# Phenylene-ethynylenes: Structure, Morphology and Photophysical Properties of Novel Pi Systems

A Dissertation
Presented to
The Academic Faculty

By

James Norbert Wilson

In Partial Fulfillment
Of the Requirements for the Degree
Doctor of Philosophy in Chemistry

Georgia Institute of Technology
December, 2004

# Phenylene-ethynylenes: Structure, Morphology and Photophysical Properties of Novel Pi Systems

| | |
|---|---|
| Dr. Marcus Weck<br>Chairman, Examining Committee | Dr. Uwe H. F. Bunz<br>Committee Member, Advisor |
| Dr. Catherine J. Murphy<br>Committee Member | Dr. Laren Tolbert<br>Committee Member |
| Dr. Mohan Srinivasarao<br>Committee Member | Dr. Thomas Orlando<br>Department Chair |

# Acknowledgement

The following people have helped me through hard times, given me encouragement, inspiration and have generally put up with me. I thank them all.

In no particular order: Uwe, for hiring an unemployed cyclist; Adrienne, for everything; my immediate family—Diane, Jim, John, Jerusha, and Julia; the Browns—Pete, Sandy and Courtney; my extended family, especially my grandfather and grandmother; my lab mates—current and those who came before me and taught me so much—Winni, Neil, Shane, Glen and Matt; Dr. Handy; Dr. Wagner; my committee members and everyone else whose names escape me.

# Table of Contents

# List of Tables

# List of Figures

# List of Schemes

# List of Abbreviations

| | |
|---|---|
| CD | circular dichroism |
| CV | cyclic voltametry |
| CPPL | circularly polarized photo luminescence |
| DSC | differential scanning calorimetry |
| eV | electron volts |
| Fc | Ferrocene |
| FTIR | Fourier transform infra red |
| GPC | Gel Permeation Chromatography |
| HOMO | highest occupied molecular orbital |
| IR | infra-red |
| LED | light emitting diode |
| LUMO | lowest unoccupied molecular orbital |
| $M_n$ | number average molecular weight |
| Mp | melting point |
| MS | mass spectrum |
| $M_w$ | weight average molecular weight |
| NBS | N-bromosuccinimide |
| NLO | non-linear optics |
| NMR | nuclear magnetic resonance |
| OLED | organic light emitting diode |

| | |
|---|---|
| PAE | poly(aryleneethynylene) |
| PDI | polydispersity index |
| PE | polyester |
| PL | photoluminescence |
| PPE | poly(*para*phenyleneethylene) |
| PPV | poly(*para*phenylenevinylene) |
| SEM | scanning electron micrscope |
| SHE | standard hydrogen electrode |
| TCE | tetrachloroethane |
| TEM | transmission electron micrscope |
| $T_g$ | glass transistion |
| TLC | thin layer chromatography |
| UV-vis | ultraviolet-visible |
| V | volts |
| XRD | X-ray diffraction |
| Φ | quantum yield |

# Summary

The syntheses of novel poly(*para*phenyleneethynylene)s, PPEs, and poly(aryleneeethynylene)s, PAEs, as well as hybrid poly(*para*phenyleneethynylene)-poly(*para*phenylenevinylene)s, PPE-PPVs, are presented. Fluorescent PPEs decorated with biologically relevant ligands are utilized in model biosensing schemes. PPE-PPV hybrids, as well as their highly emissive oligomeric, cruciform model compounds are studied in an effort to modify the bandgap of the parent PPE backbone. Improved hole and electron injection capabilities are demonstrated with these hybrid conjugated materials. Structural variation and morphological effects of PPEs, PPE-PPVs and model compounds are studied to elucidate the effects upon the photophysical properties of the emissive materials.

# Chapter 1

# PPEs: Background and Proposed Research

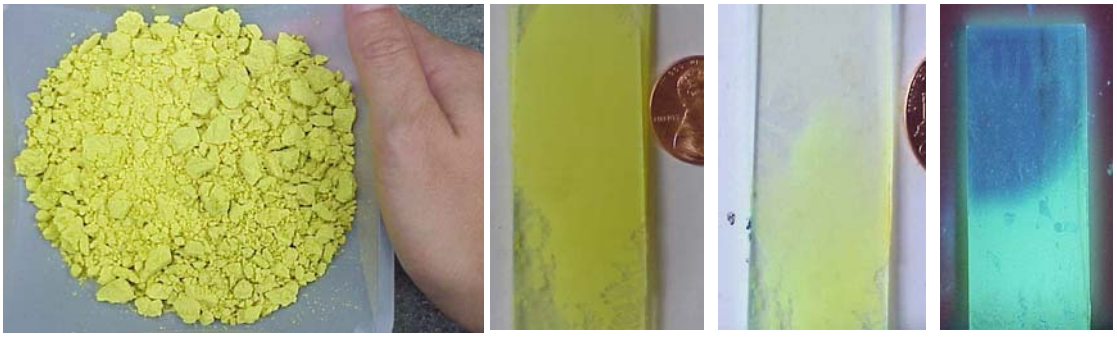

## 1.1 Introduction

Poly(*para*phenyleneethynylene)s, PPEs (Figure 1.1), and more generally poly(aryleneethynylene)s, PAEs, are an important class of conjugated polymers.[1] Conjugated polymers have far ranging applications from active layers in light emitting diodes, optical displays, thin film transistors, photovoltaics, and many sensing schemes such as electronic noses or the detection of specific sequences of DNA[6-8, 10, 11]. In most of these uses, PPEs have received less attention than PPVs. This is not to say that PPEs are unsuitable for these applications. Their chromic properties, thermal andchemical stability make them attractive candidates for many devices (Figures 1.2, 1.3) and

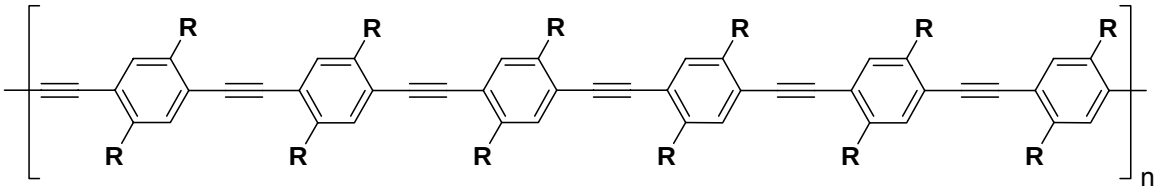


**Figure 1.1** The basic structure of a PPE. R may be a variety of sidechains, however, alkyl and alkoxy groups are typically the most common.

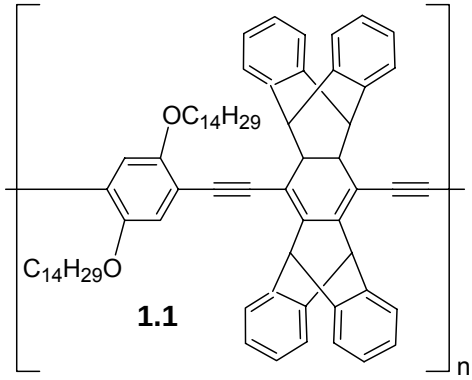


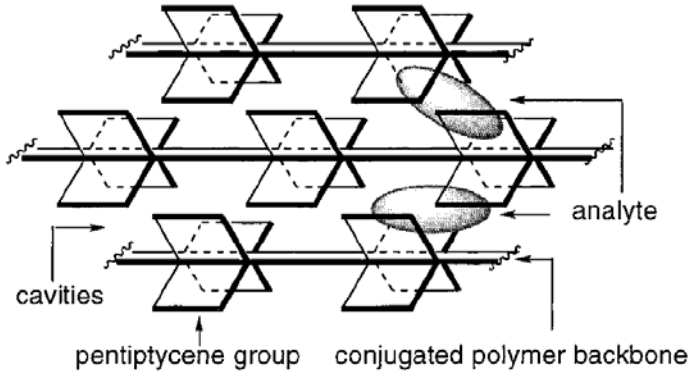


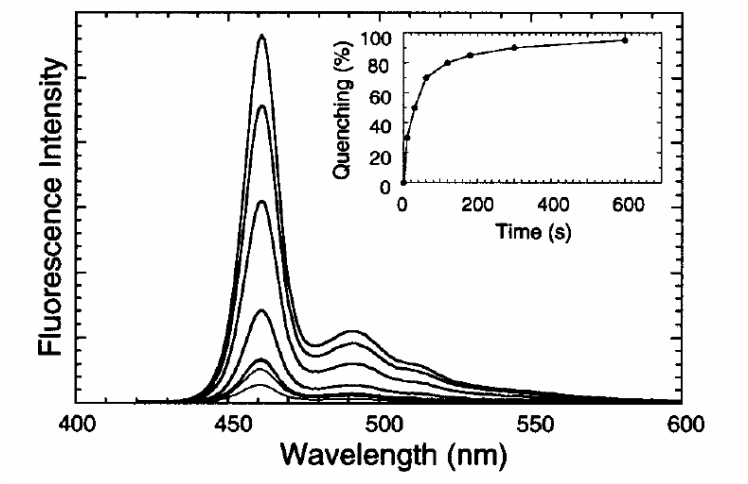


**Figure 1.2** Swager has shown that the PAE **1.1** (top) which may be cast as porous thin films (middle) displays fluorescence quenching (bottom)upon exposure to TNT and related nitro substituted degradation materials.

sensory materials. Indeed, Swager has demonstrated that PAEs may be utilized in the detection of trace amounts of by-products from TNT. Continued study of this class of polymers is warranted as is the generation of novel PPEs tailored for specific device and sensory applications.

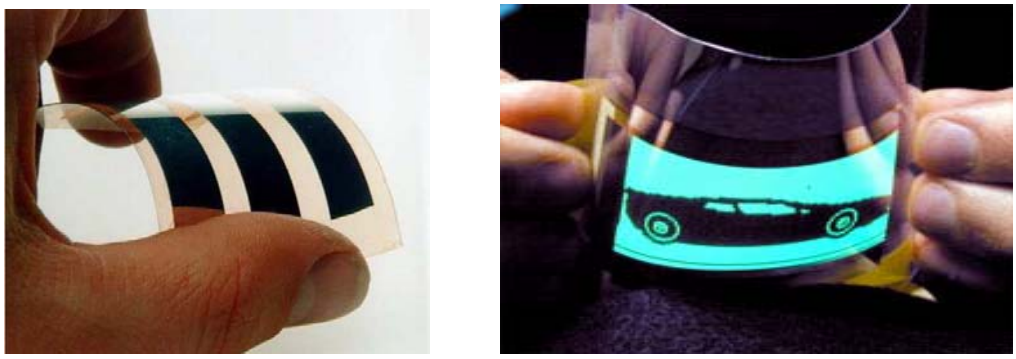

**Figure 1.3** Applications of conjugated polymers include robust, flexible photovoltaic devices (left) as well as thin, flexible and lightweight displays (right).

## 1.2 PPEs: Synthesis and Chromicity

PPEs are manufactured by either of two routes. The conventional route (Figure 1.4) utilizes a palladium catalyst in the coupling of dialkynylarenes to a dibromo- or diiodoarene.[3] This route is broadly applicable to a number of arenes and in general is tolerant of a variety of functional groups.

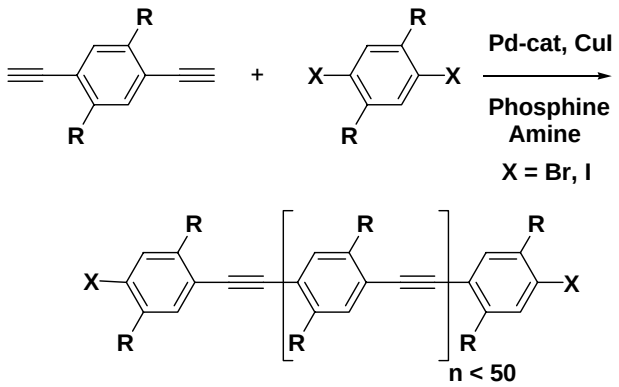


**Figure 1.4** The "classic" synthesis of PPEs utilizes the Pd catalyzed coupling of a dialkynyl benzene to a dihalogentated benzene. PPEs via this route are typically of 50 repeats or less and suffer from various structural defects.

Alternately, the route developed in the Bunz group utilizes dipropynyl arenes which are metathesized in the presence of a Mo based catalyst (Figure 1.5) with loss of 2-butyne at elevated temperatures.[2]

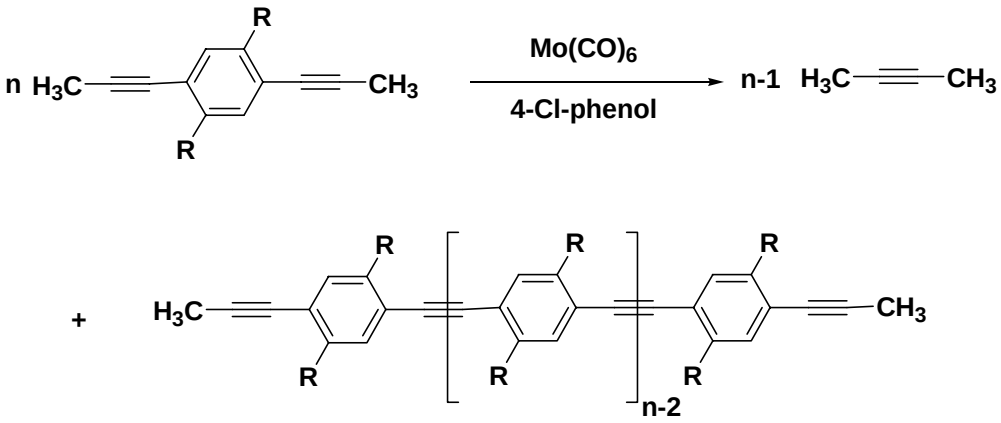


**Figure 1.5**. ADIMET or alkyne metathesis utilizes a Mo based catalyst to couple dipropynyl benzenes with elimination of 2-butyne. Reaction is run at 120-160 $^{o}$C and resulting PPEs are typically in excess of 100 repeating units.

Early work in the Bunz group reported not only a new route to PPEs but also their interesting aggregation behavior. In chloroform solutions, dialkyl PPEs display an absorbance that peaks at 390 nm. Upon aggregation there appears a red shifted sharp additional peak centered at 440 nm. This same trend is echoed in the emission spectra. In a good solvent emission peaks at 430 nm while in poor solvents or the solid state emission shifts to a maximum at 450 nm with a second peak or shoulder at 480 nm. [4a] Figure 1.6 illustrates the changes in the absorbance spectrum found with the addition of methanol, a poor solvent, to a chloroform solution of a dialkyl PPE. In Figure 1.7 a similar experiment is performed to illustrate the changes in the emission of PPEs.[4b]

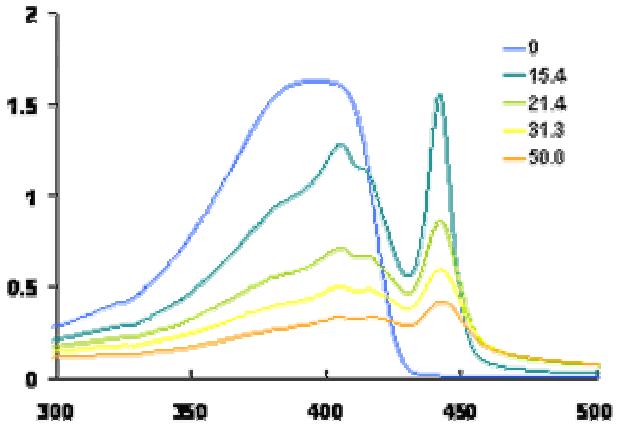


**Figure 1.6.** The addition of a non-solvent (MeOH) to a $CHCl_3$ solution of dialkyl PPE forces the planarization and aggregation of the PPE chains resulting in red shifted absorption. Figure adapted from ref 4a.

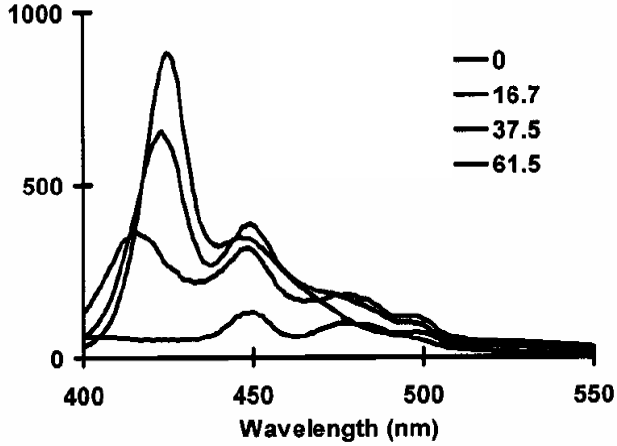


**Figure 1.7.** Addition of a non-solvent to a solution of dialkyl PPE shifts the photoluminescence to longer wavelengths. Figure adapted from ref 4b.

## 1.3 Chromicity Based Sensing Schemes

The attractive chromic behavior of PPEs results from two behaviors which are depicted in Figure 1.8. First, the planarization of the PPE backbone contributes to the lowering of the bandgap as the effective conjugation length increases. Second, formation of densely packed aggregates leads to interactions between the π systems of adjacent PPE chains allowing the formation of excimers upon excitation.

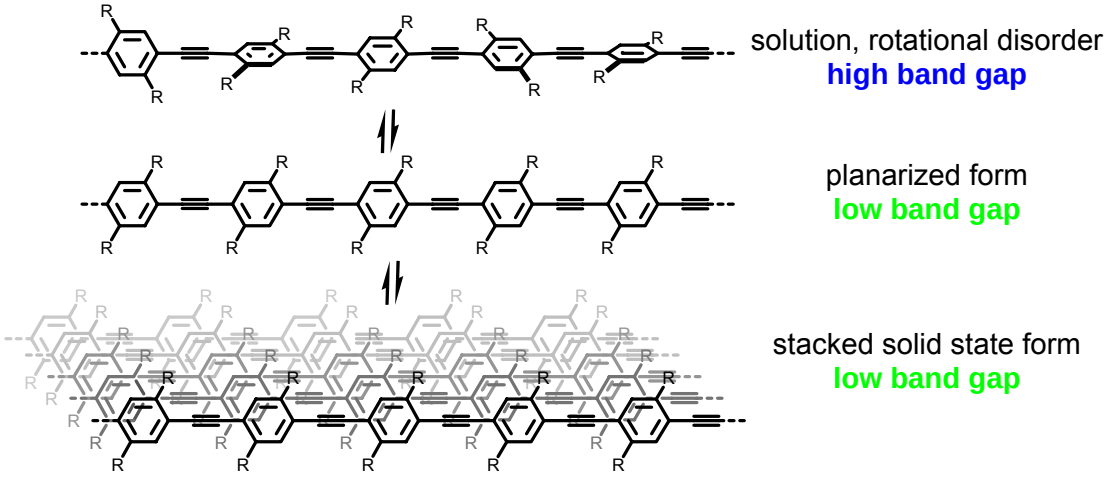


**Figure 1.8**. Cartoon depiction of the dependence of the bandgap on the conformation of the PPE backbone. In solution (at top) the phenylene rings are free to rotate leading to a relatively high band gap when compared with the planarized form (middle) which increases effective conjugation length. At bottom, aggregates of PPE chains may allow for excimer formation resulting in red-shifted emission.

In addition to the chromic shifts resulting from conformational changes induced in the conjugated backbone, PAEs may also respond to various metal ions and pH. Heterocylic arenes such as quinoline or quinoxaline may be included into the PAE backbone introducing a metal coordination site that is also responsive to pH. Figure 1.9 and 1.10 show the structures of such polymers.[5] Treatment of **1.2** with metal ions such as $Ag^{+}$ significantly alter the UV-vis spectrum as does addition of trifluoroacetic acid

(Figure 1.9). Similar behavior is observed in the case of polymer **1.3**, where trifluoroacetic acid is also found to substantially red shift the emission (Figure 1.10)

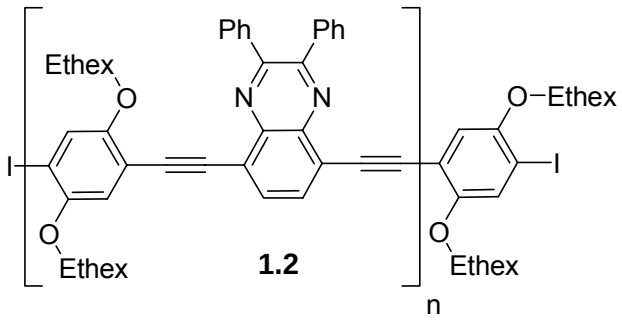


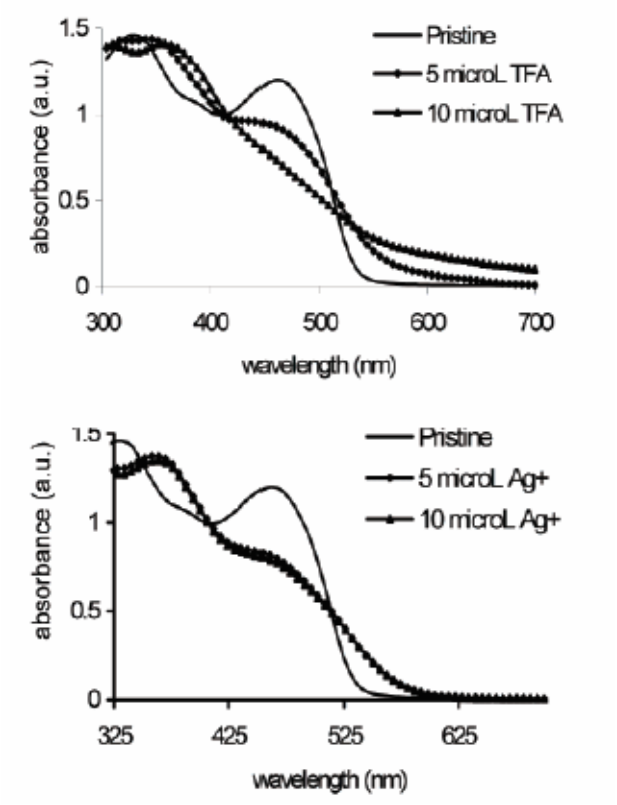


**Figure 1.9**: Quinoxaline based PPE **1.2**[5a] (top) shows changes in its UV-vis spectrum upon exposure to trifluoroacetic acid (middle) and Ag+ (bottom).

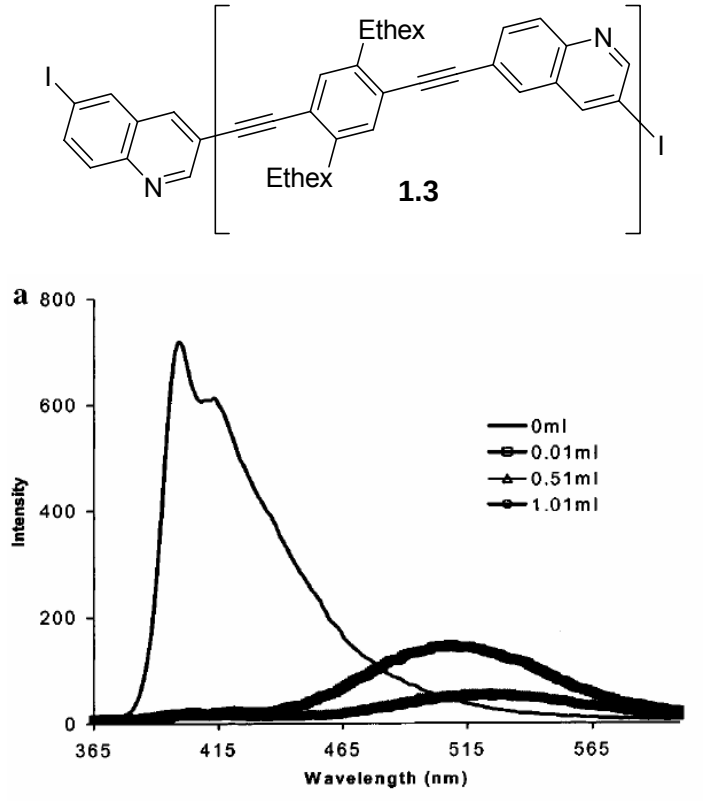


**Figure 1.10**: Quinoline based PPE, **1.3**[5b], shows a red shift from a maximum at 410 nm to 505 nm upon protonation with trifluoroacetic acid.

Encouraged by the chromicity of PPEs and the responsiveness of related PAEs to various analytes, we began to look for routes to other sensing schemes. A number of authors have reported agglutination or aggregation behaviors of saccharide decorated polymers.[12] In the case of polythiophenes decorated with mannose, sensitivity towards Conconavalin A, a sugar binding lectin, was demonstrated (Figure 1.11).[12a] While this example utilizes a colorimetric based assay, employing a strongly emissive polymer such as PPEs should lead to much more sensitive fluorescence based assays.

**Figure 1.11** Baek et al, demonstrated that polythiophenes decorated with mannose exhibit color changes upon exposure to both Influenza virus and *E. Coli*. The solutions A and D are polymer solutions without any analyte, B contains Influenza virus A, C contains Influenza virus B and E contains *E. coli*. Clearly visible is the darker red color resulting upon binding of the toxins. Adapted from Ref 12a.

We predict that ligand substituted PPEs will aggregate upon binding of the appropriate biomolecule (Figure 1.12). The resulting shift in emission should mimic the behavior of PPEs in solution as they aggregate due to introduction of non-solvents (Figures 1.6 and 1.7, above). It should be possible to introduce a series of biologically relevant ligands such as mono- and oligosaccharides onto the side chains of PPEs. Saccharides are important biomolecules forming a number of cellular receptors and recognition sites including the receptors which define blood groups. Saccharides may be bound by various lectins forming the basis for a simple bioassay. For example, Con A, the lectin of the jack bean, may be utilized as a non-toxic analogue to the toxin Ricin, which is the lectin of the castor bean and a significant bioterrorist threat. We hope that the synthesis of PPEs with biologically relevant substituents will serve as an important class of sensors in the future.

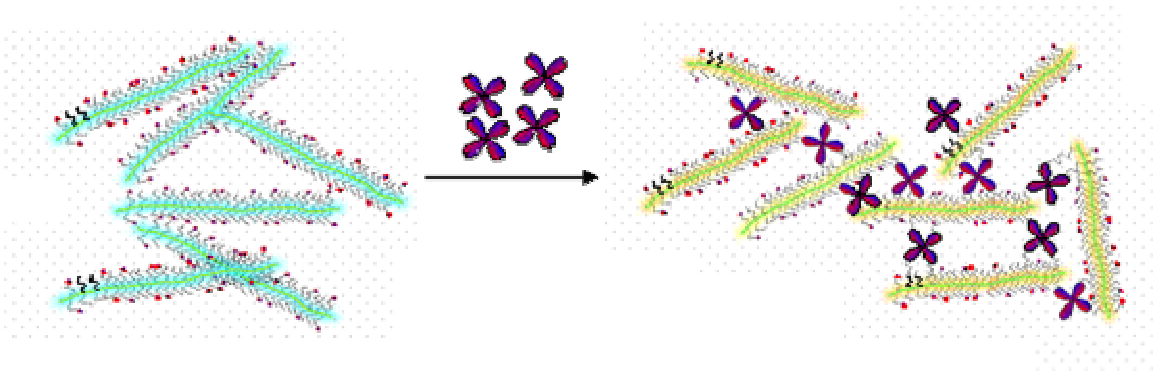

**Figure 1.12** Cartoon demonstrating the anticipated chromic response due to aggregation of a PPE decorated with saccharides when exposed to a lectin such as Conconavalin A.

## 1.4 PAEs in Light Emitting Devices

PAEs have been incorporated into functional light emitting diodes.[4b] While these devices demonstrate the ability of these PAEs to form active emitting layers, there remain significant obstacles to their widespread use. The turn-on voltages remain high and the alignment of the HOMO and LUMO levels with conventional electrodes is less than ideal. PPVs were the first conjugated polymer reported as an emitting layer in a PLED in 1990 by Burroughes *et al.*[10a] Despite their susceptibility to thermal and oxidative stress, the frontier orbitals of PPVs conveniently mesh with standard electrode materials (Figure 1.13) allowing more facile hole and electron injection and this has recently propelled them to commercial applications. If PPEs are to meet with the same success, we must demonstrate that both their hole and electron injection barriers can be lowered to more easily match with typical device construction and energy requirements. Through substitution of the basic PPE backbone, it may be possible to produce a polymer that combines the electronic capabilities of the PPVs with the stability of the PPEs.

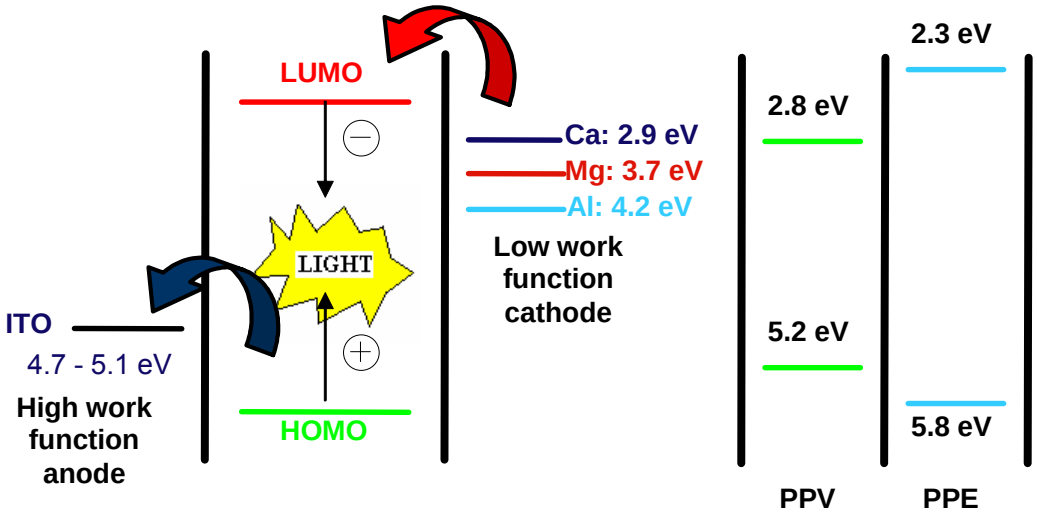


**Figure 1.13** Schematic of a light emitting device showing the relative positions of electrodes, HOMO and LUMO (left). At right is a comparison of the HOMO and LUMO values of PPV and PPE. Note that PPV conveniently matches with conventional electrode materials such as Ca and ITO.

## 1.5 Conclusion and Outlook

PPEs present stability, chromicity and fluorescence properties that make them attractive materials for both biological sensing schemes as well as device construction. Their relatively facile synthesis, adaptability to a broad range of functional groups, as well as their interesting chromic properties should see their successful application as "biosensors" in the immediate future. Additionally, the recent realization of conjugated polymers as commercially available light emitting devices should also stir interest in PPEs as candidates for a number of device applications. We propose the following research goals as steps in the development of PPEs for such applications:

1. Developing a PPE suitable for post-polymerization functionalization with biomolecules such as saccharides or other ligands and/or producing bio-substituted PPEs by conventional polymerization routes.
2. Demonstrating the applicability of PPEs in a model biosensing scheme.
3. Generating a series of PPEs and/or model compounds to improve both hole and electron injection capabilities—i.e. bandgap "engineering".

With these the completion of these goals we will progress a few small, yet significant steps forward in the implementation of PPEs as biosensors as well as understanding some of the fundamental photophysical properties of these interesting conjugated materials.

## 1.6 References and Notes


1. (a) Bunz, U. H. F. *Chem. Rev.*, **2000**, *100*, 1905-1644. (b) Giesa, R. *J. M. S.—Rev. Macromol. Chem. Phys.*, **1996**, *36*, 631.

2. Kloppenburg, L.; Song, D.; Bunz, U. H. F. *J. Am. Chem. Soc.* **1998**, *120*, 7973.

3. (a) Giesa, R.; Schulz, R. C. *Macromol.Chem. Phys.***1993**, *191*, 857. (b) Dieck, H. A.; Heck, R. F. *J. Organomet. Chem.,* **1975**, *93*, 259. (c) Cassar, I. *J. Organomet. Chem.*, **1975**, *93*, 253. (d) Sonogashira, K.; Tohda, Y.; Hagihara, N. *Tetrahedron Lett.*, **1975**, *16*, 4467.

4. (a)Halkyard, Bunz, et al. *Macromolecules.* **1998,** *31*, 8655 (b) Pschirer, N. G.; Miteva, T.; Evans, U. ; Roberts, R. S. ; Marshall, A. R. ; Neher, D. ; Myrick, M. L.; Bunz, U. H. F. *Chem. Mater*, **2001**, *13*, 2691-2696.

5. (a) Bangcuyo, C. G.; Rampey-Vaughn, M. E.; Quan, L. T.; Angel, S. M.; Smith, M. D.; Bunz, U. H. F. *Macromolecules*, **2002**, *35*, 1563. (b) Bangcuyo, C. G.; Ellsworth, J. M.; Evans, U.; Myrick, M. L.; Bunz, U. H. F. *Macromolecules*, **2003**, *36*, 546.

6. Dore, K.; Dubus, S.; Ho, H. –A.; Levesque, I.; Brunette, M.; Corbeil, G.; Boissinot, M.; Boivin, G.; Bergeron, M. G.; Boudreau, D.; Leclerc M. *J. Am. Chem. Soc.*, **2004**, *126*, 4240.

7. (a) Virji, S.; Huang, J.; Kaner, R. B.; Weiller, B. H. *Nano. Lett.*, **2004**, *4*, 591. (b) Huang, J.; Kaner, R. B., *J. Am. Chem. Soc.*, **2004**, *126*, 851.

8. Gaylord, B. S.; Heeger, A. J.; Bazan, G. C. *J. Am. Chem. Soc.*, **2003**, *125*, 896.

9. (a) Yang, J. –S.; Swager, T. M. *J. Am. Chem. Soc.*, **1998**, *120*, 5321. (b) Yang, J. –S.; Swager, T. M. *J. Am. Chem. Soc.*, **1998**, *120*, 11864.

10. (a) Burroughes, J. H.; Bradley, D. D. C.; Brown, A. R.; Marks, R. N.; Mackay, K. D.; Friend, R. H.; Burn, P. L.; Holmes, A. B. *Nature*, **1990**, *347*, 539. (b) Friend, R. H.; Gymer, R. W.; Holmes, A. B.; Burroughes, J. H.; Marks, R. N.; Taliani, C.; Bradley, D. D. C.; Dos Santos, D. A.; Bredas, J. L.; Loglund, M.; Salaneck, W. R. *Nature*, **1999**, *397*, 121. (c) Sirringhaus, H.; Tessler, N.; Friend, R. H. *Science*, **1998**, *280*, 1741.

11. Kietzke, T.; Neher, D.; Landfester, K.; Montenegro, R.; Guntner, R.; Scherf, U. *Nat. Mater.* **2003**, *2*, 408.

12. (a) Baek, M. G.; Stevens, R. C.; Charych, D. H. *Bioconjugate Chem*. **2000**, *11*, 777 (b) Fraser, C. L.; Grubbs, R. H. *Macromolecules* **1995**, *28*, 7248. (c) Nomura, K.; Schrock, R. R. *Macromolecules*, **1996**, *29*, 540. (d) Roy, R.; Tropper, F. D. *Chem. Commun*. **1988,** 1058. (e) Spaltenstein, A.; Whitesides, G. M. *J. Am. Chem. Soc*. **1991**, *113*, 686. (f) Sigal, G. B.; Mammen, M.; Dahmann, G.; Whitesides, G. M. J. *Am. Chem. Soc.* **1996**, *118*, 3789. (g) Choi, S. K.; Mammen, M.; Whitesides, G. M. *J. Am. Chem. Soc*. **1997**,*119*, 4103

# Chapter 2

# Synthesis of Poly(phenyleneethynylene)s Utilizing Acetlyene Gas as a Reagent

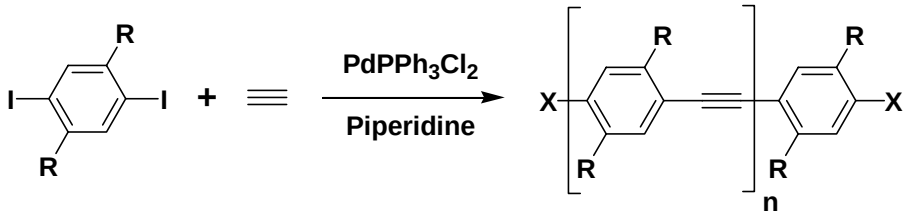


## 2.1 Introduction

Poly(*para*-phenyleneethynylene)s, (PPE)s, are conjugated polymers of importance as active materials in light-emitting diodes, as sheet polarizers, and as sensory materials in the detection of explosives.[1-3] The PPEs are of high stability and display attractive photophysical behavior in absorption and emission.[4] PPEs are made either by alkyne metatathesis or by the Pd-catalyzed coupling of aromatic diiodides to aromatic diynes.[1,6-9] Alkyne metathesis relies on $Mo(CO)_6$ for the coupling of dipropynyl benzenes with the elimination of 2-butyne (Scheme 2.1). The high temperatures (110-150 $^oC$) required for this reaction, as well as the specificity of the catalyst do not allow for R groups other than alkyl chains. The Pd-catalyzed reactions have a broad scope, and their experimental setup is facile. However, catalyst loadings are mostly in the range 1-5 mol %, and two monomers, the diiodobenzene and the dialkynylbenzene, have to be synthesized.[1] Only in a few cases acetylene gas has been utilized as reagent in these

couplings.[5] The such obtained PPEs were dark brown, suggesting defective polymers to have been formed; structurally intact PPEs are either colorless (*meta*-PPE), bright yellow (dialkyl-PPE), or orange (dialkoxy-PPE). Inspired by recent work in our own labs on the formation of tolanes utilizing acetylene gas as well as previous literature examples, we investigated the use of acetylene gas as a reagent for the synthesis of PPEs.[6] We were able to optimize the process of the Pd-catalyzed coupling of diiodoarenes to acetylene gas that allows an industrial scale synthesis of defect-free PPEs of high molecular weight.

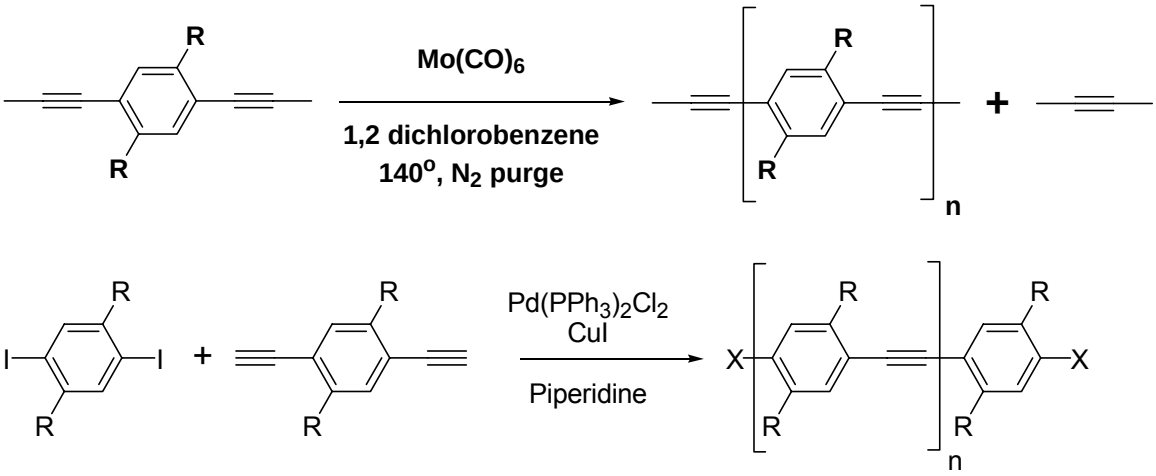


**Scheme 2.1**: The synthesis of PPEs was previously achieved by alkyne metathesis (top) utilizing a dipropynyl benzene with a molybdenum based catalyst or by the coupling of a diiodo benzene with a dialkynyl benzene utilizing a palladium based catalyst (bottom).

## 2.2 Results and Discussion

In a preliminary experiment, a Schlenk flask of known volume was used to react **2.2a** with 2 equivalents of acetylene gas in the presence of 1 mol % of catalyst [$(PPh_3)_2PPdCl_2$] and cocatalyst [CuI] in a small volume of piperidine (Scheme 2.2). The oligomer produced was of promising quality in appearance, but of low molecular weight. A set of experiments determined the best solvent to be a 1:1 mixture of toluene and piperidine.

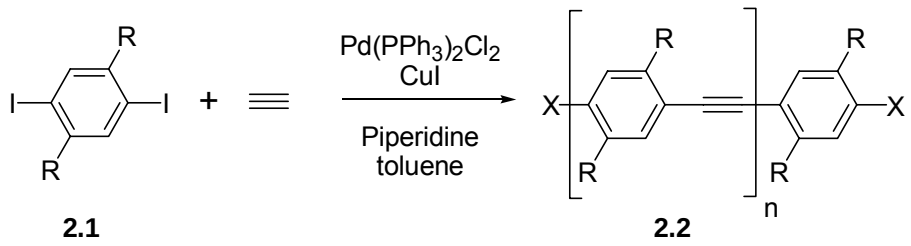


**Scheme 2.2**: The use of acetylene gas as a reagent in the synthesis of PPEs

Piperidine alone, as well as dichloromethane or chloroform as cosolvents gave polymers of low molecular weight. A second set of experiments determined that the optimum molar ratio of diiodobenzene to acetylene gas was between 1.0 and 1.1. Scale-ups based on these stoichiometries utilizing monomer **2.1a** yielded polymers of exceptionally high quality and high molecular weight (Table 2.1). We found that this approach was not only successful for the synthesis of **2.2a**,[6] but likewise efficient for the synthesis of dioctyl-PPE **2.2b**,7 and to our surprise it also worked well for the synthesis of the dialkoxy-PPEs **2.2c**,**d**[8] that were obtained in high yields and with a substantial degree of polymerization.[10] We furthermore discovered that we could decrease the amount of Pd catalyst to 0.1 mol % without impeding the catalytic activity of the system. The coupling must be a highly efficient process. Polycondensations that involve AA + BB monomers are sensitive toward imbalanced stoichiometry, and while the amount of acetylene gas we utilize is not excessive and according to the known flask volume and the general gas law represents approximately 1.1 equiv, that number can be off by 10-15%. As a consequence, it would be expected that only low molecular weight materials could form. However, this experimental setup is advantageous as the acetylene gas has to diffuse into the reaction mixture. And while slow stirring is maintained through the whole polymerization process, the concentration of free acetylene gas is perhaps low at any given moment *in* the reaction mixture. As a consequence, there is always a large excess

**Table 2.1**. Substituent key, reaction conditions, GPC results and optical data.

| Entry | Substituent key for **2.1**, **2.2** | Amt of Pd catalyst (%) | Yield of **2.2** (%) | $P_n$ GPC | $M_w/M_n$ GPC | Uv-vis Max | Emission max |
|---|---|---|---|---|---|---|---|
| 1 | a ethylhexyl | 0.2 | 87 | 259 | 2.7 | 369 | 423 |
| 2 | a ethylhexyl | 0.1 | 72 | 181 | 3.6 | 370 | 423 |
| 3 | b octyl | 0.2 | 56 | 91 | 1.8 | 391 | 428 |
| 4 | b octyl | 0.1 | 85 | 127 | 4.1 | 389 | 428 |
| 5 | c hexyloxy | 0.2 | 74 | 55 | 1.4 | 440 | 471 |
| 6 | c hexyloxy | 0.1 | 63 | 33 | 3.2 | 438 | 468 |
| 7 | d ethylhexyloxy | 0.2 | 92 | 316 | 2.4 | 460 | 480 |
| 8 | d ethylhexyloxy | 0.1 | 88 | 104 | 3.1 | 460 | 480 |

of iodine-containing reactive groups present, even in later stages of the reaction. Phenyleneethynylene oligomers with alkyne termini will immediately couple to more monomer or iodine-substituted oligomers. Because of the additional concentration decrease of acetylene gas in the vapor phase, the influx of acetylene will decrease over time, which then leads to an efficient formation of relatively high molecular weight PPEs even if only very little Pd catalyst is present.

## 2.3 Conclusions

In conclusion, we have developed a straightforward and valuable method to make high molecular weight PPEs utilizing acetylene gas in a Pd-catalyzed process. These PPEs are of better quality than many of the PPEs reported by Pd-catalyzed couplings of dialkynylarenes to diiodobenzenes;[1] the PPEs we have made here are of similar purity and quality as the metathesis-made materials.[6] Low catalyst loadings, the negligible price of acetylene gas, and the facile large-scale synthesis of diiodobenzene derivatives bodes

well for the exploitation of this reaction scheme to the synthesis of large (kilogram) amounts of high-quality PPEs.

## 2.4 Experimental

The goal of the initial experiments were simply to determine optimum reaction conditions. As such, the only analysis performed was GPC.

This first reaction set (reactions 1-4, Table 2.2) attempts to determine the optimum solvent balance between the base (piperidine) which is necessary for the reaction, but not a good solvent for the resulting polymer and chloroform which is a good solvent for the resulting polymer. For all reactions in this set 1.47 mmol of acetylene were used with 0.98 mmol of diiodide **2.1**.

**Table 2.2**. Reactions 1-4.

| Rxn | mL piperidine | mL chloroform | $Pd(PPh_3)_2Cl_2$ | CuI | **1.1** | $M_n$ GPC |
|---|---|---|---|---|---|---|
| 1 | 3.00 | 0 | 40 mg | 10 mg | 0.543 mg | 37 |
| 2 | 2.25 | 0.75 | 40 mg | 10 mg | 0.543 mg | 25 |
| 3 | 1.50 | 1.50 | 40 mg | 10 mg | 0.543 mg | - |
| 4 | 0.75 | 2.25 | 40 mg | 10 mg | 0.543 mg | - |

This second set (reactions 5-8, Table 2.3) attempts to determine the optimum solvent balance between piperidine and toluene, which has replaced chloroform from the above set. Additionally, the amount of catalyst and co-catalyst utilized has been dropped to 1 mol .

**Table 2.3**. Reactions 5-8.

| Rxn | mL piperidine | mL toluene | $Pd(PPh_3)_2Cl_2$ | CuI | diiodide | $M_n$ GPC |
|---|---|---|---|---|---|---|
| 5 | 2.5 | 0.5 | 1 mol% | 1 mol% | 0.543 mg | - |
| 6 | 2.0 | 1.0 | 1 mol% | 1 mol% | 0.543 mg | 29 |
| 7 | 1.5 | 1.5 | 1 mol% | 1 mol% | 0.543 mg | 33 |
| 8 | 0.75 | 2.25 | 1 mol% | 1 mol% | 0.543 mg | 76 |

This final block of experiments (reactions 9-12, Table 2.4) attempts to determine the optimum ratio between diiodide and acetylene gas. The acetylene gas volume was kept constant at 34 mL or 1.4 mmol.

**Table 2.4**. Reactions 9-12.

| Rxn | mL piperidine | mL toluene | $Pd(PPh_3)_2Cl_2$ | CuI | diiodide | eq. of acetylene | $M_n$ GPC |
|---|---|---|---|---|---|---|---|
| 9 | 1.5 | 1.5 | 1 mol% | 1 mol% | 0.840 mg | 1.0 | 86 |
| 10 | 1.5 | 1.5 | 1 mol% | 1 mol% | 0.755 mg | 1.1 | 84 |
| 11 | 1.5 | 1.5 | 1 mol% | 1 mol% | 0.692 mg | 1.2 | 56 |
| 12 | 1.5 | 1.5 | 1 mol% | 1 mol% | 0.640 mg | 1.3 | 43 |

**General procedure for formation of poly(phenyleneethynylene)s**: In a 25 mL Schlenk flask (real volume 37 mL), the diiodobenzene was dissolved in 3 mL of a 1:1 mixture of piperidine and toluene. Under $N_2$, $Pd(PPH_3)_2Cl_2$ (2.0 mg, 2.8 μmol, 0.2 mol%) and CuI (1.0 mg, 5.2 μmol, 0.38 mol %) were added. The reaction flask was sealed and degasses three times. A balloon was evacuated then filled with a small volume (~50 mL) of acetylene gas. The balloon was connected to the Schlenk flask and the stopcock was briefly opened allowing the gas to enter at atmospheric pressure resulting in 34 mL of gas added to the flask. The flask was sealed then allowed to stir for 24 hours. If the reaction solidified, it was placed in a warm water bath ($50^o$ C) for the remainder of the reaction time. The resulting thick solution was dissolved in 200 mL of $CH_2Cl_2$ and stirred vigorously with 150 mL of 10% $NH_4OH$ for 15 min. The aqueous layer was extracted and the organic layer was again stirred vigorously with 3M HCl for 15 min. This procedure of alternating stirring with $NH_4OH$ and HCl was repeated two times. After the final rinsing, the $CH_2Cl_2$ solution was evaporated to a few milliliters and the polymer was precipitated into MeOH. The precipitate was collected by suction filtration with a fritted funnel.

**Bis(2-ethyl)hexyl PPE 2.2a** Using the general polymerization procedure, 2,5-bis-(2-ethyl)hexyl-1,4-diiodobenzene (0.775 g, 1.40 mmol), $Pd(PPH_3)_2Cl_2$ (2.0 mg, 2.8 μmol, 0.2 mol%) and CuI (1.0 mg, 5.2 μmol, 0.38 mol %) were dissolved in piperdine/toluene. The bright yellow polymer was isolated in 83%. $^1$H NMR ($CDCl_3$) δ = 7.34 (bs), 2.82-2.64 (bm), 1.83-1.75 (bm), 0.89 (bt), 0.84 (bt).

**Dioctyl PPE 2.2b** Using the general polymerization procedure, 2,5-octyl-1,4-diiodobenzene (0.775 g, 1.40 mmol), $Pd(PPH_3)_2Cl_2$ (2.0 mg, 2.8 μmol, 0.2 mol%) and CuI (1.0 mg, 5.2 μmol, 0.38 mol %) were dissolved in piperdine/toluene. The bright yellow polymer was isolated in 56%. $^1$H NMR ($CDCl_3$) δ = 7.38 (bs), 2.86-2.66 (bm), 1.77-1.59 (bm), 1.44-1.13 (bm), 0.84 (bt).

**Dihexoxy PPE 2.2c** Using the general polymerization procedure, 2,5-hexoxy-1,4-diiodobenzene (0.742 g, 1.40 mmol), $Pd(PPH_3)_2Cl_2$ (2.0 mg, 2.8 μmol, 0.2 mol%) and CuI (1.0 mg, 5.2 μmol, 0.38 mol %) were dissolved in piperdine/toluene. The bright yellow polymer was isolated in 74%. $^1$H NMR ($CDCl_3$) δ = 7.00 (bs), 4.01 (bt), 1.91-1.77 (bm), 1.40-1.18 (bm), 0.87 (bt).

**Bis(2-ethyl)hexoxy PPE 2.2d** Using the general polymerization procedure, 2,5-bis-(2-ethyl)hexoxy-1,4-diiodobenzene (0.821 g, 1.40 mmol), $Pd(PPH_3)_2Cl_2$ (2.0 mg, 2.8 μmol, 0.2 mol%) and CuI (1.0 mg, 5.2 μmol, 0.38 mol %) were dissolved in piperdine/toluene. The bright yellow polymer was isolated in 92%. $^1$H NMR ($CDCl_3$) δ = 6.97 (bs), 3.90-3.86 (bm), 1.86-1.76 (bm), 1.74-1.40 (bm), 1.40-1.23 (bm), 0.96 (bt), 0.86 (bt).

**Gel Permeation Chromatography.** GPC was performed using a Shimadzu HPLC with a UV-vis detector module SPD 10A-VP equipped with a Waters Styragel HMW 6E (part

# WAT044204) column. The number of repeats for each polymer was determined using polystyrene standards.

**UV-vis measurements of PPEs.** The UV-Vis measurements were taken using a Jasco Inc. UV-Vis spectrometer model V-530. The PPEs were dissolved in $CHCl_3$ and diluted to a concentration of 1 mg/L. The absorbance of each PPE solution was measured from 250 nm to 600 nm. For thin film measurements, a 3 mg/mL solution was spin cast on a quartz slide at 1500 rpm. The absorbance of each film was measured from 250 nm to 600 nm.

**Fluorescence measurements.** The steady state fluorescence spectra were taken using a Jasco FP 6500. The PPE solutions used in the UV-Vis measurements were excited at the wavelength of the absorbance maxima and the emission was scanned from 10 nm above the excitation wavelength to 600 nm. While monitoring the wavelength of maximum emission, the excitation wavelengths were scanned from 250 nm to 10 nm below the monitored wavelength. The final emission spectra reported resulted from excitation at the wavelength maxima of the excitation scan. Thin film emission spectra were obtained by exciting at the maxima of the absorbance spectra.

## 2.5 References and Notes


1. Bunz, U. H. F. *Chem. Rev*. **2000**, *100*, 1605 Bunz, U. H. F., *Acc. Chem. Res*., **2001**, *34*, 998.

2. Schmitz, C.; Posch, P.; Thelakkat, M.; Schmidt, H. W.; Montali, A.; Feldman, K.; Smith, P.; Weder, C. *Adv. Funct. Mater*. **2001**, *11*, 41. Weder, C.; Sarwa, C.; Montali, A.; Bastiaansen, G.; Smith, P. *Science*, **1998**, *279*, 835. Pschirer, N. G.; Miteva, T.; Evans, U.; Roberts, R. S.; Marshall, A. R.; Neher, D.; Myrick, M. L.; Bunz, U. H. F. *Chem. Mater.*, **2001**, *13*, 2691.
3. Yang, J. S.; Swager, T. M. *J. Am. Chem. Soc.*, **1998**, *120*, 5321. Rose, A.; Lugmair, C. G.; Swager, T. M. *J. Am. Chem. Soc.*, **2001**, *123,* 11298.

4. Halkyard, C. E.; Rampey, M. E.; Kloppenburg, L.; Studer-Martinez, S. L.; Bunz, U. H. F. *Macromolecules*, **1998**, *31*, 8655. Kim, J.; Swager, T. M. *Nature (London)*, **2001**, *411*, 1030.

5. (a) Li, C. J.; Slaven, W.T.; John, V. T.; Banerjee, S. *Chem. Commun.* **1997**, *1569*. Li, C. J.; Slaven, W.T.; Chen, Y. P.; John, V. T.; Rachakonda, S. H. *Chem. Commun.* **1998**, 1351. (b) Iyoda, M.; Kabir, S. M. H.; Vorasingha, A.; Kuwatani, Y.; Yoshida, M. *Tetrahedron Lett.*, **1998**, *39*, 4701.

6. (a) Waybright, S. M. PhD Thesis, 2002. (b) Waybright, S. M.; McAlpine, K.; Laskoski, M.; Smith, M. D.; Bunz, U. H. F. *J. Am. Chem. Soc.,* **2002**, *124*, 8661.

7. Kloppenburg, L.; Song, D.; Bunz, U. H. F. *J. Am. Chem. Soc.* **1997**, *120*, 7973. Kloppenburg, L.; Jones, D. Bunz, U. H. F. *Macromolecules*, **1999**, *32*, 4194.

8. Huang, W. Y.; Gao, W.; Kwei, K.T.; Okamoto, Y. *Macromolecules,* **2001**, *34*, 1570.

9. Swanson, L. S.; Lu, F.; Shinar, J. *Proc. SPIEE*. **1993**, *191*, 101.

10. Giesa, R.; Schulz, R. C. *Macromol. Chem.* **1990**, *191*, 857. Mangel, T.; Eberhardt, A.; Scherf, U.; Bunz U. H. F.; Mullen, K. *Macromol Rapid Commun*. **1995**, *16*, 571. Weder, C.; Wrighton, M. S. *Macromolecules*, **1996**, *29*, 5157.

# Chapter 3

# The Characterization of PPEs with High G Values

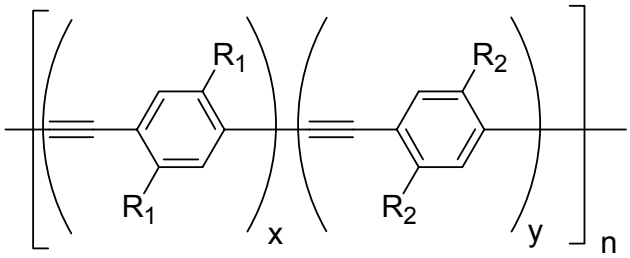


$R_1$ = 2-ethylhexyl, nonyl or dodecyl
$R_2$ = (S)-3,7-dimethyloctyl

## 3.1 Introduction

Chiroptical properties of conjugated oligomers and polymers are of fundamental interest to understand structure, conformation and interchain electronic interactions. They are important for the fabrication of advanced plastic semiconductor devices which emit circularly polarized light. Most of the earlier work on the chiroptical properties of conjugated polymers has been performed on polythiophenes, but the chiroptical properties of poly(*p*-phenylene)s[2b] and of PPEs have likewise been reported. The measured dissymmetries were, however, only moderate and did not exceed value of $|g_{CD}|$ 0.01. In most cases, the chiroptical signals in absorption of conjugated polymers are bisignate and change sign where the absorption spectrum has a maxiumum[2-4]. According to Meijer[4] this behavior is indicative of an exciton coupling within chiral assemblies of several polymer chains (interchain effect). This has changed recently with the closer examination of the liquid crystalline polyfluorenes, which show *g*-values in absorption

and emission up to 0.25[3c, 5]. The surprisingly high *g*-values in the polyfluorenes were explained by Oda *et al*.[3c, 5] by the ability of the nonlinearly linked polyfluorenes to attain a conformation in which the backbone assumes a steep helix, which apparently is stabilized in the solid state. We have investigated the amorphous poly[*p*-bis-(3,7-dimethyloctyl)phenyleneethynylene] **3a** in which all of the PE units were chirally substituted. In poor solvents and in the solid state the $|g_{CD}|$-values of **3a** were on the order of 0.006-0.008, that is, quite low even after annealing. However, when we investigated thin spin-cast and annealed films of the copolymer **3b** (5% chiral monomer), the g-values increased to 0.06.

## 3.2 Results and Discussion

In statistical copolymers, where the amount of the dimethyloctyl side chains is higher, the *g*-value at 432 nm increases dramatically to reach a maximum for **3d** where it exceeds $|g_{CD}| = 0.37$ (fig 3.1, table 3.1). The high values are observed for films which are heated to 160$^{o}$ C, just below the isotropic transition for 30 s and cooled to 140$^{o}$ C during 2h where the samples were annealed for another 16 h. Important observations are that (a) the maximum of the CD at 432 is at the maximum of the UV-vis spectrum (433 nm) and (b) that this prominent CD signal is fully monosignate within the range of the most prominent UV-vis peak (Figure 3.2).[6] Most important, the peak at 433 nm has previously been assigned to the absorption by a planarized polymer chain.[1b] Figure 3.3 shows the photoluminescence (PL) and circularly polarized photoluminescence (CPPL) spectra of a thin film of **3c** after

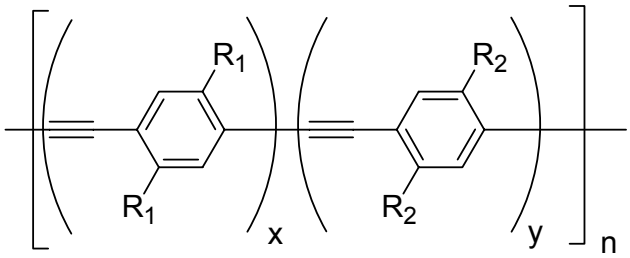


$R_1$ = 2-ethylhexyl, nonyl or dodecyl
$R_2$ = (S)-3,7-dimethyloctyl

**Figure 3.1**. General structure of PPEs with chiral side chains. Percentages of chiral monomer are in table 3.1 below.

**Table 3.1**. Substituent Key, Percentage of Chiral Monomer and $|g_{CD}|$ Values of Thin Annealed PPE Films [a,b]

| **3.3** | substituent | % chiral monomer | *g*-value annealed | *g*-value as spun |
|---|---|---|---|---|
| **a** | (S)-3,7-dimethyloctyl (dmo) | 100 | 0.008 | 0.001 |
| **b** | dmo/2-ethylhexyl | 5 | 0.060 | 0.010 |
| **c** | dmo/2-ethylhexyl | 25 | 0.292 | 0.082 |
| **d** | dmo/2-ethylhexyl | 50 | 0.378 | 0.023 |
| **e** | dmo/dodecyl | 25 | 0.042 | < 0.0001 |
| **f** | dmo/nonyl | 50 | 0.044 | 0.014 |

[a]If the content of dmo was higher than 50% (66% and 75% tested), the $|g_{CD}|$ values dropped to less than 0.05. [b]All of the herein investigated films were of uniform thickness because the spatial differences in absorbace did not exceed 8-10% in different spots of a given sample.

annealing. As has been observed in the CD spectrum, the maximum degree of CPPL at 443 nm ($g_{CPPL}$) = –0.186) is close to the maximum of the PL at 441 nm. The strong CPPL signal is fully monosignate within the range of its PL peak. The sign of the *g*-value is the same as for the pronounced feature in absorption at 432 nm. Therefore, we conclude that the prominent peaks in the CD and CPPL spectra have the same physical origin, which most likely is not an interchain exciton coupling. Evidence that excition coupling is not the dominant source for the chiroptical properties stems from the rather gradual decrease in the CPPL signal within the main emission band. In particular, the absolute value of $g_{CPPL}$ at the second emission peak (463 nm) is still more than half the

value at the first emission peak (443 nm). In contrast, exciton coupling predicts a considerably smaller circular polarization for transistions to higher vibronic states in emission.[7] The shape of the CPPL spectrum shown in Figure 3.3 is similar to the one measured for chirally substituted polyfluorenes.[3c,5] For those polyfluorenes, a helical shape of the polymer backbone has been proposed on the basis of electron diffraction experiments and quantum-chemical calculations.[5]

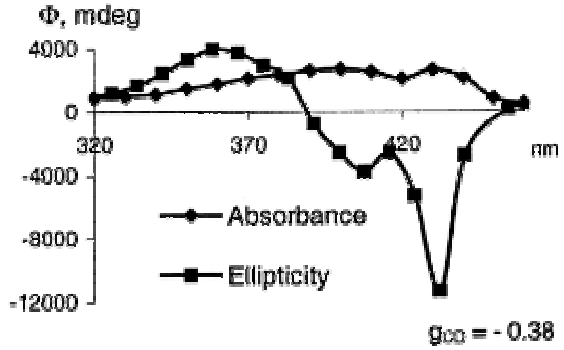


**Figure 3.2**. CD spectrum (millidegree) of a thin film of **3d** after annealing. The maximum *g*-value (-0.38) is reached at 432 nm, which corresponds to the maximum of the absorption in PPE at 433 nm.

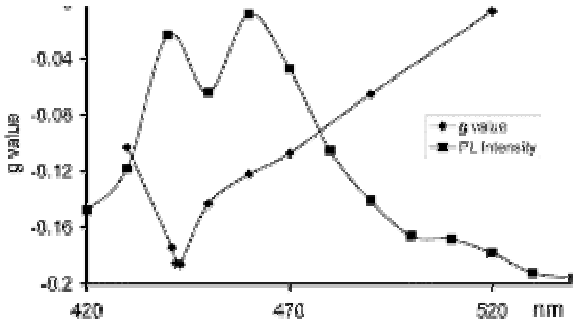


**Figure 3.3**. Solid-state emission and solid-state CPPL of **3c**. The y-axis depicts the *g*-value, the photoluminescence (PL) intensity is arbitrary.

What is the structural reason for the observed high *g*-values in the annealed as compared to the pristine films of PPEs? When examined under a polarizing microscope, the "as-spun" films of **3** are isotropic (black between crossed polarizers) and either show no or only a weak birefringence. Such samples of **3c,d** show a grainy, isotropic

morphology without any significant ordering when viewed in transmission electron microscopy (TEM). Once the films have been annealed, the PPE molecules orient parallel, adopting a nematic texture. Between crossed polarizers a distinct Schlieren texture is observed. **3e** For TEM and diffraction thin films were prepared from solution after drying and annealing. Electron diffraction of **3c** is similar to that of bis(ethylhexyl)PPE.[1e] However, we see additional innermost reflections corresponding to *d*-values near 15 Å. The strongest relfection is at 4.98 Å. We associate it with the lattice pattern produced by a staggered array of the repeating unit of the PPEs (6.8 Å).

To obtain more information a dark-field picture of a sample of **3c** was obtained in the light of the mentioned reflection. In this micrograph (Figure 3.4) all features originating from the 4.98 Å reflection appear bright. A stranded morphology with a strand thickness of approximately 40 Å is observed, similar to those reported previously for PPEs.[8] Dark-field images of nonchirally substituted PPEs display uniform brightness along the strands. Dark-field images of the stranded moieties of **3c**, however, are striated as it is visible in Figure 3.4. The striations are in an angle of 47$^{o}$ to the main axis of the strands. This angle corresponds satisfactorily with the angle under which the 4.98 Å

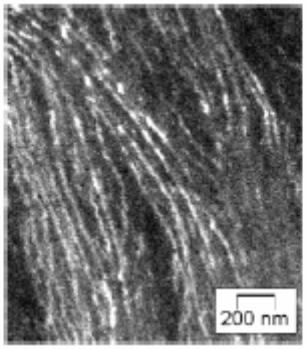


**Figure 3.4**. Transmission electron dark-field micrograph of thin polymer films of **3c** after annealing to 140$^{o}$ C for 12 h.

reflection appears off the principal direction of the strand. A further interpretation is difficult due to the restricted number of diffraction peaks that could be obtained. This is particularly true when the unit cell in the crystalline state is triclinic. However, we can conclude that the crystalline strand consists of staggered PPE molecules **3c** forming a single, helically twisted bundle. At some sites there is evidence for a helical pitch of approximately 25 nm. The screw sense of nanoscopic twisting of multiple chains into one strand seems to be caused by the chiral substituents leading to the huge dissymetries. The largest effect is visible for the 1:1 copolymer **3d**. The helical twist must be induced by the subtle interplay of chiral and racemic substituents in **3c** and **3d**. The high *g*-values are therefore *not* a property of the single chain but of the strand-shaped supramolecular assemblies that form upon annealing of **3c,d**. The nanoscopic assembly process thus seems to be critically responsible for the modulation of the chiroptical properties of **3**. It is not clear, though, if this is a conformational effect of a single chain induced by chain packing or if electronic interactions between many chains play a role.

### 3.3 Conclusion

To our knowledge, the herein reported dissymetries are the largest that have been measured for a conjugated polymer to date. While a full understanding of the phenomenon is not possible, the observed large *g*-values are exciting and seem to be caused by the strands forming upon annealing of these materials. In the future we will explore the chiroptical behavior of other chirally substituted poly(aryleneethynylene)s.

## 3.4 Experimental

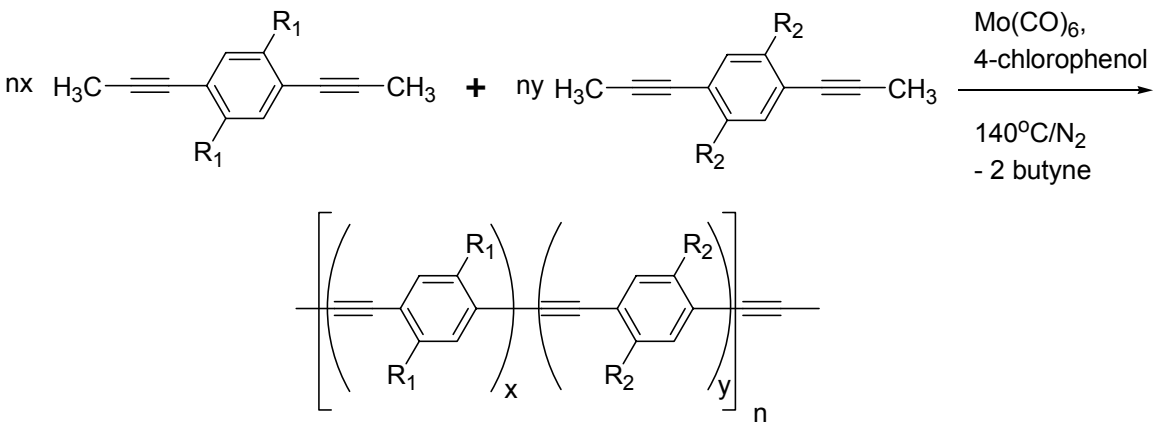


$R_1$ = {S}-3,7-dimethyloctyl, $R_2$ = 2-ethylhexyl, dodecyl, nonyl

**Table 3.2**. Substituent key, percent chiral monomer, yields and GPC data.

| Polymer | $R_1$ | $R_2$ | % Chiral monomer | Yield | $P_n$ GPC | PDI GPC |
|---|---|---|---|---|---|---|
| **3a** | citronellyl | | 100% | 83% | 128 | 3.2 |
| **3b** | ethylhexyl | citronellyl | 5% | 81% | 117 | 3.7 |
| **3c** | ethylhexyl | citronellyl | 25% | 83% | 107 | 3.7 |
| **3d** | ethylhexyl | citronellyl | 50% | 81% | 304 | 4.4 |
| **3e** | dodecyl | citronellyl | 25% | 84% | 176 | 2.2 |
| **3f** | nonyl | citronellyl | 50% | 70% | 195 | 4.1 |

**General Procedure for the Synthesis of Polymers 3a-f**: The monomers, the catalyst system consisting of $Mo(CO)_6$ (5%) and 4-chlorophenol (1 equiv. with respect to the monomers) were dissolved in o-dichlorobenzene and stirred for 48 h at 150°C, removing butyne by a slow stream of nitrogen. The solution was cooled and any precipitated polymer **3a-f** was dissolved by the addition of $CH_2Cl_2$. The organic layer was washed with 20 mL of each $H_2O$, 10% NaOH, and 25% HCl. Addition of methanol precipitated the polymer, which was filtered and vacuum-dried.[9]

The $^1H$ and $^{13}C$ NMR spectra were recorded with either a Bruker AM 300 MHz or a Varian Mercury 400 MHz spectrometer operating in the FT mode at 300 MHz ($^1H$) and 75.5 MHz ($^{13}C$) and at 400 MHz ($^1H$) and 100.6 MHz ($^{13}C$). The $^1H$ chemical shifts are referenced to the residual proton peaks of $CDCl_3$ at 2.24 (vs TMS). The $^{13}C$ resonances are referenced to the central peak of $CDCl_3$ at 77.0 (vs. TMS).

Citronellyl = **C**, Dodecyl = **D**, Ethylhexyl = **E**, Nonyl = **N**.

**Synthesis of 3a: C** (0.572 g, 1.31 mmol), 4-chlorophenol (0.168 g, 1.31 mmol), and $Mo(CO)_6$ (0.017 g, 0.065 mmol) in 10 mL of *o*-dichlorobenzene were reacted according to general procedure. Work up resulted in a yellow, brittle polymer. $^{13}C$ NMR ($CDCl_3$): δ 141.83, 132.43, 123.07, 93.56, 39.44, 38.24, 37.40, 33.08, 31.93, 28.02, 24.83, 22.56, 19.74, 14.01.

**Synthesis of 3b: E** (0.469 g, 1.23 mmol), **C** (0.031 g, 0.071 mmol), 4-chlorophenol (0.168 g, 1.31 mmol), and $Mo(CO)_6$ (0.017 g, 0.065 mmol) in 10 mL of *o*-dichlorobenzene were reacted according to general procedure. Work up resulted in a

yellow, brittle polymer. $^{13}C$ NMR ($CDCl_3$): δ 141.09, 133.40, 132.35, 123.29, 123.15, 93.58, 40.45, 39.44, 38.74, 38.46, 38.24, 37.41, 33.08, 32.70, 31.97, 28.95, 28.02, 25.89, 24.83, 23.11, 22.67, 22.60, 19.77, 14.01, 10.90, 10.75. UV/vis (CHCl ): λ max (ε) 382 (77453).

**Synthesis of 3c: E** (0.362 g, 0.95 mmol), **C** (0.138 g, 0.32 mmol), 4-chlorophenol (0.163 g, 1.27 mmol), and $Mo(CO)_6$ (0.016 g, 0.061 mmol) in 10 mL of *o*-dichlorobenzene were reacted according to general procedure. Work up resulted in a yellow, brittle polymer. $^{13}C$ NMR ($CDCl_3$): δ 142.14, 141.10, 133.42, 132.36, 123.31, 122.99, 93.60, 93.13, 40.48, 39.47, 38.76, 38.26, 37.43, 33.11, 32.73, 31.98, 28.99, 28.05, 25.90, 24.86, 23.13, 22.65, 19.80, 14.05, 10.93. UV/vis (CHCl3): λ max (ε) 387 (89125). DSC: heating: 60°C (-0.63 kcal/mol), 100°C (0.252 kcal/mol); cooling: 79°C (0.422 kcal/mol).

**Synthesis of 3d: E** (0.233 g, 0.615 mmol), **C** (0.267 g, 0.615 mmol), 4-chlorophenol (0.158 g, 1.23 mmol), and $Mo(CO)_6$ (0.016 g, 0.061 mmol) in 10 mL of *o*-dichlorobenzene were reacted according to general procedure. Work up resulted in a yellow, brittle polymer. $^{13}C$ NMR ($CDCl_3$): δ 142.30, 141.10, 134.35, 134.07, 133.48, 132.41, 123.29, 122.98, 93.56, 93.20, 77.99, 40.84, 40.47, 39.98, 39.43, 38.76, 38.20, 37.39, 33.06, 32.74, 31.92, 28.98, 27.98, 25.92, 24.79, 23.05, 22.57, 19.74, 13.93, 10.87

**Synthesis of 3e: D** (0.390 g, 0.795 mmol), **C** (0.110 g, 0.253 mmol), 4-chlorophenol (0.135 g, 1.05 mmol), and $Mo(CO)_6$ (0.014 g, 0.053 mmol) in 10 mL of *o*-dichlorobenzene were reacted according to general procedure. Work up resulted in a yellow, brittle polymer. $^{13}C$ NMR ($CDCl_3$): δ 141.97, 132.46, 122.97, 93.21, 39.43,

38.22, 37.38, 34.27, 33.06, 32.96, 31.95, 30.75, 29.74, 29.69, 29.53, 29.37, 28.01, 24.84, 22.68, 22.59, 19.79, 14.03, 1.00

**Synthesis of 3f: N** (0.242 g, 0.60 mmol), **C** (0.258 g, 0.60 mmol), 4-chlorophenol (0.154 g, 1.20 mmol), and $Mo(CO)_6$ (0.016 g, 0.061 mmol) in 10 mL of *o*-dichlorobenzene were reacted according to general procedure. Work up resulted in a yellow, brittle polymer. $^{13}C$ NMR ($CDCl_3$): δ 42.28, 142.03, 132.49, 132.34, 123.16, 123.05, 93.28, 39.48, 38.23, 38.12, 37.43, 37.32, 34.29, 34.21, 33.95, 33.10, 33.02, 31.96, 31.74, 30.74, 30.51, 29.67, 29.54, 29.37, 28.03, 24.85, 22.67, 22.60, 19.81, 19.75, 14.00, 4.38

**Gel Permeation Chromatography**: Molecular weight determinations were performed using a Waters Styragel HMW 6E (7.8 mm i.d. × 300 mm) GPC column (20 m particles/10 m frits) eluted with CHCl3 at ambient temperature (flow rate of 1 mL/min). Molecular weight results were based on 10 polystyrene standards (Mw = 3 900 000, 1 980 000, 996 000, 629 000, 210 000, 70 600, 28 600, 10 900, 3000, and 1300) purchased from Waters (type SM-105). $P_n$ was determined by dividing $P_n$ resulting from the GPC by 100.

**Film Preparation for Spectroscopy**: The films were prepared utilizing a spin caster. Films were prepared beginning with a saturated chloroform solution of the polymer. The solution was syringed through a 0.2 micrometer pore size filter (Whatman) to remove particulate and aggregates. The film was deposited onto a quartz slide then spun at 1500 rpm for 40 s. The films were protected from dust and scratches while being annealed and throughout the subsequent measurements. All films measured were found to be between 50 and 90 nm in thickness according to contact mode AFM measurement

(Digital Instruments Nanoscope IIIa). The film thickness was measured by scratching spin cast and annealed thin films (on a glass slide) with a razor blade, to produce an edge.

**Instrumentation for Optical Measurements:** A JASCO V-530 was utilized for absorbance measurements. CD measurements were performed using an OLIS RSM 1000 CD spectrophotometer. To exclude that the samples would show artifacts, the samples were rotated by $90^{o}$ and the measurement was performed again. After that operation the sample was turned upon its other side and the measurement was performed again. In all of the cases the measurements were reproducible with an error of 5-10 %. Circularly polarized photoluminescence (CPPL) spectra were measured with a commercial photoluminescence spectrophotometer, in combination with a home-built differential photon counting (DPC) system, based on the principle design described by Dekkers et al. (Rexwinkel, R. B.; Schakel, P.; Meskers, S. C. J.; Dekkers, H. P. J. M., Appl. Spectrosc. **1993**, 47, 731). Excitation was via an optical fiber with a 1 mm core diameter in combination with an appropriate interference filters. Only light emitted from a small region of ca. 2 mm diameter was passed through a piezo elastic modulator (PEM) by Hinds co. and detected by a photomultiplier tube. This way, the setup was only weakly sensitive to artifacts due to polarization-sensitive light scattering in the layer.

**DSC data** was determined on a Metler Toledo DSC821e with two repeated heating and cooling cycles:

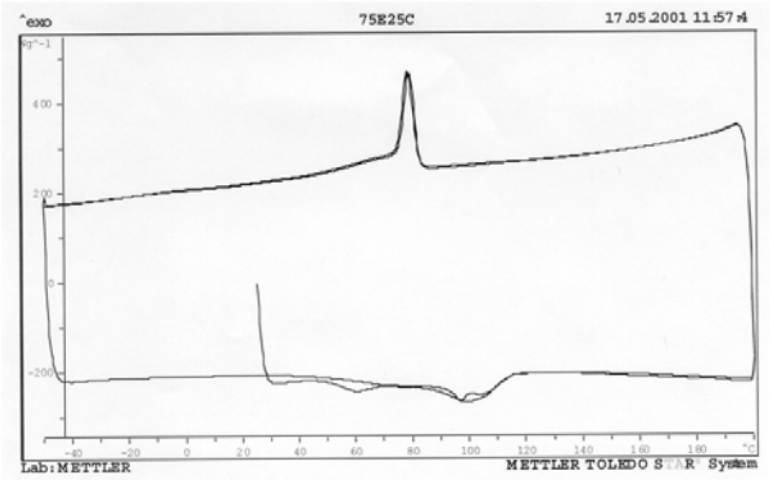


**Figure 3.5**. Polymer **3c**. Two cycles showing broad isotropic transition at 100°C and sharp liquid crystalline transition at 79°C (0.42 kcal/repeat).

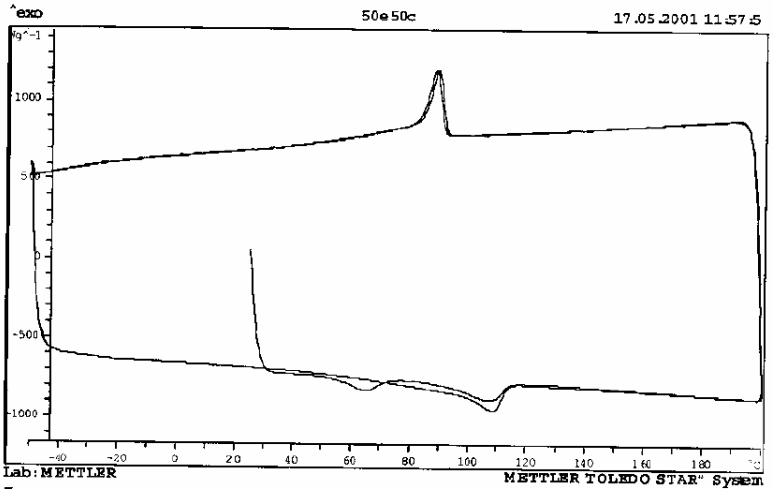


**Figure 3.6** Polymer **3d** Two cycles showing broad isotropic transition between 110°C and sharp liquid crystalline transition at 88°C (0.54 kcal/repeat).

**Supplemental TEM Images (Figures 3.7-3.9) and Electron Microscopy Details**

Electron microscopy was performed of the thin films was performed on a 1 EM 912 (Leo) and a Jeol 100 CX II. Thin films were obtained by dropping a solution of 1c in chloroform on a glass slide. The solvent was allowed to evaporate over 6 hours in a chloroform atmosphere inside a closed Petri dish. After the sample was dry carbon was evaporated onto the glass slide in high vacuum. The carbon film with the polymer was subsequently floated off the slide and transferred to copper supporting grids. Transmission electron microscopy and diffraction were performed at zero energy loss in a LEO EM 912, equipped with an -electron energy loss spectrometer at a high voltage of 120 kV. In order to minimize electron irradiation damage of the sample, the investigation was performed at –130°C by means of a GATAN cooling holder. Electron micrographs were recorded with Ilford PAN F 35 mm photographic film. Circular areas from which electron diffraction patterns were recorded had diameters of either 1.5 μm or 2.7 μm.

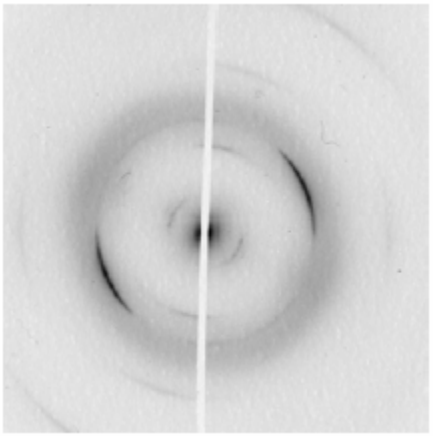

**Figure 3.7** Electron diffraction of **3c** after annealing.

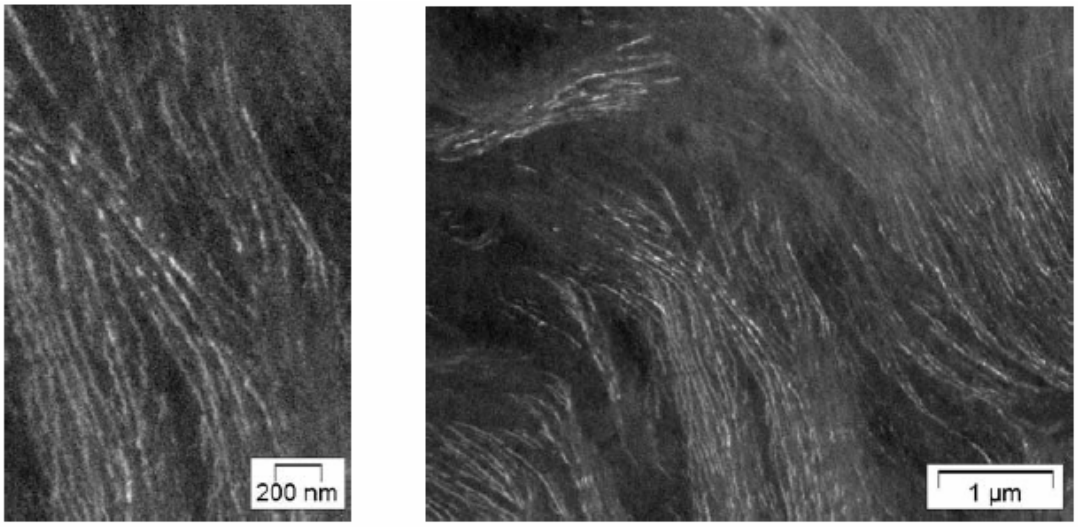


**Figure 3.8** Dark field transmission electron micrographs of **3c** after annealing

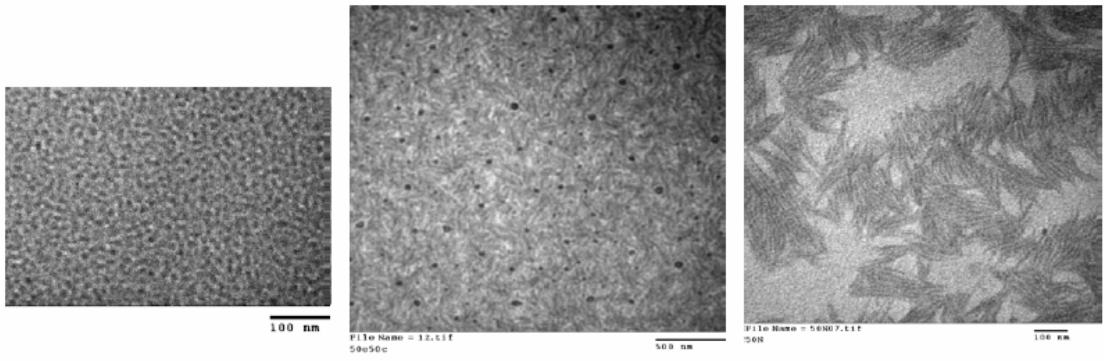


**Figure 3.9** Transmission electron micrographs of thin polymer films of **3f** (right) and of **3d** (middle) after annealing to 130°C for 12h. On the left hand side is a film of **3f** before annealing. Only a grainy structure is visible.

## 3.5 References and Notes


1. (a) Kloppenburg L.; Song, D.; Bunz, U. H. F. *J. Am. Chem. Soc.* **1998**, *120*, 7973. (b) Halkyard, C. E.; Rampey, M. E.; Kloppenburg, L.; Studer-Martinez, S. L.; Bunz, U. H. F. *Macromolecules* **1998**, *31*, 8673. (c) Fiesel,R.; Halkyard, C. E.; Rampey, M. E.; Kloppenburg, L.; Scherf, U.; Studer-Martinez, S. L.; Bunz, U. H. F. *Macromol. Rapid Commun.* **1999**, *20*, 107. (d) Miteva, T.; Palmer, L.; Kloppenburg, L.; Neher, D.; Bunz, U. H. F. *Macromolecules* **2000**, *33*, 652. (e) Kloppenburg, L.; Jones, D.; Claridge, J. B.; zur Loye, H. C.; Bunz, U. H. F. *Macromolecules* **1999**, *32*, 4460. (f) Bunz, U. H. F.; Enkelmann, V.; Kloppenburg, L.; Jones, D.; Shimizu, K. D.; Claridge, J. B.; zur Loye, H. C.; Lieser, G. *Chem. Mater.* **1999**, *11*, 1416.

2. (a) Prince, R. B.; Brunsveld, L.; Meijer, E. W.; Moore, J. S. *Angew. Chem.* **2000**, *39*, 228. Prince, R. B.; Barnes, S. A.; Moore, J. S. *J. Am. Chem. Soc.* **2000**, *122*, 2758. (b) Fiesel, R.; Scherf, U. Fiesel, R. *Macromol.Rapid. Commun.* **1998**, *19*, 427.

3. (a) Boumann, M. M.; Havinga, E. E.; Janssen, R. A. J.; Meijer, E. W. *Mol. Cryst. Liq. Cryst.* **1994**, *256*, 439. Langeveld-Voss, B. M. W.; Janssen, R. A. J.; Christiaans, M. P. T.; Meskers, S. C. J.; Dekkers, H. P. J. M.; Meijer, E. W. *J. Am. Chem. Soc.* **1996**, *118*, 4908. Peeters, E.; Delmotte, A.; Janssen, R. A. J.; Meijer, E. W. *Adv. Mater.* **1997**, *9*, 493. (b) Fiesel, R.; Neher, D.; Scherf, U. *Synth. Met.* **1999**, *102*, 1457. Oda, M.; Meskers, S. C. J.; Nothofer, H. G.; Scherf, U.; Neher, D. *Synth. Met.* **2000**, *111*, 575. (c) Oda, M.; Nothofer, H. G.; Lieser, G.; Scherf, U.; Meskers, S. C. J.; Neher, D. *Adv. Mater* **2000**, *12*, 362.

4. Langenveld-Voss, B. M. W.; Beljonne, D.; Shuai, Z.; Janssen, R. A. J.; Meskers, S. C. J.; Meijer, E. W.; Bredas, J. L. *Adv. Mater.* **1998** *10,* 1343.

5. Lieser, G.; Oda, M.; Miteva, T.; Meisel, A.; Nothofer, H.-G.; Scherf, U.; Neher, D. *Macromolecules* **2000**, *33*, 4490.

6. For all films the *linear* dichroism was ,0.01, which discounts that the large *g*-values are due to an artifact. In addition, the samples were rotated, and no angular dependence was apparent. Circularly polarized photoluminescence spectra were obtained by a differential photon counter, combined with a PTI photoluminescence spectrometer.

7. Meskers, S. C. J.; Peeters, E.; Langeveld-Voss, B. M. W.; Janssen, R. A. J. *Ad*V. *Mater*. **2000**, *12*, 589.Samori, P.; Francke, V.; Mu¨llen, K.; Rabe J. P. *Chem. Eur. J.* **1999**, *5*, 2312.

8. Samori, P.; Severin, N.; Müllen, K.; Rabe J. P. *Ad*V. *Mater.* **2000**, *12*, 579. Perahia, D.; Traiphol, R.; Bunz, U. H. F. *Macromolecules* **2001**, *34*, 151.

9. Kloppenburg, L.; Jones, D.; Bunz, U. H. F. *Macromolecules* **1999**, *32*, 4194.

# Chapter 4

# Cross Conjugated PPE/PPV Hybrids

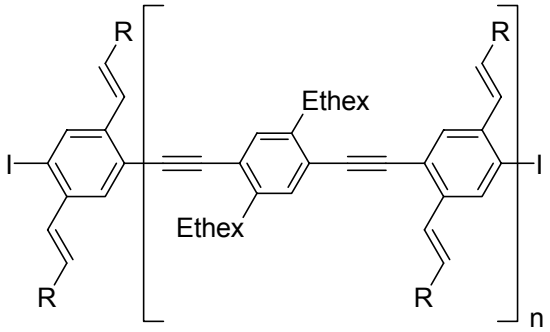


## 4.1 Introduction

The PPEs,[4] dehydrogenated congeners of the poly(*para*-phenylenevinylene)s (PPV), are a class of conjugated polymers with demonstrated sensory and device applications. [6-9] Their superb photophysical properties combined with their high stability and high electron affinity make them attractive and in many ways complementary to the PPVs. However, compared to the PPVs, the PPEs are at a disadvantage for applications in OLEDs: Their poor hole injection capability witnesses the electron withdrawing nature of the alkyne groupings and PPEs lowered HOMO.[8,9] It would be of interest to have materials that combine the stability, electron affinity, and high emissive quantum yield of the PPEs with the excellent hole injection capabilities[1] of the PPVs.[10] Cross-

conjugated PPE-PPV hybrids **4.5**, in which styryl side chains decorate a PPE main chain, are presently unknown and combine PPE and PPV motifs.

## 4.2 Results and Discussion

We report novel, luminescent, cross-conjugated poly-(*p*-phenyleneethynylene) (PPE) derivatives (**4.5**) with unsaturated side chains.[1-4] The synthetic scheme (Scheme 4.1) allows the facile appendage of substituents to PPE monomers via a *trans*-configured alkene formed in a double Horner[5] reaction of **4.2** with aldehydes. We present a simple approach for the synthesis of the monomers **4.4a-f** and their novel cross-conjugated polymers **4.5a-f** (Scheme 4.1). 2,5-Bis(bromomethyl)-1,4-diiodobenzene (**4.1**)[11] combines quantitatively

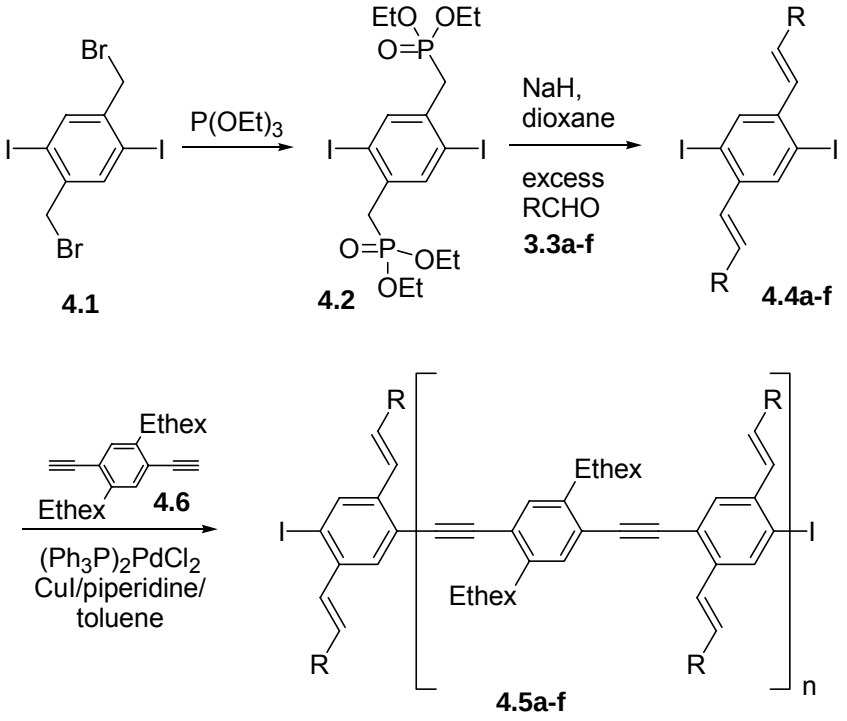


**Scheme 4.1** Synthetic route to monomers **4.4a-f** and PPE derivatives **4.5a-f**.

with triethyl phosphite to the bisphosphonate **4.2**. Reaction of **4.2** with the aldehydes **4.3a-f** in the presence of sodium hydride in THF furnishes the diiodides **4.4** (Table 4.1) in excellent yields (70-95%) as yellow, crystalline, air- and waterstable materials. In the monomers **4.4** the stilbenoid double bond is exclusively *trans*-configured according to $^{1}$H NMR spectroscopy, as expected for a Horner olefination.[5] The synthetic access to the monomers **4.4** seems to be general and depends only upon availability and reactivity of a suitable aldehyde **4.3**. While the monomers **4.4** are soluble in dichloromethane, chloroform, and toluene, their alkyne-bridged homopolymers would expected to be insoluble. Consequently, we coupled **4.4a-f** with 1,4-diethynyl-2,5-bis(ethylhexyl)-benzene utilizing $(Ph_3P)_2PdCl_2$/CuI as the catalyst system in a mixture of toluene/dichloromethane/piperidine. The cross-conjugated PPE derivatives **4.5a-f** were obtained in fair to good yields after aqueous workup and 3-fold precipitation into methanol. They appear as fluorescent, yellow or orange, moderately to well organosoluble powders/films after drying in high vacuum. $^{1}$H NMR and $^{13}$C NMR spectroscopy confirmed the proposed structures (See Section 4.4 Experimental below) of **4.5a-f** unequivocally. The degree of polymerization ($P_n$) of the PPEs **4.5** was determined by gel permeation chromatography (GPC, Table 4.1). As expected, the number of repeating units ($P_n$) in these polymers is moderate and ranges from $P_n$ = 38 to $P_n$ = 55. Exceptions are **4.5b** and **4.5f**. The GPC values of several different samples of **4.5b** and **4.5f** were spuriously high ($M_w$ ) 3 x $10^8$); dilute solutions of **4.5f** are strongly gelating. We assume that aggregate formation is the reason for the extremely high *apparent* molecular weight of these two polymers. According to powder diffraction, the polymers **4.5** are amorphous, probably due to the introduction of the styrene side chains that induce

**Table 4.1**. Yields, Substitution Pattern Properties for **4.3-5**, and Electrochemical Properties of Thin Films of Polymers **4.5a-f**.

| 4.3-4.5 | a | b | c | d | e | f | PPE |
|---|---|---|---|---|---|---|---|
| Substituent |  |  | 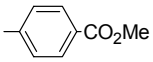 | 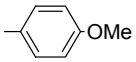 | 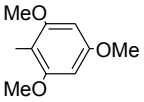 | 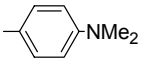 | - |
| Yield **4.4** | 97% | 70% | 95% | 95% | 93% | 91% | - |
| Yield **4.5** | 80% | 25% | 81% | 38% | 55% | 56% | - |
| $P_n$ of **4.5** | 55 | - | 38 | 50 | 52 | - | - |
| $M_w/M_n$ of **4.5** | 2.8 | - | 3.2 | 2.0 | 3.2 | - | - |
| Tg ($^oC$) | - | 119 | 123 | 183 | - | 79 | - |
| $\lambda_{max,sol}$ **4.5**(nm) | 354<br>417, sh | 350<br>410, sh | 366<br>414, sh | 389<br>414, sh | 374 | 386<br>432, sh | 385 |
| $\lambda_{max,film}$ **4.5** (nm) | 450 | 420 | 448 | 442 | 380 | 390 | 439 |
| Emission $\lambda_{max,sol}$ **4.5** (nm) | 442 | 450 | 451 | 436 | 496 | 530 | 425 |
| Emission $\lambda_{max,film}$ **4.5** (nm) | 527 | 476 | 504 | 522 | 511 | 550 | 450<br>480 |
| $\Phi$ (PL) solution | 0.58 | 0.02 | 0.24 | 0.21 | 0.08 | 0.09 | 0.99 |
| Peak $E^{ox}$ (V vs. $Fc/Fc^+$) | 1.25 | 1.55 | 1.40 | 1.87 | 0.83 | 0.72 | 1.3 |
| $E^{ox}$ (V) onset | 0.9 | 0.8 | 0.6 | 1.1 | 0.15 | 0.25 | 1.1 |
| Peak $E^{red}$ (V) | -1.68 | -1.61 | -1.75, -2.26 | -2.3 | - | -1.7 | -2.5 |
| $E^{red}$ (V) onset | -1.55 | -1.3 | -1.5 | -1.3 | -1.3 | -1.3 | -2.3 |
| Maximum electrochemical bandgap (eV) | 2.93 | 3.16 | 3.15 | 4.21 | >3.3 | 2.43 | 3.80 |
| Minimum electrochemical bandgap (eV) | 2.45 | 2.10 | 2.10 | 2.60 | 1.50 | 1.50 | 3.40 |
| Midpoint electrochemical bandgap (eV) | 2.69 | 2.63 | 2.63 | 3.40 | 2.40 | 2.00 | 3.60 |
| Thin film optical bandgap from Abs/Em intercept (eV) | 2.64 | 2.78 | 2.67 | 2.72 | 2.64 | 2.49 | 2.82 |

a step in the polymer and inhibit efficient solid-state packing/ordering. While some of the polymers form gels in organic solvents, spincast films of **4.5a-f** of good quality are obtained from toluene or chloroform. Differential scanning calorimetry measurements did show the presence of a glass transition or other thermal processes in some of the polymers (Table 4.1).

To elucidate the effect of the substituents on the electronic properties of **4.5,** we recorded their UV-vis and emission spectra in solution and in the solid state (Table 4.1, Figure 4.1). In solution, the cross-conjugated PPEs show absorption between 355 and 390 nm with an additional shoulder at 410-430 nm. Their solid-state absorption is broad and featureless with a $\lambda_{max}$ that ranges from 360 to 455 nm. There are only moderate differences between solution and solid-state spectra.[12] The emission spectra of **4.5a-f** display relatively broad and red-shifted features with respect to that of the PPEs and show a Stokes shift that is considerably larger than those of the PPEs. Their strong solid-state emission ($\lambda_{max}$ = 521, 551 nm) is red-shifted compared to that of the PPEs ($\lambda_{max}$ = 480 nm). Figure 4.1 shows the absorption and emission spectra of **4.5e** and **4.5f**. Both polymers display broad and featureless absorption in solution and in the solid state. Planarization of the chains in the solid state, so significant in the dialkyl-PPEs,[9] is not very distinct in the polymers **3.5** because of their bulky side chains. The loss of conformational order probably leads to the broader absorption and emission spectra.

PPE is relatively difficult to oxidize[8b] (1.3 V) and to reduce (-2.5 V). It was of interest to evaluate how the substituted styryl side chains would modulate the electrochemical behavior of **4.5**. Thin film samples of the styryl-substituted derivatives

**4.5** are irreversibly oxidized at peak potentials (with exception of **4.5d**) that range from 0.4 to 1.5 V (Table 4.1). As expected, the two derivatives **4.5e** and **4.5f** are particularly easily oxidized due to their strongly electron-donating side chains. Interestingly enough,

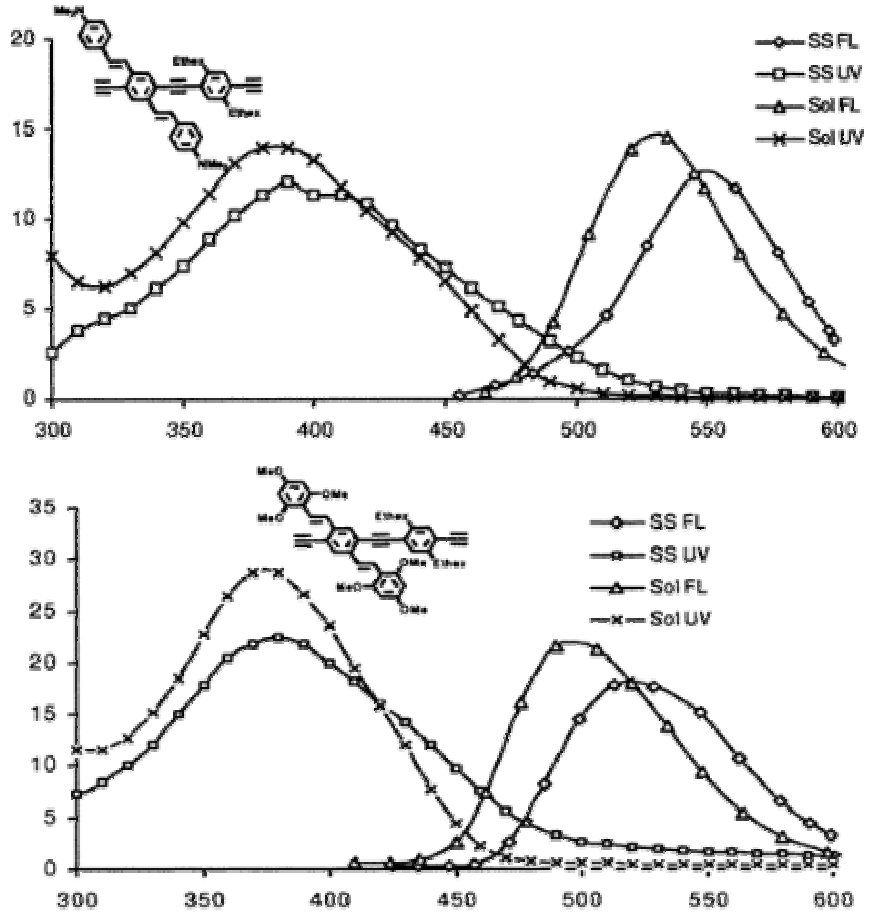


**Figure 4.1** UV-vis and emission spectra of **4.5f** (top) and **4.5e** (bottom).

the reduction potential of the derivatives of **4.5** is in the range of -1.6 to -1.7 V; an exception is **4.5e**, which does not show a reduction peak to -2.5 V. However, **4.5e** does show a reduction *onset* above -1.3 V. From these data (see Figure 4.2) one can obtain two series of band gaps that correspond either to the *onset* of oxidation and reduction (small values) or to the peak-to-peak distances (larger values). Janietz *et al*.[13] suggest that the difference in the onset of reduction and oxidation is a good measure for the band gap given an ideal sample (monodisperse, defect free). Our materials are polydisperse and

amorphous and have multiple degrees of rotational freedom with respect to both the main and side chains. A significant distribution of electrochemical/electronic and optical properties results in broad bands in absorption and emission. We estimate the optical

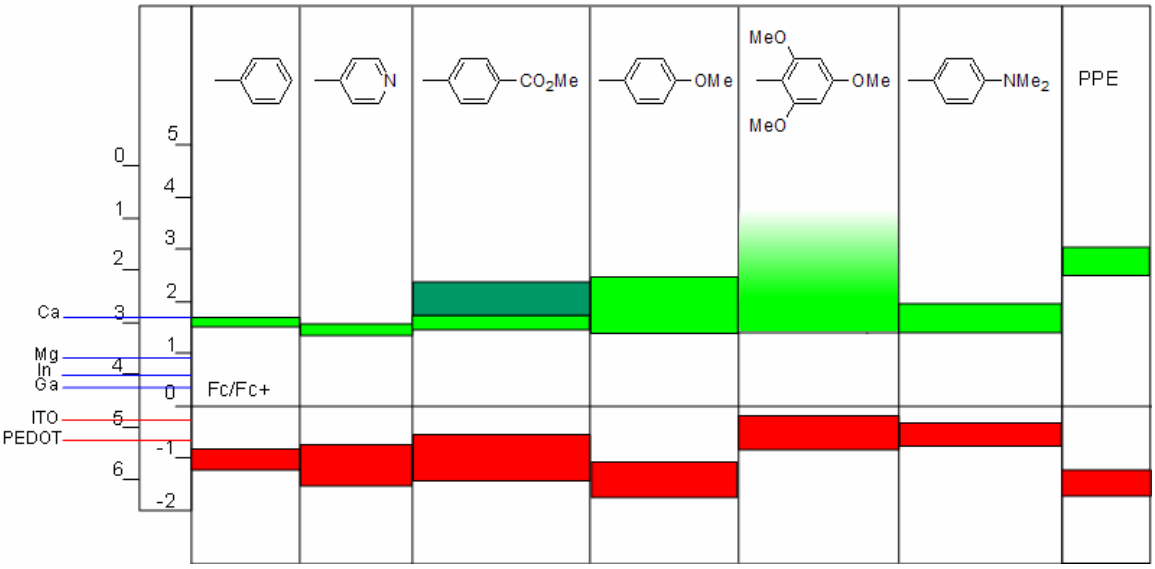


**Figure 4.2.** Schematic for relative band gaps of **4.5** and PPE obtained by cyclic voltammetry. Reduction potentials are shown in green, and oxidation potentials are shown in red. The dark green block indicates a second reduction wave. The lower absolute values indicate the onset of oxidation or reduction, while the higher absolute values indicate the peak potentials. In the case of **4.5e** there is an onset of the reduction, but no peak potential is reached. The oxidation and reduction values of dialkyl-PPEs are likewise shown. As comparison, the work functions of several common electrode materials (cathodes, anodes, and ferrocene) are shown.

band gaps of **4.5** as the point where normalized emission and absorption intersect. These values are shown in Table 4.1 and fall between the two extremal values for the electrochemical band gap. Both the oxidation and the reduction potentials are affected by the attachment of the styryl side chain to the PPE main chain (Figure 4.2). The effect of the styryl side chains is twofold: they act as slightly electronwithdrawing substituents for the PPE main chain and thus decrease the reduction potential of all of the new polymers as compared to dialkyl-PPEs. This is almost independent of the nature of the arene on the side unit. On the other hand, the nature of the distyrylbenzene core largely determines the

oxidation potential of the polymers **4.5**, suggesting that its HOMO has a significant electron density on the styryl sidearms. Whether the two crossed systems are electronically coupled or only topologically cross-conjugated is difficult to say, but attachement of styryl side chains significantly modulates the electronic properties of these PPE derivatives.

## 4.3 Conclusion

In conclusion, we have modified Bazan's oligomer concept to allow the synthesis of the hitherto unknown cross-conjugated PPV-PPE copolymers **3.5**. Because myriads of ketones and aldehydes are commercially available or easily made, their reaction with **4.2** bodes for the generation of libraries of distyrylbenzenes **4.4**. These monomers can be used in the synthesis of diversets[13] of cross-conjugated PPE-PPV derivatives with fine-tuned optical/electronic properties. We are continuing our studies of these materials to discern to what extent cross-conjugation exists as an electronic coupling of the PPV arms to the PPE backbone beyond the topological aspect.

## 4.4 Experimental

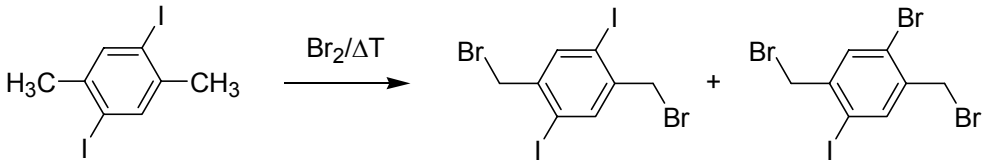


2,5-Diiodo-1,4 bis(bromomethyl) benzene, **4.1**. Diiodoxylene (20.0 g, 0.056 mol), NBS (44.0 g, 0.248 mol) and benzoylperoxide (1.00 g, 4.13 mmol) in 500 mL of chloroform were irradiated with UV light under stirring. After 8 h of irradiation while refluxing, the

solution was allowed to cool to room temperature. A saturated aqueous solution of sodium sulfite was added to the reaction mixture and stirred until the solution turned clear. The chloroform solution was dried with magnesium sulfate and reduced by rotary evaporator until a precipitate began to form. The mixture was then heated until the precipitate dissolved. The solution was allowed to cool slowly in the dark. Yield 7.19 g (25%) of 4.1a. Approximately 10 % of the material is 4.1b. The mixture is inseparable and used for further reactions. mp = 211 °C. $^{1}$H-NMR (CDCl3, 400 MHz): δ = 7.87 (s, 2H), 4.46 (s, 4H).

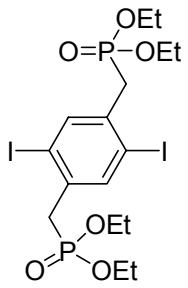


**4.2**

2,5-Diiodo-1,4 bis(triethyphosphonatemethylene)benzene **4.2**: A mixture of **4.1a,b** (10.0 g, 0.0195 mol) and triethylphosphite (30 mL, 0.175 mol) was placed in a round bottom flask and heated to reflux for 12 h. Colorless crystals formed while cooling the mixture to room temperature. The excess triethylphosphite was decanted. The remaining white solid was washed 3 times with hexanes, then stirred while heating in hexanes to extract the remaining traces of triethylphosphite. The solid was filtered off after cooling to room temperature. The resulting solid was dried under vacuum in a warm water bath (12.04 g, 98 %). mp. 162°C $^{1}$H-NMR ($CDCl_3$, 300 MHz): δ = 7.85 (d, 2H, $J_{3\ H,H}$ = 1.922 Hz, Ar-H), 4.03 ( m, 8H, P-$CH_2$), 3.29 (d, 4H, $J_{1\ H,H}$ = 20.6 Hz, Bz-H), 1.26 (t, 12H, $J_{3\ H,H}$ = 7.32

Hz). $^{13}$C-NMR ($CDCl_3$, 100 MHz): δ = 140.65, 136.13, 136.06, 100.68, 100.62, 62.33, 62.28, 62.24, 38.13, 36.30, 16.33, 16.29, 16.25.

General procedure for compounds **4.4a-f**: An oven-dried Schlenk flask cooled under nitrogen was charged with **4.2**, NaH (2.5 eq), and dry THF (25 mL). The flask was closed with a septum, a nitrogen-filled balloon was fitted to the arm and the stopcock was opened. With mild heating (40 °C), the solution turned a vivid purple-red. The aldehyde (**4.3a-f**) was introduced in small portions over an hour's time with a syringe either as the pure oil or dissolved in dry THF. The reaction was allowed to stir with heat for another 30 minutes before work-up. The small excess NaH was quenched with water and the mixture was extracted three times with chloroform. The chloroform layer was rinsed with brine and dried with magnesium sulfate and reduced until a precipitate formed. The mixture crystallized from hexanes and collected by suction filtration and dried under vacuum.

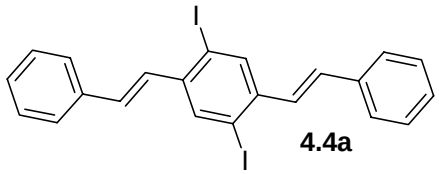


**4.4a**

**Compound 4.4a**: Following the general procedure, **4.2**(0.630 g, 1.00 mmol), NaH (0.060 g, 2.50 mmol), and 25 mL THF were combined. Benzaldehyde, (233 mg, 2.20 mmol) was then added. Work up and recrystallization yielded (378 mg, 71%)of pale yellow crystals. MP: 228°C. IR: 2915.2, 2840.2, 1458.8, 1437,3, 1348.1, 1069.7, 1041.1, 951.9, 887,6, 855.5, 809.1, 748.4, 691.3, 587.8. $^1$H NMR (CDCl3): δ 8.09 (s, 2H, Ar-H), 7.55 (d, 4H, Ar-H, $J_{3\ H,H}$ = 7.52 Hz), 7.38 (t, 4H, Ar-H, $J_{3\ H,H}$ = 7.33 Hz), 7.30 (t, 2H, Ar-H, $J_{3\ H,H}$ = 7.15 Hz), 7.20 (d, 2H, C=C-H, $J_{3\ H,H}$ = 15.95 Hz), 6.99 (d, 2H, C=C-H, $J_{3\ H,H}$ =

16.13 Hz). $^{13}$NMR (CDCl3): δ 140.79, 136.54, 136.34, 135.36, 130.48, 128.82, 128.40, 126.96, 100.28.

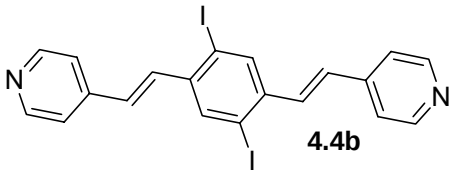


**4.4b**

**Compound 4.4b**: Following the general procedure, **4.2** (0.630 g 1.00 mmol), NaH (0.060 g, 2.50 mmol), and 25 mL THF were combined. 4-pyridine carboxaldehyde, (0.236 g 2.20 mmol) was then added. Work up and recrystallization yielded of pale yellow crystals (0.413 g, 77.0%). MP: 273 °C. IR: 3047.4, 3030.7, 3026.6, 1560.1, 1555.6, 1051.9, 956.1, 856.1, 801.9, 731.1, 672.8. $^{1}$H NMR (300 MHz, $CDCl_3$): δ = 8.62 (d, 4H, $J_{3\ H,H}$ = 3.84 Hz, Ar-H), 8.09 (s, 2H, Ar-H), 7.40 (m, 6H, Ar-H, C=C-H), 6.93 (d, 2H, $J_{3\ H,H}$ = 16.2 Hz, C=C-H). $^{13}$C-NMR (400 MHz, $CDCl_3$): δ = 150.40, 143.56, 140.62, 136.91, 130.13, 128.32, 121.13, 100.42.

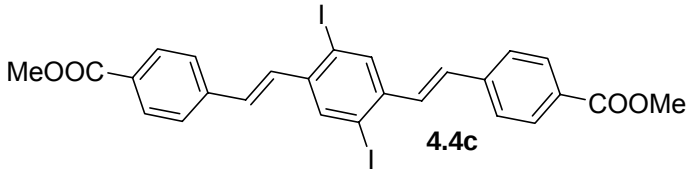


**4.4c**

**Compound 4.4c**: Following the general procedure, **4.2** (0.630 g 1.00 mmol), NaH (0.060 g, 2.50 mmol), and 25 mL THF were combined. 4-Formylmethylbenzoate, (361 mg, 2.20 mmol) was then added. Work up and recrystallization yielded yellow crystals (452 mg, 69.5%). MP: 254 $^{o}$C. IR: 2961.7, 2920.8, 2850.0, 1718.3, 1558.2, 1290.1, 1178.4, 1107.7, 955.0, 762.2. 2 $^{1}$H NMR (300 MHz, $CDCl_3$): δ = 8.08 (s, 2H, Ar-H), 8.05 (d, 4H, $J_{3\ H,H}$ = 8.23, Ar-H), 7.30 (d, 2H, $J_{3\ H,H}$ = 16.2, C=C-H), 7.02 (d, 2H, $J_{3\ H,H}$ = 15.92, C=C-H), 3.92 (s, 6H, $COOCH_3$). $^{13}$C-NMR (400 MHz, $CDCl_3$): δ = 166.97, 141.06, 136.88, 132.98, 131.70, 129.94, 127.05, 100.66, 52.42.

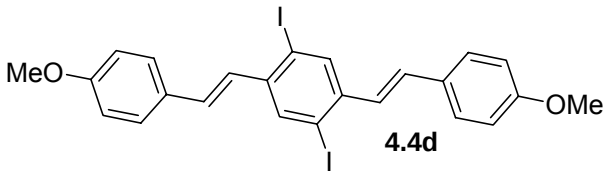


**4.4d**

**Compound 4.4d**: Following the general procedure, **4.2** (0.630 g 1.00 mmol), NaH (0.060 g, 2.50 mmol), and 25 mL THF were combined. 4-Methoxybenzaldehyde, (300 mg, 2.20 mmol) was then added. Work up and recrystallization yielded of yellow crystals (362 mg, 60.9%). MP: 213 $^{o}$C. IR: 2920.6, 2899.3, 1506.7, 1503.1, 1244.3, 1175.0, 1029.3, 956.5, 845.6, 814.4. $^{1}$H NMR (300 MHz, $CDCl_3$): δ = 8.03 (s, 2H, Ar-H), 7.49 (m, H, Ar-H), 7.17 (d, 2H, $J_{3\ H,H}$ = 23.1 Hz, CH=CH), 7.06 (d, 2H, $J_{3\ H,H}$ = 23.1 Hz, CH=CH), 6.97 (m, 6H, Ar-H, C=C-H), 3.83 (s, 6H, $CO_2CH_3$). $^{13}$C-NMR (400 MHz, $CDCl_3$): δ = 160.11, 140.91, 136.24, 131.94, 129.67, 128.62, 128.50, 114.49, 100.43, 55.60.

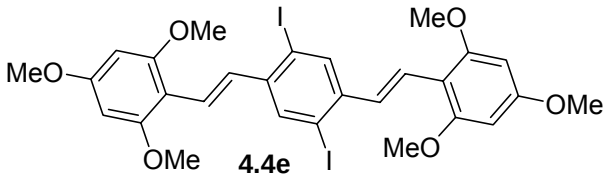


**4.4e**

**Compound 4.4e**: Following the general procedure, **4.2** (0.630 g 1.00 mmol), NaH (0.060 g, 2.50 mmol), and 25 mL THF were combined. 2,4,6-Trimethoxy-benzaldehyde, (432 mg 2.20 mmol) was then added. Work up and crystallization yielded of deep yellow crystals (522 mg 73%). MP: 259 °C. IR: 2918.1, 2846.3, 1609.3, 1571.5, 1450.5, 1412.6, 1321.9, 1208.4, 1155.4, 1117.6, 1060.9, 1026.8, 973.9, 951.2, 803.6. $^{1}$H NMR (300 MHz, $CDCl_3$): δ = 8.06 (s, 2H, Ar-H), 7.63 (d, 2H, $J_{3\ H,H}$ = 16.47 Hz, C=C-H), 7.26 (d, 2H, $J_{3\ H,H}$ = 16.2 Hz, C=C-H), 6.15 (s, 4H, Ar-H), 3.90 (s, 12H, O-$CH_3$), 3.83 (s, 6H, O-$CH_3$). $^{13}$C NMR (400 MHz, $CDCl_3$): δ = 160.72, 159.81, 159.78, 141.92, 135.92, 131.97, 128.90, 122.44, 107.79, 100.80, 90.69, 90.21, 62.39, 55.88, 55.34.

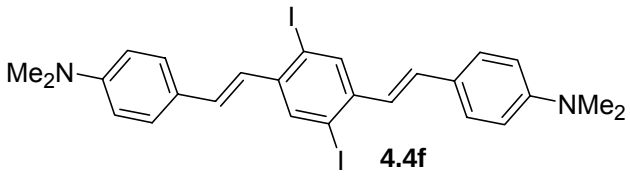


**4.4f**

**Compound 4.4f**: Following the general procedure, **4.2** (0.630 g, 1.00 mmol), NaH (0.060 g, 2.50 mmol), and 25 mL THF were combined. 4-Dimethylamino benzaldehyde, (328 mg, 2.20 mmol) was then added. Work up and crystallization yielded bright orange crystals. (476 mg, 77%). MP: 278 $^{o}$C. IR: 2922.6, 2846.3, 2794.2, 1597.5, 1519.6, 1504.0, 1367.8, 1301.6, 1219.8, 1192.6, 1044.6, 947.3, 807.9, 731.7. $^{1}$H NMR (300 MHz, $CDCl_3$): $\delta$ = 8.02 (s, 2H, Ar-H), 7.4 (d, 4H, $J_{3\ H,H}$ = 8.78 Hz, Ar-H), 6.99 (d, 2H, $J_{3\ H,H}$ = 15.9 Hz, C=C-H), 6.90 (d, 2H, $J_{3\ H,H}$ = 15.9 Hz, C=C-H), 6.72 (d, 4H, $J_{3\ H,H}$ = 8.78 Hz, Ar-H), 2.99 (s, 12H). $^{13}$C-NMR (400 MHz, $CDCl_3$): $\delta$ = 150.44, 140.48, 1355.56, 128.06, 126.08, 124.97, 112.25, 100.11, 40.34.

General Procedure for Polymerization of **4.5a-f**: A tubular Schlenk flask (25 mL) was charged under nitrogen stream with of diiodide (**4.4a-f**, 200 mg), **4.6** (1.02 eq), piperidine (1 mL), toluene(1 mL), $PdCl_2(PPh_3)_2$ (10 mg) and CuI (10 mg). The flask was capped with a septum and placed in a warm water bath (50) for 24 hours (usually solidified within 12 h). The reaction solid was dissolved in hot chloroform and rinsed 3 times with 10% w/w ammonium hydroxide and 3 times with 10% w/w hydrochloric acid. The chloroform mixture was reduced to a few mL and poured into methanol to precipitate the polymer. The polymer was collected over a fritted funnel resulting in a rubbery thin film which was dried under vacuum.

Compound **4.5a**: Following the general procedure, **4.4a** (0.200 g, 0.374 mmol) and dialkyne, **4.6** (0.134 g, 0.381 mmol) were reacted. The reaction produced yellow polymer. (0.228 g, 95 %). IR: 2956.4, 2925.3, 2855.8, 1498.3, 1259.2, 959.5, 895.0,

746.2. $^{1}$H NMR (300 MHz, $CDCl_3$): δ =7.94 (s), 7.74 (bd, $J_{3\ H,H}$ = 15.9 Hz), 7.57 (bm), 7.47 (bs), 7.38 (bm), 7.29 (bm), 2.83 (bs), 1.82 (bs), 1.33 (bm), 0.89 (bt, $J_{3\ H,H}$ = 6.86 Hz), 0.78 (bt, $J_{3\ H,H}$ = 6.6 Hz). $^{13}$C NMR (D-TCE, 80 $^{o}$C): δ = 141.42, 137.37, 137.16, 133.68, 130.86, 128.78, 128.12, 126.85, 125.64, 123.08, 122.56, 95.06, 92.48, 40.56, 38.68, 32.53, 28.83, 25.59, 23.09, 14.08, 10.89.

Compound **4.5b**: Following the general procedure, **4.4b** (0.200 g, 0.373 mmol) and dialkyne, **4.6** (0.133 g, 0.380 mmol) were reacted. The reaction produced yellow-orange polymer (164 mg, 70 %). IR: 2956.6, 2926.8, 2856.5, 1605.0, 1511.5, 1462.5, 1251.3, 11.73.6, 1037.2, 957.7, 816.2. $^{1}$H -NMR (D-TCE, 400 MHz): δ = 8.52 (bs), 7.91 (bs), 7.82, (bm), 7.39 (bs), 7.17 (bd $J_{3\ H,H}$ = 16.2 Hz, ), 2.76 (bs), 1.73 (bs), 1.21, (bs), 0.81 (bs), 0.70 (bs). $^{13}$C NMR (D-TCE, 80 $^{o}$C): δ = 150.19, 144.08, 141.52, 137.06, 133.60, 130.64, 129.89, 129.56, 128.75, 123.03, 120.89, 95.81, 91.89, 40.42, 38.60, 32.53, 28.73, 25.66, 22.89, 13.88, 10.82.

Compound **4.5c**: Following the general procedure, **4.4c** (0.200 g, 0.308 mmol) and dialkyne, **4.6** (0.110 g, 0.314 mmol) were reacted. The reaction produced yellow polymer (0.218 g 95 %). IR: 2955.3, 2924.2, 2854.8, 1722.5, 1605.3, 1497.3, 1434.8, 1277.3, 1178.2, 1107.8, 1016.2, 1107.8, 1016.2, 954.0, 764.1. $^{1}$H -NMR ($CDCl_3$, 400 MHz): δ = 8.04 (bm), 7.82 (bd, $J_{3\ H,H}$ = 15.9 Hz), 7.59 (bm), 7.46 (bs), 7.33 (bm), 3.92 (bs), 2.83 (bs), 1.57 (bs), 1.23 (bm), 0.88 (bm), 0.76 (bm). $^{13}$C NMR (D-TCE, 80 $^{o}$C): δ = 166.71, 141.47, 137.29, 133.72, 130.14, 129.91, 129.45, 129.20, 128.07, 127.65, 126.67, 122.94, 95.48, 92.21, 52.14, 40.61, 38.69, 32.55, 29.69, 28.86, 25.58, 23.09, 14.04, 10.86.

Compound **4.5d**: Following the general procedure, **4.4d** (0.200 g, 0.337 mmol) and dialkyne, **4.6** (0.120 g, 0.344 mmol) were reacted. The reaction produced bright yellow

polymer (0.221 g, 95 %). IR: 2957.1, 2927.4, 2856.9, 1605.3, 1511.7, 1484.2, 1463.0, 1378.7, 1251.6, 1173.7, 1037.3, 957.6, 896.9, 848.9, 816.0, 755.9. $^{1}$H -NMR (D-TCE, 400 MHz): δ 7.96 (s), 7.43 (d, $J_{3\ H,H}$ = 8.9 Hz), 7.23 (s), 6.92 (s), 6.86 (d, $J_{3\ H,H}$ = 8.8 Hz), 3.75 (bs), 2.58 (bs), 1.55 (bs), 1.21 (bs), 0.79 (bm). $^{13}$C NMR (D-TCE, 80 $^{o}$C): δ = 159.86, 142.81, 140.73, 135.98, 134.18, 131.71, 129.37, 128.41, 128.18, 122.26, 114.36, 100.03, 82.29, 79.13, 55.35, 40.36, 38.31, 32.55, 28.75, 25.76, 22.83, 13.90, 10.76.

Compound **4.5e**: Following the general procedure, **4.4e** (0.200 g, 0.280 mmol) and dialkyne, **4.6** (0.100 g, 0.286 mmol) were reacted. The reaction produced bright yellow polymer (0.210 g 93 %). IR: 3004.4, 2957.6, 2929.8, 2857.06, 1603.0, 1580.4, 1497.0, 1456.2, 1416.9, 1379.0, 1327.3, 1204.7, 1157.2, 1122.1, 1062.3, 1040.1, 977.1, 954.6, 900.0, 812.4, 758.8. $^{1}$H -NMR (D-TCE, 400 MHz): δ = 8.03 (bd, $J_{3\ H,H}$ = 16.2 Hz), 7.85 (bs), 7.50, (bd, $J_{3\ H,H}$ = 18.1 Hz), 7.38 (bm), 6.10 (bs), 3.76, (bs), 2.70 (bs), 2.06, (bs), 1.73 (bs), 1.20, (bs), 0.80 (bs), 0.68 (bs). $^{13}$C NMR (D-TCE, 80 $^{o}$C): δ = 160.39, 159.62, 141.26, 138.80, 134.27, 127.68, 122.98, 121.83, 121.28, 107.92, 94.12, 90.64, 40.28, 38.55, 32.33, 28.69, 25.57, 22.93, 14.12, 13.96, 10.77.

Compound **4.5f**: Following the general procedure, **4.4f** (0.200 g, 0.322 mmol) and dialkyne, **4.6** (0.115 g, 0.328 mmol) were reacted. The reaction produced bright orange polymer. (0.209 g, 91 %). IR: 2956.4, 2923.0, 2852.5, 1604.1, 1522.6, 1444.4, 1356.7, 1186.3, 1157.8, 958.4, 895.0, 847.7, 807.3. $^{1}$H-NMR ($CDCl_3$, 400 MHz): δ 7.80 (bs), 7.39 (bs), 7.14 (bs), 6.63 (bs), 2.90 (bs), 1.18 (bs), 0.76 (bs). $^{13}$C NMR (D-TCE, 80 $^{o}$C): δ = 150.53, 141.16, 137.43, 133.46, 130.80, 127.90, 125.93, 124.70, 123.63, 121.74, 116.02, 112.55, 94.86, 93.16, 40.49, 40.07, 38.79, 32.81, 28.88, 26.04, 22.85, 13.73, 10.88.

## 4.5 References and Notes


1. (a) Cross-conjugated systems: Nielsen, M. B.; Schreiber, M.; Baek, Y. G.; Seiler, P.; Lecomte, S.; Boudon, C.; Tykwinski, R. R.; Gisselbrecht, J. P.; Gramlich, V.; Skinner, P. J.; Bosshard, C.; Gu¨ nther, P.; Gross, M.; Diederich, F. *Chem.Eur. J.* **2001**, *7*, 3263. (b) Hopf, H.; Maas, G. *Angew. Chem., Int. Ed. Engl.* **1992**, *31*, 931.

2. For linear PPE-PPV hybrids, see: (a) Brizius, G.; Pschirer, N. G.; Steffen, W.; Stitzer, K.; zur Loye, H. C.; Bunz, U. H. F. *J. Am. Chem. Soc.* **2000**, *122*, 12435. (b) Egbe, D. A. M.; Tillmann, H.; Birckner, E.; Klemm, E. *Macromol. Chem. Phys.* **2001**, *202*, 2712. (c) Pautzsch, T.; Klemm, E. *Macromolecules***2002**, *35*, 1569. (d) Egbe, D. A. M.; Roll, C. P.; Birckner, E.; Grummt, U. W.; Stockmann, R.; Klemm, E. *Macromolecules* **2002**, *35*, 3825.

3. For the synthesis of oligo-PVs by a Wittig approach, see: (a) Oldham, W. J.; Lachicotte, R. J.; Bazan, G. C. *J. Am. Chem. Soc.* **1998**, *120*, 2987. Wang, S. J.; Oldham, W. J.; Hudack, R. A.; Bazan, G. C. *J. Am. Chem. Soc.* **2000**, *122*, 5695. (b) Meier, H.; Lehmann, M. *Angew. Chem.* **1998**, *37*, 643. (c) Schenk, R.; Gregorius, H.; Meerholz, K.; Heinze, J.; Mu¨ llen, K. *J. Am. Chem. Soc.* **1991**, *113*, 2634. (d) Deb, S. K.; Maddux, T. M.; Yu, L. P. *J. Am. Chem. Soc.* **1997**, *119*, 9079.

4. Bunz, U. H. F. *Chem. Rev.* **2000**, *100*, 1605. Bunz, U. H. F. *Acc. Chem. Res.* **2001**, *34*, 998.

5. Horner, L.; Hoffmann, H.; Wippel, H. G. *Chem. Ber.* **1958**, *91*, 61. Horner, L.; Klink, W. *Tetrahedron Lett.* **1964**, *36*, 2467. Wadsworth, W. S. *Org. React.* **1977**, *25*, 73.

6. Yang, J. S.; Swager, T. M. *J. Am. Chem. Soc.* **1998**, *120*, 11864.

7. Weder, C.; Sarwa, C.; Montali, A.; Bastiaansen, G.; Smith, P. *Science* **1998**, *279*, 835. Montali, A.; Bastiaansen, G.; Smith, P.; Weder, C. *Nature (London)* **1998**, *392*, 261.

8. (a) Pschirer, N. G.; Miteva, T.; Evans, U.; Roberts, R. S.; Marshall, A. R.; Neher, D.; Myrick, M. L.; Bunz, U. H. F. *Chem. Mater.* **2001**, *13*, 2601. (b) Evans, U.; Soyemi, O.; Doescher, M. S.; Bunz, U. H. F.; Kloppenburg, L.; Myrick, M. L. *Analyst* **2001**, *126*, 508.

9. Montali, A.; Smith, P.; Weder, C. *Synth. Met.* **1998**, *97*, 123. Schmitz, C.; Posch, P.; Thelakkat, M.; Schmidt, H. W.; Montali, A.; Feldman, K.; Smith, P.; Weder, C. *Adv. Funct Mater.* **2001**, *11*, 41.

10. (a) Scherf, U.; List, E. J. W. *Adv. Mater.* **2002**, *14*, 477. (b) Kraft, A.; Grimsdale, A. C.; Holmes, A. B. *Angew. Chem.* **1998**, *37*, 402. (c) Mitschke, U.; Ba¨ uerle, P. *J. Mater. Chem.* **2000**, *10*, 1471.

11. Wheland, R. C.; Martin, E. L. *J. Org. Chem.* **1975**, *40*, 3101. The radical bromination of 1,4-diiodo-2,5-dimethylbenzene gives an inseparable 9:1 mixture of **3.1** and 1-iodo-4-bromo-2,5-bis(bromomethyl)benzene. The monomer synthesis is carried on with this mixture. In the final step, the formation of polymers **3.5**, both the iodine and the bromine substituents are reactive under the coupling conditions utilized.

12. Halkyard, C. E.; Rampey, M. E.; Kloppenburg, L.; Studer-Martinez, S. L.; Bunz, U. H. F. *Macromolecules* **1998**, *31*, 8655.

13. Jainetz, S.; Bradley, D. D. C.; Grell, M.; Giebler, C.; Inbasekaran, M.; Woo, E. P. *Appl. Phys. Lett.* **1998**, *73*, 2453.

14. The term diverset was suggested by R. Hoffmann (Hoffmann, R. *Angew. Chem.* **2001**, *40*, 3337).

# Chapter 5

# Synthesis and Mesoscopic Order of a Sugar-Coated Poly(*p*-phenyleneethynylene)

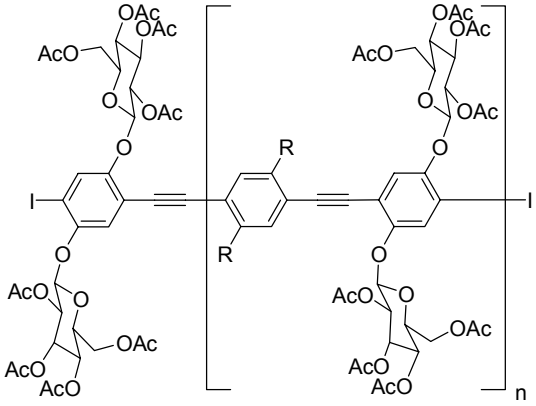


## 5.1 Introduction

We describe the facile Pd-catalyzed synthesis, supramolecular ordering, and spectroscopic behavior of glycosylated poly(*para*-phenyleneethynylene)s (PPE). Sugarsscarbohydratessare ubiquitous in bioscience. Their cellular receptors, lectins, define blood groups and modulate cell agglutination, inflammatory responses, and pathogen/host interactions.[1a] At the same time sugars are hydrophilic modules that can make polymers biocompatible and potentially useful for highly specific biosensory and biodevice applications in the detection of pathogens.[1b]

In a structural sense, sugars are attractive as building blocks in polymer science. Attachment of sugars to macromolecules will guide supramolecular nanoscale organization of polymers and organic materials, even though this aspect has attracted less interest than biosensing and disease-related applications. While Grubbs, Schrock, Whitesides, Kiessling, Roy, and others[2-6] have made significant contributions to the field of nonconjugated neoglycopolymers, much less is known about sugar-decorated conjugated polymers. Notable exceptions are sugar-coated polydiacetylenes[7] and sugar-coated polythiophenes[8] which have been investigated by Charych.

PPEs are fascinating conjugated polymers that show high fluorescence in solution and in the solid state.[9] They have successfully been used in light-emitting and sensory devices, and while several ionic, water-soluble PPEs have been reported by now, PPEs with biologically active substituents are not known.[10-13] We present herein the first example of a sugar-coated PPE.

## 5.2 Results and Discussion

Reaction of 2,5-diiodohydroquinone with penta-*o*-acetyl-,-D-glucose in the presence of $BF_3$-etherate according to the literature[14] furnished the sugar substituted monomer **5.1** in 39% yield (see Scheme 5.1). Reaction of **5.1** with 1,4-diethynyl-2,5-bisethylhexylbenzene under standard Pd-catalyzed coupling conditions furnished a yellow, highly blue-green emissive solid in almost quantitative yields. The polymer was

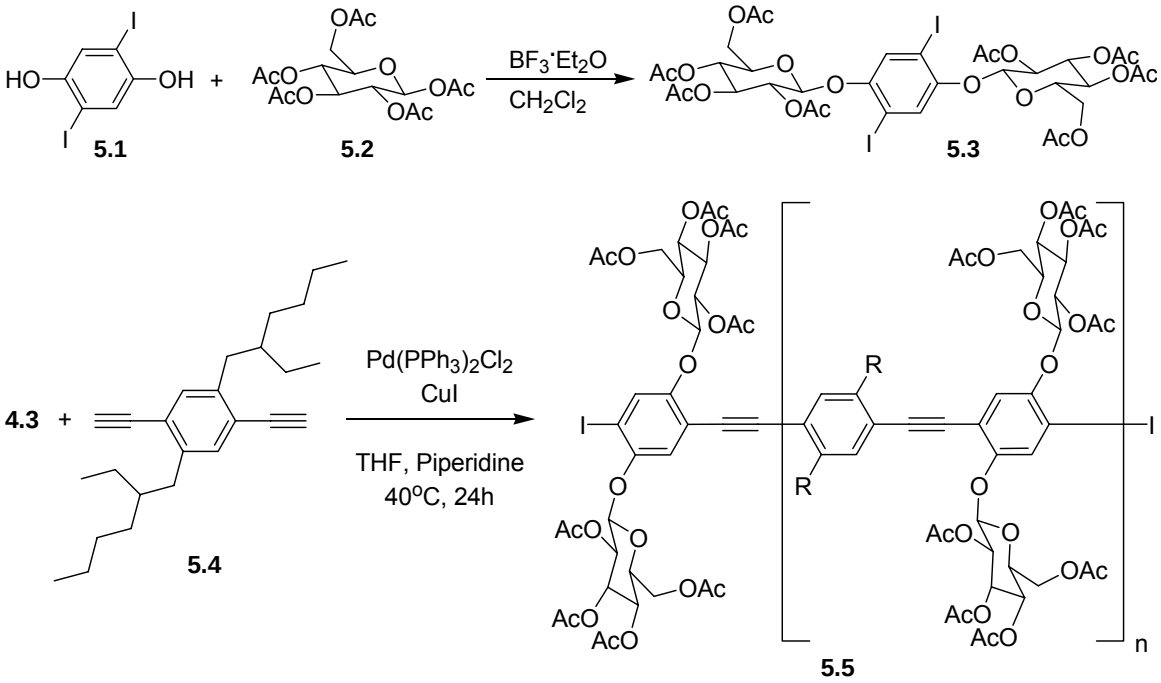


**Scheme 5.1** Synthesis of glucose substituted PPE **5.5**

soluble in THF, hot DMSO, and hot DMF but surprisingly insoluble in chloroform and in aromatic solvents. IR and NMR spectroscopy revealed that under the reaction conditions the deacetylated polymer **5.2** had formed. The characteristic band for the ester C=O stretch in the IR and the characteristic band for the methyl protons of the acetyl groups in the $^1$H NMR spectrum of the polymer were not present. Under the reaction conditions of the synthesis of the sugar-coated polymer the acetyl groups are hydrolyzed off cleanly to furnish **5.2** directly. Gel permeation chromatography in THF shows that the polymer has a degree of polymerization ($P_n$) of 75 with an $M_w/M_n$ ) 2.2.[15]

To obtain more information about the electronic and structural properties of **5.2**, absorption and emission spectroscopy was performed (Figure 5.1) in a series of different solvents and in thin solid films. As expected, the primary absorption of **5.2** is significantly dependent upon solvent and aggregation state. In hexane the absorption is

most blue-shifted in comparison to the absorption spectrum of **5.2** in THF. The difference of the spectra of **5.2** in THF solution and in thin solid films is relative small. It suggests

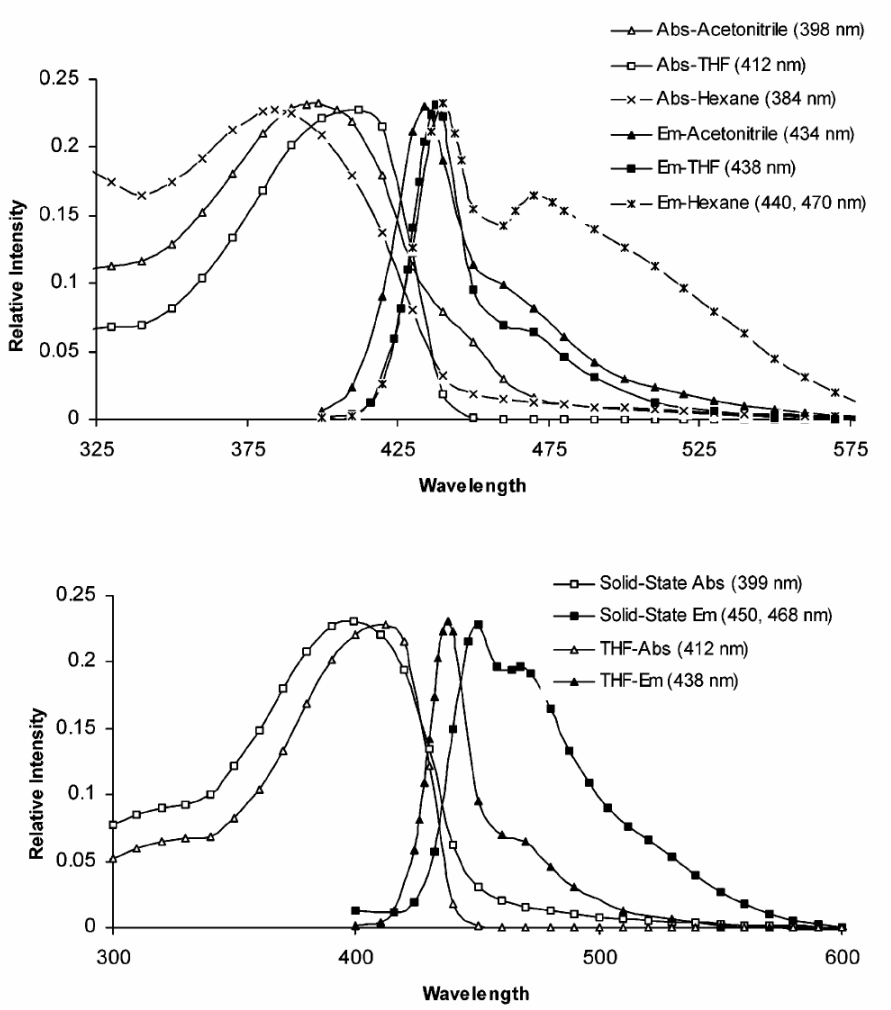


**Figure 5.1.** Top: absorption and emission of polymer **5.2** in different solvents (THF $\lambda_{max}$ 412 nm; em 438 nm. $CH_3CN$ $\lambda_{max}$ 398 nm (sh); em 434 nm. Hexanes $\lambda_{max}$ 384 nm; em 440, 470 nm). Bottom: absorption and emission spectra of **2** in the solid state ($\lambda_{max}$ 399 nm, em 450, 468 nm) and in THF ($\lambda_{max}$ 412 nm, em 438 nm).

that the large glucose substituents diminish planarization of the main chain and interchain interactions at the same time. The relatively small differences in the solution and solid-state emission spectra give likewise testimony to this interpretation. Macroscopic samples of **5.2** form fibrous mats of significant mechanical strengths and are not powdery as the

dialkyl-PPEs. Concentrated solutions of **5.2** in THF show birefringence, and dried lyotropic samples display a small but distinctive Schlieren texture under crossed polarizers, similar to those observed for the dialkyl-PPEs.

To elucidate the nature of the phase, we performed transmission electron microscopy upon dried samples of **5.2** (Figure 5.2). This polymer forms a lamellar morphology, with the lamellae showing a width of approximately 30-50 nm. Upon higher magnification, the lamellae are doubled and display a fine structure with an apparent interstrand connection every 50 nm. The two-dimensional picture could represent an intertwined composite formed from two PPE strands. The curious double-stranded feature has been observed earlier in another hydrophilic PPE derivative[16] where its genesis likewise is not clear.

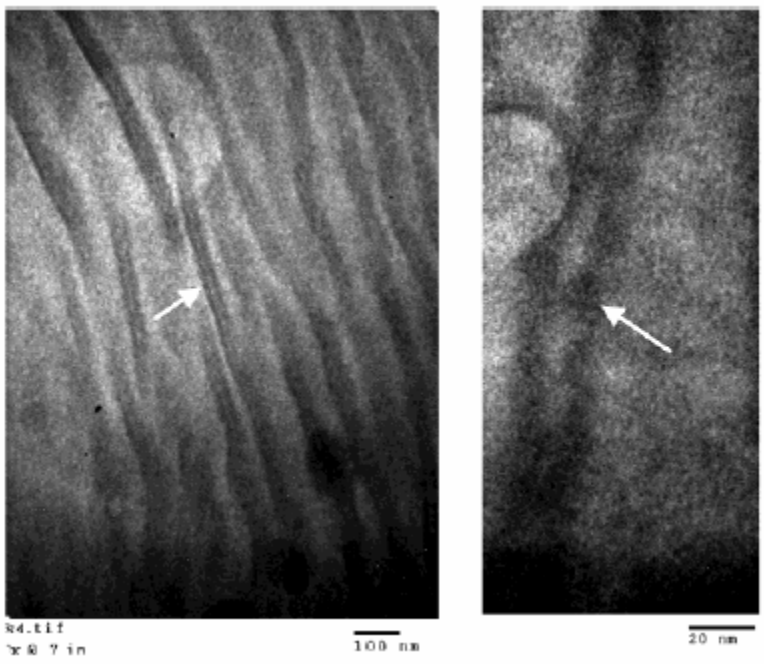


**Figure 5.2.** Transmission electron micrographs of thin films of **5.2** obtained by evaporation of a drop of a solution of **5.2** in a mixture of $H_2O$/THF. Scale bars are shown; no staining reagent or shadowing was utilized.

## 5.3 Conclusion

In conclusion, we have prepared the first sugar-substituted PPE derivative and have examined its supramolecular ordering and its spectroscopic behavior. In the future we will report upon interaction of the sugar-coated PPEs with biomolecules and novel PPE-based morphologies.

## 5.4 Experimental

α-D-Glucosepentaacetate **5.2** (2.00 g, 5.24 mmol, Aldrich Sigma) and 2,5-diiodohydroquinone **5.1** (843 mg, 2.33 mmol) were dissolved in 15 mL of anhydrous $CH_2Cl_2$. Then $BF_3{\cdot}Et_2O$ (0.6 mL, 4.7 mmol) was added slowly. The reaction mixture was stirred at room temperature for 24 h and then poured into 40 mL of 5% aqueous $NaHCO_3$. The organic layer was separated, washed with aqueous $NaHCO_3$ and water. The solution was dried over $MgSO_4$ and the solvent was removed. The crude product was crystallized from ethanol to give **5.3** (0.92 g, 39%). $^1$H NMR (DMSO): δ 7.49 (s, 2H), 5.47-5.44 (d, 2H), 5.32-5.39 (t, 2H), 5.07-5.13 (q, 2H), 5.01-4.94 (t, 2H), 4.30-4.23 (m, 2H), 4.17-4.08 (m, 4H), 2.09, 2.04, 2.01, 1.96 (4s, 24H, 8 acetyl groups). $^{13}$C NMR (DMSO): δ 170.033, 169.562, 169.390, 168.889, 152.136, 125.847, 98.474, 87.417, 71.796, 71.123, 70.204, 68.129, 62.088, 20.859, 20.821, 20.339, 20.276. IR (KBr, $cm^{-1}$ ): ν 2954, 2869, 1746, 1462, 1369, 1223, 1046, 900, 808. m/z (M+H)calcd. 1023, found 1023. mp: 187 $^o$C.

Monomer **5.4** (0.125 g, 0.360 mmol), monomer **5.3** (0.345 g, 0.340 mmol), $Pd(PPh_3)_2$ $Cl_2$ (4.9 mg, 7.0 μmol), CuI (1.3 mg, 7.0 μmol), THF (2 mL) and piperidine (2

mL) were combined under inert conditions and heated to 40°C for 24h. The product was diluted with THF and crystallized in $H_2O$. Filtering, washing with %10 $NH_4OH$ (50 ml) and water (100 ml) and removing of solvent under vacuum give a yellow-fluffy solid (0.255 g, 99 %), **5.5**. During the reaction the acetyl groups have been lost. The material is freely soluble in THF and DMSO but insoluble in aromatic solvents and chloroform or dichloromethane. $^1$H NMR (DMSO): δ 7.41 (bs, 2H), 7.27 (bs, 2H), 5.18-5.07 (bd, 2H), 3.63 (bs, 2H), 3.55-3.14 (bm, 6H), 2.07 (s, 4H), 1.70 (bs, 2H), 1.22 (bs, 16H), 0.86-0.79 (bd, 12 H). $^{13}$C NMR (DMSO): δ 151.97, 141.17, 133.22, 122.64, 118.64, 114.02, 100.52, 94.19, 90.50, 76.806, 73.34, 69.55, 60.70, 39.50, 38.99, 31.77, 28.12, 25.08, 22.49, 20.37, 13.92, 10.76. IR (KBr, $cm^{-1}$ ): ν 3400.0, 2923.1, 2861.5, 1730.8, 1630.8, 1500.0, 1453.8, 1376.9, 1261.5, 1207.7, 1061.5, 892.3. GPC (polystyrene standard in THF as solvent): $P_n = 95$ $M_w/M_n = 2.2$.

## 5.5 References and Notes


1. Mammen, M.; Choi, S.-K.; Whitesides, G. M. Angew. Chem. 1998, 37, 2754. Glycochemistry; Wang, P. G., Bertozzi, C. R., Eds.; Marcel Dekker: New York, 2001. Davies, B. G. *J. Chem. Soc., Perkin Trans.* **1999**, *3215*. (b) Langer, R. Acc. Chem. Res. **2000**, 33, 94.

2. (a) Fraser, C. L.; Grubbs, R. H. *Macromolecules* **1995**, *28*, 7248. (b) Nomura, K.; Schrock, R. R. *Macromolecules* **1996**, *29*, 540.

3. Roy, R.; Tropper, F. D. *Chem. Commun.* **1988**, 1058. Reuter,J. D.; Myc, A.; Hayes, M. M.; Gan, Z. H.; Roy, R.; Qin, D. J.;Yin, R.; Piehler, L. T.; Esfand, R.; Tomalia, D. A.; Baker, J.R. *Bioconjugate Chem.* **1999**, *10*, 271. Sashiwa, H.; Shigemasa,Y.; Roy, R. *Macromolecules* **2001**, *34*, 3211.

4. Mortell, K. H.; Weatherman, R. V.; Kiessling, L. L. *J. Am. Chem. Soc*. **1996**, *118*, 2297. Kiessling, L. L.; Pohl, N. L. *Chem. Biol*. **1996**, *3*, 71.

5. Spaltenstein, A.; Whitesides, G. M. J. Am. Chem. Soc. 1991, 113, 686. Sigal, G. B.; Mammen, M.; Dahmann, G.; Whitesides, G. M. *J. Am. Chem. Soc*. **1996**, *118*,

3789. Choi, S. K.; Mammen, M.; Whitesides, G. M. *J. Am. Chem. Soc*. **1997**,*119*, 4103.

6. (a) Rixman, M. A.; Tsai, Z. H.; Wu, D.; Njus, J. M.; Stark, J. C.; Hankins, J.; Sandman, D. J. *Macromolecules* **2001**, *34*, 7576. Kim, M.; Sandman, D. J. J. *Macromol. Sci.*, *Pure Appl. Chem*. **2001**, *38,* 1291. (b) Meier, S.; Reisinger, H.; Haag, R.; Mecking, S.; Mülhaupt, R.; Stelzer, F. *Chem. Commun*. **2001**, 855.

7. Okada, S.; Peng, S.; Spevak, W.; Charych, D. E. *Acc. Chem. Res*. **1998**, 31, *229*. Lio, A.; Reichert, A.; Ahn, D. J.; Nagy, J. O.; Salmeron, M.; Charych, D. H. *Langmuir* **1997**, *13*, 6524.

8. Baek, M. G.; Stevens, R. C.; Charych, D. H. *Bioconjugate Chem*. **2000**, *11*, 777.

9. Bunz, U. H. F. *Chem. Rev*. **2000**, *100*, 1605. Bunz, U. H. F. *Acc. Chem. Res.* **2001**, *34,* 998.

10. Pschirer, N. G.; Miteva, T.; Evans, U.; Roberts, R. S.; Marshall, A. R.; Neher, D.; Myrick, M. L.; Bunz, U. H. F. *Chem. Mater*. **2001**, *13*, 2691.

11. Weder, C.; Sarwa, C.; Montali, A.; Bastiaansen, G.; Smith, P. *Science* **1998**, *279*, 835. Montali, A.; Bastiaansen, G.; Smith, P.; Weder, C. *Nature* (London) **1998**, *392*, 261.

12. Zhou, Q.; Swager, T. M. *J. Am. Chem. Soc*. **1995**, *117*, 12593. Yang, J. S.; Swager, T. M. *J. Am. Chem. Soc*. **1998**, *120*, 11864.

13. Water-soluble PPEs: Häger, H.; Heitz, W. *Macromol. Chem. Phys*. **1998**, *199*, 1821. Tan, C.; Pinto, M. R.; Schanze, K. S. *Chem. Commun*. **2002**, 446.

14. Smits, E.; Engberts, J. B. F. N.; Kellog, R. M.; van Doren, H. A. *J. Chem. Soc., Perkin Trans. 1* **1996**, 2873.

15. As a testament to its self-organizing properties, there was an additional broad feature at much higher molecular weight.

16. Schnablegger, H.; Antonietti, M.; Göltner, C.; Hartmann, J.; Cölfen, H.; Samori, P.; Rabe, J. P.; Häger, H.; Heitz, W. J. *Colloid Interface Sci*. **1999**, *212*, 24.

17. For other ribbonlike supramolecular structures of PPEs, see: (a) Samori, P.; Severin, N.; Müllen, K.; Rabe, J. P. *Adv. Mater*. **2000**, *12*, 579. Samori, P.; Francke, V.; Müllen, K.; Rabe, J. P. *Chem. Eur. J*. **1999**, *5*, 2312. Samori, P.; Sikharulidze, I.; Francke, V.; Müllen, K.; Rabe, J. P. *Nanotechnology* **1999**, *10*, 77. (b) Perahia, D.; Traiphol, R.; Bunz, U. H. F. *Macromolecules* **2001**, *34*, 151. Wilson, J. N.; Steffen, W.; Oda, M.; Lieser, G.; Neher, D.; Bunz, U. H. F. *J. Am. Chem. Soc*. **2002**, *124*, 6830.

# Chapter 6

# Towards Bio-sensing PPEs: Synthesis of a polyester sidechain PPE with –OH handles

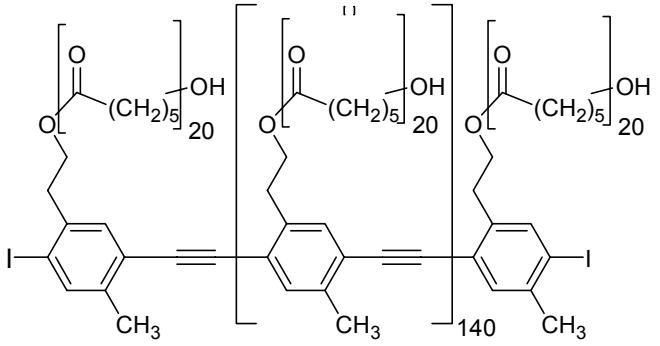

## Introduction

Poly(*para*phenyleneethynylene)s (PPEs)[1] are a specific class of conjugated polymers in which benzene groups are linked by alkyne units. Their high fluorescence quantum yield and their well developed chromicity[2,3] make the PPEs attractive as sensors4 and as active layers in semiconductor devices.[5,6] While structural variations on PPEs[7–11] have been reported, to our knowledge, PPEs with macromolecular substituents have not been described. Such graft copolymers would be of interest a) as novel macromolecular architectures, b) as a means to obtain the optical properties of PPEs in the solid state at high intrinsic backbone dilution, and c) as embedded, nanoscale separated materials with potentially unusual mechanical and solubility properties.

## 6.2 Results and Discussion

The synthesis of a grafted PPE starts by reacting **6.1** with ecaprolactone catalysed by $Sn(O–C=OCHEtBu)^2$. The telechelic macromonomer **6.2** (Scheme 6.1) forms in 48% yield. It is dissolved in a mixture of THF and piperidine.

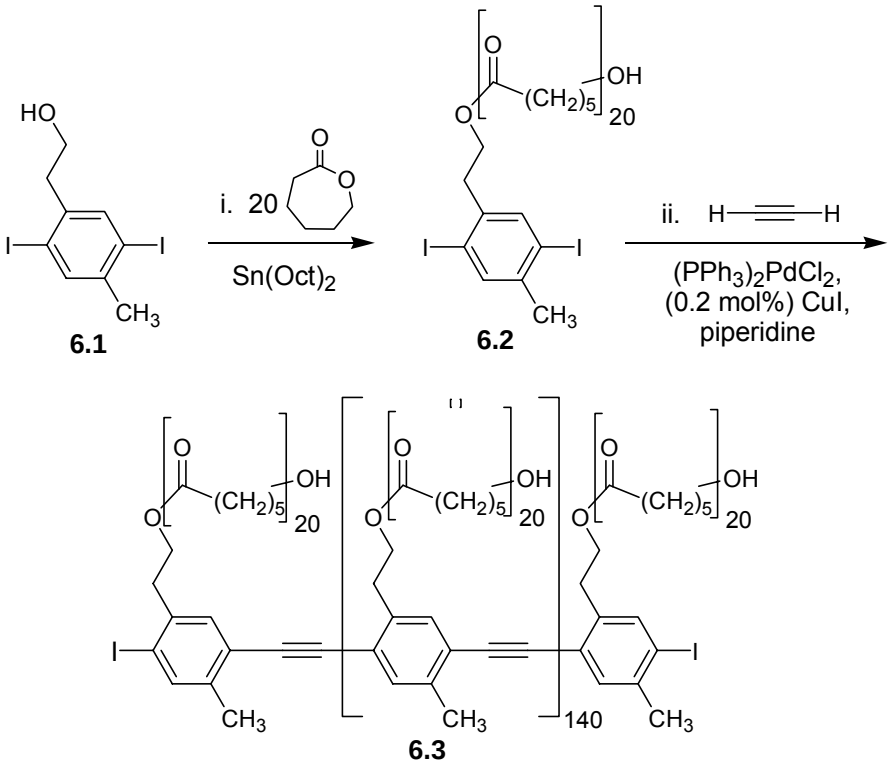


**Scheme 6.1** Synthesis of the PPE **6.3** with a macromolecular polyester substituent. Yield of **6.2**: 48%, PDI = 1.3, *M*n = 2.4 3 103 (GPC *vs.*polystyrene); yield of **6.3**: 78%, PDI = 5.3, *M*n = 336 x $10^3$ (gpc), *P*n =

Addition of a trace amount of $(Ph_3P)_2PdCl_2$ (0.2 mol%), CuI, and a measured quantity of acetylene gas[12] furnishes a deep-yellow, flaky material after precipitation from methanol. The color and the following gel permeation chromatography (GPC, *vs.* polystyrene) showed that **6.3** had formed in 78% yield. The GPC trace of **6.3** is monomodal but with a

broad distribution of molecular weights. The polydispersity index (PDI) is 5.3 and the $M_n$ of **6.3** is recorded to 3.36 x $10^5$. The polymer has a degree of polymerization ($P_n$) of 140 repeating units. In the $^{13}C$ NMR spectra of **6.3** the resonances of the grafted-on polyesters are prominent, but the signals attributable to the conjugated main chain are weak and thus difficult to discern. Due to the substitution pattern at the benzene ring and the innate non-regioselectivity of the Pd coupling, the alkyne carbons in **6.3** should show four resonances and the benzene rings should show six resonances in its $^{13}C$ NMR spectrum, exacerbating the problem of the low signal to noise ratio of the backbone carbon resonances.

To demonstrate that Pd-catalysis works well for this substitution pattern (Scheme 6.2) we prepared a model polymer that shares the backbone with **6.3** but features simpler solubilizing groups. The microwave-mediated coupling (5 min reaction time) of **6.1** with chlorotriisopropylsilane in imidazole furnished the monomer **6.4** in a 98% yield after

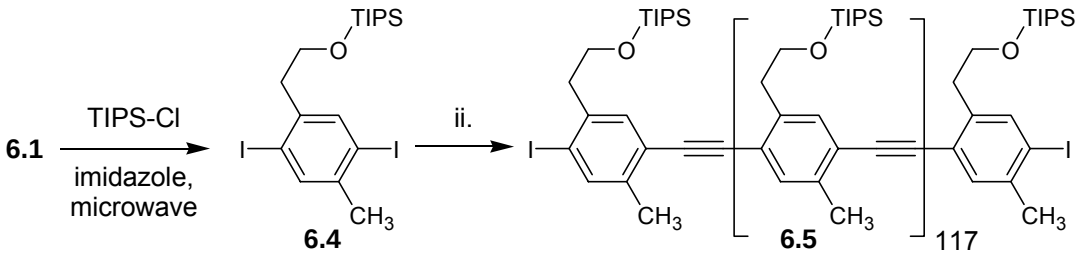


**Scheme 6.2** Synthesis of a PPE **6.5** with TIPS substituents. i. Yield of **6.4** = 98%. ii. See Scheme 1. Yield of **6.5** = 98%, $M_n$ = 37 3 103 (GPC), PDI = 3.9, $P_n$ = 117.

chromatography as a colorless oil. Treatment of **6.4** under conditions optimized for the synthesis of **6.3** gave a high molecular weight polymer **6.5** that is soluble in halogenated organic solvents. At concentrations higher than 2.5 wt% **6.5** forms a blue-fluorescent *but clear* jelly in dichloromethane or in chloroform. The aromatic and alkyne regions of the

$^{13}$C NMR spectrum of **6.5** are superimposable with that of **6.3** and shown in Fig. 6.1. As expected, the signals of the alkyne carbons and the benzene rings are split due to the non-equivalency of the side chains in the monomer **6.4** and the inset shows the split of the alkyne resonances at 92 ppm into four signals.

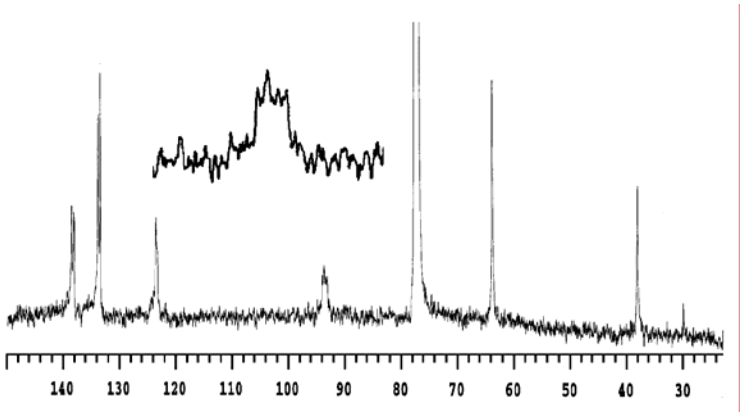


**Fig. 6.1** $^{13}$C NMR of model polymer **6.5**. Visible are the four alkyne peaks at $\delta$ = 92 (see inset) and the five resolved signals for the benzene rings. The large signal at $\delta$ = 77 is due to CDCl3. TIPS signals are not shown. The signal at $\delta$ = 31 is a hydrocarbon impurity.

The UV-vis and emission spectra of the polymers **6.3** and **6.5** in chloroform solution and in thin films are shown in Fig. 5.2. Their optical properties are similar to each other and in accord with the spectroscopic data recorded for dialkyl-PPEs[1] where lmax (solution) is 388 nm and $\lambda_{max}$ (thin film) is 439 nm. The silyloxy substituent in **6.5** seems to have a slight electron withdrawing effect. As a consequence, $\lambda_{max}$ (absorption) is somewhat blue shifted in **6.5**. The optical properties of **6.3** in the solid state are unusual. As-spun films show a $\lambda_{max}$ (absorption) of 436 nm, typical of dialkyl-PPEs. Upon annealing (4 h, 100 °C) these thin films, *their absorption changes back to $\lambda_{max}$ = 406 nm, which is similar to the absorption of* ***6.3*** *recorded in chloroform* (Fig. 6.2). In addition, the absorption loses almost all structure. The emission of the films changes much less

upon annealing and only a small shift from 519 to 504 nm is observed when going from the pristine to the annealed films. The fluorescence intensity does not change visibly upon annealing. At the same time the annealed thin films of **6.3** are now insoluble in common organic solvents. We assume that the insolubility of the polymers upon

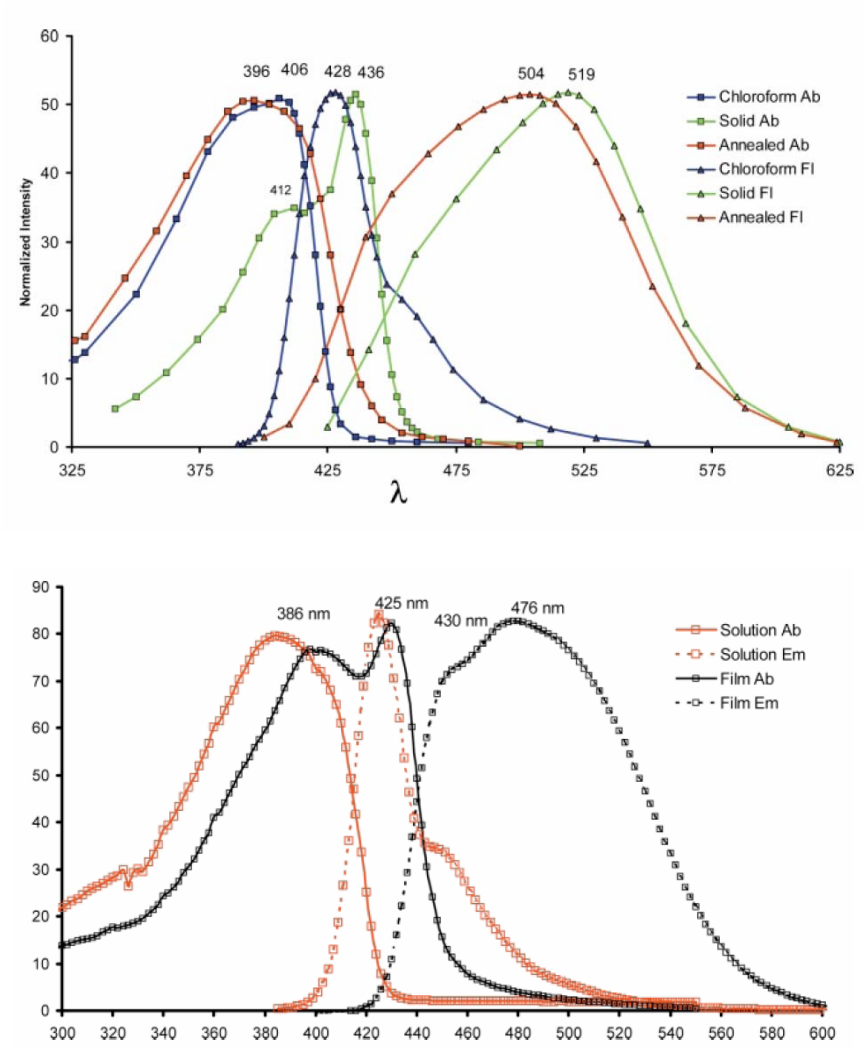


**Fig. 6.2** UV-vis and emission spectra of **6.3** and **6.5**. Top: spectra of **6.3**; bottom: spectra of **6.5**.

annealing is due to an increased order in the polyester side chain. Powder X-ray diffraction (Fig. 6.3) shows that the intensity of the polyester diffraction peaks at 5.6,

4.14, 3.74, and 3.0 Å increases upon annealing, while a diffuse intensity of diffraction that is visible as a hump at 2θ = 20–22° disappears during the annealing process. This broad diffraction peak at 2θ = 20–22° is typical for the π-π-stacking of the PPEs and is the most intense diffraction in these materials.[13,14] The annealing increases the ordering

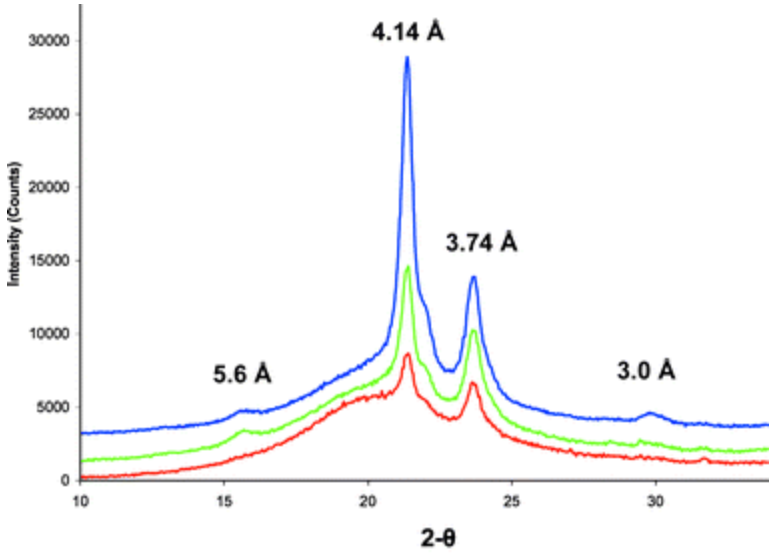


**Fig. 6.3** X-Ray diffraction of different polyester substituted PPEs. Bottom curve: gel phase. Middle curve: pristine powder. Top curve: annealed powder.

of the polyester side chains, but it seems to *decrease* the ordering of the PPE main chain, *i.e.* in the competition of main chain and side chains, the side chains win and lead to a twist and a gross disorder of the PPE main chain in the solid. In the powder diffraction of the annealed sample there are no signs of the diffraction of the main chain left.

## 6.3 Conclusion

In conclusion we have made two new *dialkyl*-PPE derivatives **6.3** and 6**5.5** with a macromolecular polyester substituent and triisopropylsilyloxy side groups. The attachment of the polyester side chain to the PPE leads to a graft copolymer that shows an

unusual chromic behavior, in that its $\lambda_{max}$ (UV-vis) blueshifts upon annealing. In future we will investigate the structural pecularities of both **6.3** and **6.5** further.

## 6.4 Experimental

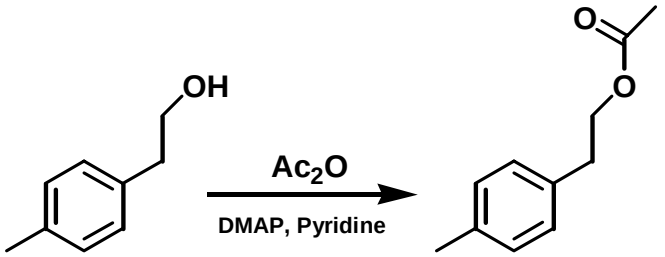


93%

To a nitrogen purged flask were added 4-methylphenethyl alcohol (21.2 g, 156 mmol), acetic anhydride (79.6 g, 780 mmol), pyridine (400 mL) and 4-dimethylaminopyridine (catalytic amount). The mixture was stirred at room temperature for 6 h. The solvent and excess acetic anhydride were removed in vacuo to afford the desired product as a colorless liquid. The acetate was purified by column chromatography by using hexane / dichloromethane (1:3) as an eluent. The product was obtained as a colorless oil (25.9 g, 93%). IR (KBr, $cm^{-1}$ ): ν 3460, 2864, 2732, 2073, 1900, 1740, 1514, 1365, 1223, 976, 908, 812, 718, 640, 606, 550. $^{1}H$ NMR ($CDCl_3$) $\delta$ = 7.13 (s, 4H), 4.30-4.26 (t, 2H, $J_{3H,H}$ = 7.0 Hz), 2.94-2.89 (t, 2H, $J_{3H,H}$ = 7.0 Hz), 2.35 (s, 3H), 2.05 (s, 3H) $^{13}C$ NMR ($CDCl_3$) $\delta$ = 170.82, 135.88, 134.56, 129.04, 128.62, 64.92, 34.50, 20.87, 20.79.

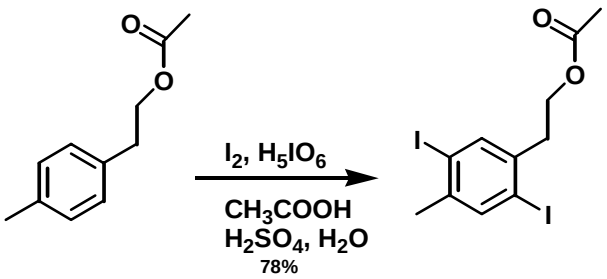


To a nitrogen purged flask, 4-methylphenethylacetate (25.0 g, 140 mmol), iodine (39.1 g, 154 mmol), periodic acid (0.639 g, 2.81 mmol), acetic acid (500 mL), $H_2O$ (100 mL) and $H_2SO_4$ (15.0 mL) were added. The mixture was heated up to 80 $^oC$ for 3 h under $N_2$. The solvent was removed in vacuo. The residue was dissolved in ethylacetate and washed with $H_2O$, then 1N (aq) $K_2CO_3$ and 1N (aq) $Na_2SO_3$. The organic phase was dried over $MgSO_4$ and the solvent was evaporated. The resulting solid was purified by silica gel chromatography using 1:3 kexane / dichloromethane to give product as a colorless solid (51.7 g, 78%). Mp = 55 $^oC$ IR (KBr, $cm^{-1}$ ): ν 2945, 2870, 1738, 1516, 1452, 1369, 1232, 1041, 984, 878, 802, 700, 656, 606. $^1H$ NMR ($CDCl_3$) $\delta$ = 7.65 (s, 1H), 7.62 (s, 1H), 4.24–4.19 (t, 2H, $J_{3H,H}$ = 7.0 Hz), 2.98-2.94 (t, 2H, $J_{3H,H}$ = 7.0 Hz), 2.33 (s, 3H), 2.03 (s, 3H) $^{13}C$ NMR ($CDCl_3$) $\delta$ = 170.73, 141.76, 139.76, 139.70, 139.60, 100.76, 100.01, 63.16, 38.48, 26.90, 20.87.

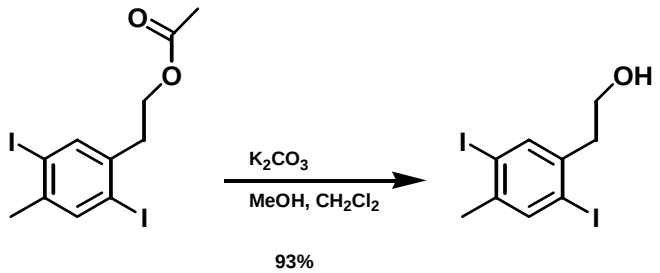


2,5-diiodo-4-methylphenethyl alcohol (50.0 g, 116 mmol) was dissolved in 65 mL of dichloromethane. After addition of 1.5 L of MeOH and $K_2CO_3$ (161 g, 1.16 mol), the mixture was stirred at room temperature for 16 h. The solvent was evaporated and the

resultant solid was transferred into funnel and washed with $H_2O$. Recrystallized from hexane, the product was a colorless solid (41.9 g, 93%). Mp = 118 $^oC$. IR (KBr, $cm^{-1}$ ): ν 3273, 2950, 2874, 1439, 1371, 1342, 1163, 1041, 1018, 995, 876, 781, 704, 654, 606. $^1H$ NMR ($CDCl_3$) $\delta$ = 7.66-7.65 (d, 2H), 3.83-3.79 (t, 2H, $J_{3H,H}$ = 6.8 Hz), 2.93-2.88 (t, 2H, $J_{3H,H}$ = 6.8 Hz), 2.33 (s, 3H), 1.42 (bs, 1H). $^{13}C$ NMR ($CDCl_3$) $\delta$ = 141.65, 140.39, 139.86, 139.76, 100.91, 100.23, 62.02, 42.49, 26.93.

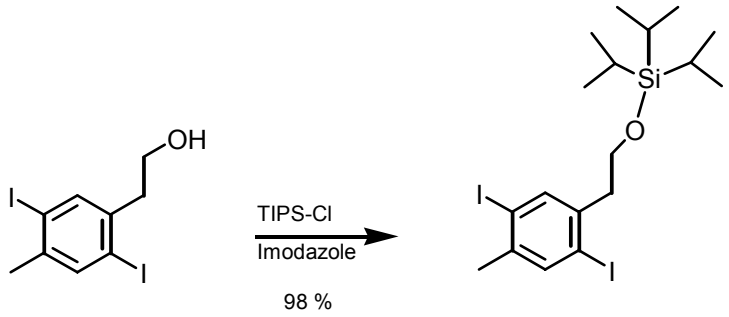


2, 5-diiodo-4-methylphenethyl alcohol (2.00 g, 5.16 mmol), triisopropylsilylchloride (3.96 g, 20.7 mmol), and imidazole (0.975 g, 15.5 mmol) were placed into a pressure tube and capped. The tube was placed in a microwave oven (Emerson, 600 watt) and irradiated for 4 x 1 minute pulses. The progress of the reaction was monitored by TLC. The reaction mixture was separated by flash column (hexane: ethyl acetate, 80:20) and excess triisopropylsilyl chloride was removed by vacuum distillation. The silyl ether was obtained as a light yellow oil. Yield 2.75 g (98%). IR (KBr, $cm^{-1}$ ): ν 2939.3, 2889.2, 2862.2, 1506.3, 1461.9, 1446.5, 1379.0, 1365.5, 1247.9, 1188.1, 1103.2, 1068.5, 1012.6, 996.2, 921.9, 881.4, 746.4, 680.8, 657.7. $^1H$-NMR ($CDCl_3$, 300 MHz): $\delta$ = 7.71 (s, 1H), 7.65 (s, 1H), 3.83(t, 2H, $J_{3H,H}$ = 6.9 Hz), 2.88(t, 2H, , $J_{3H,H}$ = 6.9 Hz), 2.34 (s, 3H), 1.55-0.99 (m, 21H). $^{13}C$-NMR ($CDCl_3$, 400 MHz): $\delta$ = 141.47, 141.43, 140.69, 139.74, 100.87, 100.35, 62.81, 43.18, 27.16, 18.24, 12.16.

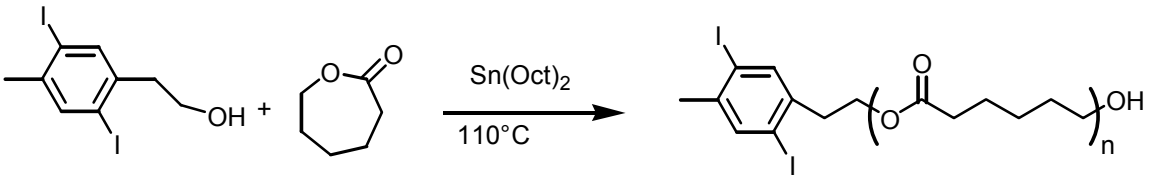


An oven-dried Schlenk flask cooled under nitrogen was charged with 2,5-diiodo-4-methylphenethylalcohol (2.00 g, 5.16 mmol), ε-caprolactone (11.8 g, 103 mmol), and tin(II)-2-ethylhexanoate (127 mg, 313 μmol). The flask was heated while stirring to 110°C. The reaction was stopped after 12 h. The highly viscous product was diluted with 10.0 mL chloroform, then precipitated into 300 mL of methanol. The diiodo-polyester was obtained as a colorless solid. Yield 6.56 g, 48%. GPC (vs. polystyrene standards in chloroform): $M_n = 2400$, $M_w/M_n = 1.3$ IR (KBr, $cm^{-1}$ ): ν 2941.2, 2893.0, 2866.0, 1722.3, 1683.7, 1652.9, 1506.3, 1471.6, 1456.2, 1394.4, 1294.1, 1244.0, 1190.0, 1107.1, 1045.3, 962.4, 933.5, 877.6, 840.9, 731.0, 709.8. $^1$H NMR ($CDCl_3$, 400 MHz): δ = 7.67 (s, 1H), 7.63 (s, 1H), 4.24 (t, $J_{3H,H}$ = 6.8 Hz, 2H), 4.05 (t, $J_{3H,H}$ = 6.8 Hz, 38H), 3.64 (t, $J_{3H,H}$ = 6.6 Hz, 2H), 2.98 (t, $J_{3H,H}$ = 6.8 Hz, 2H), 2.30 (t, $J_{3H,H}$ = 7.5 Hz, 40H), 1.68-1.60 (m, 80H), 1.41-1.33 (m, 40H) $^{13}$C NMR ($CDCl_3$, 400 MHz): δ = 173.73, 173.54, 173.29, 141.91, 139.91, 139.87, 139.82, 100.76, 100.03, 64.54, 64.14, 63.95, 63.10, 62.62, 38.64, 34.23, 34.12, 33.95, 33.82, 33.34, 28.53, 28.35, 28.18, 26.96, 25.93, 25.53, 25.31, 24.98, 34.69, 24.58, 24.39.

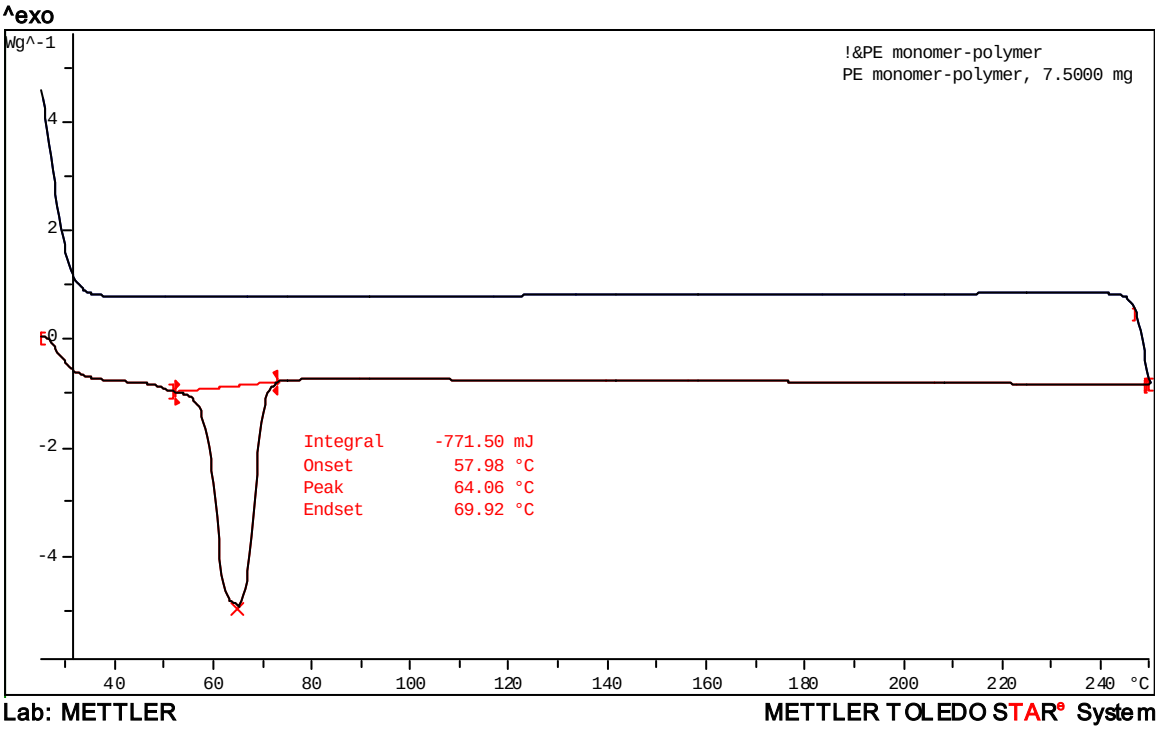


**Figure 6.4**. DSC of **6.2** showing 13.3 kJ/mole repeat.

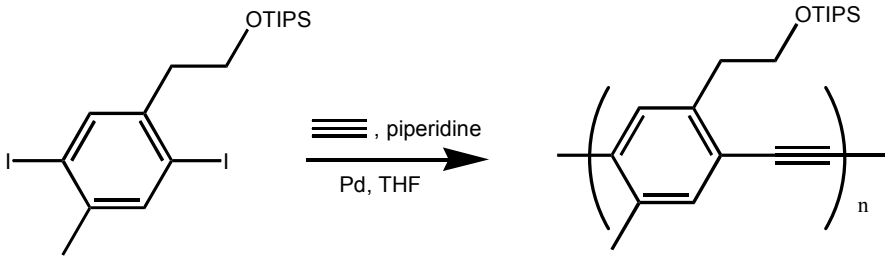


A Schlenk flask of known volume (37 mL) was charged with **6.5** (0.761 g, 1.39 mmol), THF (1.5 mL), piperidine (1.5 mL), $(PPh_3)_2PdCl_2$ (2.0 mg, 2.8 μmol, 0.2 mol%) and CuI (1.0 mg, 5.3 μmol, 0.4 mol%). The flask was degassed by three freeze-pump-thaw cycles. The acetylene gas (34 mL, 1.4 mmol) was added through the purged sidearm by a balloon. The reaction was allowed to stir at room temperature for 48 h during which time the reaction mixture solidified. The reaction mixture was filtered over a small

volume of silica (~10 mL) on a fritted funnel with hexane as solvent. The hexane was evaporated, the polymer re-dissolved and precipitated into methanol. A bright yellow polymer (0.514 g, 62%) was obtained. GPC (vs. polystyrene standards in chloroform): $M_n$ = 37200, $M_w/M_n$ = 3.9. IR (KBr, $cm^{-1}$ ): ν 2941.2, 2891.1, 2864.1, 2194.8, 1504.4, 1461.9, 1360.9, 1103.2, 1070.4, 1012.6, 996.2, 918.1, 883.3, 742.5, 680.8, 569.6. $^1$H NMR (300 MHz, $CDCl_3$): 7.45 (2H, term. Ph-H), 7.42-7.36 (bm, 2H), 3.94 (bs, 2H), 3.07 (bs, 2h), 2.47 (bs, 3H). $^{13}$C-NMR (400 MHz, $CDCl_3$): $\delta$ = 138.39, 138.00, 133.69, 123.36 (broad—2 carbons), 93.58, 63.77, 37.99, 20.53, 18.24, 12.22.

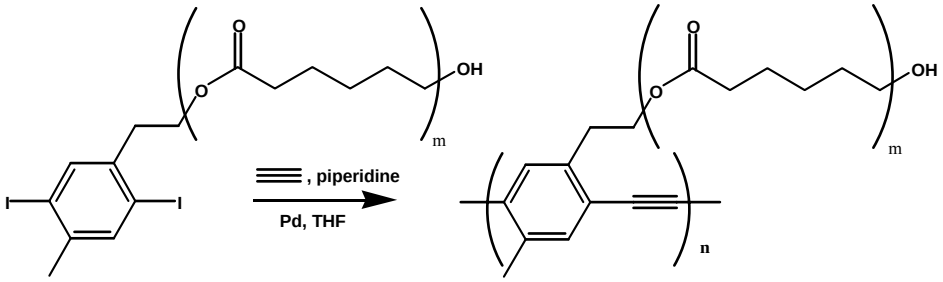


The diiodo polyester was combined with (3.29 g, 1.39 mmol), piperidine (1.5 mL), THF (1.5 mL), $(PPh_3)_2PdCl_2$ (2.0 mg, 2.8 μmol, 0.2 mol%) and CuI (1.0 mg, 5.3 μmol, 0.4 mol%) in a Schlenk flask (37 mL). Acetylene gas (34 mL, 1.4 mmol) was added through the purged side arm with a balloon. The reaction solidified after 36 h. The resultant polymer was filtered over a cotton plug using dichloromethane as a solvent before precipitating into methanol. The polymer was collected over a fritted funnel, re-dissolved in dichloromethane and precipitated again. A bright yellow polymer was obtained (2.31 g, 78 % yield). GPC (vs. polystyrene standard in chloroform): 336,000 $M_n$ vs polystyrene standards. Repeat = 2400 g/mol, $P_n$ = 140, $M_w/M_n$ = 5.3 IR (KBr, $cm^-$

[1] ): ν 2941.2, 2864.1, 1718.5, 1419.5, 1363.6, 1292.2, 1238.2, 1174.6, 1047.3, 960.5, 933.5, 840.9, 732.9, 709.8. $^{1}$H NMR (400 MHz, $CDCl_3$): 7.41 (bs), 4.36 (bs, 2H), 4.04 (bt, $J_{3H,H}$ = 6.6 Hz, 38H), 3.62 (bs, 2H), 2.94 (bs, 2H), 2.28 (bt, $J_{3H,H}$ = 7.4 Hz, 40H), 1.62 (bm, 80H), 1.36 (bm, 40H). $^{13}$C NMR (400M Hz, $CDCl_3$): δ= 173.69, 173.50, 13.8.32, 136.73, 133.40, 132.84, 123.85, 123.18, 93.18, 92.54, 65.15, 64.09, 63.05, 62.55, 34.06, 32.27, 28.29, 25.47, 25.25, 24.52, 20.29.

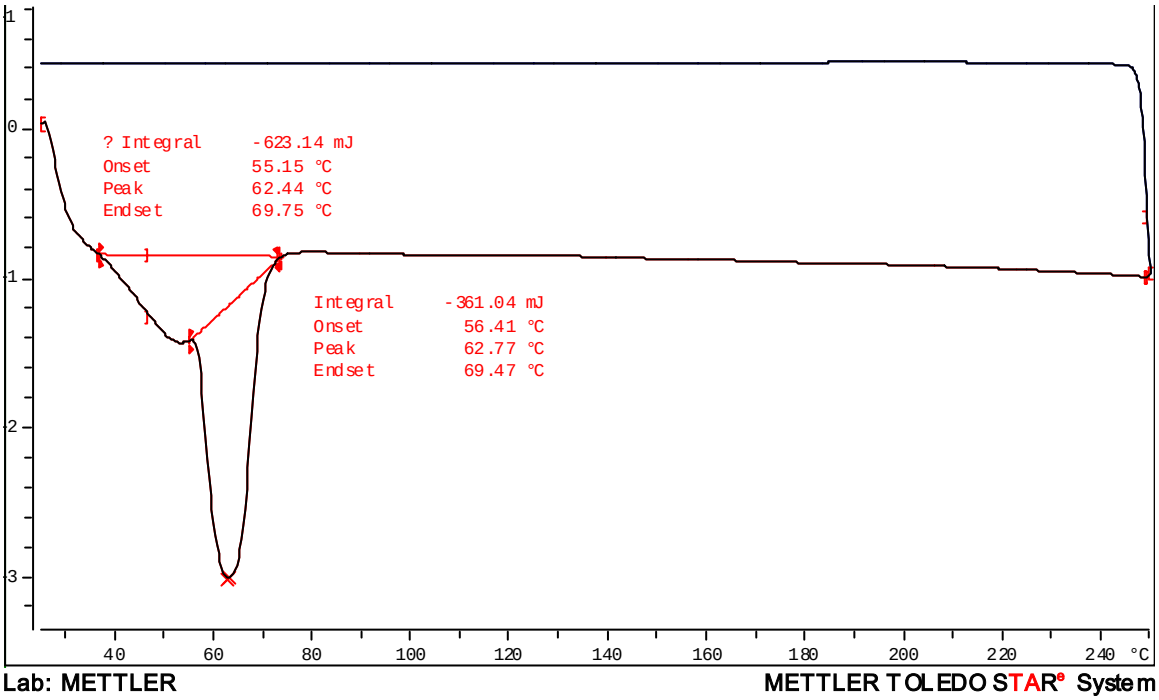


**Figure 6.5**. DSC of polymer **6.3** showing 216 kJ/mol repeat for the total curve and 124 kJ/mol repeat for the "peak" of the curve.

**XRD**

Samples were prepared for powder XRD (Rigaku D\Max-2100 Powder X-Ray Diffractometer, Bragg-Bretano geometry, Cu Kα radiation. All samples utilized the same plate to maintain a consistent background and sample thickness. The samples were

run at a step of 0.04 $^{o}$ 2θ from 5$^{o}$ to 42$^{o}$, 2θ. The precipitated PE-PPE was packed into the well and pressed smooth with a glass slide to obtain the plot for "packed aggregates". A concentrated chloroform solution of the polymer was layered onto the sample holder. This gelatinous sample was run under identical conditions to obtain the "gel" plot. This gel was then annealed at 100 $^{o}$C for 4h to produce the plot for "annealed gel".

## 6.5 References


1. U. H. F. Bunz, *Chem. Rev.*, 2000, **100**, 1605; U. H. F. Bunz, *Acc. Chem. Res.*, 2001, **34**, 998.

2. C. E. Halkyard, M. E. Rampey, L. Kloppenburg, S. L. Studer Martinez and U. H. F. Bunz, *Macromolecules*, 1998, **31**, 8655; T. Miteva, L. Palmer, L. Kloppenburg, D. Neher and U. H. F. Bunz, *Macromolecules*, 2000, **33**, 652.

3. J. Kim and T. M. Swager, *Nature*, 2001, **411**, 1030.

4. Q. Zhou and T. M. Swager, *J. Am. Chem. Soc.*, 1995, **117**, 12593; J. S. Yang and T. M. Swager, *J. Am. Chem. Soc.*, 1998, **120**, 11864; T. M. Swager, *Acc. Chem. Res.*, 1998, **31**, 201.

5. A. Montali, P. Smith and C. Weder, *Synth. Met.*, 1998, **97**, 123; C. Schmitz, P. Posch, M. Thelakkat, H. W. Schmidt, A. Montali, K. Feldman, P. Smith and C. Weder, *Adv. Funct. Mater.*, 2001, **11**, 41; A. Kokil, I. Shiyanovskaya, K. D. Singer and C. Weder, *J. Am. Chem. Soc.*, 2002, **124**, 9978; C. Weder, C. Sarwa, A. Montali, G. Bastiaansen and P. Smith, *Science*, 1998, **279**, 835.

6. N. G. Pschirer, T. Miteva, U. Evans, R. S. Roberts, A. R. Marshall, D. Neher, M. L. Myrick and U. H. F. Bunz, *Chem. Mater.*, 2001, **13**, 2691.

7. T. Sato, D. L. Jiang and T. Aida, *J. Am. Chem. Soc.*, 1999, **121**, 10658.

8. J. N. Wilson, W. Steffen, T. G. McKenzie, G. Lieser, M. Oda, D. Neher and U. H. F. Bunz, *J. Am. Chem. Soc.*, 2002, **124**, 6830.

9. S. Zahn and T. M. Swager, *Angew. Chem., Int. Ed.*, 2002, **41**, 4225.

10. C. Y. Tan, M. R. Pinto and K. S. Schanze, *Chem. Commun.*, 2002, 446; N. DiCesare, M. R. Pinto, K. S. Schanze and J. R. Lakowicz, *Langmuir*, 2002, **18**, 7785.

11. C. G. Bangcuyo, J. M. Ellsworth, U. Evans, M. L. Myrick and U. H. F. Bunz, *Macromolecules*, 2003, **36**, 546; B. Erdogan, J. N. Wilson and U. H. F. Bunz, *Macromolecules*, 2002, **35**, 7863; C. G. Bangcuyo, U. Evans, M. L. Myrick and U. H. F. Bunz, *Macromolecules*, 2001, **34**, 7592.

12. J. N. Wilson, S. M. Waybright, K. McAlpine and U. H. F. Bunz, *Macromolecules*, 2002, **35**, 3799.

13. U. H. F. Bunz, V. Enkelmann, L. Kloppenburg, D. Jones, K. D. Shimizu, J. B. Claridge, H.-C. zur Loye and G. Lieser, *Chem. Mater.*, 1999, **11**, 1416; L. Kloppenburg, D. Jones, J. B. Claridge, H.-C. zur Loye and U. H. F. Bunz, *Macromolecules*, 1999, **32**, 4460.

14. D. Ofer, T. M. Swager and M. S. Wrighton, *Chem. Mater.*, 1995, **7**, 418.

# Chapter 7

# Streptavidin Sensing by a Biotin Decorated PPE: A Model Bio-Sensing Scheme

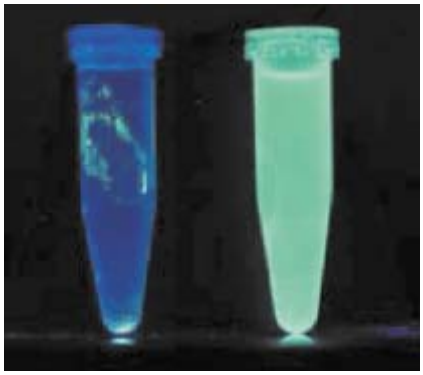

## 7.1 Introduction

Conjugated materials are valuable sensors[1] that just begin to penetrate the biological world.[2] Spectacular examples are the sensing of DNA strands by cleverly designed polythiophenes, water soluble poly*para*phenylenvinylene derivatives,[3–5] and the use of polydiacetylene vesicles for toxin detection.[6] Efficient fluorescence[7] and chromic behavior[8] make poly-(*para*phenyleneethynylene)s (PPE) attractive as candidates in sensory schemes1 and water soluble PPE-derivatives are known.[9] However, PPEs substituted with biogenic moieties are largely uncharted waters,[5,10] and we were interested in a biotinsubstituted PPE as a model compound to study interactions of suitably functionalized conjugated polymers with bacterium. In this study, a streptavidin coated polystyrene bead is a primitive model for a cell/bacterium and the

biotin/streptavidin interaction mimics the recognition process between conjugated polymer and a "cell surface".

## 7.2 Results and Discussion

To obtain a biotinylated PPE, the polymer **7.1**[11] was dissolved in dry THF and treated with the biotin-attached acid chloride **7.2**[12] at 0 °C (Scheme 7.1).[1] The acid chloride **7.2** was prepared according to literature procedures. After allowing the reaction mixture to reach ambient temperature stirring was continued for 4 h. The reaction mixture

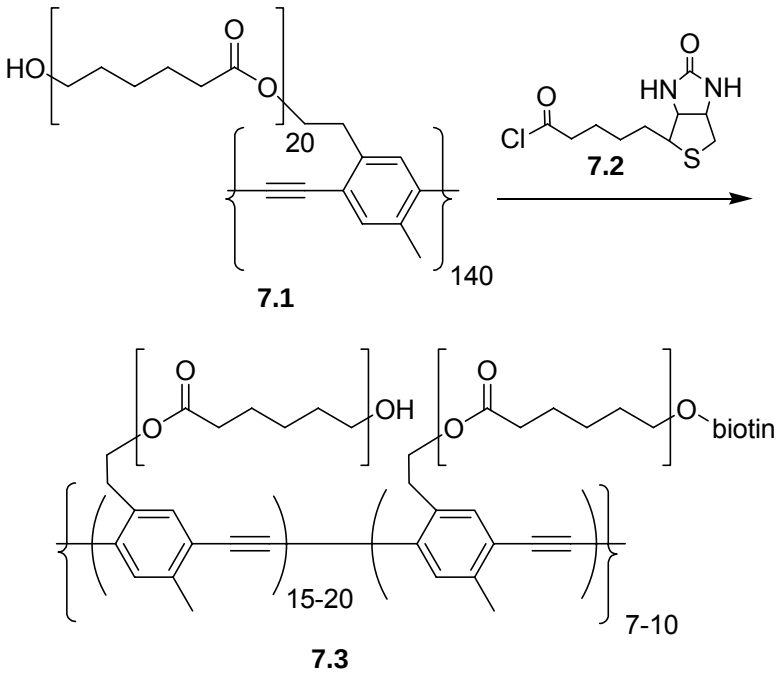


**Scheme 7.1** Synthesis of a biotinylated PPE

was precipitated into 250 mL of methanol under vigorous stirring. The polymer **7.3** was isolated by suction filtration, redissolved in 1 mL of THF and precipitated into water to remove all excess of biotin. The successful biotinylation was qualitatively evidenced by IR spectroscopy of the polymer **7.3**, while its approximate degree of biotinylation was determined by an agglutination assay utilizing free streptavidin. Based upon this assay

every 15$^{th}$ to 20$^{th}$ monomer unit in the PPE chain ($P_n$ = 140, gel permeation chromatography) was biotinylated. As a consequence only 7–14 biotin units are attached to a single polymer chain. This low "loading" of the PPE made it impossible to evidence the presence of biotin by $^1$H NMR spectroscopy. However, the agglutination studies showed convincingly the presence of biotinylated PPEs.

It was of interest to see if the biotinylated PPE **7.3** and its precursor **7.1** would behave differently when exposed to streptavidin-coated microspheres. In a first experiment polymer **7.1** was mixed with streptavidin-covered microspheres. Fig. 7.1 (right) shows that the polymer solution is unchanged and does not alter its emission color. If a solution of **7.3** was mixed with a suspension of streptavidin-coated microspheres (Fig. 7.1, left), the polymer precipitated out as a consequence of the tight binding of the polymer bound biotin to the immobilized streptavidin.

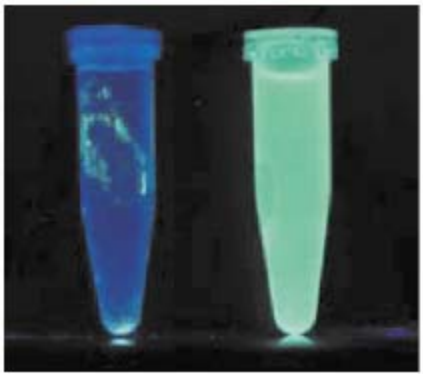

**Fig. 7.1** Left: composite of polymer **7.3** and streptavidin-coated microspheres agglutinated at the bottom of the Eppendorf cap. The blueish fluorescence is innate to the Eppendorf cap. Right: control experiment in which polymer **7.2** and streptavidin coated microspheres are mixed. No agglutination is observed.

The precipitate obtained by the reaction of **7.3** with streptavidin-coated beads was examined by fluorescence microscopy (Fig. 7.3 a,b,d). The formation of dense "mats" of

beads was observed. Surprisingly the beads appeared both blue and red fluorescent when viewed through a DAPI or Texas Red filter respectively (Fig. 7.3 a,b). Preparations of polymer **7.1** exposed to streptavidin beads produced isolated islands of fluorescence upon co-evaporation under otherwise identical conditions. The isolated islands of PPE-fluorescence are only visible under a DAPI filter, while under a Texas Red filter the sample is non-fluorescent. PPE aggregated onto spheres therefore has a measurable fluorescence in the red, while the PPE itself in the solid state does not show this red-shifted feature. To explain this behaviour we took emission spectra of **7.3** in solution, **7.1** with streptavidin in solution and the complex of **7.3** with streptavidin as a suspension. The change in fluorescence is significant (Fig. 7.2) and the aggregation causes a disappearance of the blue shoulder visible for (**7.1** + streptavidin) and for uncomplexed **7.3**. To get a better idea of the microstructure of this composite, we performed scanning electron microscopy of the complex. In Fig. 7.4a. the egg crate structure of the composite is visible. The conjugated polymer covers the beads evenly giving testimony to the

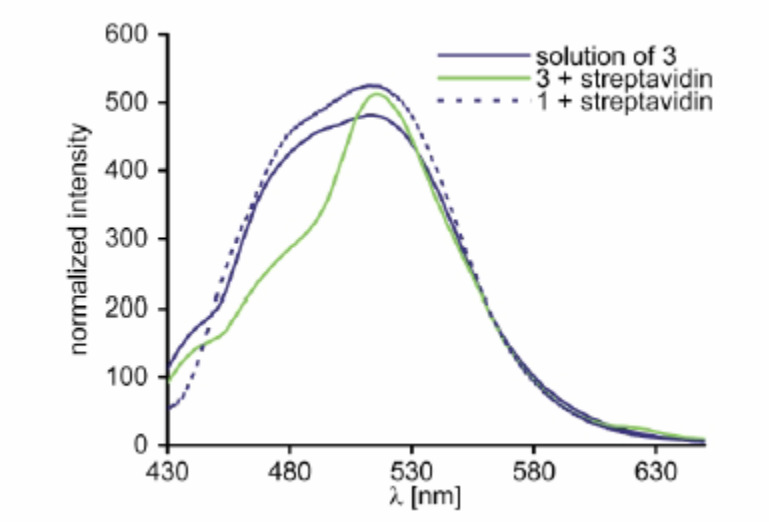


**Fig. 7.2** Emission spectra of **7.3**, **1** with streptavidin and **7.3** with streptavidin (suspension).

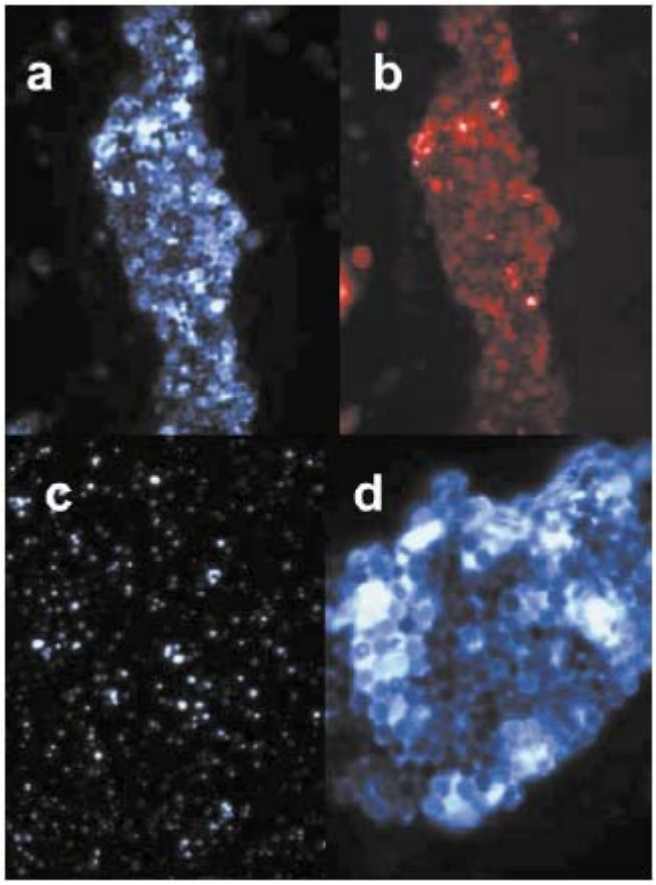


**Fig. 7.3** Fluorescence micrographs of a) aggregates of polymer **7.3** with streptavidin-covered microspheres viewed under DAPI filter; b) same preparation but viewed under Texas Red filter; c) control experiment: non-biotinylated polymer **7.2** co-preciptated with streptavidin-coated microspheres viewed under DAPI filter. Viewed under Texas Red filter the same preparation is non emissive. In a–c the base (width) of the picture is 250 µm; d) magnified picture of the cemented microspheres. The base in d) is 165 µm.

binding between biotin and streptavidin. In Fig. 7.4b. the 3-dimensional arrangement of the polymer covered beads is apparent. The control experiment (**7.1** + streptavidin-coated beads) on the other hand (Fig. 7.4c) does not show *any* defined structure, only islands of polymer **7.1** are visible in the upper half, while three streptavidin-coated beads are isolated in the lower half of the picture.

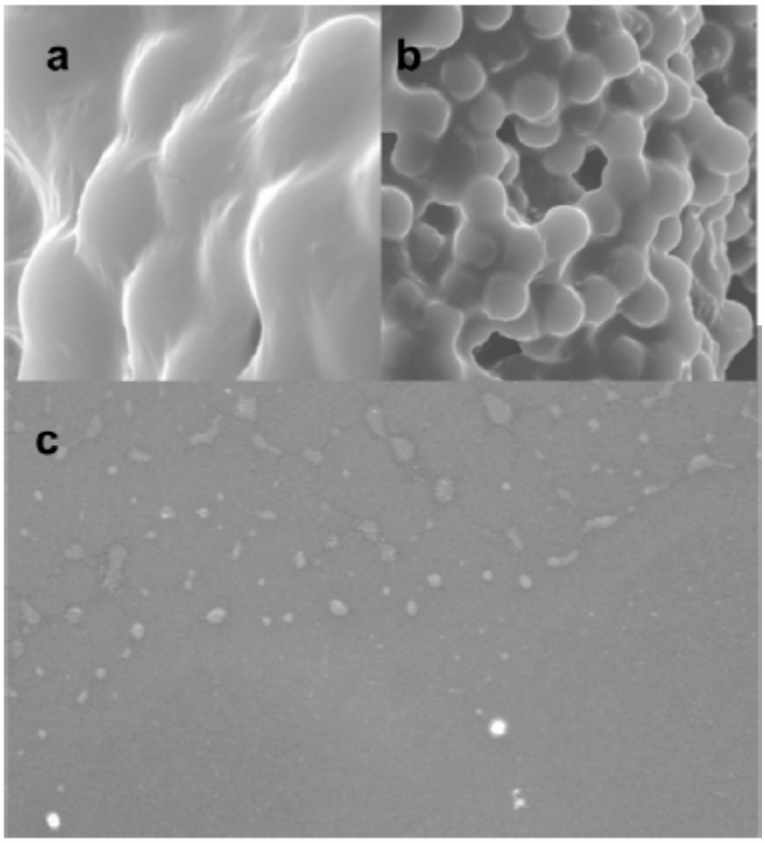


**Fig. 7.4** Scanning electron micrographs of a) complex of **7.3** and streptavidin coated microspheres (18 μm 3 18 μm), b) same as in a) but with lower magnification (53 μm x 53 μm), c) control experiment in which nonbiotinylated polymer **7.2** is co-precipitated with streptavidin-coated microspheres. There are no apparent interactions between polymer (islands on top half) and microspheres (bottom white spots, size 452 μm x 452 μm.). The size of the microspheres is in all cases 5 μm.

## 7.3 Conclusion

In conclusion we have demonstrated that lightly biotin functionalized PPEs form nanocomposites with streptavidincoated microspheres. This primitive system can be seen as a model for the interaction of cells (emulated by the beads) with functionalized conjugated polymers. This model could play an important role in the simple, colorimetric or fluorimetric detection of pathogens and toxins by PPE-types.

## 7.4 Experimental

Biotinylation of **7.1** to form **7.3**: An oven-dried Schlenk flask with stirbar was cooled under $N_2$ gas and charged with biotin (122 mg, 0.500 mmol). Excess (~2 mL) thionyl chloride was added and the reaction was capped with a septum and placed into an ice bath. The reaction was occasionally vented with a needle as it reached ambient temperature over a 2 h period. Excess thionyl chloride was removed by vacuum distillation. The product **7.2** was used without purification. Polymer **7.1** (120 mg, 0.0500 mmol) was dissolved in a freshly distilled mixture of THF/triethylamine (5:1) (~2 mL). This solution was pipetted into the reaction vessel containing 2. The reaction mixture was placed again into an ice bath and allowed to reach ambient temperature over the course of 4 hours. The polymer **7.3** was precipitated into excess methanol, collected over a fritted funnel, re-dissolved in THF and precipitated again into water (110 mg collected).

Characterization of **7.1, 3** and biotin by IR (Figures 7.5-7.10): Spectra were obtained on a Shimadzu 8400 FTIR with a Pike Technologies Diffuse Reflectance attachment and processed with Shimadzu Hyper-IR v 1.57 software including the Kubelka-Munk fuction to help resolve the peaks. All samples were scanned 3000 times. The characteristic bands observed at 3307 and 3358 $cm^{-1}$ were visible in the expansion in the region of 3500 $cm^{-1}$ to 3200 $cm^{-1}$ for polymer **7.3**.

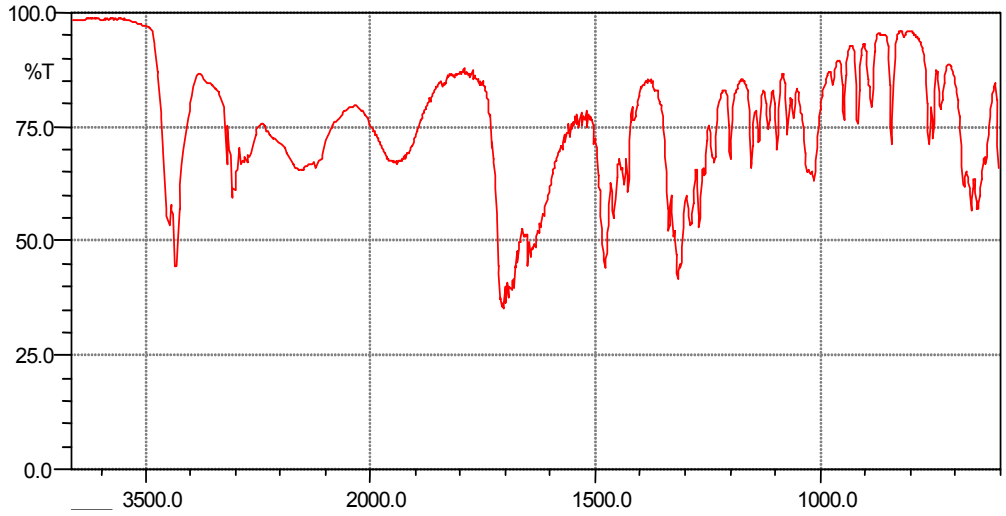


**Figure 7.5** IR of Biotin.

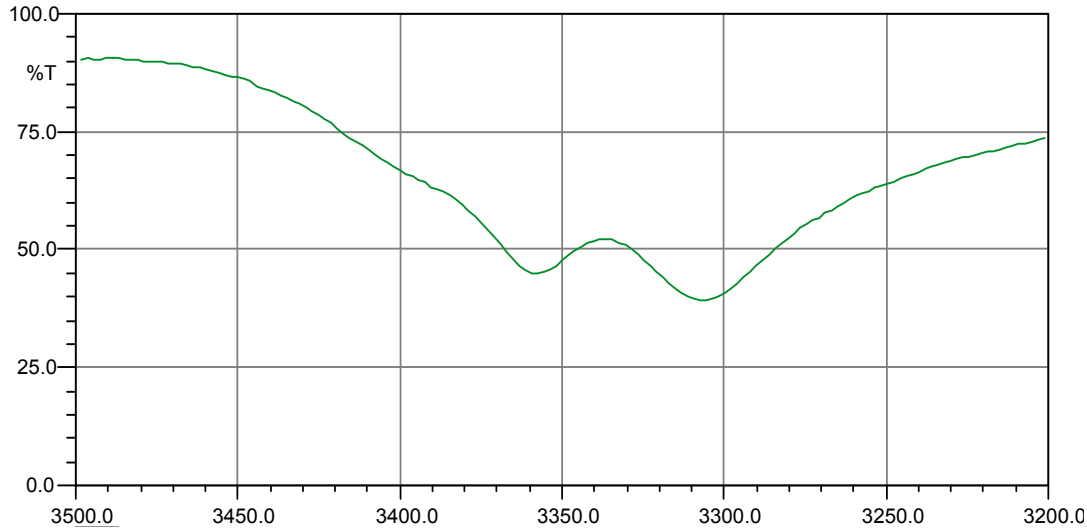


**Figure 7.6** IR of Biotin (expansion from 3500 $cm^{-1}$ to 3200 $cm^{-1}$).

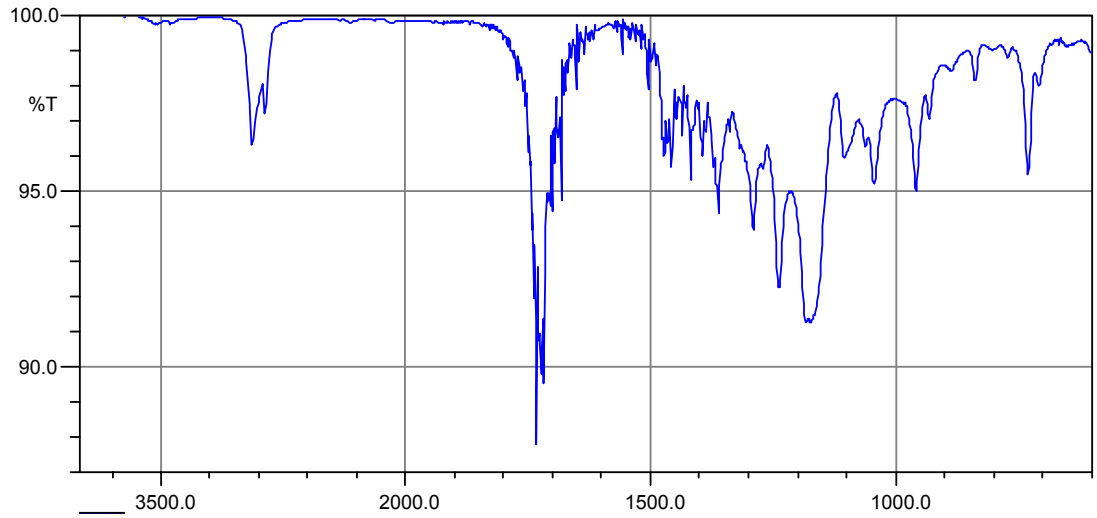


**Figure 7.7** IR of Polymer **7.1**.

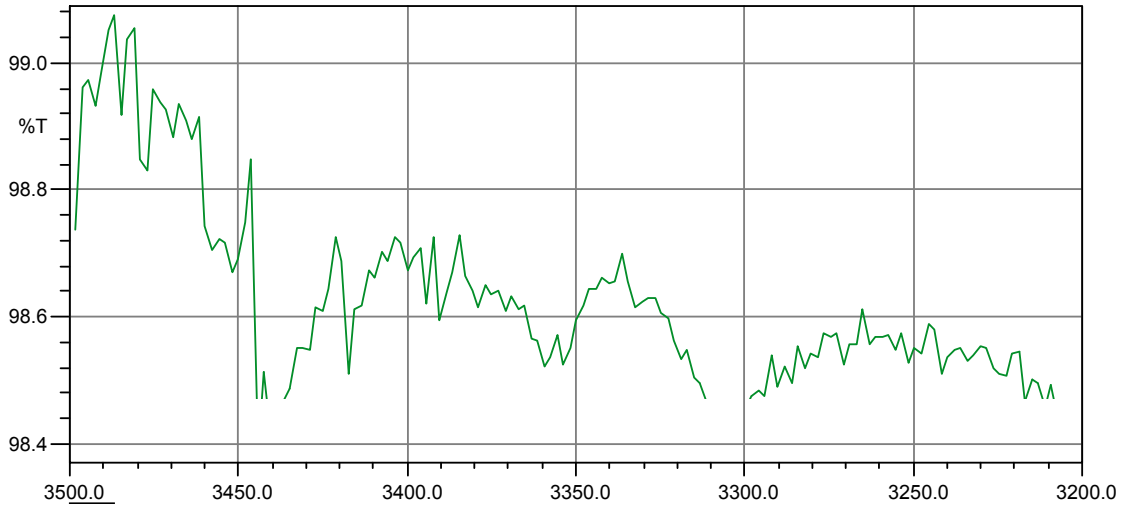


**Figure 7.8** IR of Polymer **7.1** (expansion from 3500 $cm^{-1}$ to 3200 $cm^{-1}$).

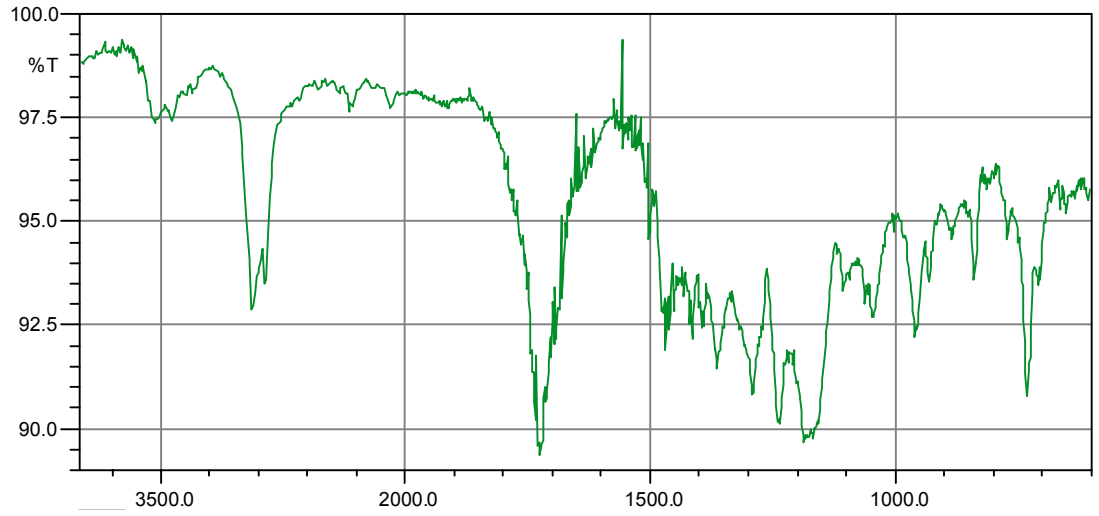


**Figure 7.9** IR of Polymer **7.3**:

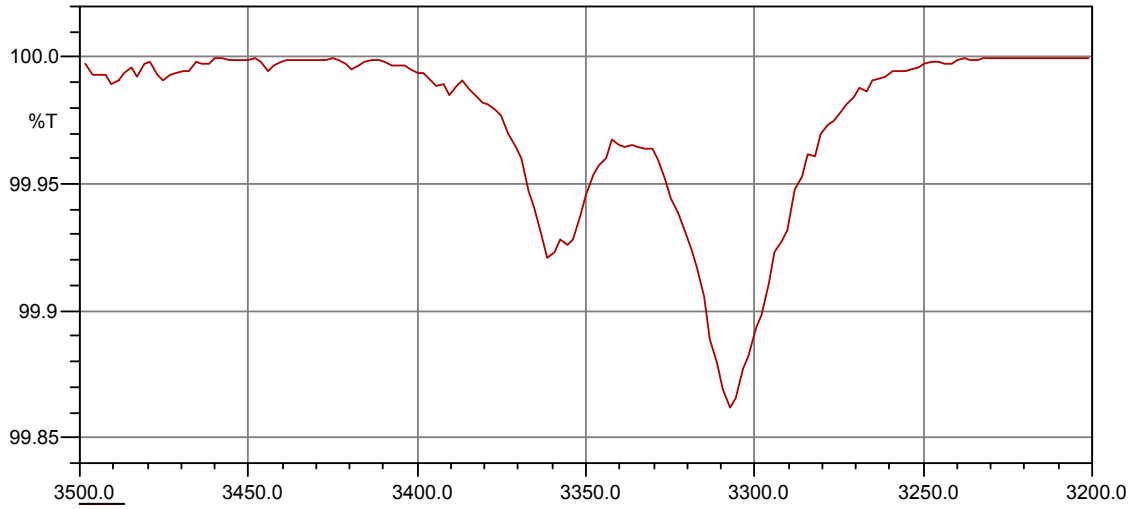


**Figure 7.10** IR of Polymer **7.3** (expansion from 3500 $cm^{-1}$ to 3200 $cm^{-1}$).

**Preparation of the polymer solutions for exposure to microspheres:**

Polymer **7.3** (20.0 mg, 5.95 x $10^{-5}$ mmol) was taken up in a small amount (~1 mL) of THF. Dioctyl sulfosuccinate, sodium salt (100 mg, 0.225 mmol) was dissolved in 100 mL of water. The THF solution was added dropwise to the vigorously stirred surfactant solution. This mixture was then heated at ~50$^{o}$ C for 12 hours, then diluted to a total volume of 1.0 L (Stock A). 10 mL of Stock A was lyophilized, then redissolved in 20 mL of 0.1 M sodium phosphate buffer. 1 mL (containing 10 μg of polymer) of this buffered polymer solution was placed into an Eppendorf tube containing 0.5 mg of streptavidin coated polystyrene microspheres. The Eppendorf tube was capped and placed onto a mechanical wrist shaker for 12 h. The agglutinated composite was found to be immobilized on the side of the capsule as seen in Figure 7.1.

**SEM Images:**

Samples of **7.1** and **7.3** exposed to streptavidin coated beads were prepared for SEM by placing them onto an aluminum sample plate which was covered with a conducting graphitic tape. The samples were placed in a vacuum sputterer and coated with 0.40 nm of gold. Images were obtained digitally on a Hitachi 2500 Delta (Figures 7.11-7.13).

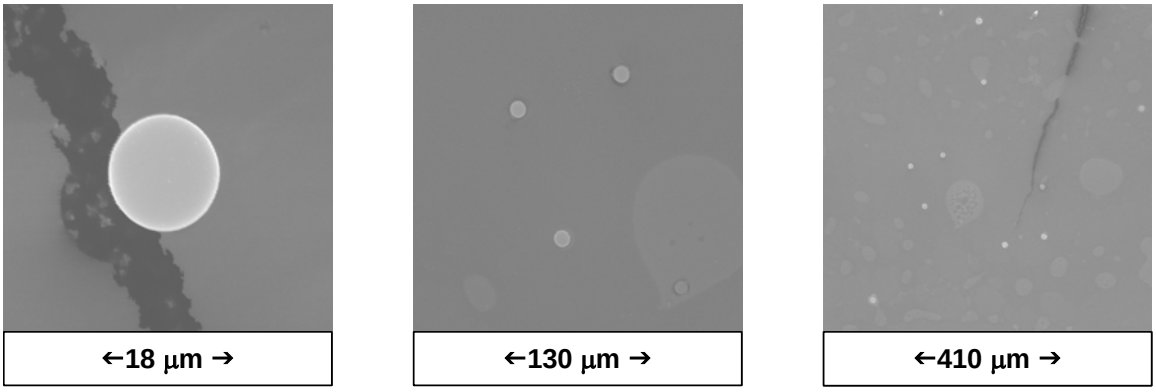


**Figure 7.11** Control Sample: Polymer **7.1** + streptavidin coated polystyrene microspheres.

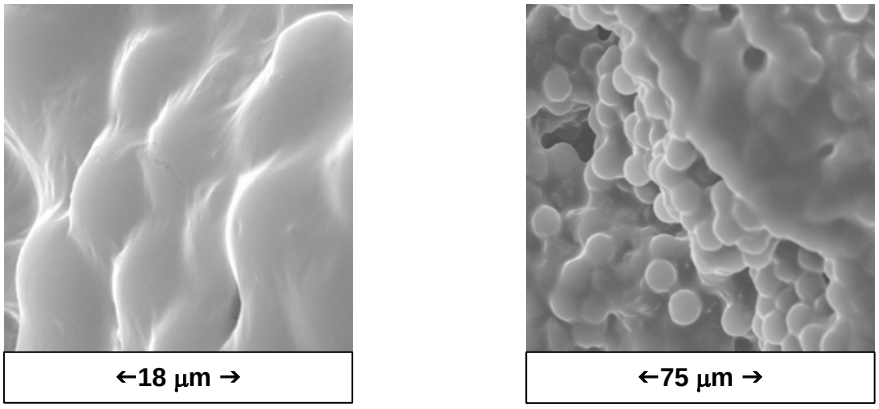


**Figure 7.12** Polymer **7.3** combined with streptavidin coated polystyrene spheres.

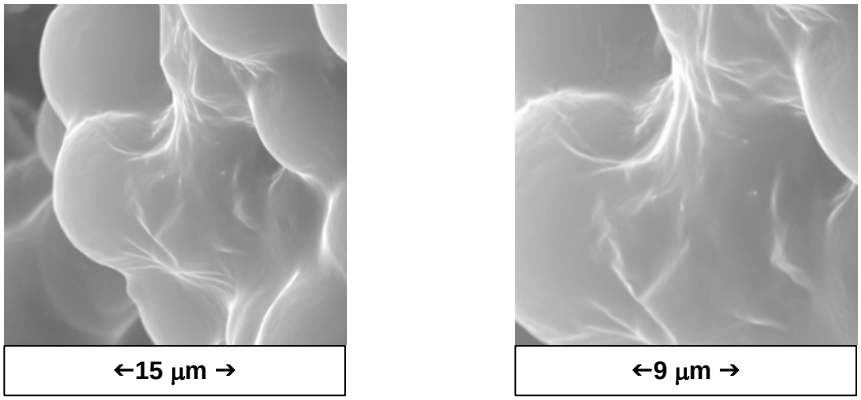


**Figure 7.13** Polymer **7.3** combined with streptavidin coated polystyrene spheres.

**Stoichiometric Calculations:** Initial calculations used to estimate the approximate percent functionalization of the polymer:

Bangs Laboratories states that 1 mg of streptavidin coated polystyrene microspheres (Product Code: CP01N/5622) can bind 0.098 μg of biotin. Thus, the 0.5 mg of beads utilized in this experiment must bind 0.049 μg of biotin. Assuming perfect binding (1:1 streptavidin:biotin) this would mean that 10 μg of polymer (2400 g/mol-repeat) would be ~5% functionalized.

A titration experiment was then performed with free streptavidin to confirm this approximation. A buffered polymer solution of 15 mg/L (Stock B) was prepared for this experiment—the dilutions per flask are listed in the table below. 1 μg of streptavidin was added to each flask. Aldrich strepavidin can bind 14 pg (0.057 pmol) of biotin per μg. Streptavidin *may* bind up to four biotin molecules, but aggregation can occur if only 2 biotin molecules from separate polymer molecules are bound. To further complicate the matter, *inter*polymer biotin binding must compete with *intra*polymer biotin binding. Thus, the table below shows a range of binding modes (2,3,4). As the spectroscopic changes began with the third dilution (flask 3), the minimum percent functionalization can be found here assuming a binding mode of only 2 biotin molecules per streptavidin.

**Table 7.1** Serial dilutions of polymer **7.3** and titration assay with biotin to determine percent loading.

| Flask | 1 | 2 | 3 | 4 | 5 |
|---|---|---|---|---|---|
| mL stock B | 1.0 | 0.20 | 0.04 | 0.008 | 0.00016 |
| μg polymer | 15.0 | 3.0 | 0.6 | 0.12 | 0.024 |
| pmol of polymer | 6.25 | 1.25 | 0.250 | 0.050 | 0.010 |
| 4:1 biotin:streptavidin | - | - | 0.057 / 0.250 = 23% | - | - |
| 3:1 biotin:streptavidin | - | - | 0.043 / 0.250 = 17% | - | - |
| 2:1 biotin:streptavidin | - | - | 0.029 / 0.250 = 12% | - | - |

## 7.5 References and Notes


1. M. Schlupp, T. Weil, A. J. Berresheim, U. M. Wiesler, J. Bargon and K. Müllen, *Angew. Chem.*, 2001, **40**, 4011; T. M. Swager, *Acc. Chem. Res*, 1998, **31**, 201; D. T. McQuade, A. E. Pullen and T. M. Swager, *Chem.Rev.*, 2000, **100**, 2537; Q. Zhou and T. M. Swager, *J. Am. Chem. Soc.*, 1995, **117**, 12593.

*2.* L. A. Samuelson, D. L. Kaplan, J. O. Lim, M. Kamath, K. A. Marx and S. K. Tripathy, *Thin Solid Films*, 1994, **242**, 50; K. Faid and M. Leclerc, *Chem. Commun.*, 1996, 2761; M. Hiller, C. Kranz, J. Huber, P. Bäuerle and W. Schuhmann, *Adv. Mater.*, 1996, **8**, 219.

3. S. Bernier, S. Garreau, M. Bera-Aberem, C. Gravel and M. Leclerc, *J. Am. Chem. Soc.*, 2002, **124**, 12463; H. A. Ho, M. Boissinot, M. G. Bergeron, G. Corbeil, K. Dore, D. Boudreau and M. Leclerc, *Angew. Chem.*, 2002, **41**, 1548.

4. B. S. Gaylord, A. J. Heeger and G. C. Bazan, *J. Am. Chem. Soc.*, 2003, **125**, 896; B. S. Gaylord, A. J. Heeger and G. C. Bazan, *Proc. Nat. Acad.Sci.*, 2002, **99**, 10954; D. L Wang, X. Gong, P. S. Heeger, F. Rininsland, G. C. Bazan and A. J. Heeger, *Proc. Nat. Acad. Sci.*, 2002, **99**, 49.

5. S. A. Kushon, K. D. Ley, K. Bradford, R. M. Jones, D. McBranch and D. Whitten, *Langmuir*, 2002, **18**, 7245.

6. S. Okada, S. Peng, W. Spevak and D. Charych, *Acc. Chem. Res.*, 1998, **31**, 229; J. J. Pan and D. Charych, *Langmuir*, 1997, **13**, 1365.

7. U. H. F. Bunz, *Chem. Rev.*, 2000, **100**, 1605.

8. C. E. Halkyard, M. E. Rampey, L. Kloppenburg, S. L. Studer-Martinez and U. H. F. Bunz, *Macromolecules*, 1998, **31**, 8655; T. Miteva, L. Palmer, L. Kloppenburg, D. Neher and U. H. F. Bunz, *Macromolecules*, 2000, **33**, 652.

9. N. DiCesare, M. R. Pinto, K. S. Schanze and J. R. Lakowicz, *Langmuir*, 2002, **18**, 7785; C. Y. Tan, M. R. Pinto and K. S. Schanze, *Chem. Commun.*, 2002, 446; M. R. Pinto and K. S. Schanze, *Synthesis*, 2002, 1293.

10. B. Erdogan, J. N. Wilson and U. H. F. Bunz, *Macromolecules*, 2002, **35**, 7863; F. Babudri, D. Colangiuli, P. A. Di Lorenzo, G. M. Farinola, O. H. Omar and F. Naso, *Chem. Commun.*, 2003, 130.

11. Y. Wang, B. Erdogan, J. N. Wilson and U. H. F. Bunz, see attached ms.

12. S. Crapatureanu, R. Serbanescu, S. B. Brevitt and R. Kluger, *Bioconjugate Chem.*, 1999, **10**, 105.

# Chapter 8

# Nanostructuring of Poly(aryleneethynylene)s: Formation of Nanotowers, Nanowires, and Nanotubules by Templated Self-Assembly

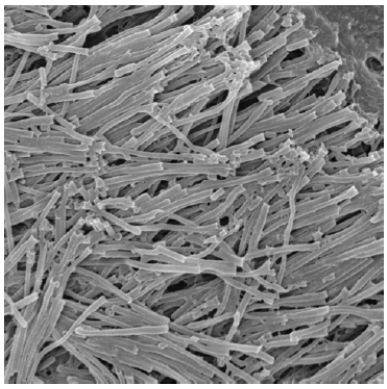

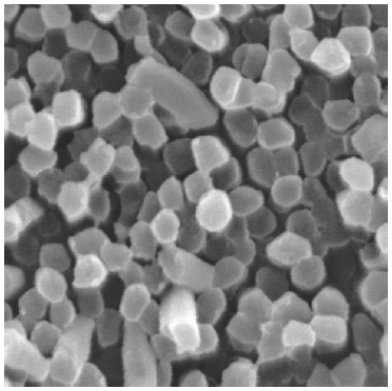

## 8.1 Introduction

We report novel, nanoscale polyaryleneethynylene (PAE) morphologies that are created by a solution molding process utilizing nanostructured anodiscs (Whatman filter disks, alumina wafers). Depending upon the molecular structure of the utilized PAE, different selfassembled nanostructures are formed during templating. Nanostructuring of conjugated polymers is an important process that modifies their electronic and electron transport properties.[1-3]

Nanostructuring plays a crucial role in device applications, for example in the fabrication of photovoltaic cells, where self-assembly of an interpenetrating network of a conjugated polymer and an *n*-semiconductor is the critical factor for success.[4]

Nanostructuring is of interest in photonic band gap materials[5] and fabrication of heterojunction devices in which two different conjugated polymers have to interact intimately to increase their interface.[4] In many cases, conjugated polymers show self-assembly into nanoscopic structures; however, their self-assembly modes are difficult to control and not always predictable.[6] Thus, it is of interest to develop processes that furnish conjugated polymers with an engineered nanoshape. A potent and elegant solution for this problem was developed by Martin for organic, inorganic, and metallic nanostructures utilizing templating procedures.[3] This approach utilizes filter anodiscs that are commercially available, are inexpensive, and display pores of defined size and diameter. The material of choice is deposited into these pores, and the anodisc is dissolved in dilute base or acid to give nanotubes of excellent quality. While metallic and insulator nanostructures have been made by this method, only very few examples of conjugated polymers have been structured by this method.[3] Polyaniline, polythiophene, and polypyrrole are examples of polymers that form electrochemically *in* the preformed pores of the filter disk.[3] However, there is a large number of conjugated polymers available that do *not* form by electropolymerization. As a result, these materials have to be nanostructured in a different way. In this paper, we describe the fabrication of semiconducting nanotowers, nanowires, and nanotubules by solutionphase self-assembly of poly(aryleneethynylene)s **8.1**-**5** (Figure 8.1).[7]

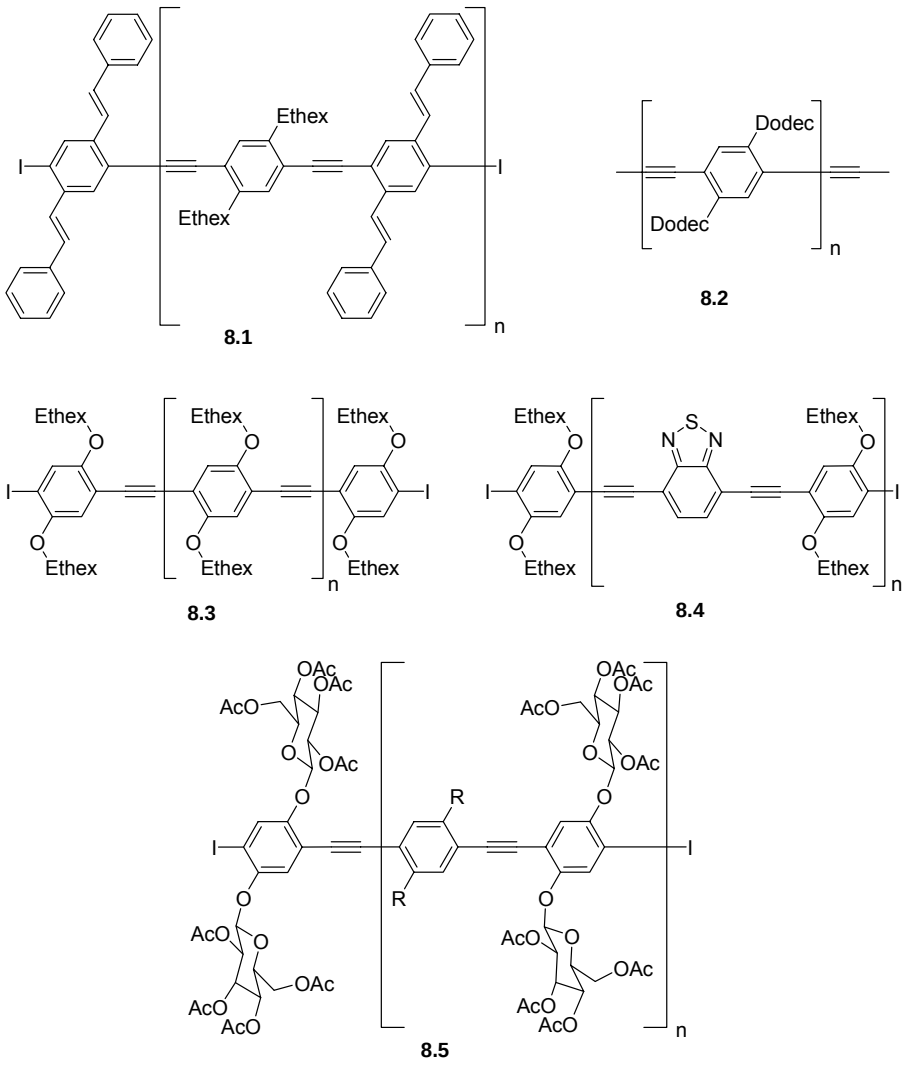


**Figure 8.1** Polymers **8.1-5** utilized in the preparation of nanostructures

## 8.2 Results and Discussion

In the first experiment, a dilute solution of polymer **8.1** was drop cast (Figure 8.2, geometry II) onto a Whatman filter anodisc[8] and allowed to dry. Subsequent dissolution of the alumina mask led to products that had formed nanotubes of poor quality (by SEM). Utilizing dilute solutions of **8.1** led to fragile nanostructures that were washed away when dissolving the anodisc. In subsequent experiments, we utilized more concentrated solutions (10 g/mL, see experimental details in the Supporting Information). These

solutions were utilized mostly in geometry II, and gave more robust products that were examined by SEM. Polymer **8.1** forms both

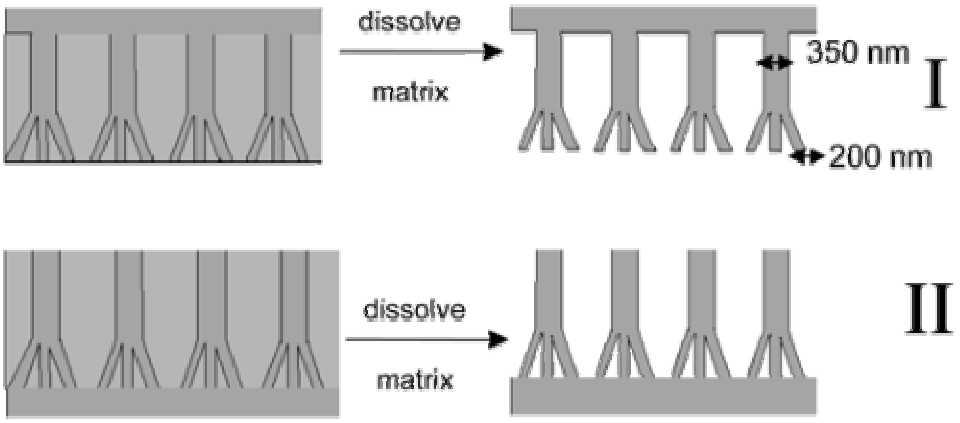


**Figure 8.2.** Schematic of the formation of PAE nanotowers and nanotubes.

filled and hollow nanotubes with an aspect ratio of approximately 32 (Figure 8.3a). The width of the tubes ranges from 300 to 350 nm, which is in good agreement with the specifications of the filter pores. The length of the tubes ranges from 2 to 10 $\mu$m. The aspect ratio is quite low (7-32). Even though the length of the channels in the Whatman filters is 60 $\mu$m, the pores of the disk are only slightly penetrated by the viscous polymer solution. annealing of the anodisc/polymer hybrid structure did not lead to better penetration of the polymer into the inorganic pores. Similarly dimensioned nanostructures were observed after dissolution of the anodisc. We wanted to explore the influence of PAE structure on the process of the nanowire formation. As a consequence, we investigated PAEs **8.2-5.** The heterocyclic polymer **8.4** (Figure 8.3b) formed well-developed wires that seemed to penetrate the pores almost completely. The dimension of these wirelike structures is 350 nm x 30 $\mu$m, and the aspect ratio of these solid wires is approximately 90. The wires are well developed over the entire area of the film. Visible

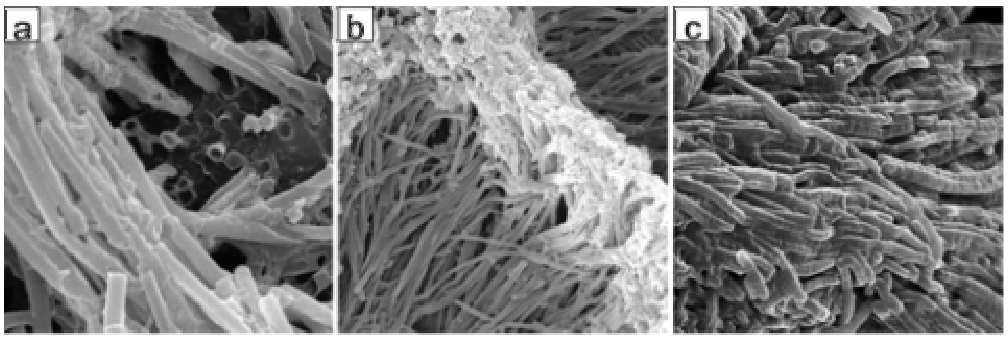


**Figure 8.3.** (a) Polymer **8.1.** Picture dimensions are 6 x 6 $\mu$m. Drop-cast films are observed. The junction of hollow and solid tubules is shown. (b) Polymer **8.4**. Picture dimension is 18 x 18 $\mu$m. Well visible is the wire-like characteristic of the polymer preparation. The aspect ratio of the wires is in excess of 50. The nanostructures are almost defect-free. The cauliflower geometry of the top is visible. (c) PPE **8.3.** The picture dimension is 6 x 6 $\mu$m (right). Particularly interesting is the horizontal striation of 140 nm in these blunted wires. The aspect ratio of tubes **8.3** is approximately 140.

is the splicing of the template that is preserved in the top part of the wires. This splicing leads to a cauliflowerlike topology that is typical for a geometry II (Figure 8.2) preparation. The heterocyclic polymer **8.4**, an excellent film-former, is almost ideal for the generation of tubules and wires of great length. The more polar, sugar-substituted, and methanolsoluble PPE **8.5** forms a different nanoscale morphology altogether. For **8.5**, short "macaroni" tubules are formed (Figure 8.4a). Their outer diameter is 330 nm, while the diameter of the "eye" is 210 nm. The tubules are 2 $\mu$m long, and their aspect ratio is only slightly above 6. Concentrated solutions give isolable macaroni structures, while dilute solutions give materials that fragment upon dissolution of the anodisc. In the case of **8.5,** the hollowness of the tubes is visible via defects that lead to some holes in the walls of the tubes. The highly hydrophobic didodecyl-PPE **8.2** forms short nanotubes that show the cauliflower geometry of the spliced matrix (Figure 8.4b). We examined as well a moderately polar PPE, bisethylhexyloxy-PPE **8.3**. This PPE furnished long, welldeveloped wire-type structures that seem to be solid, completely filled, 200-300 nm

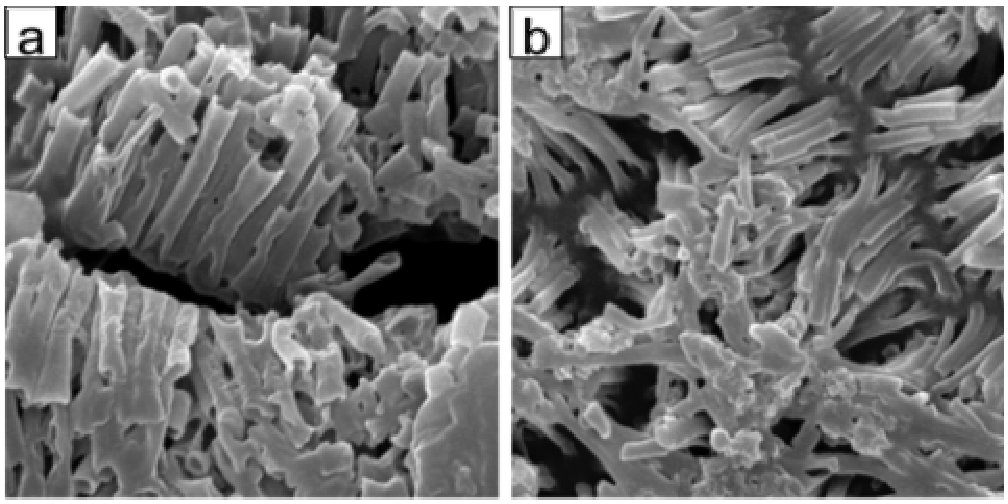


**Figure 8.4.** Sugar-PPE **8.5** forms thick macaroni-type structures. The thickness of the wall in these tubes is 60 nm and the picture dimensions are 6 x 6 $\mu$m. On the right-hand a picture of the cauliflower geometry of the didodecyl-PPE **8.2.** The picture dimensions are 9 x 9 $\mu$m. The splitting into the narrow base-wires is well visible and represents the topology of the Whatman filter anodisc.

thick, and up to 43 $\mu$m long. Aspect ratios of 140-215 result. These materials seem to penetrate the membrane almost completely. Additionally, these tubules show (Figure 8.2c) horizontal striations that are slightly irregular but have an average width of 140 nm. In all of the examined cases, we obtain nanostructures which are covered by the bulk material in the form of a thin film on the bottom. An interesting observation is that the formation of the nanostructures (see Experimental) is not visibly correlated with the molecular weights[9] of the examined PAEs.

## 8.3 Conclusion

In conclusion, we have extended Martin's nanostructuring process to PAE's. Up to now, conjugated polymers have been *formed* inside the pores of anodiscs. We have demonstrated that PAE's can be *cast* into the mesopores of anodiscs to give free-standing, high aspect ratio nanostructures of excellent quality after the removal of the template. The nanostructuring of conjugated materials may lead to advancement in

semiconductor applications by increasing the surface area of the polymer under consideration. At the moment, we are attempting to process the nanostructrures into thin films of homogeneous thickness by spin casting, and our future work in this area will focus on the construction of photovoltaic and light emitting devices in collaboration with electrical engineers.

## 8.4 Experimental

Synthesis of the polymers **8.1-5** has been described.[10] Solutions of the polymers were prepared in chloroform or THF by heating the respective polymer. Dilute solutions were approximately 1 mg polymer/mL solvent and concentrated solutions were 10-15 mg polymer/mL solvent. Films were drop-cast from chloroform onto the commercially available anodiscs[8] (Whatman Anodisc 47; 0.2 μm pore size); approximately 0.5 mL of the solution were utilized per film. After allowing the solvent to evaporate for 1 h, the discs were affixed onto a stationary phase (3M clear packing tape), and placed in a 1 mol/L NaOH solution for 1 h to allow the template to dissolve completely (See Table 8.1 below for geometry details). The films were rinsed three times with deionized water, and dried briefly in a vacuum oven at 90-100 $^{o}$C. The samples were cut into small portions (pie pieces, 1 cm length) to fit as many as possible samples on the sample holder. The samples were placed into a sputterer (Denton Vacuum Inc., Desk II), and 0.4 nm of Au was sputtered onto the films. The samples were then placed in an scanning electron microscope (Hitachi 2500 Delta), and the pictures were obtained digitally (Figures 8.5-8.8).

**Table 8.1.** Properties of Nanostructures Formed by Poly(aryleneethynylene)s **8.1-5** Utilizing Whatman Filter Anodiscs

| **Polymer** | **1** | | **2 3** | | **4** | **5** | |
|---|---|---|---|---|---|---|---|
| Sample Geometry | **I** | **II** | **II** | **II** | **I** | **II** | **I** |
| Observed structure, pristine | Only tubules | Tubules and towes | Towers | Towers | Towers, with cauliflower tops Towers and tubules | | Only tubules |
| Length | Thin films 2.5 µm | Thick films > 9.5 µm | Thin films 7 µm | Thick Films 43 µm | Thick film 30 µm | Thick films tower 12 µm tubule 3 µm | Thin films 2.1 µm |
| Width | Thin films DI 250 nm Do 350 nm | Thick films 300 nm | Thin films 300 nm | Thick films 200 – 300 nm | Thick film 350 nm | Thick films DI 270 nm Do 340 nm | Thin films DI 210 nm Do 330 nm |
| Aspect ratio | 7 | > 32 | 23 | Up to 140 | 86 | Towers 34 Tubules 8.6 | 6.4 |
| Pn<br>PDI | 55<br>2.8 | | 512<br>3.2 | 316<br>2.4 | 19<br>2.8 | | 75<br>2.2 |
| Comment | Thin films give fragile tubules. | High density of fibers prevented accurate measuremen t of length of towers. | Predomina ntly rigid towers randomly spaced Geometry I did not give useful structures | Thick films show highly textured fibers. Geometry I did not give useful structures | Dense well developed towers, and some tubules observed at base for thick films | Dense well developed towers, and some tubules observed on top of film | Thin films give fragile tubules. |
| The utilized filters have pore width of 340 nm, Anodisc 47, 0.2 µm. | | | | | | | |

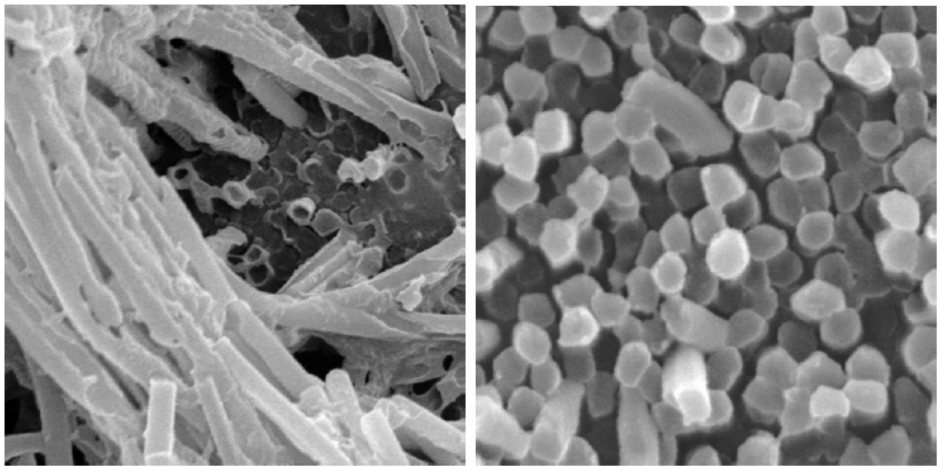

**Figure 8.5** Polymer **8.1** Picture dimensions are 6 x 6 µm (left) and 4.5 x 4.5 µm (right). Drop-cast films. On the left picture the junction of hollow and solid tubules is shown. The right picture shows a perfect fill of the mesopores.

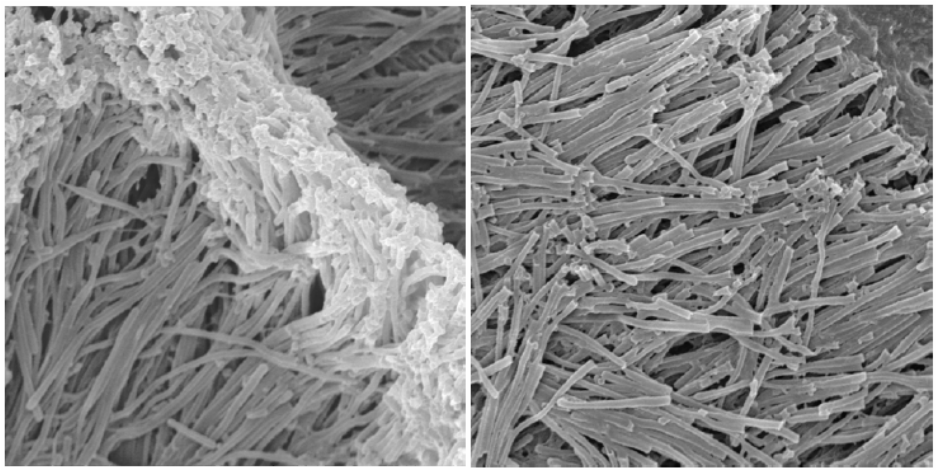

**Figure 8.6** Polymer **8.4**. Picture dimensions are 18 x 18 µm in both cases. Well visible is the wire-like characteristic of the polymer preparation. The aspect ratio of the wires is in excess of 50. Especially remarkable is that the nanostructures are almost defect-free. On the left side the cauliflower geometry of the top is visible. This geometry mirrors the geometry of the utilized Whatman mask.

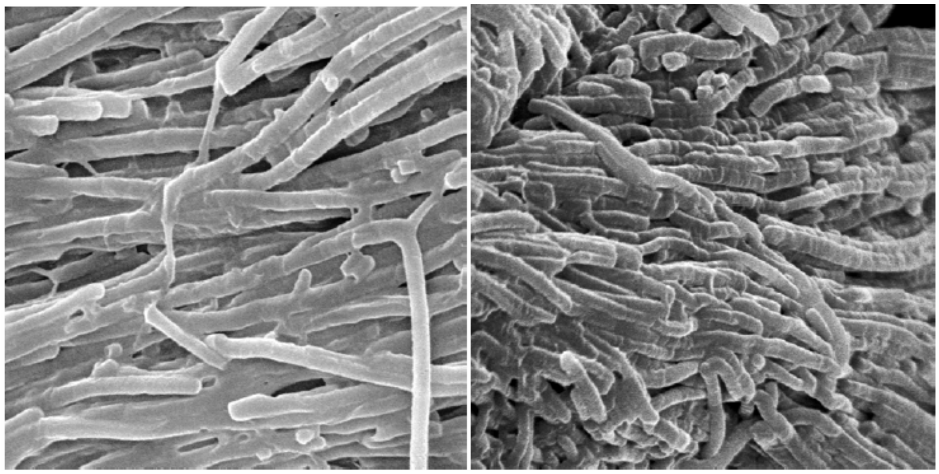

**Figure 8.7** PPE **8.3.** The picture dimensions are 9 x 9 µm (left) and 6x6 µm (right). Particularly interesting is the horizontal striation of 140 nm in these blunted wires. The aspect ratio of **8.3** is approx. 30.

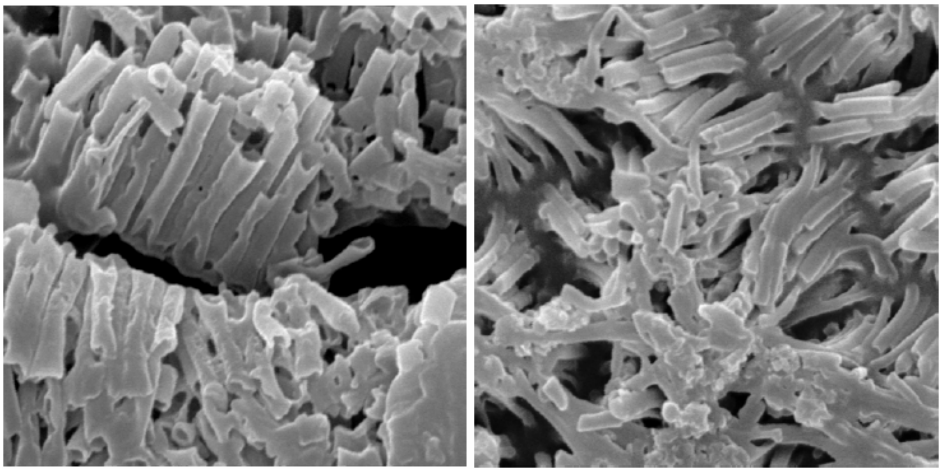

**Figure 8.8** Sugar-PPE **8.5** forms thick macaroni-type structures. The thickness of the wall in these tubes is 60 nm and the picture dimensions are 6 x 6 µm. On the right hand a picture of the cauliflower geometry of the didodecyl-PPE **8.2**. The picture dimensions are 9 x 9 µm. The splitting into the narrow base-wires is well visible and represents the topology of the Whatman filter anodisc.

## 8.5 References and Notes


1. Landfester, K.; Montenegro, R.; Scherf, U.; Guntner, R.; Asawapirom, U.; Patil, S.; Neher, D.; Kietzke, T. *Adv. Mater*. **2002**, *14*, 651. (b) Kulbaba, K.; Cheng, A.; Bartole, A.; Greenberg, S.; Resendes, R.; Coombs, N.; Safa-Sefat, A.; Greedan, J. E.; Stover, H. D. H.; Ozin, G. A.; Manners, I. *J. Am. Chem. Soc.* **2002**, *124*, 12522. Raez, J.; Manners, I.; Winnik, M. A. *J. Am. Chem. Soc.* **2002**, *124*, 10381.

2. (a) Grimsdale, A. C.; Bauer, R.; Weil, T.; Tchebotareva, N.; Wu, J. S.; Watson, M. *Synthesis* **2002**, *1229*. (b) Wiesler, U. M.; Weil, T.; Müllen, K. Top. *Curr. Chem.* **2001**, *212*, 1. (c) Morgenroth, F.; Kübel, C.; Müllen, K. J. Mater. Chem. **1997**, 7, 1207. (d) Moon, J. H.; Swager, T. M. *Macromolecules* **2002**, *35*, 6086.

3. (a) Sapp, S. A.; Mitchell, D. T.; Martin, C. R. *Chem. Mater*. **1999**, *11*, 1183. (b) Cepak, V. M.; Hulteen, J. C.; Che, G.; Jirage, K. B.; Lakshmi, B. B.; Fisher, E. R.; Martin, C. R.;Yoneyama, H. *Chem. Mater*. **1997**, *9*, 1065. (c) Martin, C. R. *Chem. Mater.* **1996**, *8*, 1739. (d) Martin, C. R. *Acc. Chem. Res*. **1995**, *28*, 61. (e) Cai, Z. H.; Martin, C. R. *J. Am. Chem. Soc*. **1989**, *111*, 4138. (f) Kros, A.; van Hovell, W. F. M.; Sommerdijk, N. A. J. M.; Nolte, R. J. M. *Adv. Mater*. **2001**, *13*, 1555.

4. (a) Wudl, F. J. *Mater. Chem*. **2002**, 1959. (b) Yu, G.; Gao, J.; Hummelen, J. C.; Wudl, F.; Heeger, A. J. *Science* **1995**, *270*, 1789. (c) Friend, R. H. *Phys. Scr.* **1996**, *T66*, 9. (d) Granstrom, M.; Petritsch, K.; Arias, A. C.; Lux, A.; Andersson, M. R.; Friend, R. H. *Nature* **1998**, *395*, 257.

5. (a) Müller, M.; Zentel, R.; Maka, T.; Romanov, S. G.; Torres, C. M. S. *Adv. Mater.* **2000**, *12*, 1499. (b) Deutsch, M.; Vlasov, Y. A.; Norris, D. J. *Adv. Mater*. **2000**, *12*, 1176.

6. For the self-assembly of PPEs into nanocables see: (a) Samori, P.; Severin, N.; Müllen, K.; Rabe, J. P. *Adv. Mater*. **2000**, *12*, 579. (b) Samori, P.; Francke, V.; Müllen, K.; Rabe, J. P. *Chem. Eur. J*. **1999**, *5*, 2312. (c) Samori, P.; Francke, V.; Mangel, T.; Müllen, K.; Rabe, J. P. *Opt. Mater.* **1998**, *9*, 390. (d) Perahia, D.; Traiphol, R.; Bunz, U. H. F. *Macromolecules* **2001**, *34*, 151. (e) Altmann, M.; Bunz, U. H. F. *Angew. Chem.* **1995**, *34*, 569.

7. (a) Bunz, U. H. F. *Chem. Rev*. **2000**, *100*, 1605. (b) Bunz, U. H. F. *Acc. Chem. Res*. **2001**, *34*, 998. (c) Kloppenburg, L.; Song, D.; Bunz, U. H. F. *J. Am. Chem. Soc.* **1998**, *120*, 7973. (d) Kloppenburg, L.; Jones, D.; Bunz, U. H. F. *Macromolecules* **1999**, *32*, 4194. (e) Erdogan, B.; Wilson, J. N.; Bunz, U. H. F. *Macromolecules* **2002**, *35*, 7863. (f) Wilson, J. N.; Windscheif, P. M.; Evans, U.; Myrick, M. L.; Bunz, U. H. F. Macromolecules 2002, 35, 8681. (g) Wilson, J. N.; Waybright, S. M.; McAlpine, K.; Bunz, U. H. F. *Macromolecules* **2002**, *35*, 3799. (h) Bangcuyo, C. G.; Evans, U.; Myrick, M. L.; Bunz, U. H. F. *Macromolecules* **2001**, *34*, 7592. (i) Halkyard, C. E.; Rampey, M. E.; Kloppenburg, L.; Studer-Martinez, S. L.; Bunz, U. H. F. *Macromolecules* **1998**, *31*, 8655.

8. Whatman claims a pore size of 0.2 μm. Our observations of blank disks reveal that only one side displayed pores of 0.2 μm. The opposite side cleary displays pores of greater size (0.3-0.35 μm) but they are less numerous. Obviously a fusion of channels must take place during the anodization process, which is in fact revealed by the observed geometries of the polymer structures.

9. Ricks, H.; Choudry, U. H.; Marshall, A. J.; Bunz, U. H. F. *Macromolecules* **2003**, *36*, 1424.

10. (a) Kloppenburg, L.; Song, D.; Bunz, U. H. F. *J. Am. Chem. Soc.* **1998**, *120*, 7973. (b) Kloppenburg, L.; Jones, D.; Bunz, U. H. F. *Macromolecules* **1999**, *32*, 4194. (c) Erdogan, B.; Wilson, J. N.; Bunz, U. H. F. *Macromolecules* **2002**, *35*, 7863. (d) Wilson, J. N.; Windscheif, P. M.; Evans, U.; Myrick, M. L.; Bunz, U. H. F. *Macromolecules* **2002**, *35*, 8681. (e) Wilson, J. N.; Waybright, S. M.; McAlpine, K.; Bunz, U. H. F. *Macromolecules* **2002**, *35*, 3799. (f) Bangcuyo, C. G.; Evans, U.; Myrick, M. L.; Bunz, U. H. F. *Macromolecules* **2001**, *34*, 7592.

# Chapter 9

# Cruciform π-systems: Hybrid phenylene-ethynylene/phenylene-vinylene oligomers

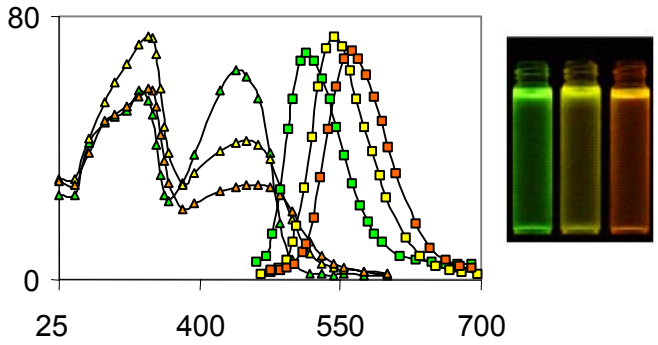


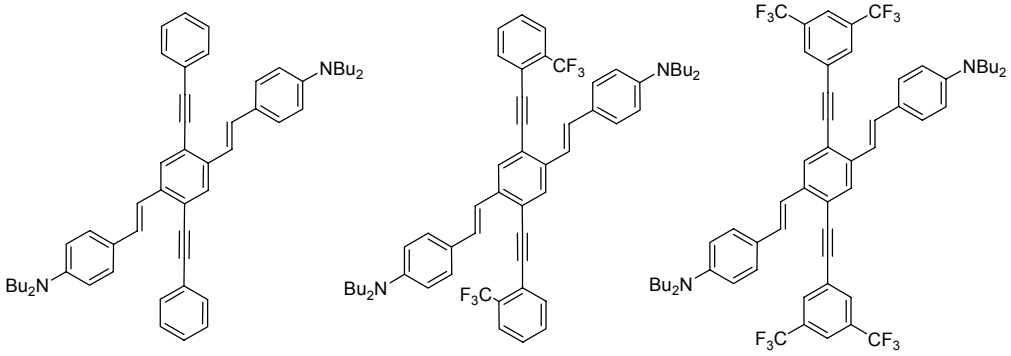


## 9.1 Introduction

Conjugated materials are important as active layers in device applications. Poly(*para*-paraphenylenevinylene)s (PPV) have been tremendously successful for device fabrication, due to their balanced hole and electron injection capabilities.[2] Recently, polymers that combine structural features of poly(paraphenyleneethynylene)s (PPE), and

that of the PPVs have been reported (Figure 9.1).[3] Formal hybrids such as A behave considerably

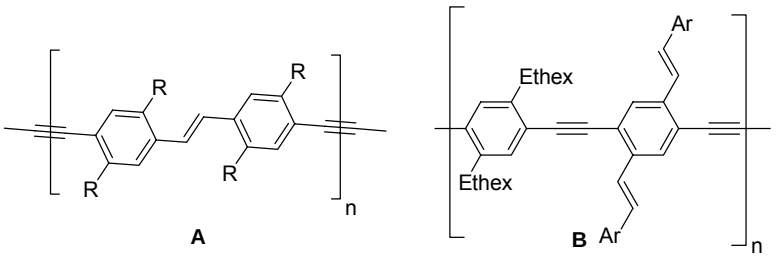


**Figure 9.1** Examples of PPE-PPV hybrids.

more like PPEs[4] than like PPVs. However, if stilbene groups are laterally attached to the benzene rings the electronic properties of the resulting polymer **B** are different from both PPV as well as PPEs.[5] Is the change in properties indigenous to the polymer backbone, or are single, isolated, cruciform pentamers "cut out" of **B** responsible for the observed electronic effects? We find that the optical, electronic and redox properties of **B** reside mostly in their pentameric cruciform modules **9.5**. The incorporation of **9.5** into the conjugated polymer chain does not influence the electronic properties of the system much.

## 9.2 Results and Discussion

Starting from the bisphosphonate **9.1** a Horner[6] reaction produced the distyrylbenzenes **9.3a-e** in good to excellent yields (Scheme 9.1, Table 9.1). In the second step **9.3a-e** were coupled to terminal alkynes utilizing $(Ph_3P)_2PdCl_2$ and CuI in piperidine.[7] In the case of the synthesis of **8.5g** triethylamine was utilized to avoid nucleophilic addition of the piperidine to the aromatic nucleus. In the cases of **9.5c,d** the products were quite insoluble and therefore the yield was lower than average (53% and 63%); **9.5a-g** were purified by double crystallization.

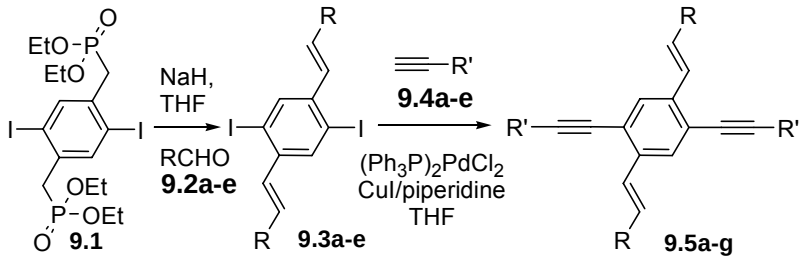


**Scheme 9.1.** Formation of cruciforms **9.5a-g**.

**Table 9.1.** Substituent key and reaction yields for **9.3a-e** and **9.5a-g.**

| | **9.5a** | **9.5b** | **9.5c** | **9.5d** | **9.5e** | **9.5f** | **9.5g** |
|---|---|---|---|---|---|---|---|
| R | 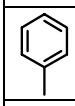 | 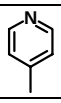 | 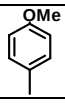 | 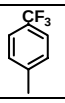 | 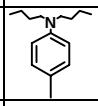 | 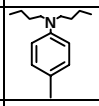 | 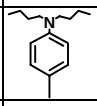 |
| R' |  |  |  |  |  |  |  |
| **9.3** | 97% | 77% | 61% | 72% | 72% | - | - |
| **9.5** | 81% | 77% | 53% | 63% | 91% | 67% | 76% |

The absorption data of **9.5a-g** are shown in Figure 9.2 and in Table 9.2. The $\lambda_{max}$ values correspond qualitatively well with the expected ordering predicted from the substituent patterns. Cruciform **9.5d** has the largest and **9.5g** the lowest optical band gap. The three oligomers **9.5e-g** show a nice correlation of decreasing band gap with increasing $CF_3$ substitution. The donor-acceptor interaction decreases the band gap. To obtain more information we investigated the electrochemistry of **9.5a-g** (Figure 9.4). The cruciforms **9.5a-g** show oxidation potentials that are in qualitative agreement with their calculated (RHF 6-31G**, Fig. 9.3 ) HOMO values. The electrochemical reduction data is difficult

**Table 9.2** Summary of absorbance and emission data for cruciforms **9.5** in chloroform and hexane; **9.5d** is not not soluble in hexane. **9.5a-d** show similar spectra in both hexane and chloroform, while **9.5e-g** show dramatic solvatochromicity in emission.

| | **9.5a** | **9.5b** | **9.5c** | **9.5d** | **9.5e** | **9.5f** | **9.5g** |
|---|---|---|---|---|---|---|---|
| Ab $CHCl_3$ | 331, 365 sh | 330 | 339,374 sh | 330, 363 sh | 339, 439 | 342, 444 | 345, 458 |
| Em $CHCl_3$ | 420, 442 | 446, 526 sh | 432, 454 | 419, 434 sh | 514 | 543 | 563 |
| $\phi$ $CHCl_3$ | 0.83 | 0.28 | 0.88 | 0.92 | 0.16 | 0.20 | 0.14 |
| Ab hex | 326, 352 sh | 324, 348 sh | 334, 376 sh | - | 332, 422 | 344, 416 | 346, 420 |
| Em hex | 414, 432 | 424, 444 sh | 420, 442 | - | 472, 498 | 502, 526 sh | 524 |
| $\phi$ hex | 0.78 | 0.45 | 0.78 | - | 0.94 | 0.70 | 0.53 |

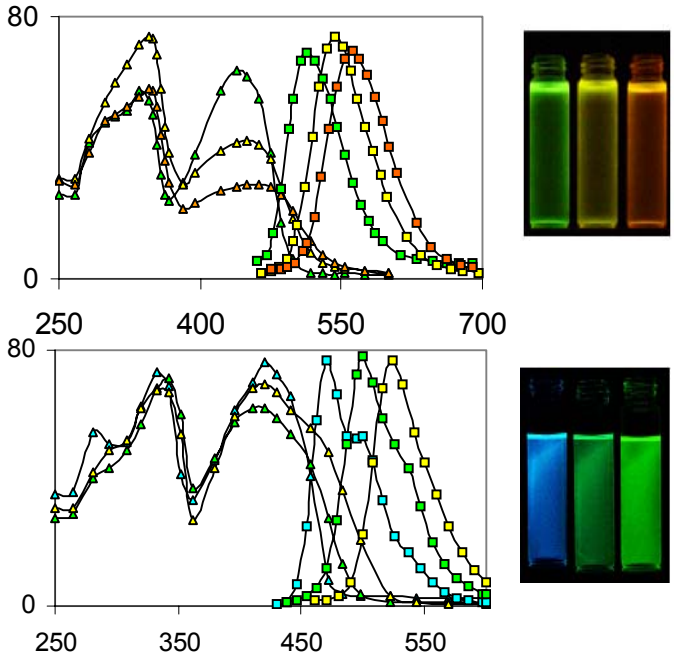


**Fig. 9.2**. Top Uv-vis and emission of **9.5e-g** in chloroform (top) and hexanes (bottom): **9.5e** (grn), **9.5f** (yel), **9.5g** (org). Absorbance (triangles) shows varying peak height, but same position, while emission (squares) clearly shows a 20+ nm shift with inclusion of $CF_3$ substituents; **9.5a-g** display solvatochromicity: their

emission in chloroform is substantially red-shifted from their emission in hexane shown at bottom, **9.5e** (blu), **9.5f** (grn), **9.5g** (yel).

to interpret for **9.5e-g** due to electron-transfer induced reactions that form dull, colored deposits on the electrodes. Thus, only onset values are given for **9.5e-g**. The reduction of **9.5c** is easier than expected in comparison to the calculated value, while reduction potential of **9.5d** is higher than expected. Not surprisingly, **9.5d** is most difficult, and **9.5e** is most easily oxidized while the electron-rich cruciforms **9.5e-g** show a second irreversible oxidation wave.

In solution all of the cruciforms were highly fluorescent ($0.45 < \Phi < 0.94$ in hexane. In chloroform the emission quantum yields were lower. The cruciforms **9.5a-d** are blue emitters but **9.5e-g** show dramatic differences in their emission that are additionally solvent dependent. In chloroform (Figure 9.2 top) the emission of **9.5e-g** changes from green to orange, while in hexane a similar trend is observed, however, the color changes from blue-green to yellow (Fig 9.2. bottom, Table 9.1). In methanol the emission of **9.5g** is weak and red. Similar effects are observed for **9.5e** and **9.5f**.

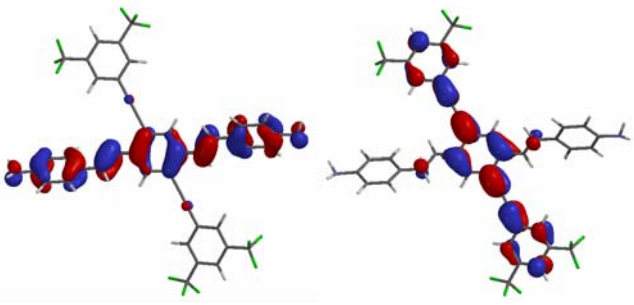

**Figure 9.3**. Frontier orbitals of **9.5g**.

The frontier orbitals of **9.5g** were inspected (RHF 6-31G**, Spartan). The HO-MO is localized on the PV branch of the cruciform while the LUMO is localized on the

PE part. HOMO and LUMO overlap only in the central benzene ring. The insensitivity of the oxidation potential of **9.5e-g** upon introduction of -$CF_3$ groups into the molecule is a consequence of the spatial separation of the HOMO and the LUMO. For **9.5a** this type of de-mixing of HOMO and LUMO is not observed and both orbitals are almost evenly distributed over the whole molecule. The excited states of **9.5e-g** must show of charge separation, which explains the sensitivity of their emission wavelength towards the polarity of the solvent. An increasingly polar solvent stabilizes the excited state and leads to a bathochromically shifted emission.

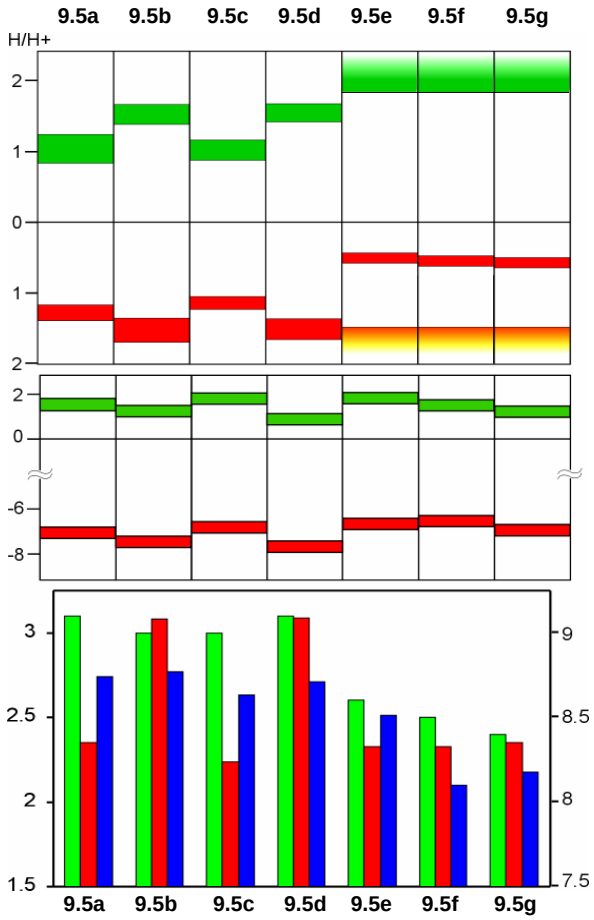


**Fig. 9.4**. Top, electrochemical bandgap with reduction in green and oxidation in red (**9.5a-g**). Faded regions correspond to an onset of oxidation/reduction that

does not reach a peak value. The range of each bar corresponds to the onset and peak values. Middle, Calculated bandgaps (reduction: green, oxidation: red). Bottom, comparison of optical (green), electrochemical (red), and calculated (blue, scale at right) bandgaps.

## 9.3 Conclusion

In summary we have made cruciforms **9.5** and examined their electronic properties. They are model compounds for the polymers of the type **B**. Conjugation along the backbone does not seem to make a large contribution in **B**. The cruciforms **B** are versatile and tune-able chromophores where the position of HOMO and LUMO can be changed almost at will by the introduction of electron donating and electron accepting substituents. The localization of the HOMO on the PV branch and that of the LUMO at the PE branch makes **9.5** cross- conjugated in a non-classical sense and extends this concept.[8,9]

## 9.4 Experimental

**General procedure for compounds 9.3a-e**: An oven-dried Schlenk flask cooled under nitrogen was charged with **9.1**, NaH (2.5 eq), and dry THF. The flask was closed with a septum, a nitrogen-filled balloon was fitted to the arm and the stopcock was opened. With mild heating (40 °C), the solution turned a vivid purple-red. The aldehyde was introduced in small portions over 1 h with a syringe either as the pure oil or dissolved in dry THF. The reaction was allowed to stir with heat for another 30 min before work-up. The small excess NaH was quenched with water and the mixture was extracted three times with chloroform. The chloroform layer was rinsed with brine and

dried with magnesium sulfate and reduced until a precipitate formed. The mixture crystallized from hexanes and was collected by suction filtration and dried under vacuum.

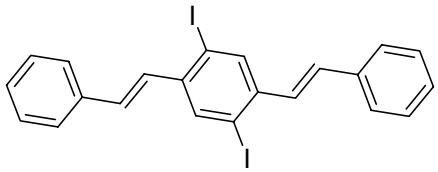

**Compound 9.3a**: Following the general procedure, **9.1** (0.630 g, 1.00 mmol), NaH (60.0 mg, 2.50 mmol), and 25.0 mL THF were combined. Benzaldehyde, (233 mg, 2.20 mmol) was then added. Work up and recrystallization yielded (422 mg, 79%) of pale yellow crystals. MP: 228°C IR: 2915.2, 2840.2, 1458.8, 1437,3, 1348.1, 1069.7, 1041.1, 951.9, 887,6, 855.5, 809.1, 748.4, 691.3, 587.8. $^{1}$H NMR ($CDCl_3$): δ8.09 (s, 2H, Ar-H), 7.55 (d, 4H, Ar-H, $J_{H,H}$ = 7.52 Hz), 7.38 (t, 4H, Ar-H, $J_{H,H}$ = 7.33 Hz), 7.30 (t, 2H, Ar-H, $J_{H,H}$ = 7.15 Hz), 7.20 (d, 2H, C=C-H, $J_{H,H}$ = 15.95 Hz), 6.99 (d, 2H, C=C-H, $J_{H,H}$ = 16.13 Hz). $^{13}$C NMR ($CDCl_3$): δ140.79, 136.54, 136.34, 135.36, 130.48, 128.82, 128.40, 126.96, 100.28.

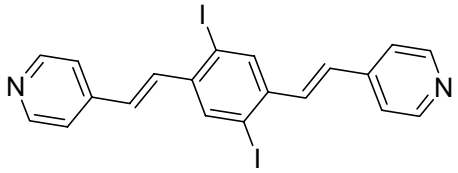

**Compound 9.3b**: Following the general procedure, **9.1** (0.630 g 1.00 mmol), NaH (60.0 mg, 2.50 mmol), and 25.0 mL THF were combined. 4-pyridine carboxaldehyde, (0.236 g 2.20 mmol) was then added. Work up and recrystallization yielded pale yellow crystals (0.413 g, 77.0%). MP: 273°C IR: 3047.4, 3030.7, 3026.6, 1560.1, 1555.6, 1051.9, 956.1, 856.1, 801.9, 731.1, 672.8. $^{1}$H NMR (300 MHz, $CDCl_3$): δ = 8.62 (d, 4H, $J_{H,H}$ = 3.84 Hz, Ar-H), 8.09 (s, 2H, Ar-H), 7.40 (m, 6H, Ar-H, C=C-H), 6.93 (d, 2H, $J_{H,H}$ = 16.2

Hz, C=C-H). $^{13}$C-NMR (400 MHz, $CDCl_3$): $\delta$ = 150.40, 143.56, 140.62, 136.91, 130.13, 128.32, 121.13, 100.42.

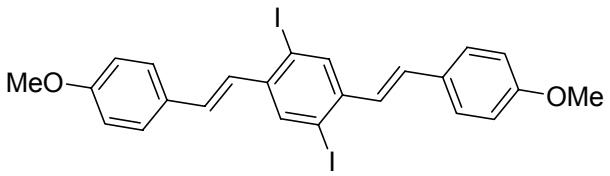


**Compound 9.3c**: Following the general procedure, **9.1** (0.630 g, 1.00 mmol), NaH (60.0 mg, 2.50 mmol), and 25.0 mL THF were combined. 4-Methoxybenzaldehyde, (300 mg, 2.20 mmol) was then added. Work up and recrystallization yielded yellow crystals (362 mg, 60.9%). MP: 213 $^{o}$ C IR: 2920.6, 2899.3, 1506.7, 1503.1, 1244.3, 1175.0, 1029.3, 956.5, 845.6, 814.4. $^{1}$H NMR (300 MHz, $CDCl_3$): $\delta$ = 8.03 (s, 2H, Ar-H), 7.49 (m, H, Ar-H), 7.17 (d, 2H, $J_{3H,H}$ = 23.1 Hz, CH=CH), 7.06 (d, 2H, $J_{3H,H}$ = 23.1 Hz, CH=CH), 6.97 (m, 6H, Ar-H, C=C-H), 3.83 (s, 6H, $CO_2CH_3$). $^{13}$C-NMR (400 MHz, $CDCl_3$): $\delta$ = 160.11, 140.91, 136.24, 131.94, 129.67, 128.62, 128.50, 114.49, 100.43, 55.60.

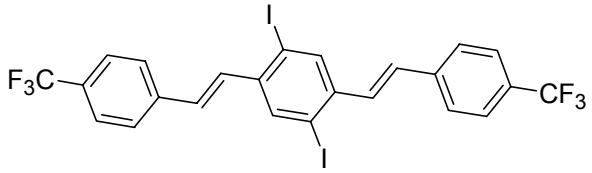


**Compound 9.3d**: Following the general procedure, **9.1** (2.00 g, 3.17 mmol), NaH (228 mg, 9.51 mmol), and 50 mL THF were combined. 4-(trifluoromethyl)-benzaldehyde, (1.22 g, 6.98 mmol) was then added. Work up and crystallization yielded bright yellow crystals (1.53 g, 72%). MP: 213-215$^{o}$ C IR: 3041.5, 2927.7, 1926.8, 1907.5, 1610.5, 1456.2, 1415.7, 1326.9, 1168.8, 1103.2, 1064.6, 956.6, 879.3, 813.9, 756.0, 732.9. $^{1}$H

NMR (300 MHz, $CDCl_3$): δ = 8.09 (s, 2H, Ar-H), 7.64 (m, 8H, Ar-H), 7.29 (d, 2H, $J_{3H,H}$ = 16.0 Hz, CH=CH), 7.02 (d, 2H, $J_{3H,H}$ = 16.2 Hz, CH=CH). $^{13}$C-NMR (400 MHz, $CDCl_3$): δ = 140.87, 140.04, 136.82, 132.96, 131.24, 131.1-129.8 (m), 128.4-120.2 (m), 127.30, 126.04, 100.66. $^{19}$F-NMR (400 MHz, $CDCl_{3)}$: δ = 22.02.

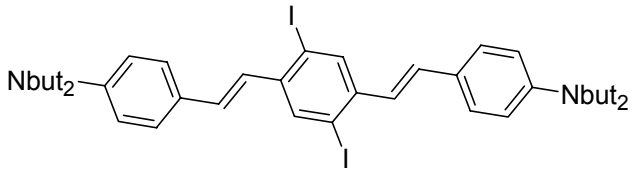


**Compound 9.3e**: Following the general procedure, **9.1** (5.65 g, 8.57 mmol), NaH (1.00 g, 25.0 mmol), and 250 mL THF were combined. 4-Dibutylamino benzaldehyde, (5.00 g, 21.4 mmol) was then added. Work up and crystallization yielded bright orange crystals (5.18 g, 72%). MP: 165$^{o}$ C IR: 2947.0, 2925.8, 2866.0, 1596.9, 1521.7, 1456.2, 1369.4, 1355.9, 1284.5, 1220.9, 1186.1, 1149.5, 1041.5, 954.7, 925.8, 802.3. $^{1}$H NMR (300 MHz, $CDCl_3$): δ = 8.00 (s, 2H, Ar-H), 7.40 (d, 4H, $J_{3H,H}$ = 8.78, Ar-H), 6.92-6.85 (dd, 4H, $J_{3H,H}$ = 16.2 Hz, CH=CH), 6.63 (d, 4H, $J_{3H,H}$ = 8.79 Hz, Ar-H), 3.28 (t, 8H, $J_{3H,H}$ = 7.41 Hz, α-$CH_2$), 1.60-1.52 (m, 8H, β-$CH_2$), 1.39-1.31 (m, 8H, γ-$CH_2$), 0.95 (t, 12H, $J_{3H,H}$ = 7.13 Hz, -CH3). $^{13}$C-NMR (400 MHz, $CDCl_3$): δ = 148.16, 140.42, 135.40, 131.89, 128.27, 125.39, 123.78, 111.49, 100.15, 50.77, 29.42, 20.32, 14.01.

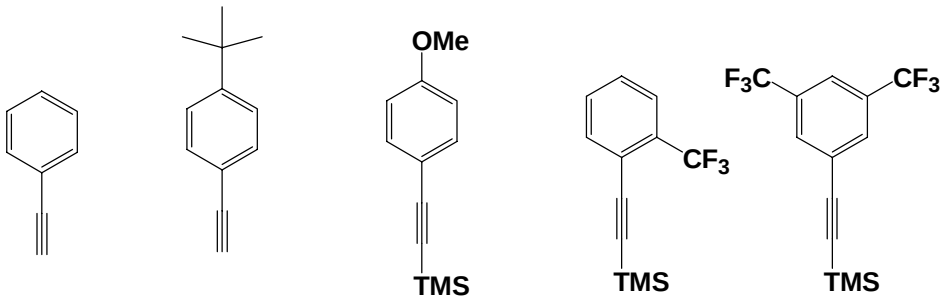


**9.4a** **9.4b** **9.4c** **9.4d** **9.4e**

The compounds **9.4b-d** have been previously reported and **9.4a** is commercially available.

Compound **9.4e**: 3,5-Bis(trifluoromethyl)iodobenzene (2.00g, 5.88 mmol) was combined with $(PPh_3)_2PdCl_2$ (50.0 mg, 72.1 μmol), CuI (50.0 mg, 333 μmol), 2.0 mL THF and 2.0 mL piperidine in a nitrogen-purged Schlenk flask. The mixture was degassed and capped with a septum. trimethylsilylacetylene (0.635 g, 6.47 mmol) was added dropwise. The reaction was allowed to stir in a warm water bath for 12 h. The crude reaction mixture was filtered over a silica plug with hexanes. The hexane mixture was reduced and the product was conveniently re-crystallized by sublimation in its own container at ambient temperature providing crystals suitable for crystallography (1.83 g, 83%). IR: 3087.8, 2960.5, 2900.7, 2173.6, 1834.2, 1807.2, 1786.0, 1608.5, 1460.0, 1409.9, 1373.2, 1300.8, 1249.8, 1181.2, 1130.2, 1107.1, 912.3, 907.7, 896.8, 891.1, 763.8. $^{1}H$ NMR (300 MHz, $CDCl_3$): $\delta$ = 7.87 (s, 2H), 7.78 (s, 1H), 0.25 (s, 9H). $^{13}C$ NMR ($CDCl_3$): $\delta$ =132.54-131.53 (q, $J_{2C,F}$ = 33.8 Hz), 132.06-132.03 (q, $J_{3C,F}$ = 3.0 Hz),, 127.19-119.06 (q, $J_{1C,F}$ = 272.9 Hz), 125.66, 122.02-121.9 (q, $J_{3C,F}$ = 3.76 Hz), 101.7 , 98.97 , 0.14.

**Compounds 9.5a-g:**

**9.5a-g** were produced by the Sonagashira coupling of either the free alkyne **9.4a,b** or by *in-situ* deprotection with potassium hydroxide and ethanol as a co-solvent (**9.4c-e**).

The reaction progress could be monitored by the development of the fluorescent products which were isolated by precipitating twice into non-solvents.

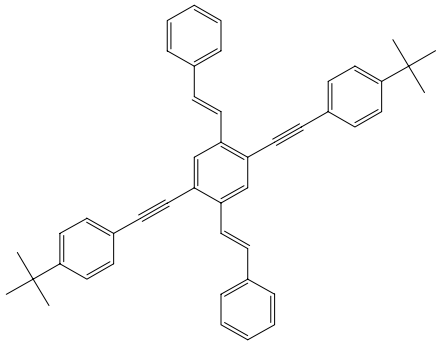

Compound **9.5a**: **9.3a** (236 mg, 0.442 mmol) was combined with **9.4b** (175 mg, 1.11 mmol), $(PPh_3)_2PdCl_2$ (5.0 mg, 7.1 μmol), CuI (5.0 mg, 33 μmol) and dissolved in 4.0 mL of piperidine/THF 1:1. The crude reaction mixture was precipitated twice from dichloromethane into hexane. The resulting yellow powder was recrystallized by evaporation of dichloromethane from hexane yielding 213 mg yellow crystals suitable for crystallographic analysis. Yield: 81% MP: 240°. IR: 3037.7, 2960.5, 2356.6, 2204.4, 1801.4, 1631.7, 1596.9, 1498.6, 1406.0, 1365.5, 1265.2, 1101.3, 1026.1, 956.6, 891.1, 831.3, 752.2, 690.5. $^1$H NMR (300 MHz, $CDCl_3$): δ = 7.99 (s, 2H, Ar-H), 7.69 (d, 2H, C=C-H, $J_{3\ H,H}$ = 16.3 Hz), 7.57 (m, 8H), 7.43 (m, 8H), 7.30 (m, 4H), 1.34 (s, 18H, t-butyl). $^{13}$C NMR ($CDCl_3$): δ = 152.16, 137.58, 137.50, 131.60, 130.76, 129.02, 128.18, 127.06, 126.00, 125.77, 122.63, 120.38, 65.97, 87.50, 35.12, 31.46. MS (DEP) ($C_{46}H_{42}$): *m/z* = 594.

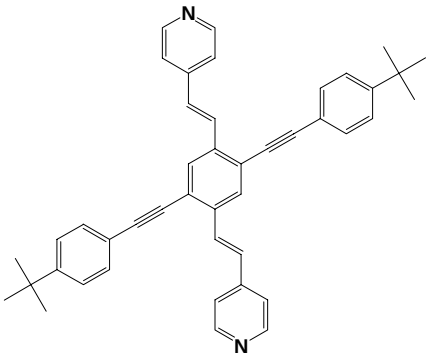

Compound **9.5b**: Compound **9.3b** (250 mg, 0.466 mmol) was combined with **9.4b** (184 mg, 1.17 mmol), $(PPh_3)_2PdCl_2$ (5.0 mg, 7.1 μmol), CuI (5.0 mg, 33 μmol) and dissolved in 4.0 mL of piperidine/THF 1:1. The crude reaction mixture was precipitated twice from dichloromethane into hexane. The resulting yellow powder was recrystallized by evaporation of dichloromethane from hexane yielding 214 mg yellow crystals suitable for crystallographic analysis. Yield: 77% MP: 264°. IR: 2960.5, 2868.0, 2358.8, 2208.3, 1593.1, 1506.3, 1461.9, 1363.6, 1267.1, 1217.0, 1103.2, 1016.4, 962.4, 866.0, 833.2, 800.4. $^1$H NMR (300 MHz, $CDCl_3$): δ = 8.61 (bs, pyridine-H), 7.91 (s, 2H, Ar-H), 7.87 (d, 2H, C=C-H, $J_{3\ H,H}$ = 16.5 Hz), 7.54(d, 4H, Ar-H, 8.51), 7.44 (m, 8H), 7.22 (d, 2H, C=C-H, $J_{3\ H,H}$ = 16.5 Hz), 1.34 (s, 18H, t-butyl). $^{13}$C NMR ($CDCl_3$): δ = 152.34, 150.22, 144.23, 136.76, 131.31, 129.85, 129.18, 128.06, 125.62, 122.90, 121.20, 119.62, 96.55, 86.53, 34.88, 31.14. MS (DEP) ($C_{44}H_{40}N_2$): *m/z* = 596.

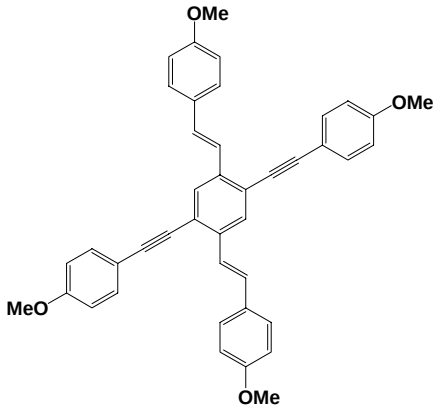


Compound **9.5c**: Compound **9.3d** (500 mg, 0.842 mmol) was combined with **9.4c** (518 mg, 2.53 mmol), $(PPh_3)_2PdCl_2$ (5.0 mg, 7.1 μmol), CuI (5.0 mg, 33 μmol), KOH (0.500 g, 8.9 mmol), 2.0 mL of piperidine, 2.0 mL THF, and 2.0 mL EtOH in a nitrogen purged Schlenk flask. The solution was degassed, capped with a septum and placed in a 50°C water bath for 24 h. The solution was reduced then precipitated twice from dichloromethane into methanol. The resulting yellow powder was recrystallized from xylenes yielding 269 mg yellow crystals. Yield: 53% MP: 199°. IR: 2929.7, 1604.7, 1512.1, 1456.2, 1440.7, 1419.5, 1292.2, 1253.6, 1174.6, 1107.1, 1031.8, 958.6, 852.5, 831.3. $^1$H NMR (300 MHz, $CDCl_3$): δ = 7.83 (s, 2H, Ar-H), 7.54 (m, 10H), 7.84 (s, 2H, Ar-H), 7.22 (d, 2H, C=C-H, $J_{3\ H,H}$ = 16.2 Hz), 6.93 (m, 8H), 3.84 (s, 6H, O-$CH_3$), 3.83 (s, 6H, O-$CH_3$). $^{13}$C NMR ($CDCl_3$): δ = 160.04, 159.75, 137.31, 133.29, 130.49, 130.00, 128.59, 128.26, 123.98, 122.25, 115.65, 114.46, 114.38, 95.53, 87.15, 55.57. MS (DEP) ($C_{42}H_{34}O_4$): *m/z* = 602.

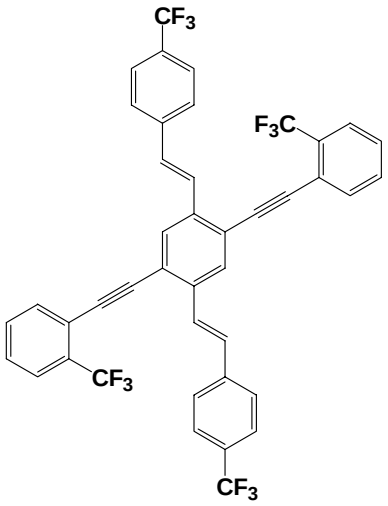


Compound **9.5d**: Compound **9.3d** (670 mg, 1.00 mmol) was combined with **9.4d** (606 mg, 2.50 mmol), $(PPh_3)_2PdCl_2$ (5.0 mg, 7.1 μmol), CuI (5.0 mg, 33 μmol), KOH (0.500 g, 8.9 mmol), 2.0 mL of piperidine, 2.0 mL THF, and 2.0 mL EtOH in a nitrogen purged Schlenk flask. The solution was degassed, capped with a septum and placed in a 50°C water bath for 24 h. The solution was reduced then precipitated twice from dichloromethane into hexane. The resulting green powder was recrystallized from xylenes yielding 475 mg greenish crystals. Yield: 63%. MP: 218-220°. IR: 2358.8, 2341.4, 1610.5, 1569.9, 1496.7, 1415.7, 1334.6, 1313.4, 1259.4, 1182.3, 1132.1, 1107.1, 1070.4, 962.4, 867.9, 823.5, 765.7. $^1$H NMR (300 MHz, $CDCl_3$): δ = 7.94 (s, 2H, Ar-H), 7.77 (m, 14H), 7.50 (t, 2H, Ar-H, $J_{3\ H,H}$ = 7.7 Hz), 7.28 (d, 2H, C=C-H, $J_{3\ H,H}$ = 16.5 Hz). $^{13}$C NMR (D-TCE, 80°C): δ= 140.44, 137.59, 134.04, 131.45, 131.15 (m), 129.98, 129.74 (m), 129.53, 128.44, 127.66, 126.92, 125.94, 125.47, 125.14, 124.69, 122.96, 122.61, 120.88, 92.69, 91.88. $^{19}$F NMR ($CDCl_3$): δ = 22.76, 22.09. MS (DEP) ($C_{42}H_{22}F_{12}$): *m/z* = 754.

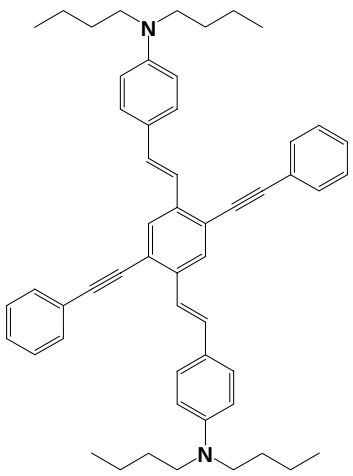

Compound **9.5e**: Compound **9.3e** (330 mg, 0.418 mmol) was combined with phenylacetylene **9.4a** (107 mg, 1.05 mmol), $(PPh_3)_2PdCl_2$ (5.0 mg, 7.1 μmol), CuI (5.0 mg, 33 μmol) and dissolved in 4.0 mL of piperidine/THF 1:1. The crude reaction mixture was precipitated twice from dichloromethane into methanol. The resulting orange powder was recrystallized from methanol yielding 280 mg orange crystals. Yield: 91%. MP: 164-168°. IR: 3033.8, 2929.7, 1795.6, 1600.8, 1521.7, 1461.9, 1400.2, 1367.4, 1257.5, 1220.9, 1147.9, 1109.0, 925.8, 804.3, 752.2, 688.5. $^1$H NMR (300 MHz, $CDCl_3$): δ = 7.84 (s, 2H, Ar-H), 7.84 (d, 4H, Ar-H, $J_{3\ H,H}$ = 7.7 Hz), 7.44 (m, 12H), 7.19 (d, 2H, C=C-H, $J_{3\ H,H}$ = 16.5 Hz), 6.64 (d, 4H, Ar-H, $J_{3\ H,H}$ = 8.8 Hz), 3.31 (t, 8H, α-C-H, $J_{3\ H,H}$ = 7.41 Hz), 1.63 (m, 8H, β-C-H), 1.39 (m, 8H, γ-C-H,), 0.97 (t, 12H, -$CH_3$, $J_{3\ H,H}$ = 7.4 Hz). $^{13}$C NMR ($CDCl_3$): δ = 147.97, 137.29, 131.57, 130.38, 128.38, 128.25, 128.09, 128.07, 124.49, 123.48, 121.41, 120.50, 111.59, 94.78, 88.51, 50.74, 29.46, 20.32, 14.00. MS (DEP) ($C_{54}H_{60}N_2$): *m/z* = 736.

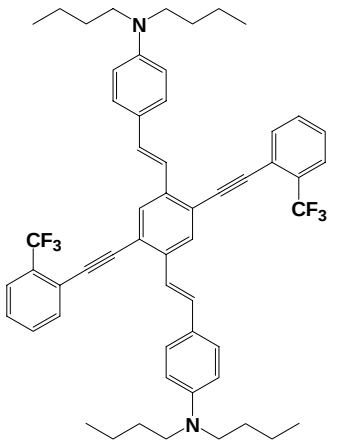


Compound **9.5f**: Compound **9.3e** (250 mg, 0.317 mmol) was combined with **9.4d** (192 mg, 0.792 mmol), $(PPh_3)_2PdCl_2$ (5.0 mg, 7.1 μmol), CuI (5.0 mg, 33 μmol), KOH (0.500 g, 8.9 mmol), 2.0 mL of piperidine, 2.0 mL THF, and 2.0 mL EtOH in a nitrogen purged Schlenk flask. The solution was degassed, capped with a septum and placed in a 50°C water bath for 24 h. The crude reaction mixture was dissolved in dichloromethane and washed three times with water. The solution was reduced then precipitated twice from dichloromethane into methanol. The resulting orange powder was recrystallized from methanol yielding 186 mg orange crystals. Yield: 67% MP: 182°. IR: 3030.0, 2954.7, 2869.9, 2208.3, 1600.8, 1521.7, 1469.7, 1398.3, 1369.4, 1315.4, 1286.4, 1259.4, 1220.9, 1174.6, 1136.0, 1109.0, 1055.0, 1031.8, 962.4, 806.2, 765.7. $^1$H NMR (300 MHz, $CDCl_3$): δ = 7.86 (s, 2H, Ar-H), 7.77 (d, 2H, Ar-H, $J_{3\ H,H}$ = 7.69 Hz), 7.73 (d, 2H, Ar-H, $J_{3\ H,H}$ = 7.69 Hz), 7.58 (t, 2H, Ar-H, $J_{3\ H,H}$ = 7.68 Hz), 7.45 (m, 8H), 7.17 (d, 2H, C=C-H, $J_{3\ H,H}$ = 16.47 Hz), 6.64 (d, 4H, Ar-H, $J_{3\ H,H}$ = 8.78 Hz), 3.31 (t, 8H, α-C-H, $J_{3\ H,H}$ = 6.59 Hz), 1.60 (m, 8H, β-C-H), 1.39 (m, 8H, γ-C-H,), 0.97 (t, 12H, -$CH_3$, $J_{3\ H,H}$ = 7.14 Hz). $^{13}$C NMR ($CDCl_3$): δ = 148.32, 137.94, 134.69, 131.71, 131.60, 131.19, 131.11, 128.64, 128.52, 128.21, 126.18, 126.11, 124.66, 121.95, 121.68, 120.32, 111.81, 94.29, 90.85, 51.00, 29.74, 20.59, 14.25. MS (DEP) ($C_{56}H_{58}F_6N_2$): *m/z* = 872.

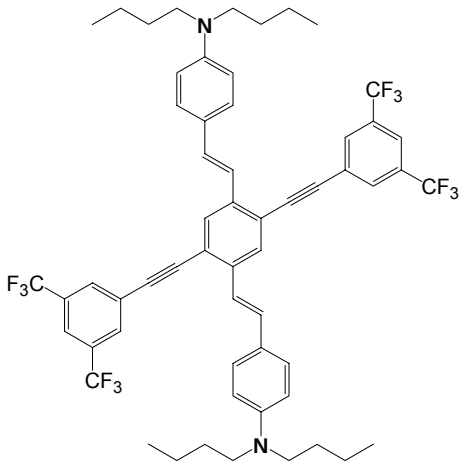

Compound **9.5g**: Compound **9.3e** (182 mg, 0.25 mmol) was combined with **9.4e** (177 mg, 0.624 mmol), $(PPh_3)_2PdCl_2$ (5.0 mg, 7.1 μmol), CuI (5.0 mg, 33 μmol), KOH (0.500 g, 8.9 mmol), 2.0 mL of piperidine, 2.0 mL THF, and 2.0 mL EtOH in a nitrogen purged Schlenk flask. The solution was degassed, capped with a septum and placed in a 50°C water bath for 24 h. The crude reaction mixture was dissolved in dichloromethane and washed three times with water. The solution was reduced then precipitated twice from dichloromethane into methanol. The resulting orange powder was recrystallized from methanol yielding 192 mg orange crystals. Yield: 76% MP: 191°. IR: 3039.6, 2960.5, 2931.6, 2864.1, 2208.3, 1600.8, 1521.7, 1373.2, 1286.4, 1182.3, 1137.9, 956.6, 893.9, 804.3, 684.7. $^1$H NMR (300 MHz, $CDCl_3$): δ = 8.02 (s, 4H, Ar-H), 7.86 (s, 2H, Ar-H), 7.84 (s, 2H, Ar-H), 7.43 (d, 4H, Ar-H, $J_{3\ H,H}$ = 8.78 Hz), 7.37 (d, 2H, C=C-H, $J_{3\ H,H}$ = 16.2 Hz), 7.19 (d, 2H, C=C-H, $J_{3\ H,H}$ = 16.3 Hz), 6.65 (d, 4H, Ar-H, $J_{3\ H,H}$ = 8.51 Hz), 3.32 (t, 8H, α-C-H, $J_{3\ H,H}$ = 6.59 Hz), 1.58 (m, 8H, β-C-H), 1.39 (m, 8H, γ-C-H,), 0.97 (t, 12H, -$CH_3$, $J_{3\ H,H}$ = 7.14 Hz). $^{13}$C NMR ($CDCl_3$): δ = 148.29, 137.80, 132.53-131.53 (m), 131.30, 131.21, 128.22, 128.13, 127.06-118.9 (m), 125.70, 123.98, 121.62, 120.82, 119.66, 111.59, 92.07, 91.94. MS (DEP) ($C_{56}H_{56}F_{12}N_2$): *m/z* = 1008.

**Cyclic Voltametry:**

Electrochemical experiments (Table 9.3)were carried out with CH Instruments model 660 electrochemical workstation. Cyclic voltammograms (CV) were obtained by using a conventional three-electrode system. A platinum foil was used as the counter electrode. A platinum disk electrode ($\phi$ = 1.2 mm) from Bioanalytical Systems serves as a working electrode. Reference electrode **A**, Ag/0.1 M $AgNO_3$ in $CH_2Cl_2$, was separated from the test by a fritted bridge containing the background electrolyte (0.1 M $Bu_4NPF_6$ in $CH_2Cl_2$ or 0.1 M $Bu_4NPF_6$ in THF). The reference electrode was calibrated before each experiment with the ferrocene/ferrocenium ($Fc/Fc^+$) redox system. The $E_{1/2}$ of 5 mM of $Fc/Fc^+$ in 0.1 M $Bu_4NPF_6$ in in $CH_2Cl_2$ was 0.89 V and in 0.1 M 0.1 M $Bu_4NPF_6$ in THF 0.141 V. The standard redox potential of the $Fc/Fc^+$ system has been determined to be 0.190 V [Bard, AJ., Faulkner LR. Electrochemical Methods; John Wiley & Sons: New York 1980 p.701].. Therefore, the potential of our reference electrode **A** was 0.289 V and 0.331 in $CH_2Cl_2$ and THF respectively vs. S.H.E. For additional experiments (oxidation of **9.3d**), the working and reference electrodes (reference electrode **B**) were a platinum wires with a platinum foil counter electrode. The reference electrode was calibrated before each experiment with the ferrocene/ferrocenium ($Fc/Fc^+$) redox system. The $E_{1/2}$ of 5 mM of $Fc/Fc^+$ in 0.1 M $Bu_4NPF_6$ in in $CH_2Cl_2$ was 0.205 V. Therefore, the potential of our reference electrode **B** was 0.395 V vs. S.H.E. All solutions were purged prior to electrochemical measurements using nitrogen gas. All solvents were dried with molecular sieves (3 Å). All the salts were used as received from Aldrich.

**Table 9.3:** Reduction and oxidation potentials of **9.5a-g**

| | **9.5a** | **9.5b** | **9.5c** | **9.5d** | **9.5e** | **9.5f** | **9.5g** |
|---|---|---|---|---|---|---|---|
| Reduction: | | | | | | | |
| onset | -0.80 | -1.44 | -0.83 | -1.46 | -1.8* | -1.8* | -1.8* |
| $E_{1/2}$ | -1.02 | -1.57 | -1.12 | -1.57 | - | - | - |
| peak | -1.26 | -1.67 | -1.15 | -1.65 | - | - | - |
| Oxidation: | | | | | | | |
| onset | 1.21 | 1.40 | 1.07 | 1.45 | 0.41, 1.47 | 0.47, 1.45 | 0.50, 1.54 |
| $E_{1/2}$ | 1.32 | 1.51 | 1.12 | 1.52 | 0.53 | 0.53 | 0.57 |
| peak | 1.42 | 1.68 | 1.19 | 1.61 | 0.61 | 0.62 | 0.66 |

***** only onsets of reduction were observed.

## 9.5 References and Notes


1. Klare, J. E. ; Tulevski, G. S. ; Sugo, K. ; de Picciotto, A. ; White, K. A. ; Nuckolls, C. *J. Am. Chem. Soc*., **2003**, *125*, 6030

2. Kraft, A.; Grimsdale, A. C. ; Holmes, A. B. *Angew. Chem. Int. Ed. Engl*. **1998**, *37*, 402.

3. Brizius, G. ; Pschirer, N. G. ; Steffen, W. ; Stitzer, K. ; zur Loye, H.-C. *J. Am. Chem. Soc*. **2000,** *122*, 12435. Egbe, D. A. M. ; Tillmann, H. ; Birckner, E. ; Klemm, E. *Macromol. Chem. Phys*. **2001**, *202*, 2712.

4. Halkyard, C. E.; Rampey, M. E.; Kloppenburg, L.; Studer Martinez, S. L.; Bunz, U. H. F *Macromolecules* **1998**, *31*, 8655.

5. Wilson, J. N.; Windscheif, P. M.; Evans, U.; Myrick, M. L.; Bunz, U. H. F. *Macromolecules*, **2002**, *35*, 8681.

6. a) Horner, L. ; Hoffmann, H.; Wippel, H. G. *Chem. Ber.* **1958**, *91*, 61. b) Horner, L.; Klink, W. *Tetrahedron Lett*. **1964**, *36*, 2467.

7. a) Sonogashira, K. J. Organomet. Chem. 2002, 653, 46. b) Neghishi, E. ; Anastasia, L. *Chem. Rev*. **2003**, *103*, 1979. Bunz, U. H. F. *Chem. Rev.* **2000**, *100*, 1605.

8. Zhao, Y. M. Tykwinski, R. R. *J. Am. Chem. Soc.* **1999**, *121*, 458. Tykwinski, R. R. ; Schreiber, M. ; Gramlich, V. ; Seiler, P. ; Diederich, F. *Adv. Mater*. **1996**, *8*, 226.

9. Hopf, H. Classics in Hydrocarbon Chemistry, Wiley-VCH, Weinheim **2000**.

# Chapter 10

# Cruciform π-systems: Effect of aggregation on emission

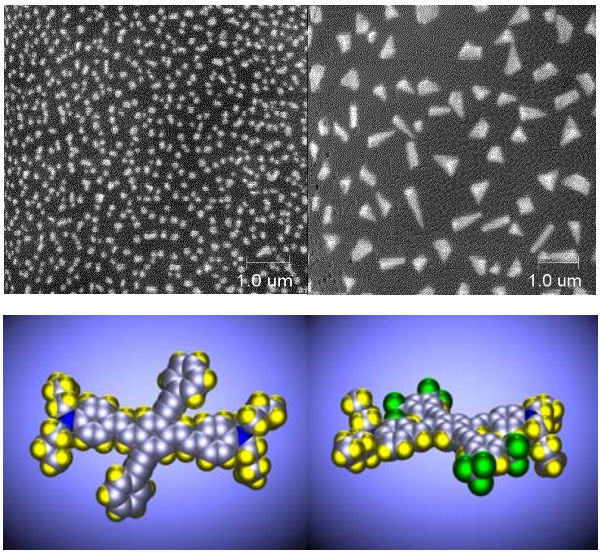


## 10.1 Introduction

The solid state properties of cruciform pentamers **10.1-4** (Figure 10.1)are examined in thin film preparation, in the single crystalline state and in nanoparticle formulations; emission behavior was found to vary substantially with the solid state morphology.

Conjugated organic oligomers have been used extensively in optical and electronic devices.[1] We recently introduced a class of cross-conjugated oligomers **10.1-4** that show unusual electronic properties in solution.[2,3] To achieve successful incorportation of these and other conjugated materials into functional solid state devices

it is necessary to understand and manipulate their solid state optical properties as a consequence of their intermolecular ordering4 and their conformtional preference.[5] We find that the morphology, i.e. crystalline or glassy state[6] of these molecules has a substantial effect upon their emission spectra, similar to the oligomers extensively examined by Curtis et al.[4]

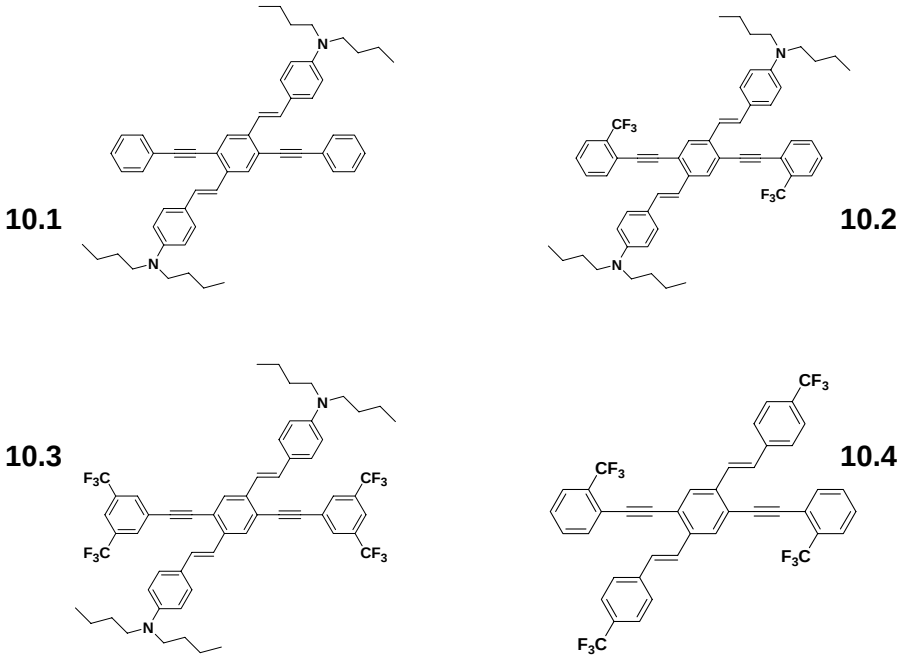


**Figure 10.1** Previously synthesized cruciforms utilized in these experiments.

## 10.2 Results and Discussion

While spin cast films of **10.1-4** were found to be amorphous, crystallization of **10.1-4** from a mixture of dichloromethane and methanol (**10.1-3**) or from xylenes (**10.4**) resulted in specimens suitable for single crystal XRD (Fig 10.2). The most striking characterisitic of these structures is the relative distortion of the π-system. While **10.3** exhibits near perfect planarity of the $\tilde{\pi}$ backbone, **10.1** and **10.2** show twisting of the phenylene-ethynylene (PE) subunits with rotations of approximately 30$^{o}$. Additionally,

the styryl groups of **10.2** show a departure from planarity. Twisting of approximately 15° of the PE unit in **10.4** is observed. While **10.2** and **10.3** pack in a herringbone fashion, **10.1** exhibits flat packing. To examine the solid state optical spectra of **10.1-4**, thin films were cast from chloroform solutions. The films were amorphous when examined under the crossed polarizers of an optical microscope. As expected, the molecules **10.1-3** showed similar absorption spectra

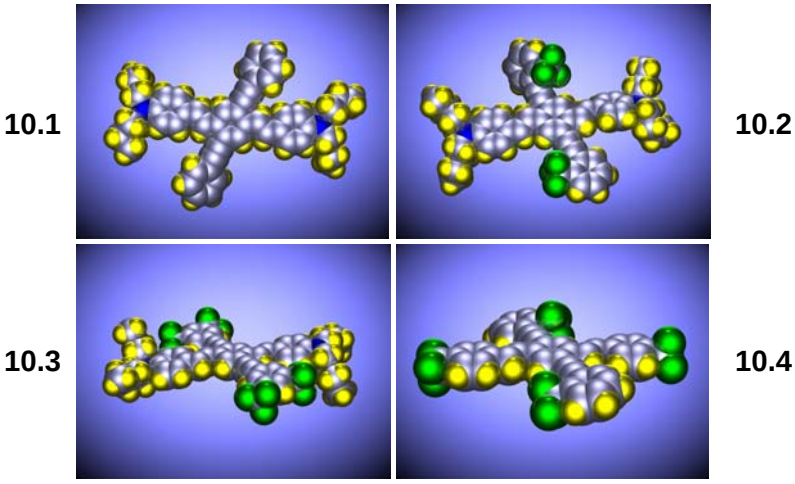


**Fig. 10.2**. Crystal structures of compounds **10.1-4** showing the twist angles of the phenyleneethynylene subunits in **10.1** and **10.2** (30° and 45° respectively), while **10.3** and **10.4** (12°) remain relatively planar.

(thin films, see Table 10.1) with a first maximum between 330 and 340 nm and a second, broader maximum between 425 and 455. Only one emission peak is observed in thin films of **10.1-3** ranging from 560 to 586 nm respectively. An absorption maximum of 332 nm and an emission maximum of 484 nm was observed for **10.4**, substantially blue shifted from its dibutylamino-substituted relatives **10.1-3**.

**Table 10.1**. Summary of the optical and crystal data for **10.1-4**.

| | **10.1** | **10.2** | **10.3** | **10.4** |
|---|---|---|---|---|
| Absorption Film | 335,440 | 340,455 | 335,425 | 332 |
| Emission Film | 560 | 574 | 586 | 484 |
| Emission Crystal | 601 | 596 | 607 | 504 |
| Emission Solution | 498 $C_6H14$ | 502 C6H14 | 579 THF | 434 (CHCl3) |
| Space group | P21/c | P21/n | C2/c | P2/c |
| *a* | 14.78 | 13.83 | 42.33 | 17.87 |
| *b* | 19.60 | 16.94 | 5.19 | 5.06 |
| *c* | 16.74 | 20.42 | 28.82 | 18.69 |
| β/° | 115.63 | 97.85 | 128.21 | 97.6 |
| Z | 4 | 4 | 4 | 2 |

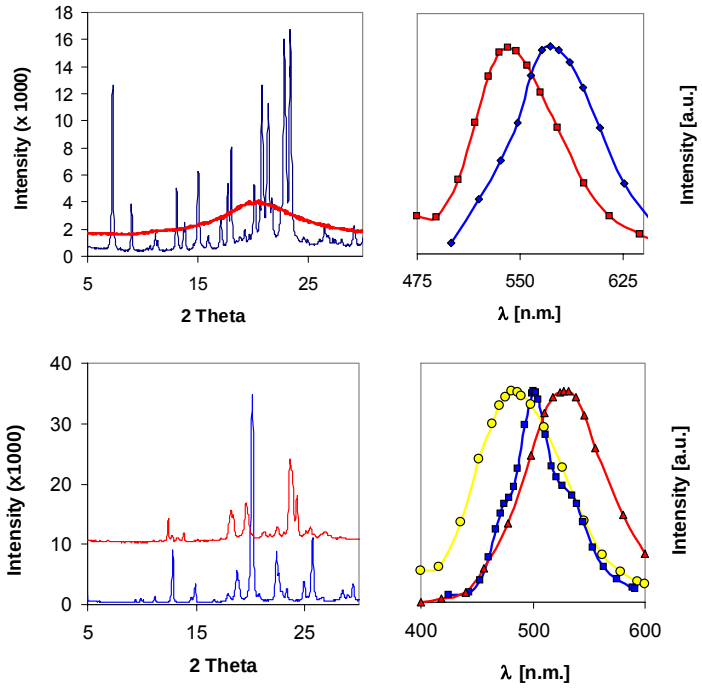


**Fig. 10.3**. Compound **10.1** (top) shows a distinct XRD pattern for the crystalline state and emission at 601 nm (blue). Melting and cooling the sample results in loss of crystallinity (red) and a hypsochromic shift of 25 nm in the emission. Crystals of **10.4** (at bottom) display a distinct XRD pattern and an emission centered at 500 nm (blue). Melting and cooling this sample results in a second crystalline state with 25 nm red shifted emission (red). Amorphous thin films display an emission (yellow) at 484 nm.

We next examined the emission of crystals of **10.1-4** (Table 10.1). A similar trend was observed as in the thin films with **10.4** showing the bluest emission at 504 nm, **10.1** and **10.2** displaying emissions near 600 while **10.3** was again the reddest at 607 nm. For **10.4** this represents a 20 nm shift from the thin film, while for **10.3** the shift is 30 nm and in **10.1** a 40 nm shift is observed. It was of interest to see whether these crystals could be converted to the glass-like state to compare the resulting emission spectra with those observed in the crystalline state. None of the compounds formed the desired glassy state with the exception of **10.1** which could easily be drawn into amorphous fibers that were up to 10 cm in length with widths of ~100 μm. Powder XRD (Fig 10.3. top, right) shows the effect of melting on **10.1**: a distinct diffraction pattern visible before and an amorphous pattern is visible after melting. This loss of crystallinity corresponds to a 25

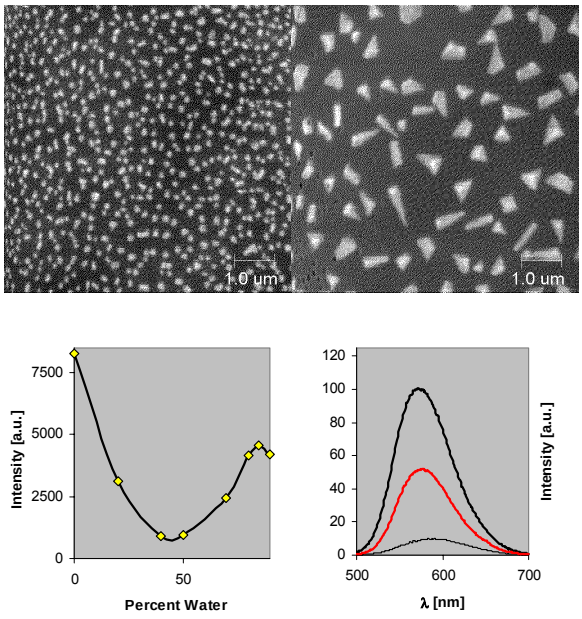


**Fig 10.4**. Nanospheres of **10.1** (top left) and nanocrystals of **10.3** (top right) with scale bar. Nanoparticles are formed by the addition of water to THF solutions of the compounds. Bottom left: relative quantum yield of **10.3** as a function of $H_2O$/THF fraction. Quantum yield of **10.3** in THF $\Phi$ = 0.10. Bottom right: With initial addition of $H_2O$ the quantum yield drops (thin line), but increases at higher $H_2O$ concentrations (red line).

nm red shift in emission confirming the observed difference between thin film and crystal. By comparison, **10.4** shows quite different behavior—attempts at melting the sample resulted in another crystalline state as observed in the XRD pattern (Fig 10.3, bottom left). The emission spectra of this second crystalline state was found to have emission red shifted by 20 nm. Thus **10.4** exhibits three solid state emissions (Fig 10.3, bottom right) amorphous thin films yielding the bluest emission at 484 nm, one crystalline state at 504 nm and a second crystalline state at 526 nm.

Preparations of nanospheres from conjugated oligomers and polymers have been reported, the simplest method being that reported by Park et al.[7] Nanospheres have been successfully incorporated into fuctional solar cells.[8] It was of interest to see if **10.1-4** could form nanospheres from THF/$H_2O$ mixtures and in how far their optical properties would be different from that of thin film and crystalline preparations. Dilute solutions (2.0 x$10^{-5}$ M) of **10.1-4** with increasing fractions of water were prepared. The effect of water could be observed as a decrease in the quantum yield and a red shift (15 nm for **10.3**, Fig. 10.4, bottom) in emission. However, above ~75% $H_2O$ concentration, the emission of **10.3**, but not that of **10.1,2**, or **10.4**, showed a dramatic increase in emission intensity accompanied by a small hypsochromic shift. We believe this behavior results from the formation of the nanoparticles: molecules of **10.3** are isolated from their polar environment (THF/$H_2O$ mixture) and thus exhibit a higher quantum yield and slight blue shift. The behavior is not observed in the nanoparticle preparation of the other cruciforms.

SEM images revealed that 1 showed nanospheres of uniform size and shape (150-250 nm, Fig. 9.4, top left) similar to those previously reported,[7] while **10.3** formed well-

developed nanocrystals (widths of 200-500 nm, lengths of up to 1 μm, Fig 10.4, top). While electron diffraction patterns were observed for **10.3**, the microspheres of **10.1** were amorphous. Electron diffraction showed that the nanocrystals of **10.3** exhibited the same packing as that observed in macroscopic single crystals according to comparison of the actual electron diffraction pattern to a simulated one obtained by the program Cerius2 (ESI) utilizing the cell data obtained from macroscopic single crystals of **10.3**.

## 10.3 Conclusions

Cruciforms **10.1-4** form distinctly different morphologies in the solid state (thin film, crystalline phases, nanoparticles) displaying greatly different emissive behavior. It is to be noted that while **10.1,2**, and **10.4** form nanospheres, **10.3** forms highly fluorescent nanocrystals. In the future we will report on the incorporation

## 10.4 Experimental

X-Ray Structure Determination, $C_{54}H_{60}N_2$ (Table 10.2)

An orange bar was mounted onto the end of a thin glass fiber using inert oil. X-ray intensity data were measured at 200.0(2) K in the nitrogen cold stream of a Bruker SMART APEX CCD-based diffractometer (Mo Kα radiation, λ = 0.71073 Å).[1] Attempts to cool the crystal further resulted in fracturing and destruction of the sample. The raw data frames were integrated with SAINT+,[9] which also applied corrections for Lorentz and polarization effects. The final unit cell parameters are based on the least-squares refinement of 5751 reflections with $I > 5(\sigma)I$ from the data set. Analysis of the data showed negligible crystal decay during data collection.

Systematic absences in the intensity data were consistent with the space group $P2_1/c$. The structure was solved by a combination of direct methods and difference Fourier syntheses, and refined by full-matrix least-squares against $F^2$, using the SHELXTL software package.[10] The molecule possesses no crystallographically imposed symmetry. Three of the four butyl groups (C19 – C22, C39 – C42, C43 – C46) are afflicted by disorder. These chains were modeled as occupying two conformations, A and B. The site occupation factors (sofs) for each disorder component were refined,

**Table 10.2.** Crystal data and structure refinement.

| | | |
|---|---|---|
| Identification code | j111a1s | |
| Empirical formula | C54 H60 N2 | |
| Formula weight | 737.04 | |
| Temperature | 200.0(2) K | |
| Wavelength | 0.71073 Å | |
| Crystal system | Monoclinic | |
| Space group | $P2_1/c$ | |
| Unit cell dimensions | a = 14.7777(7) Å | α= 90°. |
| | b = 19.5961(9) Å | β= 115.6340(10)°. |
| | c = 16.7434(8) Å | γ = 90°. |
| Volume | 4371.4(4) $Å^3$ | |
| Z | 4 | |
| Density (calculated) | 1.120 $Mg/m^3$ | |
| Absorption coefficient | 0.064 $mm^{-1}$ | |
| F(000) | 1592 | |
| Crystal size | 0.58 x 0.40 x 0.36 $mm^3$ | |
| Theta range for data collection | 1.70 to 23.28°. | |
| Index ranges | -14<=h<=16, -21<=k<=21, -18<=l<=18 | |
| Reflections collected | 26282 | |
| Independent reflections | 6288 [R(int) = 0.0406] | |
| Completeness to theta = 23.28° | 99.9 % | |
| Absorption correction | None | |
| Refinement method | Full-matrix least-squares on $F^2$ | |
| Data / restraints / parameters | 6288 / 38 / 590 | |
| Goodness-of-fit on $F^2$ | 0.977 | |
| Final R indices [I>2sigma(I)] | R1 = 0.0541, wR2 = 0.1400 | |
| R indices (all data) | R1 = 0.0840, wR2 = 0.1519 | |
| Extinction coefficient | 0.0037(5) | |
| Largest diff. peak and hole | 0.235 and -0.160 $e.Å^{-3}$ | |

constrained to sum to unity for that component. The final values are near A = 0.60 / B = 0.40 for all three. Additionally, a total of 38 restraints were employed to maintain a chemically reasonable geometry for the disordered groups; however, some displacement parameters of these atoms show highly anisotropic motion, indicating the twofold disorder model is inadequate, and that more conformations are present. These were not modeled. Eventually all non-hydrogen atoms were refined with anisotropic displacement parameters; hydrogen atoms were placed in geometrically calculated positions and refined as standard riding atoms.

---

X-Ray Structure Determination, $C_{56}H_{58}F_6N_2$ (Table 10.3)

$C_{56}H_{58}F_6N_2$ crystallizes in the form of brilliant orange plates. Evaluation of several samples showed broad diffraction peaks and weak scattering > $2\theta \sim 40^{\circ}$. The crystal judged to be the best of these was mounted onto the end of a thin glass fiber using inert oil. X-ray intensity data were measured at 150.0(2) K on a Bruker SMART APEX CCD-based diffractometer (Mo K$\alpha$ radiation, $\lambda$ = 0.71073 Å).[9] The raw data frames were integrated into reflection intensity files with SAINT+,[9] which also applied corrections for Lorentz and polarization effects. The final unit cell parameters are based on the least-squares refinement of 5134 reflections from the data set with $I > 5\sigma(I)$. Analysis of the data showed negligible crystal decay during data collection. No correction for absorption was applied.

Systematic absences in the intensity data uniquely determined the monoclinic space group $P2_1/n$. The structure was solved by a combination of direct methods and difference Fourier syntheses, and refined by full-matrix least-squares against $F^2$, using SHELXTL.[10] All atoms reside on positions of general crystallographic symmetry. Severe positional disorder of both butyl groups attached to N2 was observed. A disorder model consisting of two distinct conformations was employed. Occupation factors were adjusted manually and then fixed at values yielding reasonable displacement parameters.

**Table 10.3.** Crystal data and structure refinement

| | | |
|---|---|---|
| Identification code | dba1bm | |
| Empirical formula | C56 H58 F6 N2 | |
| Formula weight | 873.04 | |
| Temperature | 150.0(2) K | |
| Wavelength | 0.71073 Å | |
| Crystal system | Monoclinic | |
| Space group | $P2_1/n$ | |
| Unit cell dimensions | a = 13.8368(7) Å | α= 90°. |
| | b = 16.9399(8) Å | β= 97.8490(10)°. |
| | c = 20.4197(10) Å | γ = 90°. |
| Volume | 4741.4(4) $Å^3$ | |
| Z | 4 | |
| Density (calculated) | 1.223 $Mg/m^3$ | |
| Absorption coefficient | 0.087 $mm^{-1}$ | |
| F(000) | 1848 | |
| Crystal size | 0.38 x 0.28 x 0.10 $mm^3$ | |
| Theta range for data collection | 1.57 to 20.81°. | |
| Index ranges | -13<=h<=13, -16<=k<=16, -20<=l<=20 | |
| Reflections collected | 23049 | |
| Independent reflections | 4958 [R(int) = 0.0603] | |
| Completeness to theta = 20.81° | 100.0 % | |
| Absorption correction | None | |
| Refinement method | Full-matrix least-squares on $F^2$ | |
| Data / restraints / parameters | 4958 / 14 / 608 | |
| Goodness-of-fit on $F^2$ | 0.971 | |
| Final R indices [I>2sigma(I)] | R1 = 0.0596, wR2 = 0.1407 | |
| R indices (all data) | R1 = 0.1022, wR2 = 0.1581 | |
| Largest diff. peak and hole | 0.209 and -0.157 $e.Å^{-3}$ | |

A total of 14 geometric restraints were used to maintain a chemically reasonable geometry for these groups. The behavior of the displacement parameters as well as the presence of several diffuse difference peaks in this region indicate more butyl group conformations exist. One atom (C45A) of the minor disorder component was refined isotropically; all other non-hydrogen atoms were refined with anisotropic displacement parameters. Hydrogen atoms were placed in idealized positions and included as riding atoms. The relatively high final residuals reflect the poor crystal quality and side chain disorder.

---

X-Ray Structure Determination, $C_{58}H_{56}F_{12}N_2$ (Table 10.4)

**A**n orange plate was mounted onto the end of a thin glass fiber using inert oil. X-ray intensity data covering the full sphere of reciprocal space were measured at 150(1) K on a Bruker SMART APEX CCD-based diffractometer (Mo K$\alpha$ radiation, $\lambda$ = 0.71073 Å).[9] The raw data frames were integrated with SAINT+,[9] which also applied corrections for Lorentz and polarization effects. The final unit cell parameters are based on the least-squares refinement of 9712 reflections from the data set with I > 5($\sigma$)I. Analysis of the data showed negligible crystal decay during data collection.

Systematic absences in the intensity data were consistent with the space groups C2/c and Cc; intensity statistics indicated centricity. The structure was solved in C2/c by a combination of direct methods and difference Fourier syntheses, and refined by full-matrix least-squares against $F^2$, using SHELXTL.[10] The molecule resides on a center of symmetry. All non-hydrogen atoms were refined with anisotropic displacement

parameters; hydrogen atoms were placed in geometrically idealized positions and refined with isotropic displacement parameters as riding atoms.

**Table 10.4.** Crystal data and structure refinement

| | | |
|---|---|---|
| Identification code | jw06s | |
| Empirical formula | C58 H56 F12 N2 | |
| Formula weight | 1009.05 | |
| Temperature | 150(1) K | |
| Wavelength | 0.71073 Å | |
| Crystal system | Monoclinic | |
| Space group | C2/c | |
| Unit cell dimensions | a = 42.3302(15) Å | α= 90°. |
| | b = 5.1937(2) Å | β= 128.2140(10)°. |
| | c = 28.8208(11) Å | γ = 90°. |
| Volume | 4978.4(3) $Å^3$ | |
| Z | 4 | |
| Density (calculated) | 1.346 $Mg/m^3$ | |
| Absorption coefficient | 0.109 $mm^{-1}$ | |
| F(000) | 2104 | |
| Crystal size | 0.42 x 0.30 x 0.10 $mm^3$ | |
| Theta range for data collection | 1.42 to 25.04°. | |
| Index ranges | -50<=h<=49, -6<=k<=6, -34<=l<=34 | |
| Reflections collected | 16856 | |
| Independent reflections | 4406 [R(int) = 0.0428] | |
| Completeness to theta = 25.04° | 99.8 % | |
| Absorption correction | None | |
| Refinement method | Full-matrix least-squares on $F^2$ | |
| Data / restraints / parameters | 4406 / 0 / 356 | |
| Goodness-of-fit on $F^2$ | 1.056 | |
| Final R indices [I>2sigma(I)] | R1 = 0.0541, wR2 = 0.1423 | |
| R indices (all data) | R1 = 0.0675, wR2 = 0.1497 | |
| Extinction coefficient | 0.0006(2) | |
| Largest diff. peak and hole | 0.667 and -0.385 $e.Å^{-3}$ | |

X-Ray Structure Determination, $C_{42}H_{22}F_{12}$ (Table 10.5)

A yellow-green blade was mounted onto the end of a thin glass fiber using inert oil. X-ray intensity data covering the full sphere of reciprocal space were measured at 150(1) K on a Bruker SMART APEX CCD-based diffractometer (Mo Kα radiation, λ = 0.71073 Å).[9] The raw data frames were integrated with SAINT+,[9] which also applied corrections for Lorentz and polarization effects. The final unit cell parameters are based on the least-squares refinement of 6553 reflections from the data set with $I > 5(\sigma)I$. Analysis of the data showed negligible crystal decay during data collection.

Systematic absences in the intensity data were consistent with the space groups P2/c and Pc; intensity statistics indicated centricity. The structure was solved in P2/c by a combination of direct methods and difference Fourier syntheses, and refined by full-matrix least-squares against $F^2$, using SHELXTL.[10] The molecule resides on a center of symmetry. One $-CF_3$ group (C21, F4 – F6) is rotationally disordered over two orientations in the proportion 0.68(1) / 0.32 and was refined with the aid of 18 restraints (SHELX SAME). All non-hydrogen atoms were refined with anisotropic displacement parameters; hydrogen atoms were placed in geometrically idealized positions and refined with isotropic displacement parameters as riding atoms.

**Table 10.5.** Crystal data and structure refinement.

| | | |
|---|---|---|
| Identification code | jw05s | |
| Empirical formula | C42 H22 F12 | |
| Formula weight | 754.60 | |
| Temperature | 150(1) K | |
| Wavelength | 0.71073 Å | |
| Crystal system | Monoclinic | |
| Space group | P2/c | |
| Unit cell dimensions | a = 17.8688(14) Å | α= 90°. |
| | b = 5.0625(4) Å | β= 97.617(2)°. |
| | c = 18.6933(15) Å | γ = 90°. |
| Volume | 1676.1(2) $Å^3$ | |
| Z | 2 | |
| Density (calculated) | 1.495 $Mg/m^3$ | |
| Absorption coefficient | 0.133 $mm^{-1}$ | |
| F(000) | 764 | |
| Crystal size | 0.72 x 0.30 x 0.04 $mm^3$ | |
| Theta range for data collection | 2.20 to 24.11°. | |
| Index ranges | -20<=h<=20, -5<=k<=5, -21<=l<=21 | |
| Reflections collected | 9956 | |
| Independent reflections | 2664 [R(int) = 0.0360] | |
| Completeness to theta = 24.11° | 100.0 % | |
| Absorption correction | None | |
| Refinement method | Full-matrix least-squares on $F^2$ | |
| Data / restraints / parameters | 2664 / 18 / 284 | |
| Goodness-of-fit on $F^2$ | 1.010 | |
| Final R indices [I>2sigma(I)] | R1 = 0.0546, wR2 = 0.1344 | |
| R indices (all data) | R1 = 0.0662, wR2 = 0.1421 | |
| Extinction coefficient | 0.0027(10) | |
| Largest diff. peak and hole | 0.196 and -0.204 $e.Å^{-3}$ | |

---

In Figure 10.5 (below) comparison of simulated and found electron diffraction patterns are compared.

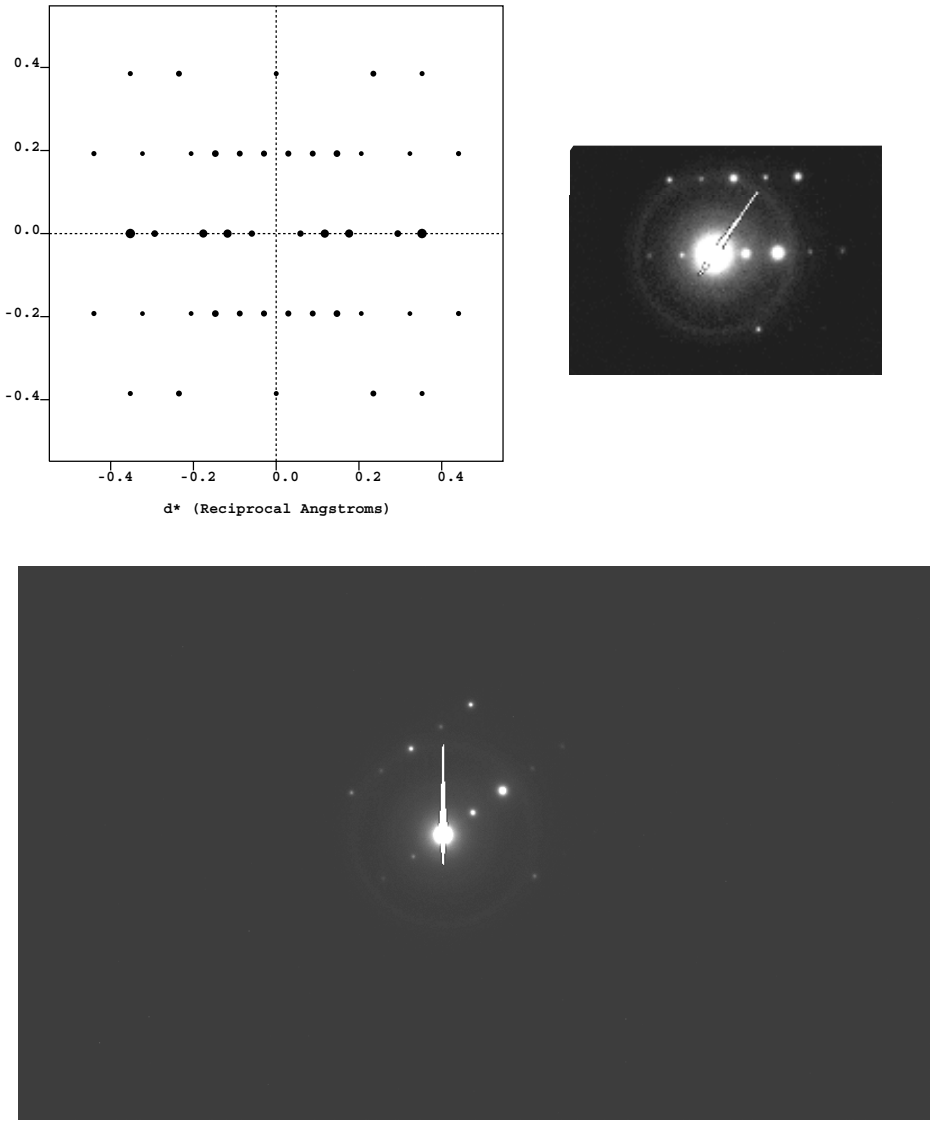


**Figure 10.5** Simulated and observed electron diffraction of a microcrystal of 9.3 ($C_{42}H_{22}F_{12}$). Top left: simulated electron diffraction obtained by cerius$^2$. Top right: corresponding experimental electron diffraction pattern, processed. Bottom: Raw diffraction pattern after contrast enhancement by Microsoft Word program. The crystals of **10.3** were very small and of comparatively low quality. They were slightly bent and not perfectly oriented with respect to the diffraction plane. As a consequence only a section of the expected diffraction pattern is visible. The calculated values are in perfect match when comparing experiment and simulation. The crystals are oriented such that one looks onto a plane that is defined by the crystallographic axes *a* and *b*.

## 10.5 References and Notes


1. Müllen, K. and Wegner, G., Eds. Electronic Materials. The Oligomer Approach. Wiley-VCH, Weinheim, **1998**.

2. Wilson, J. N.; Josowicz, M.; Y. Wang, and Bunz, U. H. F., *Chem. Commun.* **2003**, 2962.

3. For other cruciform oligomers see: Klare, J. E.; Tulevski, G. S.; Sugo, K; de Picciotto, A.; White, K. A.; Nuckolls, C., *J. Am. Chem. Soc*., **2003**, *125*, 6030.

4. Koren, A. B.;. Curtis, M. D; Francis, A. H.; Kampf, J. W. *J. Am. Chem. Soc.* **2003**, *125*, 5040-5050. Koren, A. B.; Curtis, M. D.; Kampf, J. W. *Chem. Mater*. **2000**, *12*, 1519.

5. Halkyard, C. E.; Rampey, M. E.; Kloppenburg, L.; Studer-Martinez, S. L.; Bunz, U. H. F.*Macromolecules* **1998**, *31*, 8655.

6. Strohriegl, P. and Grazulevicius, J. V. *Adv. Mater.* **2002**, *14*, 1439.

7. An, B. K.; Kwon, S. K.; Jung, S. D.; Park, S. Y.. *J. Am. Chem. Soc*., **2002**, *124*, 14410.

8. Kietzke, T.; Neher, D.; Landfester, K.; Montenegro, R.; Guntner, R.; Scherf, U. *Nat. Mater.* **2003**, *2*, 408.

9. SMART Version 5.625 and SAINT+ Version 6.02a. Bruker Analytical X-ray Systems, Inc., Madison, Wisconsin, USA, **1998**.

10. Sheldrick, G. M. SHELXTL Version 5.1; Bruker Analytical X-ray Systems, Inc., Madison, Wisconsin, USA, **1997.**

# Chapter 11

# Synthesis and electronic properties of bis-styryl substituted trimeric aryleneethynylenes: Comparison of cruciforms with iso-cruciforms

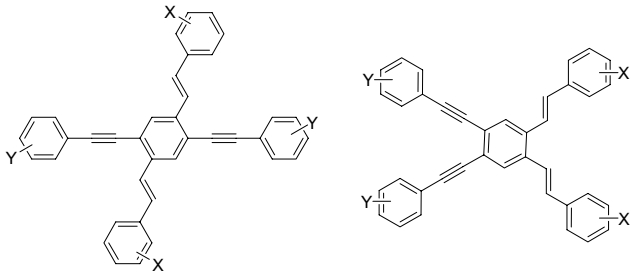



## 11.1 Introduction

Conjugated organic materials are –generally speaking– wide bandgap semiconductors.[1] Their band gap and their emissive properties are primarily manipulated by choice of the covalently assembled chemical structure. This approach leads itself to an inexhaustible variability of chromophores. Upon combination of two or more organic modules this variability increases if their connection takes place in topologically different ways; absorption and emission will change as a result.

Contrary to inorganic semiconductors that only exist in the solid state, as covalent assembly,[2] most organic semiconductors are soluble and processible from solution into amorphous or crystalline films.[1] The processing aspect adds a further layer of complexity to the behavior of most organic semiconductors, with the optical properties being dependent upon solid-state ordering and concomitant aggregation phenomena.[3] As a consequence, organic semiconductors might be compared to proteins where primary, secondary and tertiary structures are present and critically important for the correct function. While organic semiconductors are much less complex than proteins, higher order structures –as in the case of nature's polymers– most often define the organic semiconductor's electronic properties.

There has been a considerable interest in poly(*para*phenyleneethynylene)s (PPE)[3] as active layers in light emitting devices.[4] And while several encouraging reports have appeared in the literature, the hole injecting properties of PPEs present a problem in their use as OLED materials. The difficulty in hole injection is due to the electron withdrawing quality of the alkyne groups. As a consequence it would be of interest, while preserving the PPE skeleton, to improve the hole injection capabilities of these polymers.[5] As a consequence, a series of PPEs with styryl side chains was synthesized (Figure 11.1).[6] These materials are more electron rich and showed elctrooptical properties that were different from those displayed by the PPEs. To understand the properties of these polymers better, cruciform models **11.1-5** were prepared and their emission and absorption were recorded both in solution and in the solid state.[7,8]

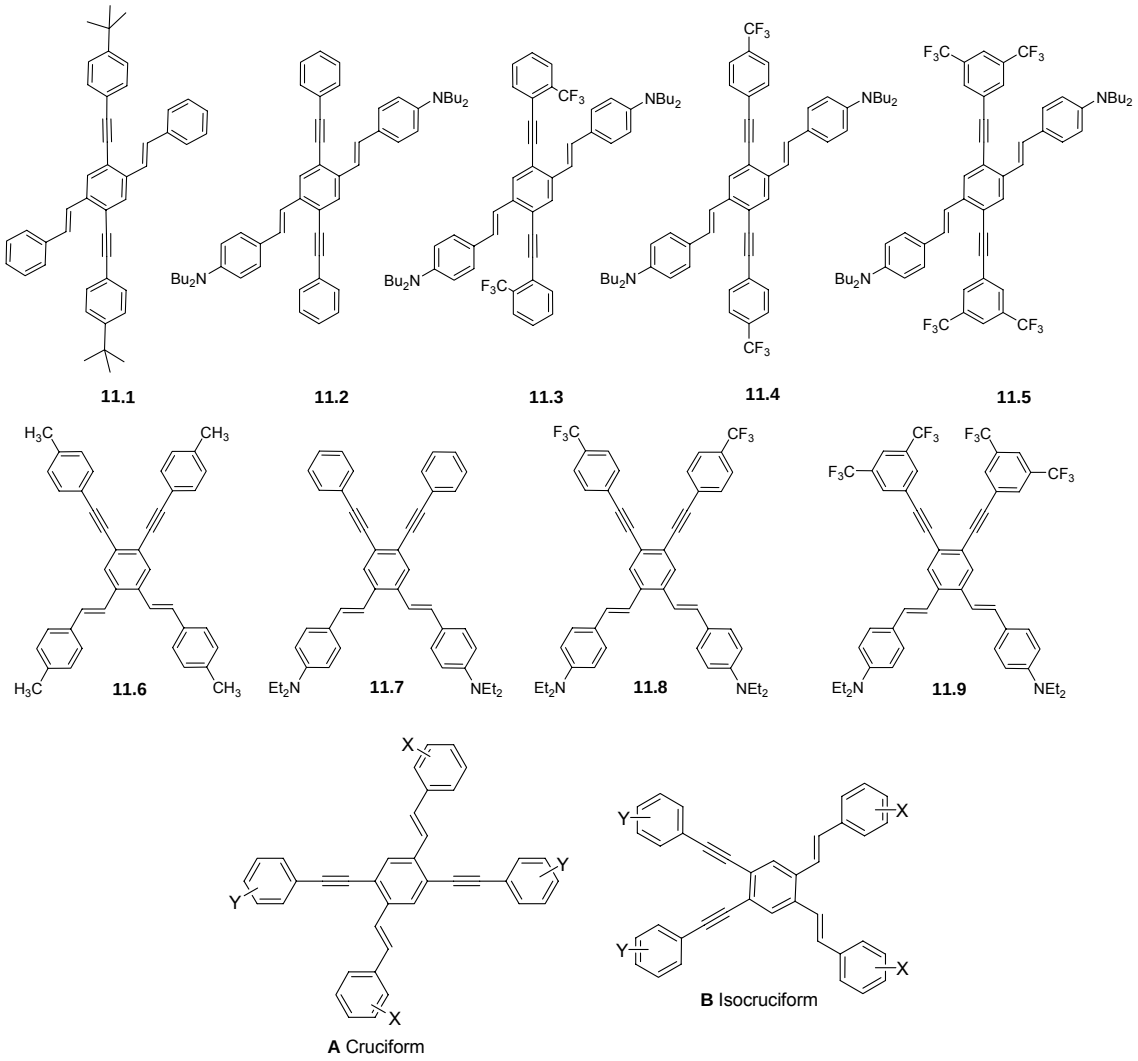


**Figure 11.1** Cruciforms **11.1-9**, broadly grouped into two types cruciforms **A** where phenylene-ethynylene subgroups are *para* to each other and isocruciforms **B** where phenylene-ethynylene subgroups are *ortho* to each other.

## 11.2 Results and Discussion

The synthesis of the cruciforms **11.1-3** and **11.5** has been described elsewhere.[7] The cruciform **11.4** and the isocruciforms **11.6-9** were prepared utilizing a similar route. Starting from the known diiodide **11.10** a Heck-Cassar-Sonogashira-Hagihara coupling with the alkyne **11.11** furnished the cruciform **11.4** (Scheme 11.1) in high yield and purity after chromatography and crystallization from hexanes.[9] For the isocruciforms

**11.6-9** (Schemes 11.2, 11.3) the central intermediates **11.17** and **11.18** were prepared. Starting from the compound **11.12** photochemical bromination furnished the tetrahalide **11.13** after multiple recrystallizations in 19% yield.

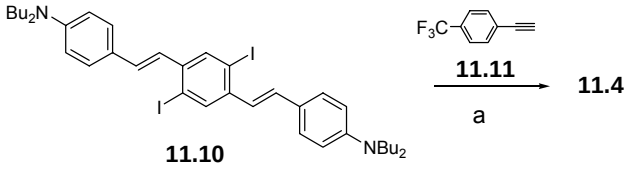


**Scheme 11.1.** (a) $(Ph_3P)_2PdCl_2$, CuI, piperidine, THF.

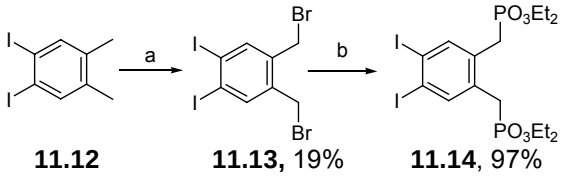


**Scheme 11.2.** (a) N-Bromo succinic imide, sun lamp, $CHCl_3$, 6h. (b) Triethylphosphite (solvent), reflux 8h.

An Arbuzov reaction transformed **11.13** into the phosphonate **11.14**, which in the presence of sodium hydride was subjected to the conditions of a Horner[10] olefination utilizing the aldehydes **11.15** and **11.6** to give the intermediates **11.17** and **11.18**. The yields in these reactions were considerably lower than those obtained in an analogous coupling for molecules of the type **11.10.** This is probably due (Scheme 11.3) to intramolecular ring closure of the sodium salt of **11.14**. The ring closed

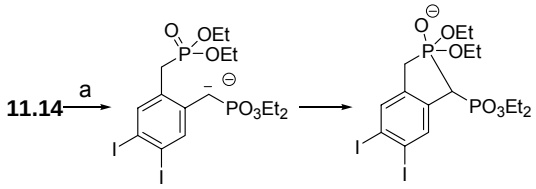


**Scheme 11.3.** (a) NaH in mineral oil

species may then decompose into further unidentified products. And indeed, this Horner reaction was always accompanied by the formation of polar, but hard to identify side products that gave rise to a forest of signals in their proton NMR spectrum. In the bisphosphonate precursor to **11.10** and similar *para*-distyrylbenzenes this intramolecular ring closure is sterically not possible and the yields of those double Horner reactions are considerably higher.[7]

The intermediate **11.17** (Scheme 11.4) is coupled to 4-methyl(phenylacetylene), and gave **11.6** in 46% yield. The intermediate **11.18** was subjected to a similar Heck-Cassar-Sonogashira-Hagihara[9] coupling utilizing phenylacetylene, 4-trifluoromethyl-phenylacetylene and 3,5-bis(trifluoromethyl)(phenylacetylene) (Scheme 11.5). This reaction furnished the isocruciforms **11.7-9** in yields between 80 and 94% after crystallization and chromatography. All of the isolated materials are yellow to yellow-orange solids, freely soluble in nonpolar organic solvents and stable crystalline materials in the solid state.

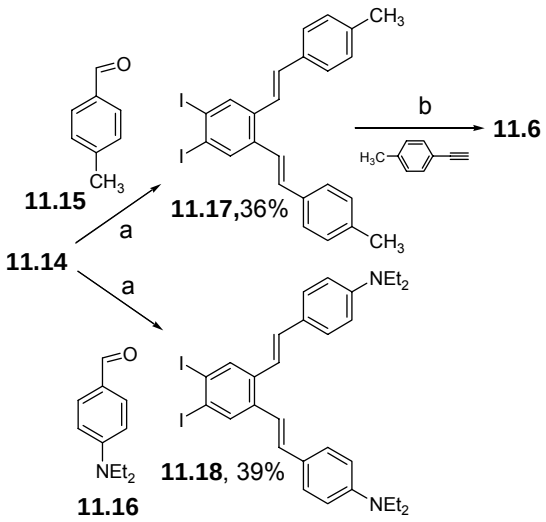


**Scheme 11.4.** (a) NaH, heat; slow addition of either **11.15** or **11.16**. (b) $(Ph_3P)_2PdCl_2$, CuI, piperidine.

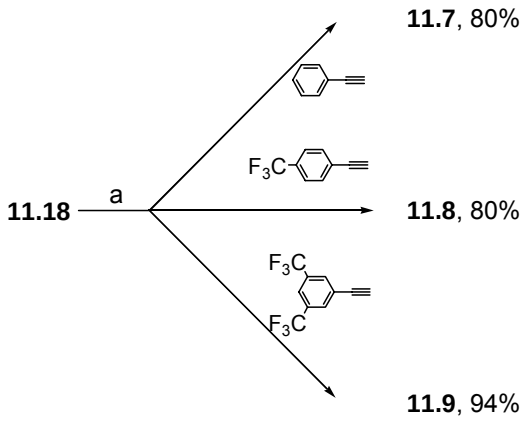


**Scheme 11.5.** (a) $(Ph_3P)_2PdCl_2$, CuI, piperidine

The optical properties of **11.1-9** are listed in Table 11.1. The absorption spectra of the conjugated crosses are unremarkable and their bandgap decreases with increasing donor-acceptor quality of the styryl and phenylethynyl side chains. As a conesquence, **11.1** and **11.6** show the highest band gaps in solution and in the solid state, while **11.5** and **11.9** show the smallest ones. The isocruciforms show a somewhat larger band gap than the cruciforms suggesting that conjugation is attenuated. In the isocruciforms all of the conjugative interactions of one type of substituent (either styryl or phenylethynyl) are of *ortho*- instead of the *para* -type.

The tetrasubstituted benzenes **11.1-9** are emissive in the solid state and in solution. Figure 11.2 shows the emission spectra of **11.5** in differrent solvents. The emission in **11.5** ranges from 521-608 nm. It is instructive to note that the emission of the pure hydrocarbon crosses **11.1** and **11.6** do not show any appreciable dependence on solvent (Figure 11.3, Table 11.1).

**Table 11.1.** Absorption and emission data for the cruciforms and isocruciforms **11.1-9**.

| Substituents Compound | Absorption [nm] | | Emission [nm] | | | | | | | |
|---|---|---|---|---|---|---|---|---|---|---|
| | $CHCl_3$ | Film | Hex. | $CHCl_3$ | THF | Acetone | EtOAc | MeOH | Film | Crystal |
| *tert*-butyl, H; **11.1** | 369 | 405 sh | 411 | 421 | 418 | 418 | 415 | 416 | 491 | 487 |
| Me,Me; **11.6** | 366 | 397 sh | 426 sh 433 | 433 | 430 | 431 | 429 | 430 | 479 | 497 |
| H,$NBu_2$; **11.2** | 442 | 474 | 471 | 510 | 515 | 535 | 510 | 532 | 560 | 603 |
| H,$NEt_2$; **11.7** | 410 | 451 | 455 | 518 | 521 | 540 | 514 | 536 | 539 | 535 |
| *o*-$CF_3$, $NBu_2$; **11.3** | 440 | 486 sh | 501 | 542 | 548 | 562 | 546 | 554 | 573 | 595 |
| *p*-$CF_3$, $NBu_2$; **11.4** | 441 | 480 sh | 492 | 539 | 549 | 564 | 546 | 555 | 584 | 594 |
| *p*-$CF_3$, $NEt_2$; **11.8** | 424 sh | 462 sh | 472 | 530 | 545 | 564 | 541 | 555 | 543 | 549 |
| *m,m*-$(CF_3)_2$, $NBu_2$; **11.5** | 470 sh | 518 sh | 521 | 558 | 573 | 591 | 568 | 583 | 585 | 608 |
| *m,m*-$(CF_3)_2$, $NEt_2$; **11.9** | 437 sh | 484 sh | 484 | 539 | 562 | 591 | 556 | 580 | 566 | 581 |

In Figure 11.3 a colored bar representation of all of the fluorescence data of **11.1-9** is displayed to give an overview of their emissive properties in different solvents and in the solid state. Some general trends can be gleaned. 1) The position of the $CF_3$-group on the phenylethynyl substituent (*ortho* or *para* with respect to the alkyne group) in **11.3** and **11.4** does not have a significant influence on their emission spectra. That is not unexpected, because the $CF_3$-groups have an inductive effect. Their position should not be critical. 2) The emission of the isocruciforms is blue shifted with respect to that of their cruciform isomers. 3) In thin film and in the crystalline state the emission of **11.1-9** is bathochromically shifted, probably due to the formation of excimers. This red shift, when going from solution into the crystalline state is significantly larger in the cruciforms

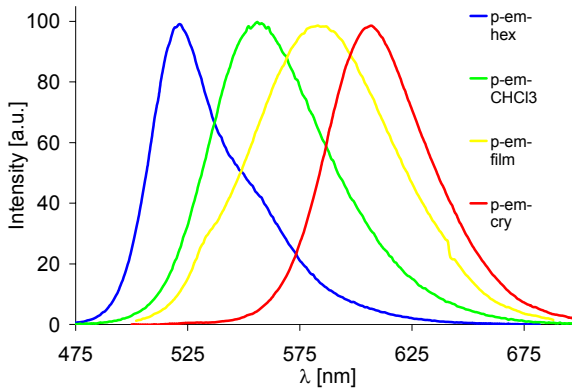


**Figure 11.2.** Emission spectra of compound **11.6** in different solvents and in the solid state. The emission maximum of **11.5** varies from 521 to 608 nm depending upon the environment.

when compared to their isocruciforms. Similar trends are observed in thin films, but the emission is generally less red-shifted. 4) The more polar the solvent, the more bathochromically shifted the emission for the donor-acceptor substituted oligomers. The distinct solvatechromicity of the emission is easily understood in terms of the stabilization of the excited state. The more donor-acceptor substituted the oligomer is, the more its excited state is charge separated, and the more red-shifted the observed emission is. In the compounds **11.3-5, 8** and **11.9** these effects are most strongly developed, due to the presence of both a donor (dialkylamino) and one or two acceptor groups ($CF_3$).

The quantum yields of **11.1,2** and **11.4-9** were determined in hexanes and in chloroform (Figure 11.4). Overall the quantum yields tend to be higher in hexanes than in chloroform, but there is no obvious correlation of the quantum efficiency with the structure or with the solvent utilized. The cruciforms **11.1-5** are photostable and do not bleach after prolonged exposure to UV light in a fluorimeter at 315 nm. In the case of the

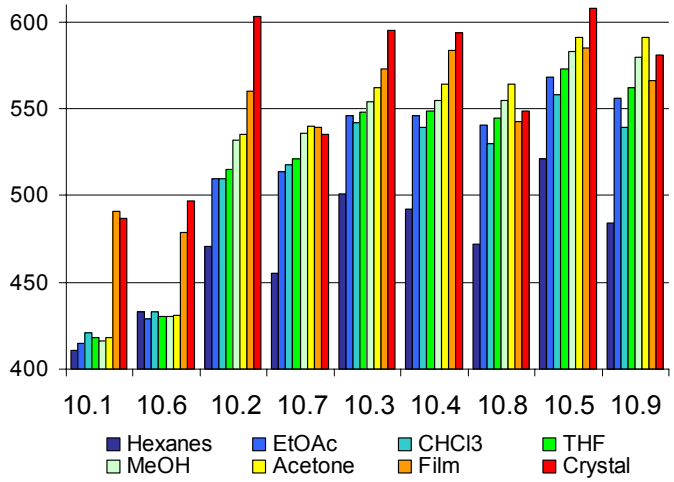


**Figure 11.3.** Bar graph of the emission spectra of **11.1-9.** The compounds are grouped according to their substituent patterns. Y-axis is the emission maximum in nm.

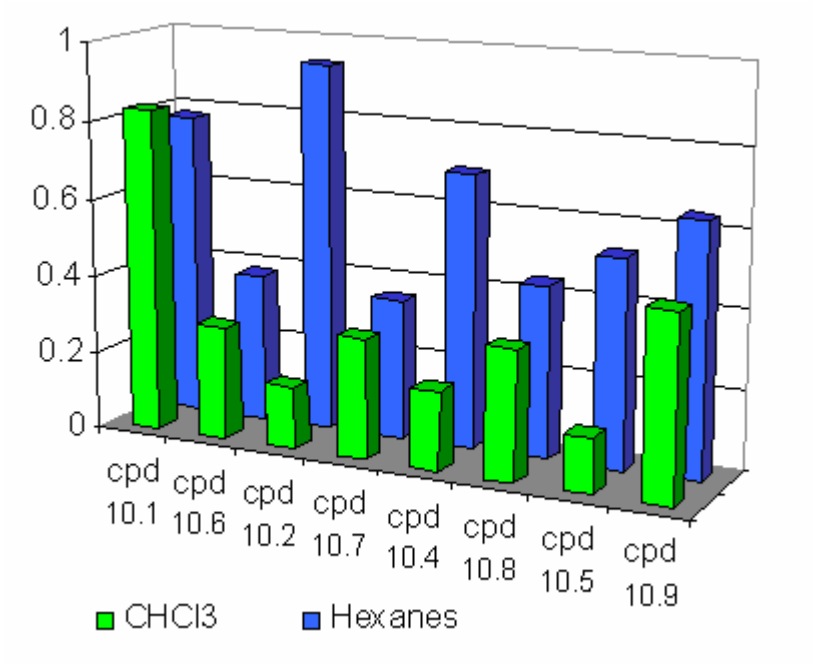


**Figure 11.4**. Quantum yield (y-axis) of **11.1,2** and **11.4-9** in hexanes and in chloroform.

isocruciforms **11.6-9** fast bleaching in dilute solution and in thin films is observed via an isosbestic point (Figure 11.6). Attempts to perform the irradiation in synthetically useful

concentrations led to the isolation of an unidentified brownish polymeric-insoluble residue that resisted attempts of a meaningful spectroscopic characterization. Müllen *et al*. had observed similar behavior when irradiating simple 1,2-distyrylbenzenes.[11] A mass spectrum taken from a very dilute sample of **11.8**, irradiated in chloroform showed the presence of a molecular ion at 794 amu suggesting the uptake of a chlorine atom under the reaction conditions. We speculate that this is a photo-induced radical process, possibly involving a Bergman-type reaction of the enediyne moieties of the isocruciforms. Further investigations of this interesting process are ongoing. In the solid state the bleaching process can be utilized to irreversibly etch patterns into thin films of **11.9**. Figure 11.5 shows such a pattern "RHG" etched into a thin film of **11.9**.


**Figure 11.5.** Thin film of **11.8** irradiated through an RHG mask at 315 nm. Irradiated areas are non fluorescent.

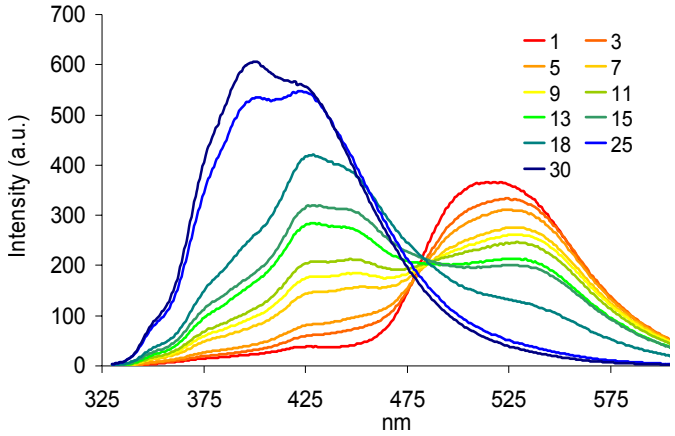


**Figure 11.6**. Emission spectra of **11.8** under irradiation in hexanes after 1,3,5….30 min. After 30 min the spectrum of **11.8** has disappeared, instead a broad emission centered at 401 nm has developed.

The electrochemistry of the isocruciforms **11.6-9** was examined by cyclic voltammetry to correlate **11.6-9**'s redox properties to their structure. Table 11.2 shows the electrochemical potentials of **11.6-9** for oxidation and for reduction. Comparison of the oxidation potentials of **11.6-9** reveals that **11.6** is oxidized at 1.1V but **11.7-9** are oxidized at a considerably lower potential, i.e. at 0.47-0.49 V. The $CF_3$-groups in **11.8** or **11.9** do not seem to play a role in the determination of the oxidation potential; the diethylamino groups do have a determining influence on the oxidation potential. The positive charge of the oxidized species -we speculate- is located on the distyrylbenzene branch of **11.7-9**. That is reasonable, because the presence of the diethylamino group pumps electron density into the already electron rich π-system. The phenyleneethynylene branch does not seem to be involved in the reversible electrochemical oxidation event.

The isocruciforms **11.6** and **11.7** are reduced between -1.63 and -1.70 V while **11.8** and **11.9** are reduced at around -1.47 V, at significantly lower negative potential than **11.6** and **11.7**. This is easily understood, because the LUMO of **11.6-9** should be located on the electron deficient bis(phenylethynyl)benzene branch of the molecules. The electron accepting trifluoromethyl substituents help to accommodate the negative charge on this branch leading to a lower reduction potential.

**Table 11.2**: Reduction and oxidation potentials of **11.6-9** vs. Standard Hydrogen Electrode, HOMO and LUMO positions of **11.6-9** calculated from oxidation and reduction potentials as well as by SPARTAN with B3LYP utilizing the 6-31G** basis set.

| | **11.6** | **11.7** | **11.8** | **11.9** |
|---|---|---|---|---|
| | Oxidation [V]: | | | |
| $E_{1/2}$ | 1.27 | 0.52 | 0.57 | 0.55 |
| peak | 1.35 | 0.56 | 0.62 | 0.63 |
| HOMO | -5.77 | -5.02 | -5.07 | -5.05 |
| | Reduction [V]: | | | |
| $E_{1/2}$ | -1.77 | -1.83 | -1.61 | -1.62 |
| peak | -1.86 | -1.94 | -1.71 | -1.70 |
| LUMO | -2.73 | -2.67 | -2.89 | -2.88 |
| Band gap | 3.04 | 2.35 | 2.18 | 2.17 |
| | Quantum Chemical Calculations [eV]: | | | |
| HOMO | -5.16 | -4.74 | -4.96 | -5.04 |
| LUMO | -2.04 | -1.68 | -2.05 | -2.20 |
| Band gap | 3.12 | 3.06 | 2.89 | 2.84 |

To understand the optical (i.e. band gap, solvatochromicity) and the redox properties of **11.6-9**, quantum chemical calculations (B3LYP utilizing 6-31G** basis set; SPARTAN) were performed. Table 11.2 contains the results of the calculations for **11.6-9.** In Figures 11.7 and 11.8 the calculated HOMOs and LUMOs of **11.6** and **11.9** are shown. The values in Table 11.2 demonstrate the decreasing band gap when going from

the hydrocarbon **11.6** to the donor-acceptor substituted arene **11.9**. The localization of the HOMO and the LUMO of **11.6** and of **11.9** are critical to understand the solvatochromic behavior of the isocruciforms. In **11.6** the HOMO as well as the LUMO are spread out over the whole π-system. Both orbitals are decidedly delocalized (Figure 11.7). In **11.9** that is not the case (Figure 11.8). Instead the HOMO is mostly located on the distyrylbenzene branch of the molecule, while the LUMO resides mostly on the aryleneethynylene branch of the isocruciform **11.9**. The central ring is an integral part of both orbitals. Upon photonic excitation, an electron from the HOMO will be advanced into the LUMO to give a highly polarized state. This polarized excited state should be significantly stabilized by polar solvents, as observed (Table 11.1). Increasing solvent

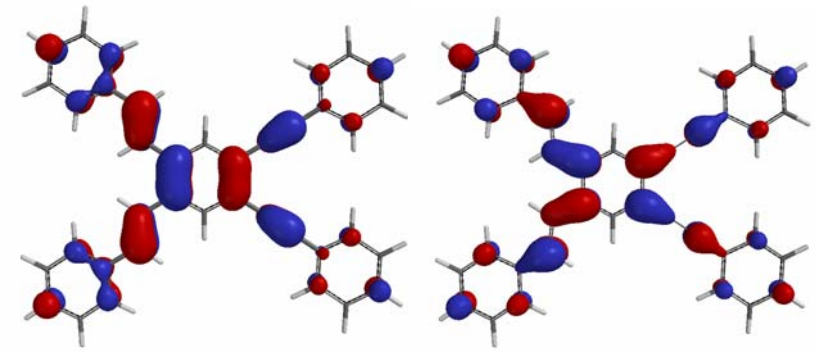

**Figure 11.7.** HOMO (left) and LUMO (right) of **11.6**. The methyl groups are omitted to minimize the time to calculate the structures.

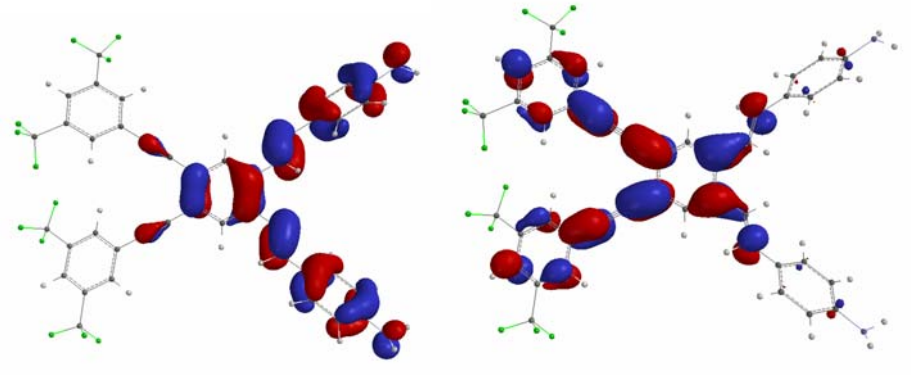

**Figure 11.8.** HOMO (left) and LUMO (right) of **11.9.** The diethylamino groups are substituted by simple $NH_2$ groups to decrease the time to calculate the structures.

polarity leads to a significantly red shifted emission but only to a small change in absorption as expected for an excited state effect. As a means of comparison we have calculated the structure and the energetics of **11.5** (B3LYP; 6-31G** basis set). In Figure 11.9 the HOMO and the LUMO of **11.5** are shown. The calculated band gap of **11.5** is 2.7 eV.

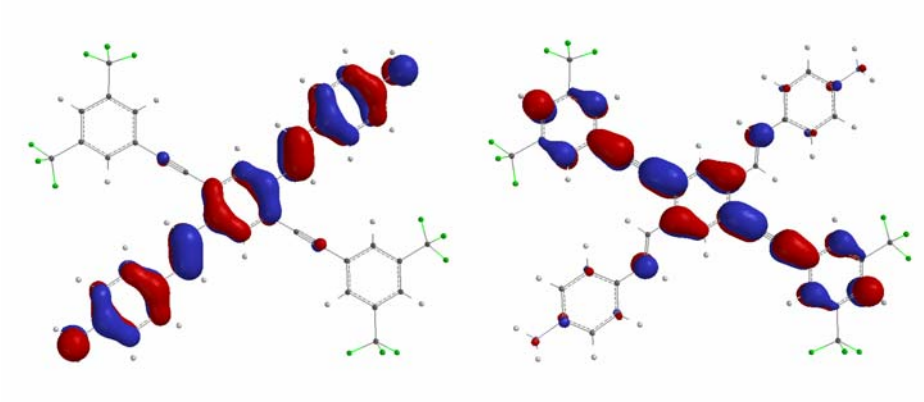

**Figure 11.9.** Calculated (B3LYP, 6-31G**, SPARTAN 04) HOMO (top, -4.98 eV) and LUMO (bottom, -2.28 eV) of **11.5**. The calculated band gap is 2.70 eV.

The band gap of **11.5** is lower than that of **11.9**, which is 2.89 eV. The HOMO and the LUMO of **11.5** (Figure 11.9) are even more localized on their relative branches than the HOMO and the LUMO of **11.9**.

The quantum chemical calculations support a self-consistent picture that explains the decreased band gap when going from **11.6** to **11.9** as well the increased solvatochromicity (Table 11.3). Both effects are due to the increased localization of the HOMO and the LUMO respectively on the distyrylbenzene and the aryleneethynylene branches in **11.9** . When the HOMO and the LUMO of **11.9** are compared to the frontier

**Table 11.3**: Band gap of **11.1,2** and **11.4-9** calculated from oxidation and reduction potentials, from the optical band gap as well as by SPARTAN with B3LYP utilizing the 6-31G** basis set. Electrochemical band gaps of **11.1-5** are from ref [7]

| | Calculated bandgap [eV] | Optical bandgap [eV] | Electro-chemical bandgap [V] |
|---|---|---|---|
| **11.1** | 3.06 | 3.08 | 2.35 |
| **11.2** | 3.08 | 2.56 | 2.33 |
| **11.4** | 2.72 | 2.47 | 2.33 |
| **11.5** | 2.68 | 2.39 | 2.35 |
| **11.6** | 3.12 | 3.08 | 3.04 |
| **11.7** | 3.06 | 2.75 | 2.35 |
| **11.8** | 2.89 | 2.63 | 2.18 |
| **11.9** | 2.84 | 2.52 | 2.17 |

orbitals of **11.5**[7] one can see that the geometrical separation of HOMO and LUMO (Figure 11.8,9) is even more succinct in **11.5**. So is **11.5**'s solvatochomicity. The herein presented calculations are in good qualitative agreement with the experimental band gap data obtained from fluorescence spectroscopy and from cyclic voltammetry and explain the observed solvatochromicity (Figure 11.10).

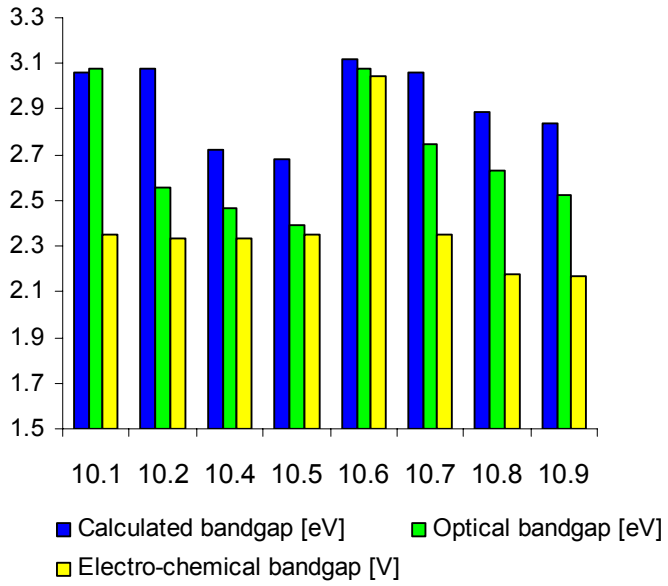


**Figure 11.10.** Comparison of the calculated and experimental band gaps of the compounds **11.1,2** and **11.4-9**. The values are taken from Table 11.3.

To get a better feel for the structures and the conformations of the isocruciforms in the solid state, single crystalline specimen of **11.6-8** were grown and their structures solved (Figures 11.11-13). Compound **11.9** did not form single crystals but a micro-crystalline powder. However, **11.6-8** are quite disordered in the solid state. The compound **11.6** crystallizes in an unusual tetragonal space group. That is due to the structural similarity of the styryl and the phenylethynyl substituents that are completely disordered in the solid state. In Figure 11.11 the ORTEP of **11.6** and two views of its packing in the solid state are shown. The alkyne/alkyne connectors are indistinguishable in the solid state. The arene rings are somewhat twisted with respect to each other. The twist angles between the central benzene and the outer rings vary from 12-32 degrees. Interestingly, pairs of oppositely located "arms" show similar torsion angles.

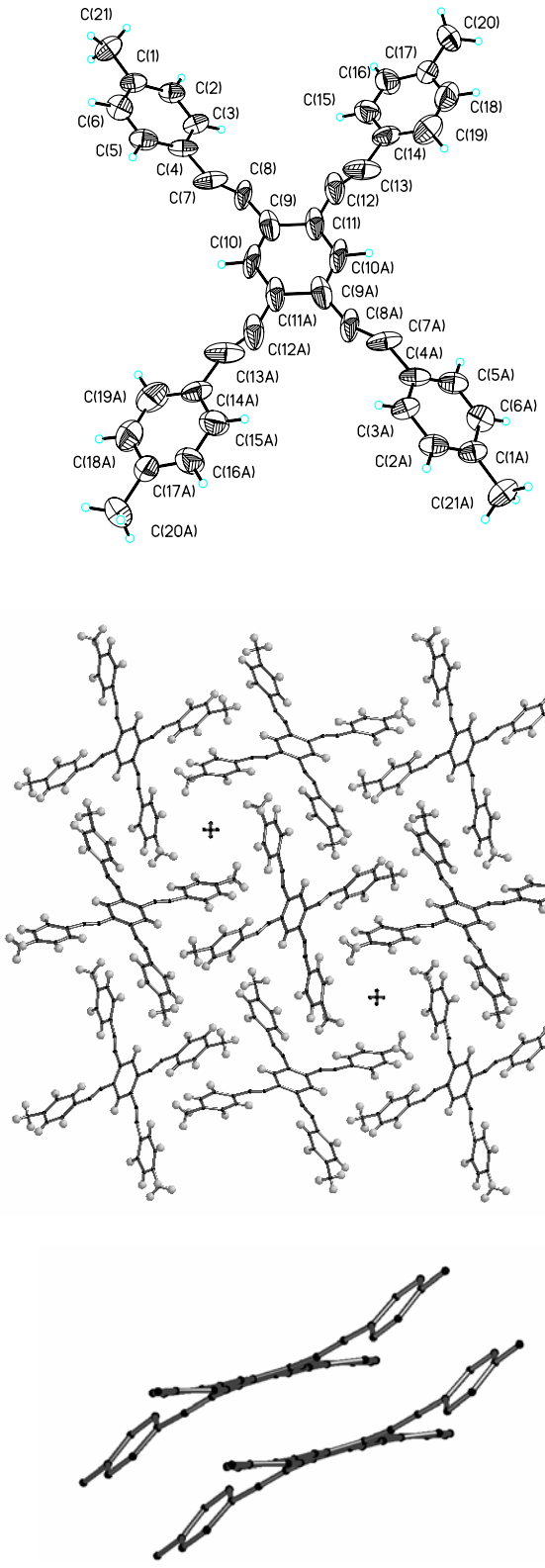


**Figure 11.11**. Top: ORTEP representation of **11.6**. Notable is the disorder, that renders alkyne and alkene units identical in the solid state. Middle, Bottom: Tetragonal packing of **11.6**. The molecules of **11.6** are packed in tilted stacks

The molecules are packed in tilted stacks with an interstack distance of approx. 3.6 A, the van der Waals radius of carbon.

An ORTEP representation and views of the packing of **11.7** are shown in Figure 11.12. The ethyl groups of the amine substituents in **11.7** are disordered, and the outer rings are twisted with respect to the central one. One of the phenyleneethynylene units is twisted around 13 degrees, while the other one is twisted around 37 degrees. The degree of twisting with respect to the central core ranges from 11 to 58 degrees.

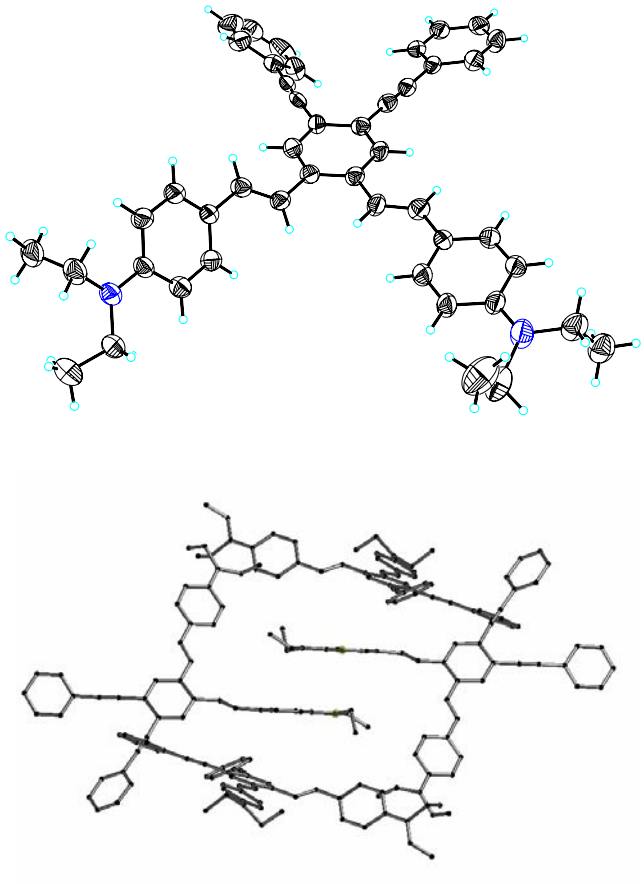

**Figure 11.12**. Top: ORTEP representation of **11.7**. Bottom: Packing diagram of **11.7**. Distance between two layers is 3.596 A.

In **11.7** two of the substituents are almost coplanar with the central ring, while the other two show a significant twist. There are 4 independent molecules in the unit cell and each of them has a set of somewhat different twist angles of the benzene rings with respect to the center ring.

In the crystals of the compound **11.8** (Figure 11.13) the situation is similar to that of **11.7**. Here as well two out of the four substituents are more twisted than the other two. An additional feature is the rotational disorder of the $CF_3$ groups that is not unexpected in this type of structures.

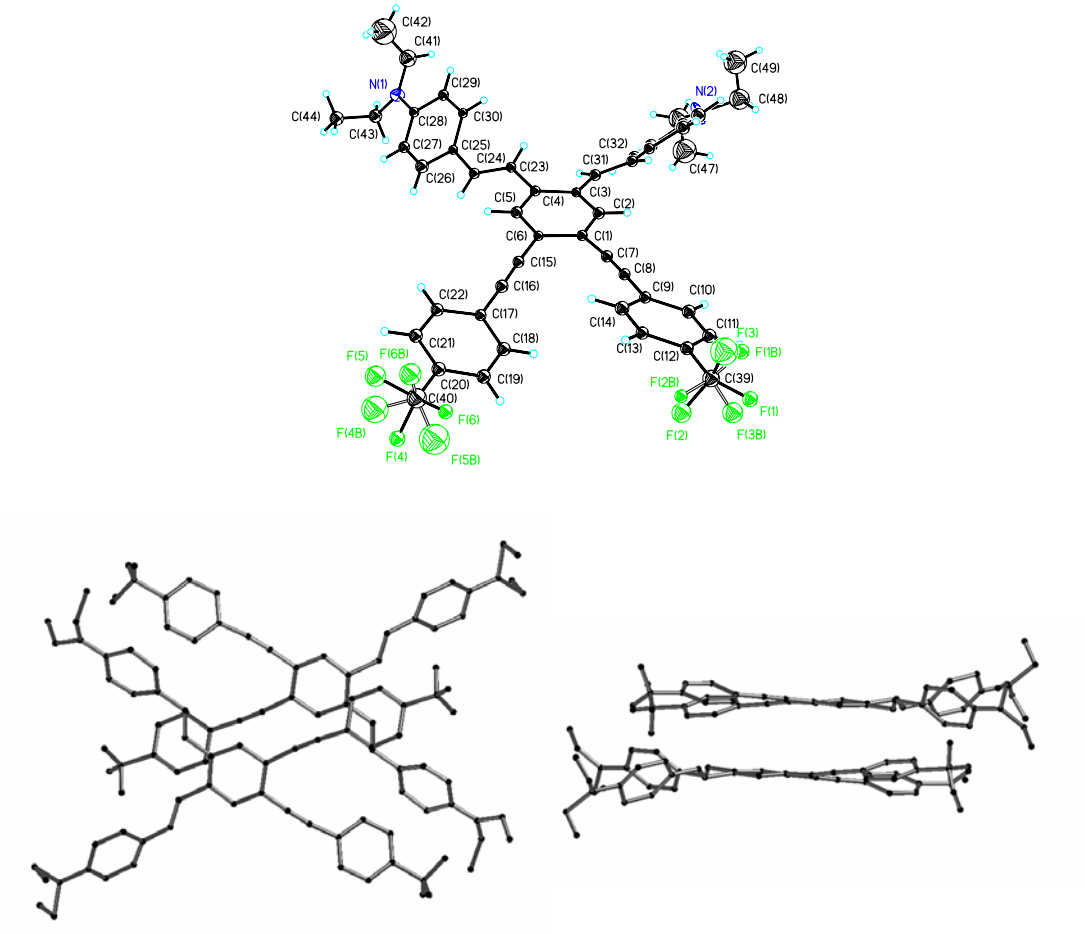


**Figure 11.13**. Top: ORTEP representation of a representative molecule of **11.8**. The trifluoromethyl groups are rotationally completely disordered. Middle, Bottom: Packing diagram of **11.8**. Distance between two layers is 3.51 A.

In all of the cases, the π-systems are packed closely and in a herringbone or a modified herringbone pattern. The distances between the π-systems are in the range of the van der Waals distance of carbon, i.e. between 3.5 and 3.8 Å. The close proximity of the π-systems leads to their interaction in the solid state, and we interpret the observed bathochromic emissions of crystalline or microcrystalline species of **11.6-9** as a sign of excimer formation of the isocruciforms in the solid state.

## 11.3 Conclusion

In conclusion we have prepared the isocruciforms **11.6-9** by a combination of Horner and Heck-Cassar-Sonogashira-Hagihara reactions. The optical and electrochemical properties of the isocruciforms are similar to those of the cruciforms **11.1-5**, however, their emission spectra are somewhat blue shifted, due to the decreased conjugative pathways in the *ortho* connected isocruciforms. The electrochemical oxidation and reduction of the isocruciforms combined with the quantum chemical calculations and the emission data in a series of different solvents shows that HOMO and LUMO of the isocruciforms are located on the distyrylbenzene and the bisphenylethynyl branch of the molecules respectively, similar to those observed for **11.1-5**. This trend is more pronounced in the donor-acceptor substituted isocruciforms **11.8** and **11.9** where an electronic decoupling of HOMO and LUMO is more prevalent. The cruciforms and the isocruciforms are cross conjugated molecules, even though in a non-classical sense.[12,13] The large bathochromic shift in emission of **11.1-9** in the crystalline state can be explained by the packing of the π-systems that leads to strong electronic interactions in the excited state.[14] The presence of the 1,2-distyrylbenzene unit in **11.6-9** makes them

potentially attractive as materials for photopatterning. In future we will report single crystal reactivity of **11.6-9** and their incorporation of into polymers. These materials have interesting properties as 3rd order NLO-phores and similar applications.

## 11.4 Experimental

1,2-Bis-bromomethyl-4,5-diiodo-benzene **(11.13)** A round bottom flask with stirbar was charged with 50.0 g (0.140 mol) of **12.12**, 120 g (0.667 mol) of N-bromosuccinimide, 1.3 L of chloroform and 1.00 g (6.85 mmol) of *t*-butyl peroxide. A condensor column was place atop the flask and the reaction mixture was irradiated with a sun lamp (120 W, General Electric 120R40/P1) while refluxing for 6 h. The reaction mixture was allowed to cool to room temperature and crystals of succinimide formed which could be filtered off. The chloroform solution was washed three times with 500 mL of 5% sodium sulfite solution followed by two washes of 500 mL of water. The chloroform was removed by roto-vap and the resulting solid was crystallized from hexane. Yield: 14.0 g, 19.4 %. MP: 98° C. $^{1}$H NMR ($CDCl_3$) δ 7.79 (s, 2H), 4.47 (s, 4H). $^{13}$C NMR ($CDCl_3$) 141.1, 137.6, 108.7, 28.0. IR ($cm^{-1}$): 3014.5, 2896.9, 2849.6, 2735.4, 2660.1, 2408.9, 2291.3, 1992.3, 1972.1, 1777.8, 1729.6, 156.5, 1451.8, 1432.1, 1341.9, 1268.1, 1212.2, 1168.3, 1142.3, 1098.4, 898.8, 877.1.

[2-(Diethoxy-phosphorylmethyl)-4,5-diiodo-benzyl]-phosphonic acid diethyl ester **(11.14)** A 250 mL round bottom flask was charged with a stirbar, 23.2 g (45.0 mmol) of **11.13**, and 100 mL of triethylphosphite. A condensor column was placed atop the reaction vessel and the reaction refluxed for 8 h. The reaction was allowed to cool briefly

before the excess triethylphosphite was distilled off. The product was crystallized from hexane to offer clear crystalline cubes. Yield: 27.5 g, 97 MP: 115° C. $^{1}$H NMR ($CDCl_3$) δ 7.70 (δ, 2H, $J_{4H,P}$ = 1.9 Hz), 4.06-3.97 (m, 8H), 3.31-3.24 (d, 4H, $J_{2H,P}$ = 20.33 Hz), 1.28–1.23 (t, 12H, $J_{3H,H}$ = 7.1 Hz). $^{13}$C NMR ($CDCl_3$) δ 141.6, 133.1, 105.7, 62.3, 31.5–29.6 (d, $J_{1P,C}$ = 137.4 Hz) , 16.5. IR ($cm^{-1}$): 2978.4, 2909.9, 2863.1, 2828.9, 2810.1, 1748.5, 1733.4, 1569.5, 1476.4, 1452.3, 1408.9, 1394.0, 1366.5, 1341.9, 1249.8, 1221.8, 1202.5, 1160.1, 1099.4, 1047.3, 1019.3, 893.0, 864.5.

1,2-Diiodo-4,5-bis-(2-p-tolyl-vinyl)-benzene **(11.17)** A 500 mL Schlenk flask was charged with a stirbar and 5.40 g (8.57 mmol) of **11.14** while under nitrogen purge. Dry THF (250 mL) was added followed by 1.2 g (50 mmol) of NaH. A condensor column was placed atop the reaction vessel and capped with a balloon. The schlenk cock was closed and the stem was capped with a septum. The reaction mixture was heated to reflux for 30 min at which point it had turned yellow. Tolualdehyde **11.15** (2.57 g, 21.4 mmol) was added via a syringe in approximately 10 0.25 mL aliquots every 5 min. The reaction was allowed to cool to room temperature. The crude reaction mixture was poured slowly into a 2L Erlenmeyer flask was filled with 1 kg of ice. The product was extracted with hexane (2x 200 mL) which was reduced and run over a fritted funnel with a silica plug. The product was obtained as a pale yellow solid (1.72 g, 36% yield). MP: 150° C. $^{1}$H NMR ($CDCl_3$) δ 8.01 (s, 2H), 7.41-7.39 (d, 4H, $J_{3H,H}$ = 7.69 Hz), 7.21-7.14 (m, 6H), 6.97-6.92 (d, 2H, $J_{3H,H}$ = 15.9 Hz), 1.53 (s, 6H). $^{13}$C NMR ($CDCl_3$) δ 138.2, 137.2, 136.7, 132.5, 129.4, 126.6, 123.1, 106.0, 99.3, 21.4. IR ($cm^{-1}$): 3045.9, 3040.1, 3017.9, 3006.8, 2965.8, 2917.1, 2853.0, 1628.3, 1624.0, 1607.6, 1568.0, 1508.7, 1456.6,

1448.0, 1436.9, 1409.4, 1376.6, 1354.9, 1325.5, 1300.4, 1281.6, 1279.2, 1262.3, 1229.5, 111.81.3, 1118.2, 1108.5, 1040.0, 1038.3, 1016.9, 949.9, 847.2.

1,2-Bis-(3,5-bis-trifluoromethyl-phenylethynyl)-4,5-bis(4-diethylaminostyryl)benzene **(11.18)** A 500 mL schlenk flask was charged with a stirbar and 3.70 g (5.87 mmol) of **11.14** while under nitrogen purge. Dry THF (250 mL) was added followed by 1.2 g (50 mmol) of NaH. A condensor column was placed atop the reaction vessel and capped with a balloon. The schlenk cock was closed and the stem was capped with a septum. The reaction mixture was heated to reflux for 30 min at which point it had turned yellow. Diethylaminobenzaldehyde **11.16** (2.30 g, 12.9 mmol) was dissolved in the minimum volume of dry THF (~8 mL) and was added via a syringe in 8 aliquots every 5 min. The reaction was allowed to cool to room temperature. The crude reaction mixture was poured slowly into a 2 L Erlenmeyer flask was filled with 1 kg of ice. This mixture was separated with the addition of NaCl and the THF portion was extracted then reduced. The crude product was redissolved in 50 mL of hexane with 10 mL of dichloromethane. This solution was run over a fritted funnel with a silica plug in the same solvent mixture. The product proceeded as a yellow band, was collected and the solution was evaporated and further purified by crystallization from hexane/dichloromethane mixture. The product was obtained as large yellow crystals (1.55 g, 39% yield). MP: 175$^{o}$ C. $^{1}$H NMR ($CDCl_3$) δ 7.94 (s, 2H), 7.36-7.35 (d, 4H, 8.24 Hz), 7.01-6.96 (d, 2H, $J_{3H,H}$ = 15.9 Hz), 6.89-6.86 (d, 2H, $J_{3H,H}$ = 15.9 Hz), 3.41-3.34 (q, 8H, $J_{3H,H}$ = 7.1 Hz), 1.52-1.14 (t, 12H, $J_{3H,H}$ = 7.1 Hz). $^{13}$C NMR ($CDCl_3$) δ 147.9, 138.0, 136.5, 132.5, 128.4, 124.5, 119.4, 111.8, 104.9, 44.7, 13.0. IR ($cm^{-1}$): 3039.1, 3006.3, 2959.6, 2923.4, 1601.8, 1596.0,

1576.2, 1557.9, 1512.6, 1495.7, 1490.4, 1479.3, 1464.8, 1441.2, 1429.6, 1373.7, 1357.8, 1355.4, 1265.2, 1200.1, 1236.6, 1138.4, 1092.1, 1078.1, 1070.4, 1025.1, 947.0, 930.1.

1,2-Bis-p-tolylethynyl-4,5-bis-(2-p-tolyl-vinyl)-benzene **(11.6)** 1.00 g (1.78 mmol) of **11.17** were placed intoa schlenk tube with stirbar under nitrogen purge. To this was added 5.0 mL of THF and 3.0 mL of piperidine. This solution was allowed to stir vigorously for 10 min. 10 mg (14 μmol) of $Pd(PPh_3)Cl_2$ and 5.0 mg (26 μmol) of CuI were added and the tube was fitted with a septum. With a syringe, 516 mg (4.45 mmol) of 4-methyl-1-ethynylbenzene were added. The reaction was allowed to proceed at room temperature for 48 h. The crude reaction mixture was diluted with hexane and run through a silica plug on a fritted funnel with hexane (100 mL) as an eluent. The hexane solution was collected and discarded. A 50:50 dichloromethane:hexane mixture (250 mL) was then passed through the silica plug and collected. This solution was reduced to yield 437 mg (46 % yield) of a green crystalline solid. To obtain crystals for XRD analysis 100 mg were dissolved in approximately 10 mL of dichloromethane. Aliquots of this solution (2-3 mL) were placed in the bottom of a test tube filled with hexane and capped with a septum. MP: 233° C. $^1$H NMR ($CDCl_3$) δ 7.78, 7.51-7.48 (d, 4H, $J_{3H,H}$ = 7.97 Hz), 7.46-7.43 (d, 4H, $J_{3H,H}$ = 7.97 Hz), 7.38-7.33 (d, 2H, 15.9 Hz), 7.21-7.16 (m, 8H), 7.09-7.03 (d, 2H, $J_{3H,H}$ = 15.9 Hz), 2.37 (s, 12H). $^{13}$C NMR ($CDCl_3$) δ 138.4, 137.9, 135.6, 134.3, 132.1, 131.5, 129.5, 129.4, 129.1, 126.6, 124.5, 124.1, 120.2, 94.0, 87.9, 21.7, 21.4. IR ($cm^{-1}$): 3024.2, 2918.1, 2855.4, 2731.0, 2203.0, 1905.1, 1792.2, 1656.7, 1629.3, 1605.6, 1512.6, 1481.7, 1447.5, 1412.3, 1377.1, 1302.3, 1281.1, 1264.7, 1209.8, 1181.8, 1118.2, 1104.7, 1039.6, 1033.3, 1016.9, 970.1, 962.4, 816.8, 806.7.

1,2-Bis-phenylethynyl-4,5-bis(4-diethylamino)styryl-benze **(11.7)** 520 mg (0.769 mmol) of **11.18** were placed into a schlenk tube with stirbar under nitrogen purge. To this was added 5.0 mL of THF and 3.0 mL of piperidine. This solution was allowed to stir vigorously for 10 min. 10 mg (14 μmol) of $Pd(PPh_3)Cl_2$ and 5.0 mg (26 μmol) of CuI were added and the tube was fitted with a septum. With a syringe, 500 mg (4.9 mmol) of phenylacetylene were added. The reaction was allowed to proceed at room temperature for 48 h. The crude reaction mixture was diluted with hexane and run through a silica plug on a fritted funnel with hexane (100 mL) as an eluent. The hexane solution was collected and discarded. A 50:50 dichloromethane:hexane mixture (250 mL) was then passed through the silica plug and collected. This solution was reduced to 25 mL and poured into 200 mL of methanol. The precipitate was collected to yield 384 mg (80 % yield) of a yellow crystalline solid. To obtain crystals for XRD analysis 100 mg were dissolved in approximately 10 mL of dichloromethane. Aliquots of this solution (2-3 mL) were placed in the bottom of a test tube filled with methanol and capped with a septum. MP: 191-193$^{o}$ C. $^{1}$H: δ 7.88 (s, 2H), 7.64-7.61 (m, 4H), 7.46-7.43 (d, 4H, $J_{3H,H}$ = 8.5 Hz), 7.41-7.35 (m, 6H), 7.24-7.19 (d, 2H, $J_{3H,H}$ = 15.9 Hz), 7.06-7.00 (d, 2H, 16.2 Hz), 6.71-6.68 (d, 4H, 8.5 Hz), 3.44-3.37 (q, 8H, $J_{3H,H}$ = 6.9 Hz), 1.23-1.18 (t, 12H, $J_{3H,H}$ = 6.9 Hz) $^{13}$C: δ 147.8, 136.5, 132.3, 131.8, 129.5, 128.5, 128.4, 124.9, 123.8, 123.6, 120.4, 111.8, 93.5, 89.3, 44.8, 13.1. IR ($cm^{-1}$): 3061.8, 3017.9, 2977.4, 2965.8, 2001.5, 1951.4, 1876.6, 1597.4, 1583.9, 1552.1, 1511.1, 1462.9, 1441.2, 1426.7, 1396.4, 1393.0, 1371.3, 1293.2, 1250.8, 1219.4, 1176.5, 1156.7, 1139.9, 1092.1, 1070.9, 1064.2

1,2-Bis(4-diethylaminostyryl)-4,5-bis-(4-trifluoromethyl-phenylethynyl)benzene **(11.8)** 510 mg (0.754 mmol) of **11.18** were placed intoa schlenk tube with stirbar under nitrogen purge. To this was added 5.0 mL of THF and 3.0 mL of piperidine. This solution was allowed to stir vigorously for 10 min. 10 mg (14 μmol) of $Pd(PPh_3)Cl_2$ and 5.0 mg (26 μmol) of CuI were added and the tube was fitted with a septum. With a syringe, 3.00 g (17.6 mmol) of 4-trifluoromethylethynylbenznene were added. The reaction was allowed to proceed at room temperature for 48 h. The crude reaction mixture was diluted with hexane and run through a silica plug on a fritted funnel with hexane (100 mL) as an eluent. The hexane solution was collected and discarded. A 50:50 dichloromethane:hexane mixture (250 mL) was then passed through the silica plug and collected. This solution was reduced to 25 mL and poured into 200 mL of methanol. The precipitate was collected to yield 457 mg (80 % yield) of a yellow crystalline solid. To obtain crystals for XRD analysis 100 mg were dissolved in approximately 10 mL of dichloromethane. Aliquots of this solution (2-3 mL) were placed in the bottom of a test tube filled with methanol and capped with a septum . MP: 220$^{o}$ C. $^{1}$H NMR ($CDCl_3$) δ 7.73 (s, 2H), 7.64-7.57 (m, 8H), 7.41 (d, 4H, $J_{3H,H}$ = 8.24 Hz), 7.18 (d, 2H, $J_{3H,H}$ = 15.9 Hz), 7.01 (d, 2H, $J_{3H,H}$ = 15.9 Hz), 6.66 (d, 4H, $J_{3H,H}$ = 8.24 Hz), 3.40-3.37 (q, 8H, $J_{3H,H}$ = 6.87 Hz), 1.21-1.17 (t, 12H, $J_{3H,H}$ = 6.59 Hz) . $^{13}$C NMR ($CDCl_3$) δ 137.05, 132.67, 131.90, 130.67-129.37 (q, $J_{2C,F}$ = 33.2 Hz), 129.68, 129.56-118.76 (q, $J_{1C,F}$ = 271.4 Hz), 128.47, 127.53, 125.54, 124.7, 122.82, 120.09, 111.76, 92.03, 91.51, 44.76, 13.03. IR ($cm^{-1}$): 2967.3, 2866.0, 2207.9, 1873.7, 1616.9, 1601.8, 1576.2, 1475.9, 1456.6, 1448.0, 1428.2, 1398.8, 1358.3, 1349.6, 1310.1, 1297.0, 1267.6, 1154.3, 1120.1, 1104.2, 1064.6, 1013.5, 1001.5, 966.8, 955.2, 931.1.

1,2-Bis-(3,5-bis-trifluoromethylphenylethynyl)-4,5-bis(4-diethylaminostyryl)benzene (**11.9**) 520 mg (0.769 mmol) of **11.18** were placed intoa schlenk tube with stirbar under nitrogen purge. To this was added 5.0 mL of THF and 3.0 mL of triethylamine. This solution was allowed to stir vigorously for 10 min. 10 mg (14 μmol) of $Pd(PPh_3)Cl_2$ and 5.0 mg (26 μmol) of CuI were added and the tube was fitted with a septum. With a syringe, 3.00 g (12.6 mmol) of 3,5-bistrifluoromethylethynylbenzene were added. The reaction was allowed to proceed at room temperature for 48 h. The crude reaction mixture was diluted with hexane and run through a silica plug on a fritted funnel with hexane (100 mL) as an eluent. The hexane solution was collected and discarded. A 50:50 dichloromethane:hexane mixture (250 mL) was then passed through the silica plug and collected. This solution was reduced to 25 mL and poured into 200 mL of methanol. The precipitate was collected to yield 646 mg (94 % yield) of a yellow crystalline solid. To obtain single crystalline specimen 100 mg were dissolved in approximately 10 mL of dichloromethane. Aliquots of this solution (2-3 mL) were placed in the bottom of a test tube filled with methanol and capped with a septum. MP: 207° C. $^1$H NMR ($CDCl_3$) δ 7.97 (s, 4H,), 7.82 (s, 2H), 7.80 (s, 2H), 7.45 (d, 4H, $J_{3H,H}$ = 8.79 Hz), 7.21 (d, 2H, $J_{3H,H}$ = 15.9 Hz), 7.06 (d, 2H, $J_{3H,H}$ = 15.9 Hz), 6.70 (d, 4H, $J_{3H,H}$ = 8.80 Hz), 3.44-3.37 (q, 8H, $J_{3H,H}$ = 7.12 Hz), 1.22-1.18 (t, 12H, $J_{3H,H}$ = 7.13 Hz). $^{13}$C NMR ($CDCl_3$) δ 148.0, 137.6, 133.2, 133.0–131.6 (q, $J_{2C,F}$ = 33.2 Hz), 131.4, 129.9, 128.5, 128.5-117.6 (q, $J_{C,F}$ = 272.6 Hz), 125.8, 124.5, 122.2, 121.2, 119.7, 111.8, 92.7, 90.5, 44.8, 13.0. IR ($cm^{-1}$): 2967.8, 2207.4, 1605.2, 1576.2, 1521.3, 1517.4, 1487.0, 1466.3, 1429.6, 1398.8, 1390.1, 1349.1, 1296.6, 1284.5, 1279.7, 1267.6, 1245.9, 1176.5, 1169.3, 1105.6, 1097.9, 1077.2, 1074.3, 959.5, 937.8.

**Cyclic Voltametry:** Electrochemical experiments were carried out with CH Instruments model 660 electrochemical workstation. Cyclic voltammograms (CV) were obtained by using a conventional three-electrode system. A platinum foil was used as the counter electrode. A platinum disk electrode ($\phi$ = 1.2 mm) from Bioanalytical Systems serves as a working electrode. Reference electrode **A**, Ag/0.1 M $AgNO_3$ in acetonitrile, was separated from the test by a fritted bridge containing the background electrolyte (0.1 M $Bu_4NPF_6$ in acetonitrile). The reference electrode was calibrated before each experiment with the ferrocene/ferrocenium ($Fc/Fc^+$) redox system. The $E_{1/2}$ of 5 mM of $Fc/Fc^+$ in 0.1 M $Bu_4NPF_6$ in in acetonitrile was 0.37 V. The standard redox potential of the $Fc/Fc^+$ system has been determined to be 0.190 V [Bard, AJ., Faulkner LR. Electrochemical Methods; John Wiley & Sons: New York 1980 p.701].. Therefore, the potential of our reference electrode **A** was 0.227 V versus S.H.E. All solutions were purged prior to electrochemical measurements using nitrogen gas. All solvents were dried with molecular sieves (3 Å). All the salts were used as received from Aldrich.

**Quantum chemical calculations:** The program SPARTAN 04 was implemented on a Windows XP platform (Dell, 3.0 GHz processor speed). The geometries were first determined utilizing an AM1 calculation. The obtained geometries were utilized in a second set of minimizations to determine the equilibrium structure utilizing B3LYP with a 6-31G** basis set.

**Single crystal structure determination.**[15-19] Suitable crystals of **11**.**6,7** and **11**.**8** were coated with Paratone N oil, suspended in a small fiber loop and placed in a cooled nitrogen gas stream at 173 K on a Bruker D8 SMART APEX CCD graphite mono-chromated MoKa (0.71073 A)diffractometer for 6 and a D8 SMART 1000 CCD graphite monochromated CuKa (1.5418 A) difractometer for **11**.**7** and **11**.**8**. Data were measured using a series of combinations of phi and omega scans with 20 s frame exposures and $0.3^{o}$ frame widths. Data collection, indexing and initial cell refinements were all carried out using SMART software. Frame integration and final cell refinements were done using SAINT software. The final cell parameters were determined from least-squares refinement on 2911, 3793 and 3786 reflections for **11**.**6**, **11**.**7** and **11**.**8**, respectively. The SADABS program was used to carry out absorption corrections. The structure was solved using Direct methods and difference Fourier techniques (SHELXTL, V6.12). Hydrogen atoms were placed their expected chemical positions using the HFIX command and were included in the final cycles of least squares with isotropic $U_{ij}$ 's related to the atom's ridden upon. The C-H distances were fixed at 0.93 Å(aromatic and amide), 0.98 Å (methine), 0.97 Å (methylene), or 0.96 Å (methyl). All non-hydrogen atoms were refined anisotropically. Scattering factors and anomalous dispersion corrections are taken from the *International Tables for X-ray Crystallography*[5]. Structure solution, refinement, graphics and generation of publication materials were performed by using SHELXTL, V6.12 software. Additional details of data collection and structure refinement are given in Table 11.4.

**Table 11.4**. X-ray data of **11.6-8.**

| | **11.6** | **11.7** | **11.8** |
|---|---|---|---|
| Empirical formula | $C_{42}H_{30}$ | $C_{46}H_{44}N_2$ | $C_{48}H_{42}F_6N_2$ |
| Formula weight | 534.66 | 624.83 | 760.84 |
| Temperature | 173(2) K | 173(2) K | 173(2) K |
| Wavelength | 0.71073 Å | 1.54178 Å | 1.54178 Å |
| Crystal system | Tetragonal | Monoclinic | Triclinic |
| Space group | P4/n | P2(1)/c | P-1 |
| Unit cell dimensions | a = 23.809(2) Å , $\alpha$= 90°. | a = 8.3889(9) Å $\alpha$= 90°. | a = 10.0454(7) Å $\alpha$= 91.787(1)°. |
| | b = 23.809(2) Å $\beta$= 90°. | b = 31.632(3) Å $\beta$= 92.992(5)°. | b = 13.88826(7) Å $\beta$= 101.471(4)°. |
| | c = 5.8229(8) Å $\gamma$ = 90°. | c = 13.489(1) Å $\gamma$ = 90°. | c = 15.3(10) Å $\gamma$ = 107.723(4)°. |
| Volume | 3300.8(6) $Å^3$ | 3574.4(6) $Å^3$ | 1981.7(2) $Å^3$ |
| Z | 4 | 4 | 2 |
| Density (calculated) | 1.076 $Mg/m^3$ | 1.161 $Mg/m^3$ | 1.275 $Mg/m^3$ |
| Absorption coefficient | 0.061 $mm^{-1}$ | 0.505 $mm^{-1}$ | 0.775 $mm^{-1}$ |
| F(000) | 1128 | 1336 | 794 |
| Crystal size | 0.75 x 0.12 x 0.12 $mm^3$ | 0.40 x 0.20 x 0.17 $mm^3$ | 0.57 x 0.12 x 0.10 $mm^3$ |
| Theta range for data collection | 1.71 to 21.24°. | 2.79 to 66.69°. | 2.96 to 38.07°. |

**Table 11.4**. continued

| | | | |
|---|---|---|---|
| Index ranges | -24<=h<=24, -24<=k<=24, -5<=l<=5 | -9<=h<=7, -37<=k<=25, -13<=l<=16 | -8<=h<=8, -11<=k<=11, -12<=l<=12 |
| Reflections collected | 23096 | 12497 | 18747 |
| Independent reflections | 1825 [R(int) = 0.0457] | 4226 [R(int) = 0.0644] | 8695 [R(int) = 0.0000] |
| Completeness to theta | 99.9 % | 67.0 % | 99.9 % |
| Absorption correction | Semi-empirical from equivalents | | |
| Max. and min. transmission | 1.000 and 0.757805 | Nd | 1.000 and 0.425485 |
| Refinement method | Full-matrix least-squares on $F^2$ | | |
| Data / restraints / parameters | 1825 / 0 / 194 | 4226 / 0 / 438 | 8695/ 0 / 252 |
| Goodness-of-fit on $F^2$ | 2.227 | 1.069 | 1.180 |
| Final R indices [I>2sigma(I)] | R1 = 0.1489, wR2 = 0.4577 | R1 = 0.0980, wR2 = 0.2759 | R1 = 0.139, wR2 = 0.3246 |
| R indices (all data) | R1 = 0.1567, wR2 = 0.4654 | R1 = 0.1692, wR2 = 0.3198 | R1 = 0.1815, wR2 = 0.3481 |
| Extinction coefficient | Nd | 0.0045(8) | Nd |
| Largest diff. peak and hole | 0.786, -0.323 e.$Å^{-3}$ | 0.371, -0.311 e.$Å^{-3}$ | 0.710 and -0.573 e.$Å^{-3}$ |
| CCDC reference number (Cambridge Crystallo-graphic Data Centre) | 238654 | 238655 | 238656 |

## 11.5 References and notes


1. Electronic materials, the oligomers approach, Müllen K. and Wegner G. Ed., Wiley-VCH, Weinheim **1998**
2. Ball, P. Made to measure, Princeton Press Paperback, Princeton, **1999.**
3. (a) Bunz U. H. F. *Chem Rev.* **2000**, *100*, 1603-1644. (b) Halkyard, C. E.; Rampey, M. E.; Kloppenburg, L.; Studer-Martinez, S. L.; Bunz, U. H. F. *Macromolecules* **1998**, *31*, 8655-8659. (c) Miteva, T.; Palmer, L.; Kloppenburg, L.; Neher, D.; Bunz, U. H. F. *Macromolecules* **2000**, *33*, 652-654. (d) Scherf, U. *Top. Curr. Chem.* **1999**, *201*, 163-222.
4. (a) Schmitz, C.; Posch, P.; Thelakkat, M.; Schmidt, H. W.; Montali, A.; Feldman, K.; Smith, P.; Weder, C. *Adv. Funct. Mater.* **2001**, *11*, 41-46. (b) Kokil, A.; Shiyanovskaya, I.; Singer, K. D.; Weder C. *Synth. Met.* **2003** *138*, 513-517.
5. Pschirer, N. G.; Miteva, T.; Evans, U.; Roberts, R. S.; Marshall, A. R.; Neher, D.; Myrick, M. L.; Bunz, U. H. F. *Chem. Mater.* **2001**, *13*, 2691-2696.
6. Wilson, J. N.; Windscheif, P. M.; Evans, U.; Myrick, M. L.; Bunz, U. H. F. *Macromolecules* **2002**, *35*, 8681-8683.
7. Wilson, J. N.; Josowicz, M.; Wang, Y. Q.; Bunz, U. H. F. *Chem. Commun.* **2003**, 2962-2963.
8. Wilson, J. N.; Smith, M. D.; Enkelmann, V.; Bunz, U. H. F. *Chem. Commun.* **2004, *1700-1701.***
9. (a) Yamamoto T**,** *Synlett* **2003,** 425-450. (b) Yamamoto T**,** *Bull. Chem. Soc. Jpn.* **1999**, *72*, 621-638. (c) Sonogashira, K. *J. Organomet. Chem.* **2002**, *653*, 46-49. (d) Sonogashira, K.; Tohda, Y.; Hagihara, N. *Tetrahedron Lett.* **1975**, 4467-4470 (e) Negishi, E.; Anastasia, L. *Chem. Rev.* **2003**, *103*, 1979-2017.
10. (a) Horner, L.; Hoffmann H.; Wippel, H. G. *Chem. Ber.*, **1958**, *91*, 61. (b) Horner L.; Klink, W. *Tetrahedron Lett.* **1964**, *36*, 2467
11. (a) Böhm, A.; Adam, M.; Mauermann, H.; Stein, S.; Müllen, K. *Tetrahedron Lett.* **1992**, *33*, 2795-2798. (b) Böhm, A.; Müllen, K. *Tetrahedron Lett.* **1992**, *33*, 611-614. (c) Müller, M.; Mauernann-Düll, H.; Wagner, M, Enkelmann, V.; Müllen, K. *Angew. Chem. Int. Ed.* **1995**, *34*, 1583-1586.
12. (a) Tykwinski, R. R.; Zhao, Y. M. *Synlett* **2002**, 1939-1953. (b) Zhao, Y. M.; McDonald, R.; Tykwinski, R. R.; *J. Org. Chem.* **2002**, *67*, 2805-2812. (c) Tykwinski, R. R.; Schreiber, M.; Carlon, R. P.; Diederich, F.; Gramlich, V. *Helv. Chem. Acta* **1996**, *79*, 2249-2281. (d) Tykwinski, R. R.; Diederich, F. *Liebigs Ann.-Recueil* **1997,** 649-661.
13. (a) Hagen, S.; Hopf, H. *Top. Curr. Chem.* **1998**, *196*, 45-89. (b) Hopf, H.; Kreutzer, M.; Jones, P. G. *Chem. Ber.* **1991**, *124*, 1471-1475.

14. (a) Cao, J.; Curtis, M. D. *Chem. Mater.* **2003**, *15*, 4424-4430. (b) Koren, A.B.; Curtis, M. D.; Francis, A. H.; Kampf J. W. *J. Am. Chem. Soc.* **2003**, *125*, 5040-5050 (c) Koren, A. B.; Curtis, M. D.; Kampf J. W. *Chem. Mater.* **2000**, *12*, 1519-1523.

15. SMART Version 5.628, **2003**, Bruker AXS, Inc., Analytical X-ray Systems, 5465 East Cheryl Parkway, Madison WI 53711-5373

16. SAINT Version 6.36A, **2002**, Bruker AXS, Inc., Analytical X-ray Systems, 5465 East Cheryl Parkway, Madison WI 53711-5373.

17. SADABS Version 2.08, **2003**, George Sheldrick, University of Göttingen,

18. SHELXTL V6.12, **2002**, Bruker AXS, Inc., Analytical X-ray Systems, 5465 East Cheryl Parkway, Madison WI 53711-5373

19. A. J. C. Wilson (ed), *International Tables for X-ray Crystallography, Volume C.* Kynoch, Academic Publishers, Dordrecht, **1992**, Tables 6.1.1.4 (pp. 500-502) and 4.2.6.8 (pp. 219-222).

# Chapter 12

# Conclusion and Final Remarks

## 12.1 Discusssion

In light of the research goals outlined at the beginning of this work, we have been successful in making a few small, yet important, steps forward in the field of PPEs. First, our desire to functionalize PPEs with biologically relevant molecules has been realized.[1] A number of saccharide substituted PPEs have been reported by the Bunz group as well as a very recent publication by Swager.[4a] With the recent surge in reports on "click" chemistry, it would appear that PPEs with a broad range of appendages are on the horizon.[2]

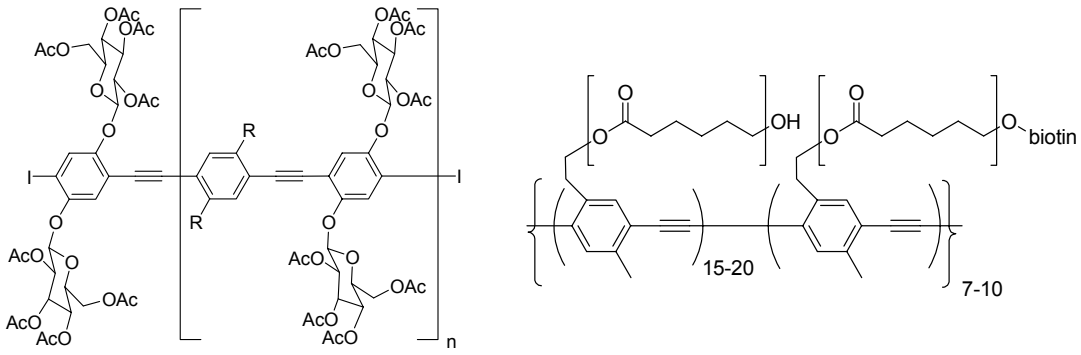


**Figure 12.1** Samples of "bio-PPEs" synthesized to date by the Bunz group.

Secondly, ligand substituted PPEs have been shown to be sensitive to a variety of biologically relevant molecules demonstrating their applicability in biosensing schemes.[3,4] The model biotin-streptavidin system clearly sets a precedent for agglutination based

assays.[3a] The work of Swager and Seeberger also demonstrates that sugar substituted PPEs are sensitive towards both lectins as well as certain bacteria.[4] Conveniently, sugar substituted PPEs have also been shown to be highly selective towards specific metal ions.[3b]

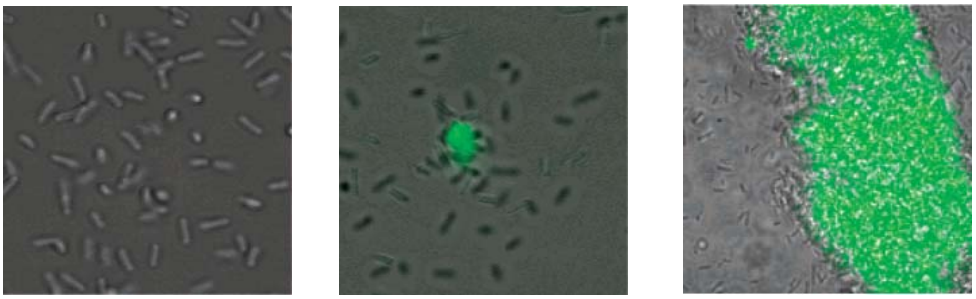

**Figure 12.2** Bacteria sensing by PPEs from the groups of Seeberger and Swager.[4a] At left, image of *E. coli*. Middle, combined light and fluorescence images of an aggregate of *E. coli*. and a mannose-containing PPE. Right, close up of aggregate.

Finally, PPEs with improved hole and electron injection susceptibilities have been produced in a "cross-conjugated" PPE-PPV system.[4a] In addition, a similarly constructed series of model compounds, or cruciforms, with attractive optical and electronic properties have been reported as well.[4b,c] A very recent publication demonstrated the applicability of one of these polymers in a polymer field effect transistor (PFET).[6] There has been progress in understanding the basic photophysics of PPEs as color tuning via two photon excitation was recently reported.[7] We hope that a number of our contributions have helped to demonstrate the important relationship between structure, morphology and photophysical properties.[8]

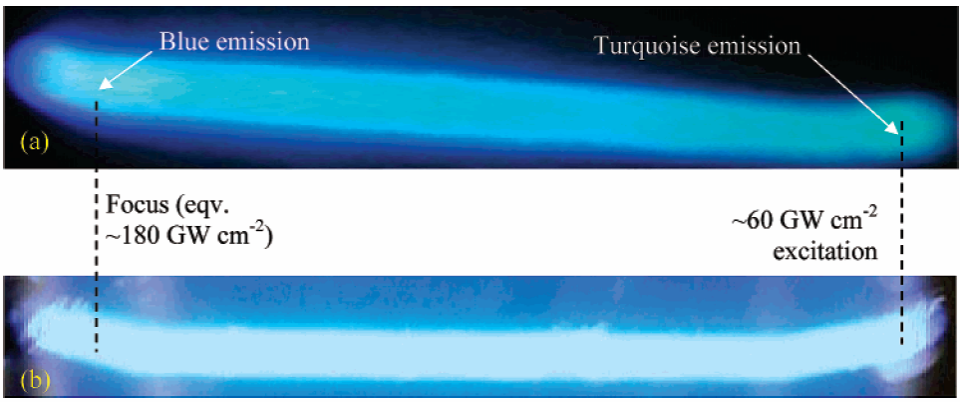


**Figure 12.3** Relationship between morphology and physical properties of PPEs: (a) Aggregated phase of dialkyl PPE displaying dual emission as a function of excitation intensity; (b) Uniform emission of the same PPE in a non-aggregated phase. Figure adapted from Ref. 7.

## 12.2 References


1. Bio (a) Erdogan, B.; Wilson J.N.; Bunz U.H.F. *Macromolecules* **2002**, *35*, 7863. (b) Wang, Y.Q.; Erdogan, B.; Wilson, J.N.; Bunz, U.H.F. *Chem. Commun.* **2003**, 1*4*, 1624-1625.

2. (a) Erdogan, B.; Song, L.; Wilson, J. N.; Park, J. O.; Srinivasarao, M.; Bunz, U. H. F. *J. Am. Chem. Soc.*, **2004**, *126*, 3678. (b) Wang, Q.; Chan, T.; Hilgraf, R.; Finn, M. G.; Valery, R. F.; Sharpless, K. B. *J. Am. Chem. Soc.*, **2003**, *125*, 3192. (c) Saxon, E.; Bertozzi, C. R. *Science*, **2000**, *287*, 2007. (d) Link, A. J.; Tirrell, D. A. *J. Am. Chem. Soc.*, **2003**, *125*, 11164.

3. (a) Wilson, J. N.; Wang, Y.; Lavigne, J. J.; Bunz, U. H. F. *Chem. Commun.*, **2003**, 1626. (b) Kim, I. –B.; Erdogan, B.; Wilson, J. N.; Bunz, U. H. F. *Chem. Eur. J.*, **2004**, ASAP Article.

4. (a) Disney, M. D.; Zheng, J.; Swager, T. M.; Seeberger, P.H.; *J. Am. Chem. Soc.*, **2004**, *126*, 13343. (b) Kwan, P. H.; MacLachlan, M. J.; Swager, T. M.; *J. Am. Chem. Soc.*, **2004**, *126*, 8638.

5. (a) Wilson, J. N.; Windscheif P.M.; Evans U.; Myrick M.L;., Bunz U.H.F. *Macromolecules,* **2002**, *35*, 8681. (b) Wilson, J.N.; Josowicz, M.; Wang, Y.Q.; Bunz, U.H.F. *Chem. Commun*. **2004**, *24*, 2962-2963. (c) Wilson, J.N.; Hardcastle, K.I.; Josowicz, M.; Bunz, U.H.F. *Tetrahedron* **2004**, *60*, 7157-7167.\

6. Xu, Y., Wilson, J. N.; Bunz, U. H. F.; Berger, P. R. *Appl. Phys. Lett.*, **2004**, *85*, 4219.

7. Schroeder, R.; Wilson, J. N.; Bunz, U. H. F.; Ullrich, B. *J. Phys. Chem. B.*, **2003**, *107*, 11604.

8. (a) Wilson, J. N.; Steffen, W.; McKenzie, T. G.; Lieser, G.; Oda, M.; Neher, D.; Bunz, U. H. F. *J. Am. Chem. Soc.*, **2002**, *124*, 6830. (b) Wilson, J.N.; Smith, M.D.; Enkelmann, V.; Bunz, U.H.F. *Chem. Commun*. **2004**, *15*, 1700-1701. (c) Wilson, J. N.; Bangcuyo, C. G.; Erdogan, B.; Myrick, M. L.; Bunz, U. H. F. *Macromolecules*, **2003**, *36*, 1426.

# Appendix A

# Additional Crystallographic Data and Structures

## A.1 Crystallographic Data and Figures

**X-Ray Structure Determination, $C_{13}H_{12}F_6Si$**

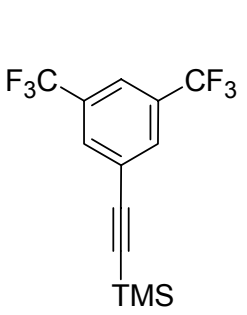


**A.1**

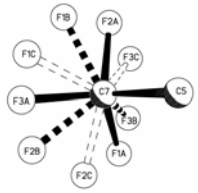


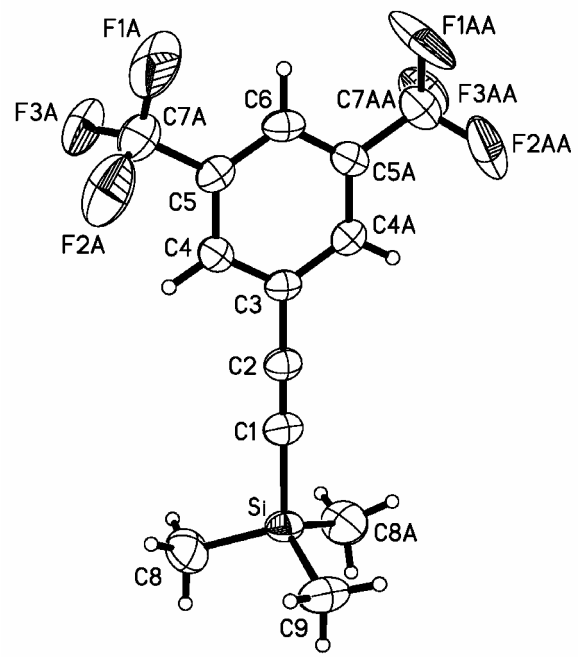


**Figure A.1**. Clockwise from top left: Structure of **A.1**, refined crystal structure showing displacement ellipsoids drawn at the 50% probability level, and at lower left the rotational disorder of a -$CF_3$ group.

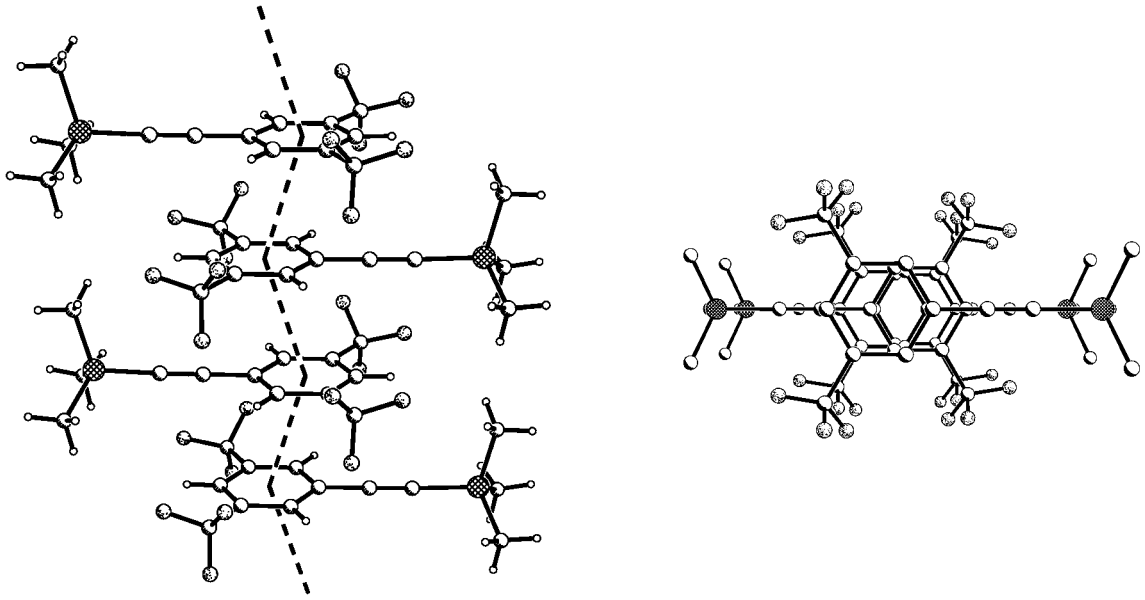

**Figure A.2.** Chains of pi-pi stacked molecules down the a axis: centroid - centroid distance = 3.604 Å, interplanar angle = 0.3 º

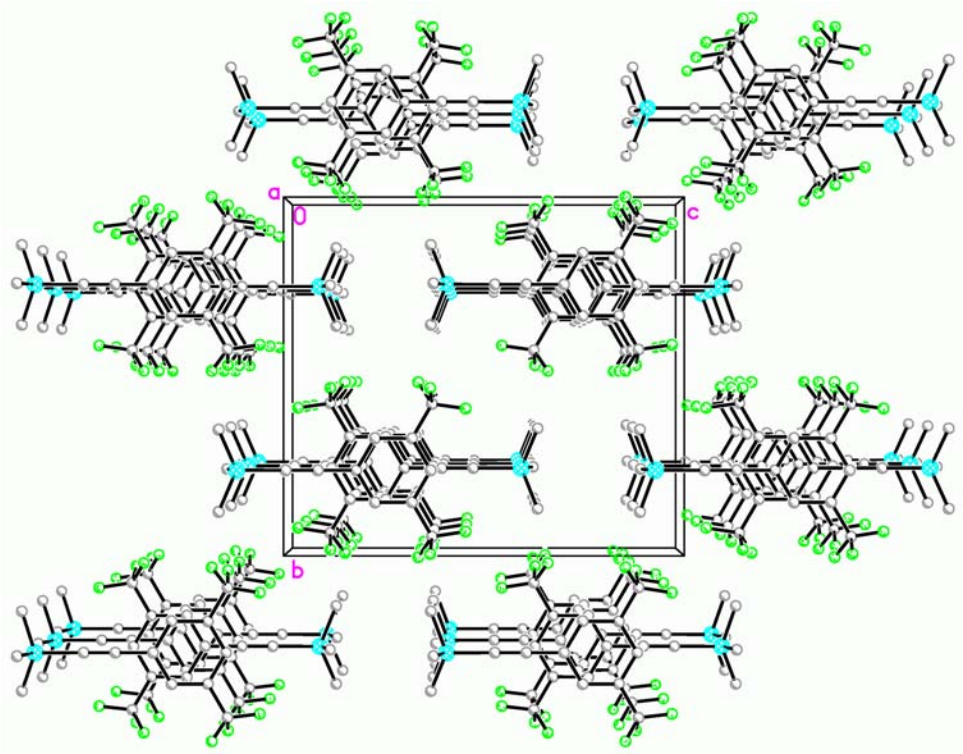


**Figure A.3.** View down the crystallographic a axis, showing the columns of pi-pi stacked molecules.

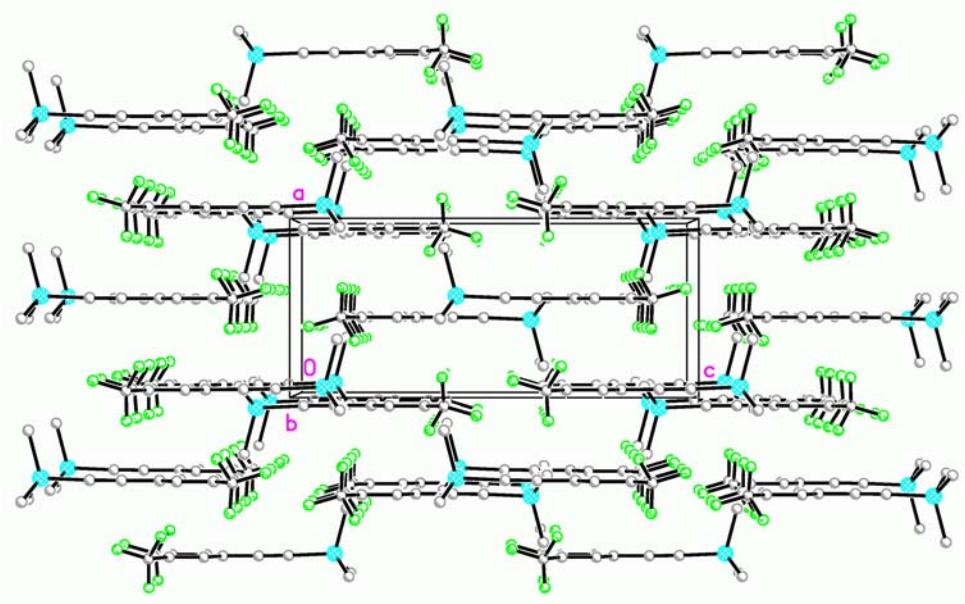


**Figure A.4.** View down the crystallographic b axis

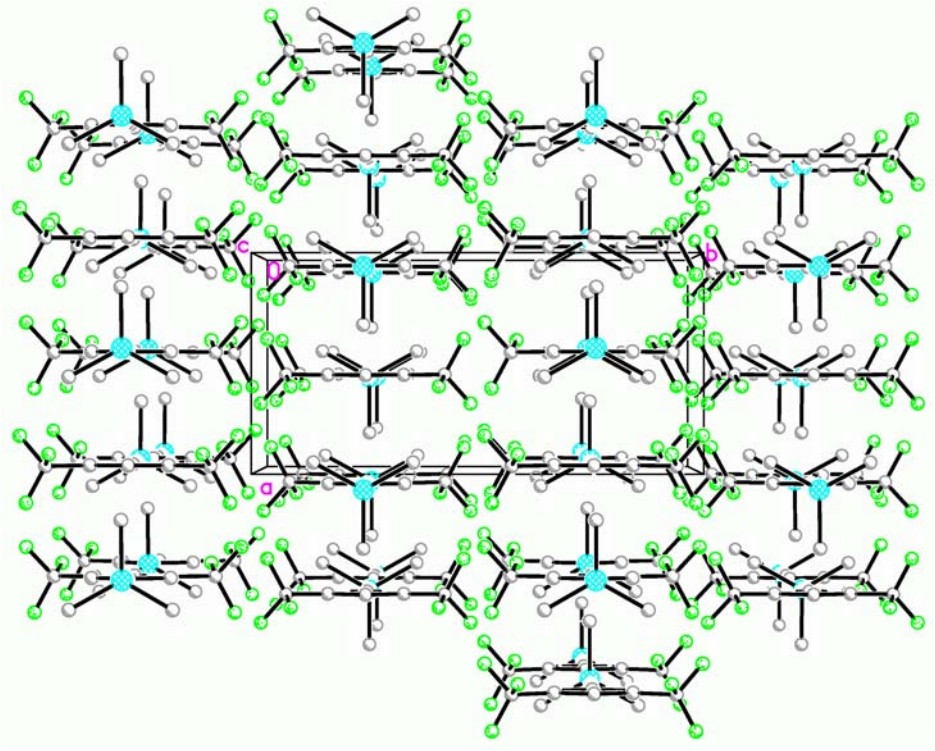


**Figure A.5.** View down the crystallographic c axis

A colorless needle was mounted onto the end of a thin glass fiber using inert oil. X-ray intensity data covereing nearly the entire sphere of reciprocal space were measured at 150.0(2) K on a Bruker SMART APEX CCD-based diffractometer (Mo Kα radiation, λ = 0.71073 Å).[1] The raw data frames were integrated with SAINT+,[1] which also applied corrections for Lorentz and polarization effects. The final unit cell parameters are based on the least-squares refinement of 4654 reflections with $I > 5(\sigma)I$ from the data set. Analysis of the data showed negligible crystal decay during data collection.

Systematic absences in the intensity data were consistent with the space groups Pnma and $Pn2_1a$; intensity statistics indicated centricity. The structure was solved in Pnma by a combination of direct methods and difference Fourier syntheses, and refined by full-matrix least-squares against $F^2$, using SHELXTL.[2] The molecule resides on a crystallographic mirror plane perpendicular to the phenyl ring plane. The $-CF_3$ group was found to be rotationally disordered and a model incorporating three distinct rotational orientations was employed. A total of 72 restraints were used to maintain a reasonable chemical geometry for the disordered species. Refinement in the acentric space group $Pn2_1a$ yielded the same $-CF_3$ disorder as well as large correlations between atoms related by mirror symmetry in Pnma; therefore Pnma was retained as the correct space group. Eventually all non-hydrogen atoms were refined with anisotropic displacement parameters. Hydrogen atoms were placed in geometrically idealized positions and included as riding atoms with refined isotropic displacement parameters.

**Table A.1**. Crystal data and structure refinement for jw07t.

| | | |
|---|---|---|
| Identification code | jw07t | |
| Empirical formula | C13 H12 F6 Si | |
| Formula weight | 310.32 | |
| Temperature | 150.0(2) K | |
| Wavelength | 0.71073 Å | |
| Crystal system | Orthorhombic | |
| Space group | Pnma | |
| Unit cell dimensions | a = 6.8886(4) Å | α= 90°. |
| | b = 14.0380(8) Å | β= 90°. |
| | c = 15.6487(9) Å | γ = 90°. |
| Volume | 1513.26(15) $Å^3$ | |
| Z | 4 | |
| Density (calculated) | 1.362 $Mg/m^3$ | |
| Absorption coefficient | 0.205 $mm^{-1}$ | |
| F(000) | 632 | |
| Crystal size | 0.66 x 0.16 x 0.06 $mm^3$ | |
| Theta range for data collection | 1.95 to 25.05°. | |
| Index ranges | -7<=h<=8, -16<=k<=16, -18<=l<=18 | |
| Reflections collected | 9598 | |
| Independent reflections | 1401 [R(int) = 0.0527] | |
| Completeness to theta = 25.05° | 99.9 % | |
| Absorption correction | None | |
| Refinement method | Full-matrix least-squares on $F^2$ | |
| Data / restraints / parameters | 1401 / 72 / 162 | |
| Goodness-of-fit on $F^2$ | 1.045 | |
| Final R indices [I>2sigma(I)] | R1 = 0.0408, wR2 = 0.1062 | |
| R indices (all data) | R1 = 0.0485, wR2 = 0.1113 | |
| Largest diff. peak and hole | 0.278 and -0.189 $e.Å^{-3}$ | |

**Table A.2.** Atomic coordinates ( x $10^4$) and equivalent isotropic displacement parameters ($Å^2$x $10^3$) for jw07t. U(eq) is defined as one third of the trace of the orthogonalized $U^{ij}$ tensor.

| | x | y | z | U(eq) |
|---|---|---|---|---|
| Si | 4339(1) | 7500 | 5913(1) | 41(1) |
| C(1) | 4451(3) | 7500 | 4736(2) | 41(1) |
| C(2) | 4472(3) | 7500 | 3969(2) | 37(1) |
| C(3) | 4480(3) | 7500 | 3052(1) | 32(1) |
| C(4) | 4479(2) | 6645(1) | 2601(1) | 35(1) |
| C(5) | 4477(2) | 6650(1) | 1718(1) | 36(1) |
| C(6) | 4469(3) | 7500 | 1274(2) | 37(1) |
| C(7A) | 4495(3) | 5731(1) | 1240(1) | 54(1) |
| F(1A) | 3960(40) | 5858(12) | 442(8) | 105(8) |
| F(2A) | 3170(20) | 5155(11) | 1580(11) | 87(5) |
| F(3A) | 6111(14) | 5310(9) | 1277(10) | 68(4) |
| C(7B) | 4495(3) | 5731(1) | 1240(1) | 54(1) |
| F(1B) | 4270(40) | 4951(5) | 1727(4) | 80(3) |
| F(2B) | 6236(15) | 5572(9) | 859(13) | 79(3) |
| F(3B) | 3210(30) | 5634(12) | 628(12) | 95(6) |
| C(7C) | 4495(3) | 5731(1) | 1240(1) | 54(1) |
| F(1C) | 5610(30) | 5098(13) | 1595(12) | 97(6) |
| F(2C) | 5130(40) | 5858(9) | 440(7) | 110(6) |
| F(3C) | 2762(14) | 5370(12) | 1171(15) | 101(6) |
| C(8) | 5577(4) | 6410(2) | 6300(2) | 68(1) |
| C(9) | 1728(5) | 7500 | 6212(2) | 64(1) |

**Table A.3**. Bond lengths [Å] and angles [°] for jw07t.

| | |
|---|---|
| Si-C(1) | 1.843(2) |
| Si-C(8) | 1.854(2) |
| Si-C(8)#1 | 1.854(2) |
| Si-C(9) | 1.858(3) |
| C(1)-C(2) | 1.201(3) |

**Table A.3**. continued

| | |
|---|---|
| C(2)-C(3) | 1.434(3) |
| C(3)-C(4) | 1.3932(19) |
| C(3)-C(4)#1 | 1.3932(19) |
| C(4)-C(5) | 1.382(2) |
| C(5)-C(6) | 1.381(2) |
| C(5)-C(7A) | 1.491(2) |
| C(6)-C(5)#1 | 1.381(2) |
| C(7A)-F(3A) | 1.262(8) |
| C(7A)-F(1A) | 1.314(9) |
| C(7A)-F(2A) | 1.328(8) |
| C(1)-Si-C(8) | 107.90(9) |
| C(1)-Si-C(8)#1 | 107.90(9) |
| C(8)-Si-C(8)#1 | 111.25(16) |
| C(1)-Si-C(9) | 106.99(12) |
| C(8)-Si-C(9) | 111.30(10) |
| C(8)#1-Si-C(9) | 111.30(10) |
| C(2)-C(1)-Si | 178.3(2) |
| C(1)-C(2)-C(3) | 179.5(2) |
| C(4)-C(3)-C(4)#1 | 119.1(2) |
| C(4)-C(3)-C(2) | 120.46(10) |
| C(4)#1-C(3)-C(2) | 120.46(10) |
| C(5)-C(4)-C(3) | 120.15(15) |
| C(6)-C(5)-C(4) | 120.52(15) |
| C(6)-C(5)-C(7A) | 119.70(17) |
| C(4)-C(5)-C(7A) | 119.78(15) |
| C(5)-C(6)-C(5)#1 | 119.6(2) |
| F(3A)-C(7A)-F(1A) | 110.7(8) |
| F(3A)-C(7A)-F(2A) | 107.5(7) |
| F(1A)-C(7A)-F(2A) | 105.7(7) |
| F(3A)-C(7A)-C(5) | 113.0(5) |
| F(1A)-C(7A)-C(5) | 110.9(8) |
| F(2A)-C(7A)-C(5) | 108.7(6) |

---

Symmetry transformations used to generate equivalent atoms:
#1 x,-y+3/2,z

**Table A.4**. Anisotropic displacement parameters ($Å^2 x\ 10^3$) for jw07t. The anisotropic displacement factor exponent takes the form: $-2\pi^2[\ h^2\ a^{*2}U^{11} + ...\ + 2\ h\ k\ a^*\ b^*\ U^{12}\ ]$

| | $U^{11}$ | $U^{22}$ | $U^{33}$ | $U^{23}$ | $U^{13}$ | $U^{12}$ |
|---|---|---|---|---|---|---|
| Si | 47(1) | 49(1) | 27(1) | 0 | 0(1) | 0 |
| C(1) | 37(1) | 52(1) | 34(1) | 0 | 2(1) | 0 |
| C(2) | 29(1) | 47(1) | 34(1) | 0 | 1(1) | 0 |
| C(3) | 23(1) | 44(1) | 28(1) | 0 | 0(1) | 0 |
| C(4) | 28(1) | 39(1) | 38(1) | 5(1) | -1(1) | 1(1) |
| C(5) | 29(1) | 44(1) | 36(1) | -7(1) | -1(1) | 1(1) |
| C(6) | 27(1) | 56(1) | 28(1) | 0 | 0(1) | 0 |
| C(7A) | 55(1) | 51(1) | 56(1) | -15(1) | -3(1) | 1(1) |
| F(1A) | 158(18) | 85(11) | 74(9) | -53(7) | -62(11) | 38(12) |
| F(2A) | 74(9) | 63(7) | 125(12) | -49(7) | -3(6) | -18(6) |
| F(3A) | 61(5) | 63(8) | 80(10) | -28(7) | -9(6) | 22(5) |
| C(7B) | 55(1) | 51(1) | 56(1) | -15(1) | -3(1) | 1(1) |
| F(1B) | 139(10) | 37(3) | 65(3) | -1(2) | -3(7) | -7(6) |
| F(2B) | 78(4) | 70(7) | 90(10) | -39(6) | 27(5) | 5(4) |
| F(3B) | 125(13) | 68(6) | 93(8) | -35(5) | -68(9) | 15(7) |
| C(7C) | 55(1) | 51(1) | 56(1) | -15(1) | -3(1) | 1(1) |
| F(1C) | 112(11) | 59(8) | 119(12) | -32(7) | -15(8) | 42(8) |
| F(2C) | 198(18) | 78(8) | 53(7) | -33(5) | 44(10) | -33(12) |
| F(3C) | 60(4) | 93(11) | 149(14) | -69(11) | -10(9) | -19(6) |
| C(8) | 85(2) | 65(1) | 54(1) | 9(1) | -11(1) | 12(1) |
| C(9) | 61(2) | 85(2) | 47(2) | 0 | 16(2) | 0 |

**Table A.5.** Hydrogen coordinates ( x $10^4$) and isotropic displacement parameters ($Å^2$x 10 $^3$) for jw07t.

| | x | y | z | U(eq) |
|---|---|---|---|---|
| H(4) | 4480 | 6056 | 2901 | 45(5) |
| H(6) | 4459 | 7500 | 667 | 56(8) |
| H(8A) | 5043 | 5852 | 6006 | 95(9) |
| H(8B) | 5374 | 6345 | 6917 | 126(11) |
| H(8C) | 6971 | 6457 | 6181 | 109(10) |
| H(9A) | 1773 | 7500 | 6838 | 105(12) |
| H(9B) | 1040 | 6923 | 6032 | 79(7) |

**Table A.6**. Torsion angles [°] for jw07t.

| | |
|---|---|
| C(8)-Si-C(1)-C(2) | 119.85(10) |
| C(8)#1-Si-C(1)-C(2) | -119.85(10) |
| C(9)-Si-C(1)-C(2) | 0.000(19) |
| Si-C(1)-C(2)-C(3) | 0.00(9) |
| C(1)-C(2)-C(3)-C(4) | -89.8(2) |
| C(1)-C(2)-C(3)-C(4)#1 | 89.8(2) |
| C(4)#1-C(3)-C(4)-C(5) | 0.0(3) |
| C(2)-C(3)-C(4)-C(5) | 179.68(16) |
| C(3)-C(4)-C(5)-C(6) | -0.2(2) |
| C(3)-C(4)-C(5)-C(7A) | 179.41(16) |
| C(4)-C(5)-C(6)-C(5)#1 | 0.4(3) |
| C(7A)-C(5)-C(6)-C(5)#1 | -179.20(13) |
| C(6)-C(5)-C(7A)-F(3A) | 107.3(9) |
| C(4)-C(5)-C(7A)-F(3A) | -72.3(9) |
| C(6)-C(5)-C(7A)-F(1A) | -17.7(13) |
| C(4)-C(5)-C(7A)-F(1A) | 162.7(13) |
| C(6)-C(5)-C(7A)-F(2A) | -133.5(11) |
| C(4)-C(5)-C(7A)-F(2A) | 46.9(11) |

Symmetry transformations used to generate equivalent atoms: #1 x,-y+3/2,z

## X-Ray Structure Determination, $C_{46}H_{42}$

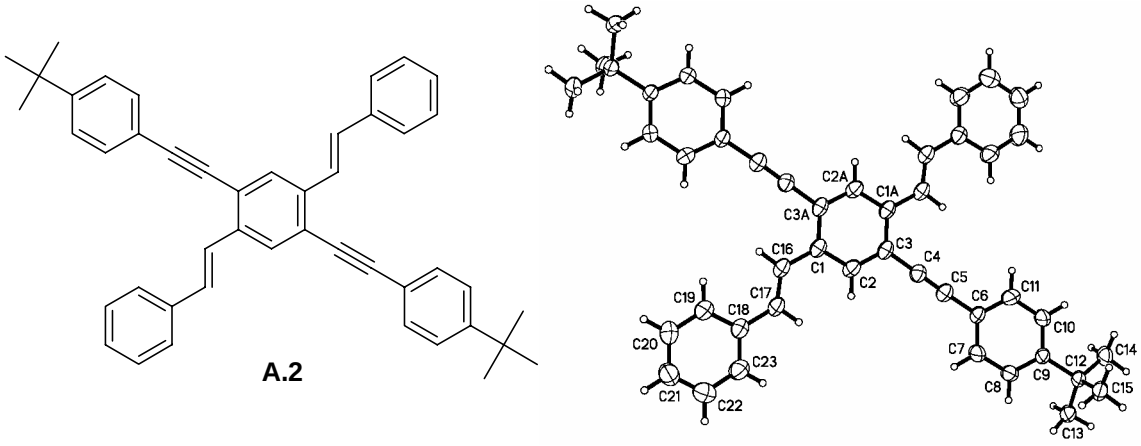


**Figure A.6**. The structure (top) and refined crystal structure (bottom) of **A.2**.

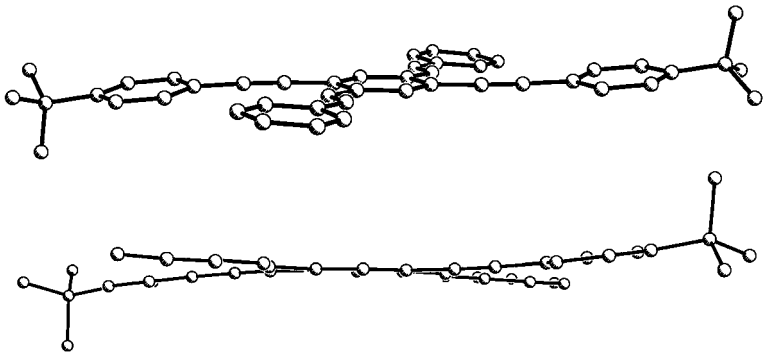

**Figure A.7**. Side view of **A.2** showing the interplane angles. Values are in Table A.7.

**Table A.7**. Dihedral angles between ring planes (º)

| | C1---C3A | C6---C11 |
|---|---|---|
| C6---C11 | 7.6 | |
| C18---C23 | 4.1 | 10.9 |

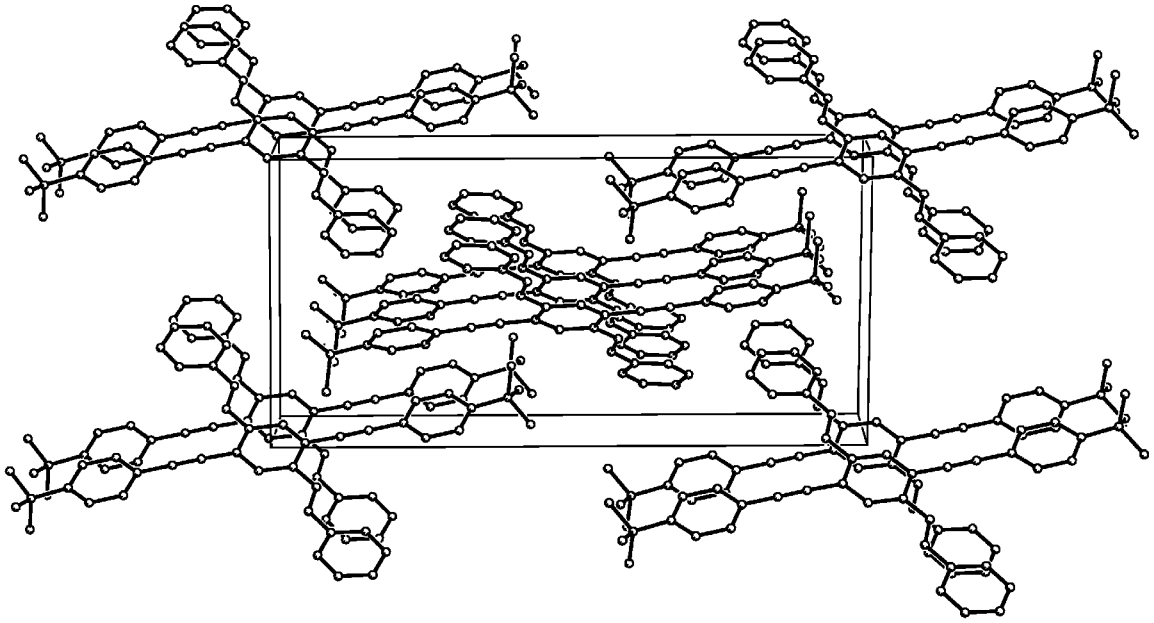

**Figure A.8**. View down the crystallographic b axis

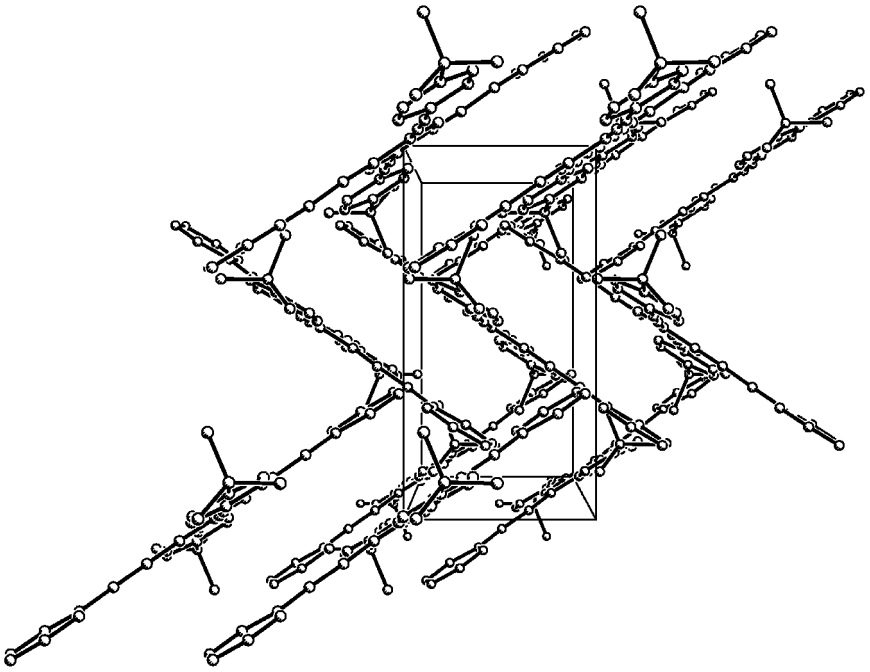

**Figure A.9**. View down the crystallographic a axis

A yellow-green needle was mounted onto the end of a thin glass fiber using inert oil. X-ray intensity data covering > 90% of reciprocal space were measured at 150(1) K on a

Bruker SMART APEX CCD-based diffractometer (Mo Kα radiation, λ = 0.71073 Å).[1] The raw data frames were integrated with SAINT+,[1] which also applied corrections for Lorentz and polarization effects. The final unit cell parameters are based on the least-squares refinement of 4862 reflections with $I > 5(\sigma)I$ from the data set. Analysis of the data showed negligible crystal decay during data collection.

Systematic absences in the intensity data were consistent with the space group $P2_1/n$. The structure was solved by a combination of direct methods and difference Fourier syntheses, and refined by full-matrix least-squares against $F^2$, using the SHELXTL software package.[2] The molecule resides on a center of symmetry. All non-hydrogen atoms were refined with anisotropic displacement parameters; hydrogen atoms were placed in geometrically idealized positions and refined with isotropic displacement parameters as riding atoms.

**Table A.8**. Crystal data and structure refinement for jw03s.

| | | |
|---|---|---|
| Identification code | jw03s | |
| Empirical formula | C46 H42 | |
| Formula weight | 594.80 | |
| Temperature | 150(1) K | |
| Wavelength | 0.71073 Å | |
| Crystal system | Monoclinic | |
| Space group | $P2_1/n$ | |
| Unit cell dimensions | a = 11.7184(14) Å | α= 90°. |
| | b = 6.0332(7) Å | β= 90.640(2)°. |
| | c = 24.063(3) Å | γ = 90°. |
| Volume | 1701.2(3) $Å^3$ | |
| Z | 2 | |
| Density (calculated) | 1.161 $Mg/m^3$ | |
| Absorption coefficient | 0.065 $mm^{-1}$ | |
| F(000) | 636 | |
| Crystal size | 0.72 x 0.12 x 0.06 $mm^3$ | |
| Theta range for data collection | 1.69 to 22.54°. | |
| Index ranges | -11<=h<=12, -6<=k<=6, -25<=l<=25 | |
| Reflections collected | 9050 | |
| Independent reflections | 2240 [R(int) = 0.0461] | |
| Completeness to theta = 22.54° | 100.0 % | |
| Absorption correction | None | |
| Refinement method | Full-matrix least-squares on $F^2$ | |
| Data / restraints / parameters | 2240 / 0 / 233 | |
| Goodness-of-fit on $F^2$ | 1.074 | |
| Final R indices [I>2sigma(I)] | R1 = 0.0549, wR2 = 0.1283 | |
| R indices (all data) | R1 = 0.0712, wR2 = 0.1370 | |
| Extinction coefficient | 0.0039(13) | |
| Largest diff. peak and hole | 0.148 and -0.167 $e.Å^{-3}$ | |

**Table A.9.** Atomic coordinates ( x $10^4$) and equivalent isotropic displacement parameters ($Å^2$x $10^3$) for jw03s. U(eq) is defined as one third of the trace of the orthogonalized $U^{ij}$ tensor.

| | x | y | z | U(eq) |
|---|---|---|---|---|
| C(1) | 4495(2) | 3517(4) | 4605(1) | 36(1) |
| C(2) | 4400(2) | 3184(4) | 5176(1) | 40(1) |
| C(3) | 4881(2) | 4604(4) | 5567(1) | 36(1) |
| C(4) | 4715(2) | 4137(4) | 6150(1) | 38(1) |
| C(5) | 4544(2) | 3761(4) | 6627(1) | 40(1) |
| C(6) | 4331(2) | 3411(4) | 7210(1) | 36(1) |
| C(7) | 3754(3) | 1591(4) | 7397(1) | 55(1) |
| C(8) | 3527(3) | 1346(5) | 7960(1) | 56(1) |
| C(9) | 3868(2) | 2866(4) | 8349(1) | 33(1) |
| C(10) | 4461(3) | 4647(5) | 8157(1) | 69(1) |
| C(11) | 4684(3) | 4936(5) | 7595(1) | 72(1) |
| C(12) | 3531(2) | 2635(4) | 8963(1) | 37(1) |
| C(13) | 3530(2) | 199(4) | 9142(1) | 45(1) |
| C(14) | 4344(2) | 3913(4) | 9349(1) | 49(1) |
| C(15) | 2327(2) | 3595(4) | 9020(1) | 48(1) |
| C(16) | 3962(2) | 2037(4) | 4198(1) | 40(1) |
| C(17) | 3331(2) | 276(4) | 4305(1) | 42(1) |
| C(18) | 2773(2) | -1233(4) | 3915(1) | 40(1) |
| C(19) | 2772(2) | -927(5) | 3345(1) | 56(1) |
| C(20) | 2243(3) | -2412(5) | 2994(1) | 68(1) |
| C(21) | 1689(2) | -4227(5) | 3194(1) | 55(1) |
| C(22) | 1698(2) | -4594(5) | 3752(1) | 55(1) |
| C(23) | 2223(2) | -3105(4) | 4107(1) | 51(1) |

**Table A.10**. Bond lengths [Å] and angles [°] for jw03s.

| | |
|---|---|
| C(1)-C(2) | 1.393(3) |
| C(1)-C(3)#1 | 1.414(3) |
| C(1)-C(16) | 1.461(3) |
| C(2)-C(3) | 1.388(3) |
| C(3)-C(1)#1 | 1.414(3) |
| C(3)-C(4) | 1.447(3) |
| C(4)-C(5) | 1.189(3) |
| C(5)-C(6) | 1.442(3) |
| C(6)-C(11) | 1.366(4) |
| C(6)-C(7) | 1.369(3) |
| C(7)-C(8) | 1.390(3) |
| C(8)-C(9) | 1.367(3) |
| C(9)-C(10) | 1.362(3) |
| C(9)-C(12) | 1.541(3) |
| C(10)-C(11) | 1.392(4) |
| C(12)-C(13) | 1.531(3) |
| C(12)-C(14) | 1.532(3) |
| C(12)-C(15) | 1.533(3) |
| C(16)-C(17) | 1.322(3) |
| C(17)-C(18) | 1.457(3) |
| C(18)-C(23) | 1.382(3) |
| C(18)-C(19) | 1.385(3) |
| C(19)-C(20) | 1.374(4) |
| C(20)-C(21) | 1.363(4) |
| C(21)-C(22) | 1.362(4) |
| C(22)-C(23) | 1.380(4) |

| | |
|---|---|
| C(2)-C(1)-C(3)#1 | 116.9(2) |
| C(2)-C(1)-C(16) | 122.3(2) |
| C(3)#1-C(1)-C(16) | 120.77(19) |
| C(3)-C(2)-C(1) | 122.9(2) |
| C(2)-C(3)-C(1)#1 | 120.2(2) |
| C(2)-C(3)-C(4) | 118.7(2) |
| C(1)#1-C(3)-C(4) | 121.1(2) |

**Table A.10**. continued.

| | |
|---|---|
| C(5)-C(4)-C(3) | 178.1(3) |
| C(4)-C(5)-C(6) | 177.4(3) |
| C(11)-C(6)-C(7) | 117.6(2) |
| C(11)-C(6)-C(5) | 120.4(2) |
| C(7)-C(6)-C(5) | 122.0(2) |
| C(6)-C(7)-C(8) | 120.4(2) |
| C(9)-C(8)-C(7) | 122.5(2) |
| C(10)-C(9)-C(8) | 116.3(2) |
| C(10)-C(9)-C(12) | 122.2(2) |
| C(8)-C(9)-C(12) | 121.3(2) |
| C(9)-C(10)-C(11) | 122.0(2) |
| C(6)-C(11)-C(10) | 121.1(3) |
| C(13)-C(12)-C(14) | 108.3(2) |
| C(13)-C(12)-C(15) | 109.5(2) |
| C(14)-C(12)-C(15) | 108.8(2) |
| C(13)-C(12)-C(9) | 111.01(18) |
| C(14)-C(12)-C(9) | 111.8(2) |
| C(15)-C(12)-C(9) | 107.31(18) |
| C(17)-C(16)-C(1) | 126.6(2) |
| C(16)-C(17)-C(18) | 128.6(2) |
| C(23)-C(18)-C(19) | 116.4(2) |
| C(23)-C(18)-C(17) | 120.2(2) |
| C(19)-C(18)-C(17) | 123.4(2) |
| C(20)-C(19)-C(18) | 121.2(3) |
| C(21)-C(20)-C(19) | 121.4(3) |
| C(22)-C(21)-C(20) | 118.7(3) |
| C(21)-C(22)-C(23) | 120.2(3) |
| C(22)-C(23)-C(18) | 122.1(2) |

---

Symmetry transformations used to generate equivalent atoms:

#1 -x+1,-y+1,-z+1

**Table A.11**. Anisotropic displacement parameters ($Å^2 x\ 10^3$) for jw03s. The anisotropic displacement factor exponent takes the form: $-2\pi^2[\ h^2\ a^{*2}U^{11} + ...\ + 2\ h\ k\ a^*\ b^*\ U^{12}\ ]$

| | $U^{11}$ | $U^{22}$ | $U^{33}$ | $U^{23}$ | $U^{13}$ | $U^{12}$ |
|---|---|---|---|---|---|---|
| C(1) | 37(2) | 45(2) | 27(1) | 5(1) | -1(1) | 5(1) |
| C(2) | 41(2) | 48(2) | 30(1) | 7(1) | 2(1) | -2(1) |
| C(3) | 38(1) | 46(2) | 26(1) | 4(1) | 0(1) | 6(1) |
| C(4) | 41(2) | 41(2) | 32(2) | 1(1) | 0(1) | 1(1) |
| C(5) | 42(2) | 46(2) | 31(2) | 3(1) | 0(1) | 1(1) |
| C(6) | 44(2) | 40(2) | 25(1) | 2(1) | 2(1) | 0(1) |
| C(7) | 88(2) | 47(2) | 29(1) | -2(1) | -1(1) | -25(2) |
| C(8) | 88(2) | 48(2) | 30(2) | 0(1) | 1(1) | -30(2) |
| C(9) | 43(2) | 31(1) | 25(1) | 2(1) | 2(1) | 1(1) |
| C(10) | 124(3) | 51(2) | 31(2) | -9(1) | 12(2) | -38(2) |
| C(11) | 116(3) | 64(2) | 36(2) | 0(2) | 16(2) | -45(2) |
| C(12) | 53(2) | 32(1) | 26(1) | -1(1) | 6(1) | -1(1) |
| C(13) | 68(2) | 35(1) | 33(1) | 3(1) | 8(1) | 0(1) |
| C(14) | 69(2) | 46(2) | 30(1) | -3(1) | -1(1) | -1(1) |
| C(15) | 66(2) | 42(2) | 36(1) | -2(1) | 15(1) | 4(1) |
| C(16) | 44(2) | 49(2) | 26(1) | 4(1) | 1(1) | 1(1) |
| C(17) | 50(2) | 48(2) | 27(1) | 3(1) | 2(1) | 0(1) |
| C(18) | 43(2) | 42(2) | 34(1) | 2(1) | 2(1) | 6(1) |
| C(19) | 73(2) | 58(2) | 36(2) | 5(1) | -1(1) | -17(2) |
| C(20) | 87(2) | 78(2) | 39(2) | -9(2) | -1(2) | -25(2) |
| C(21) | 54(2) | 56(2) | 56(2) | -12(2) | 0(1) | -4(2) |
| C(22) | 53(2) | 46(2) | 66(2) | 0(2) | 3(2) | -3(1) |
| C(23) | 56(2) | 55(2) | 42(2) | 8(1) | 2(1) | -3(1) |

**Table A.12**. Hydrogen coordinates ( x $10^4$) and isotropic displacement parameters (Å$^2$x $10^3$) for jw03s.

| | x | y | z | U(eq) |
|---|---|---|---|---|
| H(2) | 3988 | 1929 | 5302 | 42(7) |
| H(7) | 3507 | 487 | 7141 | 84(10) |
| H(8) | 3119 | 74 | 8078 | 73(9) |
| H(10) | 4729 | 5724 | 8415 | 89(10) |
| H(11) | 5089 | 6213 | 7477 | 96(11) |
| H(13A) | 3369 | 103 | 9540 | 56(7) |
| H(13B) | 4278 | -457 | 9069 | 57(8) |
| H(13C) | 2941 | -606 | 8932 | 51(7) |
| H(14A) | 4301 | 5499 | 9263 | 64(8) |
| H(14B) | 5127 | 3390 | 9295 | 51(8) |
| H(14C) | 4125 | 3669 | 9736 | 59(8) |
| H(15A) | 2341 | 5183 | 8934 | 56(8) |
| H(15B) | 2063 | 3378 | 9401 | 60(8) |
| H(15C) | 1807 | 2838 | 8760 | 57(8) |
| H(16) | 4082 | 2373 | 3817 | 66(8) |
| H(17) | 3226 | -48 | 4688 | 71(9) |
| H(19) | 3143 | 332 | 3193 | 54(8) |
| H(20) | 2264 | -2168 | 2604 | 90(10) |
| H(21) | 1305 | -5217 | 2948 | 70(9) |
| H(22) | 1341 | -5879 | 3898 | 90(11) |
| H(23) | 2207 | -3376 | 4496 | 70(9) |

**Table A.13**. Torsion angles [°] for jw03s.

| | |
|---|---|
| C(3)#1-C(1)-C(2)-C(3) | 0.3(4) |
| C(16)-C(1)-C(2)-C(3) | -178.6(2) |
| C(1)-C(2)-C(3)-C(1)#1 | -0.3(4) |
| C(1)-C(2)-C(3)-C(4) | 178.8(2) |
| C(2)-C(3)-C(4)-C(5) | -62(8) |
| C(1)#1-C(3)-C(4)-C(5) | 117(8) |
| C(3)-C(4)-C(5)-C(6) | -79(10) |
| C(4)-C(5)-C(6)-C(11) | -34(6) |
| C(4)-C(5)-C(6)-C(7) | 145(6) |
| C(11)-C(6)-C(7)-C(8) | 1.0(4) |
| C(5)-C(6)-C(7)-C(8) | -177.6(3) |
| C(6)-C(7)-C(8)-C(9) | -0.6(5) |
| C(7)-C(8)-C(9)-C(10) | -0.7(4) |
| C(7)-C(8)-C(9)-C(12) | 175.6(3) |
| C(8)-C(9)-C(10)-C(11) | 1.5(5) |
| C(12)-C(9)-C(10)-C(11) | -174.8(3) |
| C(7)-C(6)-C(11)-C(10) | -0.2(5) |
| C(5)-C(6)-C(11)-C(10) | 178.4(3) |
| C(9)-C(10)-C(11)-C(6) | -1.1(5) |
| C(10)-C(9)-C(12)-C(13) | -147.1(3) |
| C(8)-C(9)-C(12)-C(13) | 36.8(3) |
| C(10)-C(9)-C(12)-C(14) | -26.0(3) |
| C(8)-C(9)-C(12)-C(14) | 158.0(2) |
| C(10)-C(9)-C(12)-C(15) | 93.3(3) |
| C(8)-C(9)-C(12)-C(15) | -82.8(3) |
| C(2)-C(1)-C(16)-C(17) | 1.1(4) |
| C(3)#1-C(1)-C(16)-C(17) | -177.7(2) |
| C(1)-C(16)-C(17)-C(18) | 179.3(2) |
| C(16)-C(17)-C(18)-C(23) | 174.5(3) |
| C(16)-C(17)-C(18)-C(19) | -4.5(4) |
| C(23)-C(18)-C(19)-C(20) | 0.3(4) |
| C(17)-C(18)-C(19)-C(20) | 179.3(3) |
| C(18)-C(19)-C(20)-C(21) | 0.8(5) |
| C(19)-C(20)-C(21)-C(22) | -2.1(5) |

**Table A.13**. continued.

| | |
|---|---|
| C(20)-C(21)-C(22)-C(23) | 2.3(4) |
| C(21)-C(22)-C(23)-C(18) | -1.2(4) |
| C(19)-C(18)-C(23)-C(22) | -0.1(4) |
| C(17)-C(18)-C(23)-C(22) | -179.1(2) |

Symmetry transformations used to generate equivalent atoms:
#1 -x+1,-y+1,-z+1

**X-Ray Structure Determination, $C_{44}H_{40}N_2$**

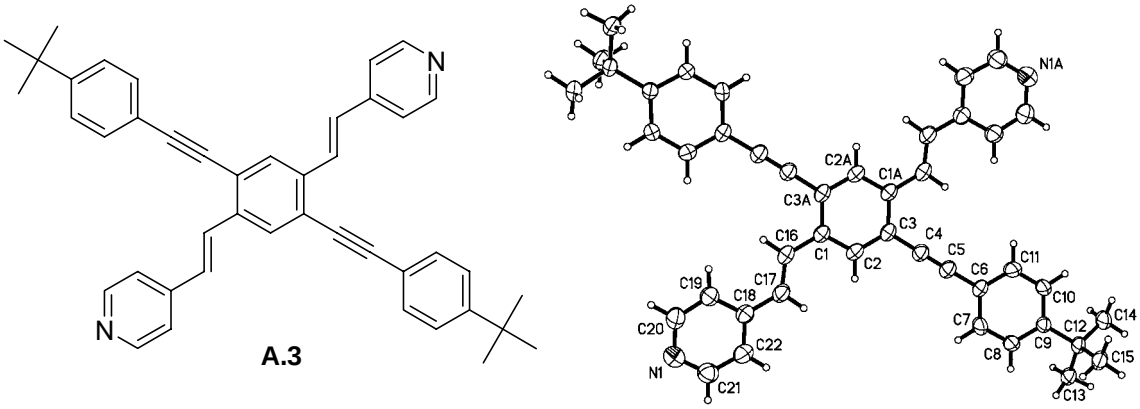


**Figure A.10**. The structure of **A.3** at left and the refined crystal structure at right. The compound is isomorphic to **A.2**.

A yellow plate was mounted onto the end of a thin glass fiber using inert oil. X-ray intensity data covering the full sphere of reciprocal space were measured at 150(1) K on a Bruker SMART APEX CCD-based diffractometer (Mo Kα radiation, λ = 0.71073 Å).[1] The raw data frames were integrated with SAINT+,[1] which also applied corrections for Lorentz and polarization effects. The final unit cell parameters are based on the least-squares refinement of 6358 reflections with I > 5(σ)I from the data set. Analysis of the data showed negligible crystal decay during data collection.

Systematic absences in the intensity data were consistent with the space group $P2_1/n$. The structure was solved by a combination of direct methods and difference Fourier syntheses, and refined by full-matrix least-squares against $F^2$, using the SHELXTL software package.[2] The molecule resides on a center of symmetry. All non-hydrogen atoms were refined with anisotropic displacement parameters; hydrogen atoms were placed in geometrically idealized positions and refined with isotropic displacement parameters as riding atoms.

**Table A.14**. Crystal data and structure refinement for jw04s.

| | | |
|---|---|---|
| Identification code | jw04s | |
| Empirical formula | C44 H40 N2 | |
| Formula weight | 596.78 | |
| Temperature | 150(1) K | |
| Wavelength | 0.71073 Å | |
| Crystal system | Monoclinic | |
| Space group | $P2_1/n$ | |
| Unit cell dimensions | a = 11.3053(6) Å | α= 90°. |
| | b = 6.1025(3) Å | β= 90.4890(10)°. |
| | c = 24.1402(14) Å | γ = 90°. |
| Volume | 1665.39(15) $Å^3$ | |
| Z | 2 | |
| Density (calculated) | 1.190 $Mg/m^3$ | |
| Absorption coefficient | 0.068 $mm^{-1}$ | |
| F(000) | 636 | |
| Crystal size | 0.40 x 0.35 x 0.08 $mm^3$ | |
| Theta range for data collection | 1.69 to 23.26°. | |
| Index ranges | -12<=h<=12, -6<=k<=6, -26<=l<=26 | |
| Reflections collected | 9379 | |
| Independent reflections | 2393 [R(int) = 0.0368] | |
| Completeness to theta = 23.26° | 100.0 % | |
| Absorption correction | None | |
| Refinement method | Full-matrix least-squares on $F^2$ | |
| Data / restraints / parameters | 2393 / 0 / 231 | |

**Table A.15**. Bond lengths

| | |
|---|---|
| Goodness-of-fit on $F^2$ | 0.997 |
| Final R indices [I>2sigma(I)] | R1 = 0.0453, wR2 = 0.1170 |
| R indices (all data) | R1 = 0.0556, wR2 = 0.1218 |
| Largest diff. peak and hole | 0.180 and -0.175 e.$Å^{-3}$ |

**Table A.16**. Bond lengths [Å] and angles [°] for jw04s.

| | |
|---|---|
| C(1)-C(2) | 1.387(2) |
| C(1)-C(3)#1 | 1.420(2) |
| C(1)-C(16) | 1.459(2) |
| C(2)-C(3) | 1.387(2) |
| C(3)-C(1)#1 | 1.420(2) |
| C(3)-C(4) | 1.434(2) |
| C(4)-C(5) | 1.200(2) |
| C(5)-C(6) | 1.436(2) |
| C(6)-C(11) | 1.378(2) |
| C(6)-C(7) | 1.388(2) |
| C(7)-C(8) | 1.378(2) |
| C(8)-C(9) | 1.384(2) |
| C(9)-C(10) | 1.382(2) |
| C(9)-C(12) | 1.538(2) |
| C(10)-C(11) | 1.375(2) |
| C(12)-C(14) | 1.528(3) |
| C(12)-C(13) | 1.529(3) |
| C(12)-C(15) | 1.534(2) |
| C(16)-C(17) | 1.328(2) |
| C(17)-C(18) | 1.445(3) |
| C(18)-C(19) | 1.388(2) |
| C(18)-C(22) | 1.391(3) |
| C(19)-C(20) | 1.366(3) |
| C(20)-N(1) | 1.337(3) |
| C(21)-N(1) | 1.310(2) |
| C(21)-C(22) | 1.377(3) |
| C(2)-C(1)-C(3)#1 | 117.76(16) |
| C(2)-C(1)-C(16) | 122.38(16) |

**Table A.16**. continued

| | |
|---|---|
| C(3)#1-C(1)-C(16) | 119.85(14) |
| C(3)-C(2)-C(1) | 122.86(16) |
| C(2)-C(3)-C(1)#1 | 119.37(15) |
| C(2)-C(3)-C(4) | 119.55(16) |
| C(1)#1-C(3)-C(4) | 121.08(16) |
| C(5)-C(4)-C(3) | 178.7(2) |
| C(4)-C(5)-C(6) | 178.9(2) |
| C(11)-C(6)-C(7) | 117.88(15) |
| C(11)-C(6)-C(5) | 120.78(16) |
| C(7)-C(6)-C(5) | 121.31(16) |
| C(8)-C(7)-C(6) | 120.20(17) |
| C(7)-C(8)-C(9) | 122.45(17) |
| C(10)-C(9)-C(8) | 116.38(15) |
| C(10)-C(9)-C(12) | 122.29(15) |
| C(8)-C(9)-C(12) | 121.15(15) |
| C(11)-C(10)-C(9) | 121.96(17) |
| C(10)-C(11)-C(6) | 121.13(17) |
| C(14)-C(12)-C(13) | 108.39(15) |
| C(14)-C(12)-C(15) | 108.54(15) |
| C(13)-C(12)-C(15) | 109.16(14) |
| C(14)-C(12)-C(9) | 112.00(14) |
| C(13)-C(12)-C(9) | 111.49(14) |
| C(15)-C(12)-C(9) | 107.18(14) |
| C(17)-C(16)-C(1) | 127.45(16) |
| C(16)-C(17)-C(18) | 126.75(16) |
| C(19)-C(18)-C(22) | 115.51(18) |
| C(19)-C(18)-C(17) | 123.67(17) |
| C(22)-C(18)-C(17) | 120.77(16) |
| C(20)-C(19)-C(18) | 120.13(18) |
| N(1)-C(20)-C(19) | 124.24(18) |
| N(1)-C(21)-C(22) | 124.8(2) |
| C(21)-C(22)-C(18) | 119.71(18) |
| C(21)-N(1)-C(20) | 115.60(18) |

Symmetry transformations used to generate equivalent atoms: #1 -x+1,-y+1,-z

**Table A.17**. Anisotropic displacement parameters ($Å^2 x\ 10^3$) for jw04s. The anisotropic displacement factor exponent takes the form: $-2\pi^2[\ h^2\ a^{*2}U^{11} + ...\ + 2\ h\ k\ a^*\ b^*\ U^{12}\ ]$

| | $U^{11}$ | $U^{22}$ | $U^{33}$ | $U^{23}$ | $U^{13}$ | $U^{12}$ |
|---|---|---|---|---|---|---|
| C(1) | 36(1) | 42(1) | 30(1) | 5(1) | 1(1) | 3(1) |
| C(2) | 39(1) | 44(1) | 31(1) | 8(1) | 4(1) | 0(1) |
| C(3) | 37(1) | 44(1) | 27(1) | 5(1) | 1(1) | 4(1) |
| C(4) | 37(1) | 44(1) | 32(1) | 3(1) | 0(1) | -1(1) |
| C(5) | 40(1) | 46(1) | 31(1) | 4(1) | 1(1) | 0(1) |
| C(6) | 38(1) | 43(1) | 28(1) | 3(1) | 2(1) | 2(1) |
| C(7) | 76(1) | 45(1) | 28(1) | -5(1) | -2(1) | -16(1) |
| C(8) | 77(1) | 45(1) | 31(1) | 0(1) | 4(1) | -24(1) |
| C(9) | 40(1) | 32(1) | 29(1) | 0(1) | 0(1) | 0(1) |
| C(10) | 70(1) | 41(1) | 31(1) | -4(1) | 1(1) | -19(1) |
| C(11) | 66(1) | 48(1) | 35(1) | 5(1) | 1(1) | -21(1) |
| C(12) | 51(1) | 38(1) | 26(1) | -2(1) | 3(1) | -3(1) |
| C(13) | 56(1) | 42(1) | 31(1) | 2(1) | 6(1) | -2(1) |
| C(14) | 76(2) | 53(1) | 29(1) | -4(1) | 0(1) | -12(1) |
| C(15) | 65(1) | 43(1) | 38(1) | -1(1) | 16(1) | 3(1) |
| C(16) | 44(1) | 49(1) | 28(1) | 5(1) | 3(1) | 3(1) |
| C(17) | 51(1) | 47(1) | 32(1) | 6(1) | 4(1) | -1(1) |
| C(18) | 40(1) | 40(1) | 38(1) | 4(1) | 2(1) | 4(1) |
| C(19) | 51(1) | 45(1) | 40(1) | 4(1) | -3(1) | -3(1) |
| C(20) | 62(1) | 56(1) | 42(1) | -1(1) | 0(1) | -2(1) |
| C(21) | 53(1) | 47(1) | 60(1) | -3(1) | 6(1) | -2(1) |
| C(22) | 52(1) | 47(1) | 46(1) | 6(1) | 7(1) | 1(1) |
| N(1) | 61(1) | 53(1) | 59(1) | -4(1) | -1(1) | -6(1) |

**Table A.18**. Hydrogen coordinates ( x $10^4$) and isotropic displacement parameters ($Å^2$x $10^3$) for jw04s.

| | x | y | z | U(eq) |
|---|---|---|---|---|
| H(2) | 3956 | 1945 | 296 | 42(5) |
| H(7) | 3476 | 567 | 2146 | 55(5) |
| H(8) | 3146 | 108 | 3082 | 88(8) |
| H(10) | 4814 | 5767 | 3405 | 56(5) |
| H(11) | 5129 | 6274 | 2473 | 71(7) |
| H(13A) | 2937 | -519 | 3948 | 49(5) |
| H(13B) | 3485 | 118 | 4540 | 40(4) |
| H(13C) | 4341 | -485 | 4037 | 52(5) |
| H(14A) | 5298 | 3252 | 4285 | 51(5) |
| H(14B) | 4276 | 3615 | 4731 | 61(6) |
| H(14C) | 4488 | 5401 | 4257 | 63(6) |
| H(15A) | 2423 | 5206 | 3961 | 60(6) |
| H(15B) | 2143 | 3423 | 4428 | 61(6) |
| H(15C) | 1828 | 2918 | 3793 | 60(6) |
| H(16) | 4202 | 2295 | -1176 | 48(5) |
| H(17) | 3038 | 121 | -339 | 60(6) |
| H(19) | 3330 | 406 | -1826 | 54(6) |
| H(20) | 2647 | -2182 | -2433 | 71(6) |
| H(21) | 1383 | -5725 | -1240 | 83(8) |
| H(22) | 2049 | -3291 | -583 | 56(6) |

**Table A.19**. Torsion angles [°] for jw04s.

| | |
|---|---|
| C(3)#1-C(1)-C(2)-C(3) | 0.3(3) |
| C(16)-C(1)-C(2)-C(3) | 179.97(15) |
| C(1)-C(2)-C(3)-C(1)#1 | -0.3(3) |
| C(1)-C(2)-C(3)-C(4) | 178.95(15) |
| C(2)-C(3)-C(4)-C(5) | -120(8) |
| C(1)#1-C(3)-C(4)-C(5) | 60(9) |
| C(3)-C(4)-C(5)-C(6) | -39(16) |
| C(4)-C(5)-C(6)-C(11) | -16(10) |
| C(4)-C(5)-C(6)-C(7) | 162(9) |
| C(11)-C(6)-C(7)-C(8) | 0.1(3) |
| C(5)-C(6)-C(7)-C(8) | -178.26(18) |
| C(6)-C(7)-C(8)-C(9) | -0.2(3) |
| C(7)-C(8)-C(9)-C(10) | -0.1(3) |
| C(7)-C(8)-C(9)-C(12) | 175.19(18) |
| C(8)-C(9)-C(10)-C(11) | 0.5(3) |
| C(12)-C(9)-C(10)-C(11) | -174.69(17) |
| C(9)-C(10)-C(11)-C(6) | -0.7(3) |
| C(7)-C(6)-C(11)-C(10) | 0.3(3) |
| C(5)-C(6)-C(11)-C(10) | 178.70(17) |
| C(10)-C(9)-C(12)-C(14) | -28.3(2) |
| C(8)-C(9)-C(12)-C(14) | 156.71(18) |
| C(10)-C(9)-C(12)-C(13) | -149.96(17) |
| C(8)-C(9)-C(12)-C(13) | 35.1(2) |
| C(10)-C(9)-C(12)-C(15) | 90.6(2) |
| C(8)-C(9)-C(12)-C(15) | -84.3(2) |
| C(2)-C(1)-C(16)-C(17) | 8.1(3) |
| C(3)#1-C(1)-C(16)-C(17) | -172.32(17) |
| C(1)-C(16)-C(17)-C(18) | -178.72(17) |
| C(16)-C(17)-C(18)-C(19) | -7.0(3) |
| C(16)-C(17)-C(18)-C(22) | 170.16(18) |
| C(22)-C(18)-C(19)-C(20) | -1.0(3) |
| C(17)-C(18)-C(19)-C(20) | 176.33(17) |
| C(18)-C(19)-C(20)-N(1) | 1.4(3) |
| N(1)-C(21)-C(22)-C(18) | -0.3(3) |

**Table A.19**. continued

| | |
|---|---|
| C(19)-C(18)-C(22)-C(21) | 0.4(3) |
| C(17)-C(18)-C(22)-C(21) | -176.94(17) |
| C(22)-C(21)-N(1)-C(20) | 0.7(3) |
| C(19)-C(20)-N(1)-C(21) | -1.2(3) |

Symmetry transformations used to generate equivalent atoms:
#1 -x+1,-y+1,-z

## A.2 References and Notes


1. SMART Version 5.625 and SAINT+ Version 6.02a. Bruker Analytical X-ray Systems, Inc., Madison, Wisconsin, USA, 1998.

2. Sheldrick, G. M. SHELXTL Version 5.1; Bruker Analytical X-ray Systems, Inc., Madison, Wisconsin, USA, 1997.

# Appendix B

# Additional Synthesis and Characterization of Cruciform π Systems

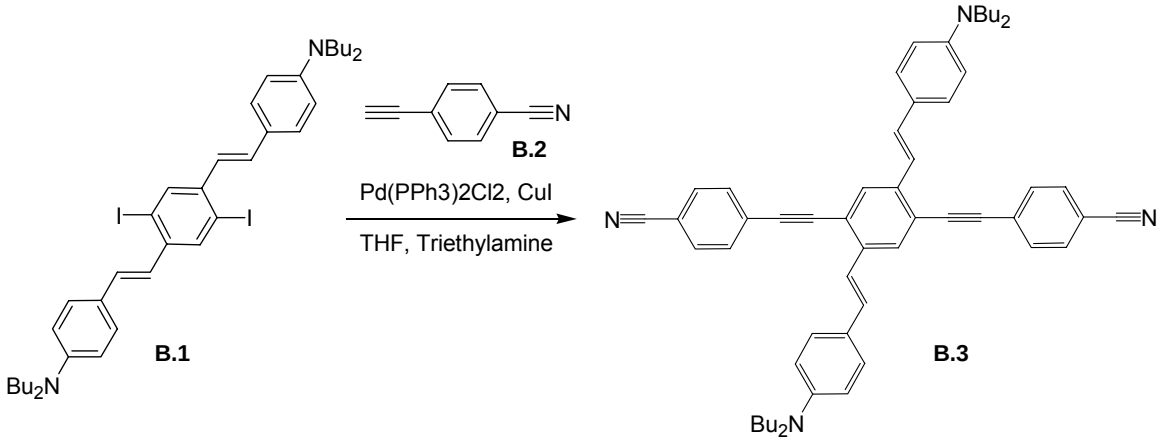


**Scheme B.1**. The formation of **B.3** from the previously described **B.1**.

Compound **B.3**: **B.1** (683 mg, 0.866 mmol) was combined with **B.2** (330 mg, 2.60 mmol), $(PPh_3)_2PdCl_2$ (5.0 mg, 7.1 μmol), CuI (5.0 mg, 33 μmol) and dissolved in 4.0 mL of triethylamine/THF 1:1. The crude reaction mixture was precipitated twice from dichloromethane into hexane. The resulting orange-red powder was purified by flash chromatography beginning with hexane and gradually switching to 1:2 dichloromethane:hexane. Yield: 78% MP: 239-241°. IR: 3037.7, 2952.8, 2927.7, 2925.8, 2918.1, 2859.2, 2222.8, 2205.4, 1600.8, 1550.6, 1521.7, 1509.1, 1465.8, 1457.1, 1427.2, 1399.2, 1367.4, 1314.4, 1284.5, 1252.6, 1221.8, 1183.2, 1149.5, 1109.9, 1104.1, 983.6, 954.7, 924.8, 887.1, 846.6, 835.1, 822.5, 801.3. $^1$H NMR (300 MHz, $CDCl_3$): δ = 7.84 (s,

2H), 7.68 (m, 8H), 7.42 (d, 4H, $J_{3\ H,H}$ = 8.71 Hz), 7.36 (d, 2H, $J_{3\ H,H}$ = 16.16 Hz), 7.19 (d, 2H, $J_{3\ H,H}$ = 16.21 Hz), 6.66 (d, 4H, $J_{3\ H,H}$ = 8.81 Hz), 3.34 (d, 8H, $J_{3\ H,H}$ = 7.15 Hz), 1.63 (m, 8H), 1.41 (m, 8H), 1.00 (t, 12H, $J_{3\ H,H}$ = 7.31 Hz). $^{13}$C NMR ($CDCl_3$): δ = 148.37, 137.84, 132.33, 132.21, 131.35, 128.63, 128.42, 128.34, 124.24, 121.22, 119.92, 118.76, 111.80, 93.06, 51.11, 29.84, 20.74, 14.43.

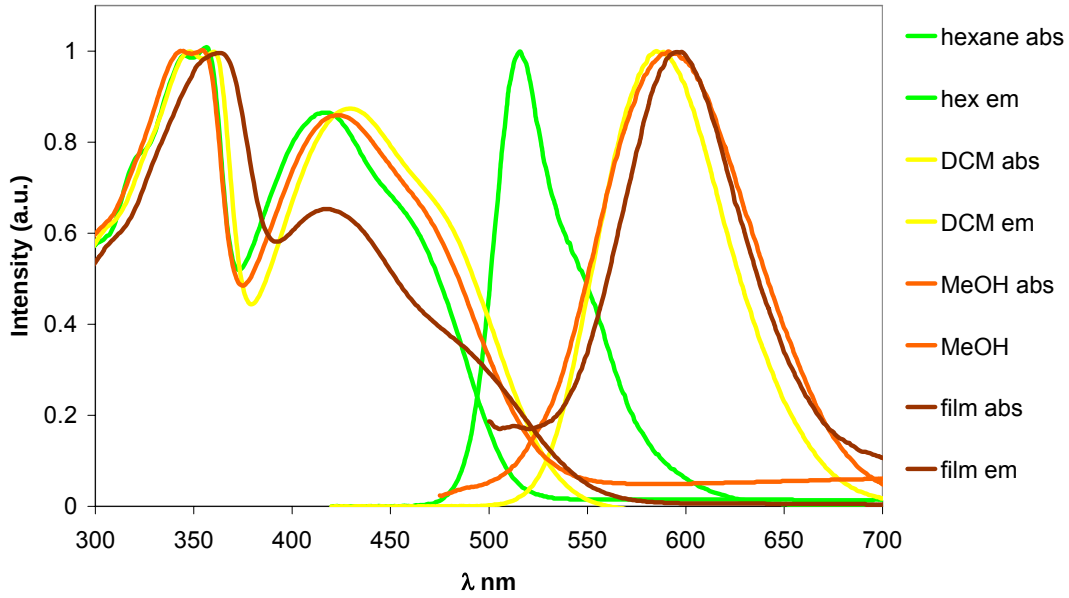


**Figure B.1**. Absorbance and emission spectra for **B.3**. Absorbance spectra are at right, emission spectra are at left.

**Table B.1**. Summary of optical data for compound **B.3**.

| | Hexane | DCM | MeOH | Thin film |
|---|---|---|---|---|
| Absorbance $\lambda_{max}$ (nm) | 357, 417 | 357, 431 | 355, 423 | 364, 418 |
| Emission $\lambda_{max}$ (nm) | 516 | 586 | 592 | 598 |

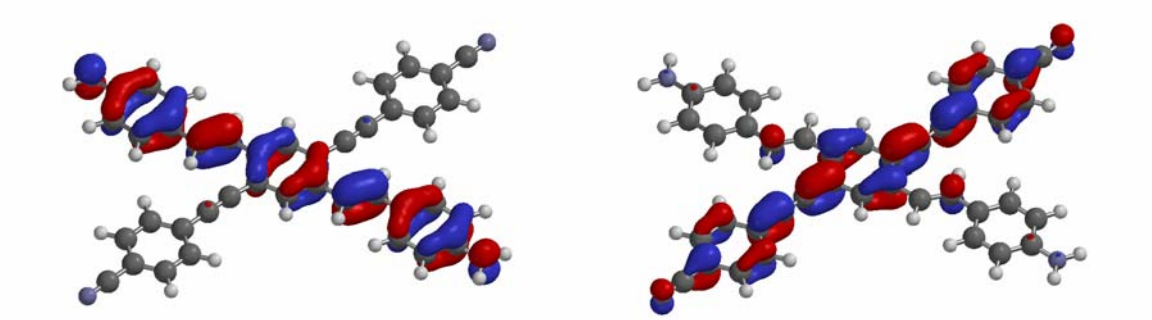

**Figure B.2**. Frontier orbitals for **B.3**. HOMO: -4.79 eV at left. LUMO: -2.48 eV at right. Values calculated by SPARTAN with B3LYP utilizing the 6-31G** basis set.

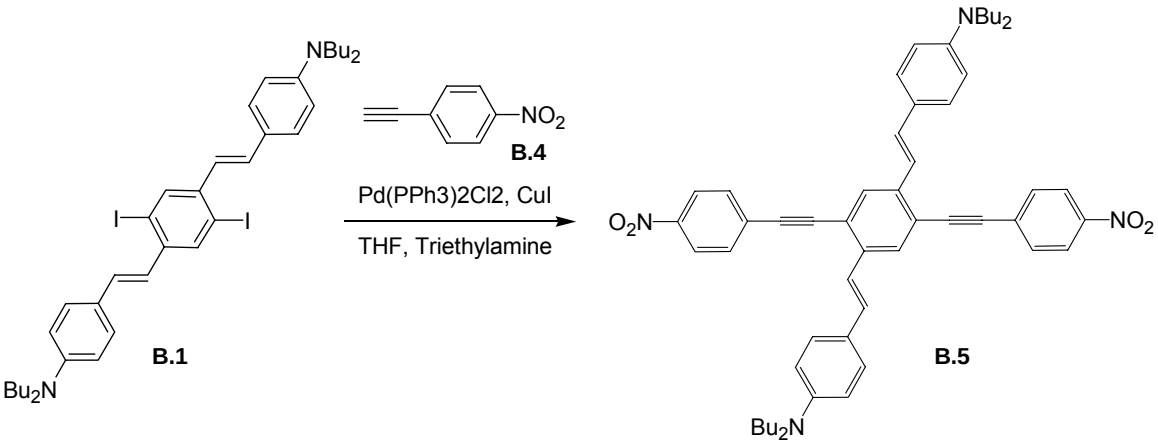


**Scheme B.2**. The formation of **B.5** from the previously described **B.1**.

Compound **B.5**: **B.1** (2.00 g, 2.50 mmol) was combined with **B.4** (3.00 g, 20.0 mmol), $(PPh_3)_2PdCl_2$ (5.0 mg, 7.1 μmol), CuI (5.0 mg, 33 μmol) and dissolved in 4.0 mL of triethylamine/THF 1:1. The crude reaction mixture was precipitated from dichloromethane into hexane and a second time from dichloromethane into cold methanol. The resulting black powder was purified by flash chromatography beginning with hexane and gradually

switching to 1:1 dichloromethane:hexane. Yield: 83% MP: 221-223°. IR: 3036.7, 2952.8, 2921.9, 2867.9, 2859.2, 2838.0, 2438.8, 2234.3, 2206.4, 1599.8, 1591.1, 1551.6,1513.0, 1495.6, 1469.6, 1454.2, 1427.2, 1404.0, 1370.3, 1338.5, 1282.5, 1220.8, 1184.2, 1148.5, 1108.0, 957.5, 951.8, 922.8, 886.2, 858.2, 847.6, 817.7, 801.3, 747.3, 729.0, 688.5. $^{1}$H NMR (300 MHz, $CDCl_3$): δ = 8.25 (d, 4H, $J_{3\ H,H}$ = 8.86 Hz), 7.82 (s, 2H), 7.71 (d, 4H, $J_{3\ H,H}$ = 8.69 Hz), 7.41 (d, 2H, $J_{3\ H,H}$ = 8.57 Hz), 7.34 (d, 2H, $J_{3\ H,H}$ = 16.22 Hz), 7.17 (d, 2H, $J_{3\ H,H}$ = 16.21 Hz), 6.64 (d, 4H, $J_{3\ H,H}$ = 8.61 Hz), 3.32 (d, 8H, $J_{3\ H,H}$ = 7.15 Hz), 1.61 (m, 8H), 1.40 (m, 8H), 0.98 (t, 12H, $J_{3\ H,H}$ = 7.31 Hz). $^{13}$C NMR ($CDCl_3$): δ = 148.40, 147.11, 137.87, 132.38, 131.38, 130.40, 128.65, 128.37, 124.20, 123.92, 121.19, 119.81, 111.78, 94.04, 93.53, 51.10, 29.85, 20.74, 14.43.

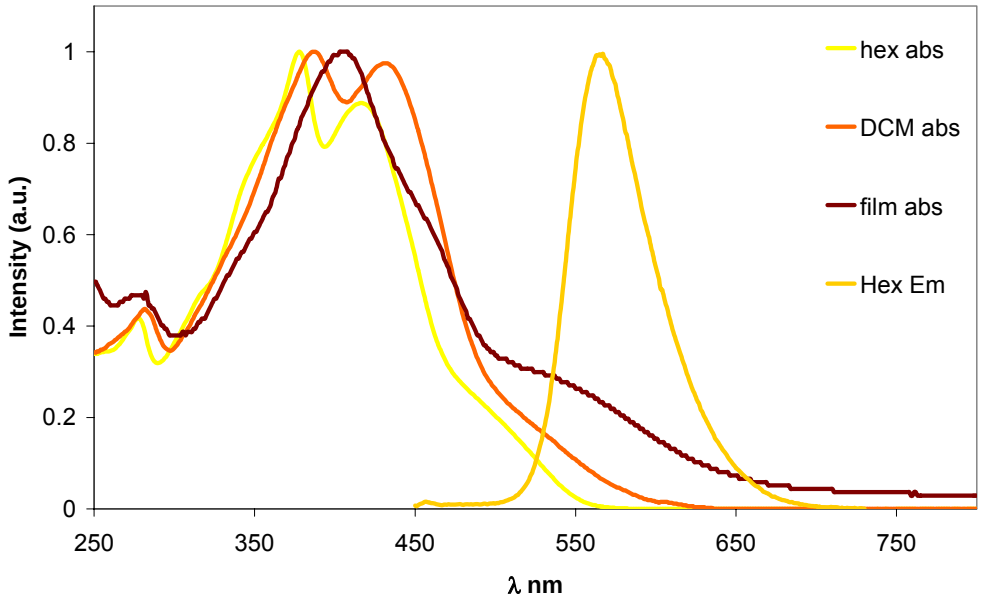


**Figure B.3**. Absorbance and emission spectra for **B.5**. The compound is non-emissive in the solid state and polar solvents.

**Table B.2**. Summary of optical data for compound **B.5**.

| | Hexane | DCM | MeOH | Thin film |
|---|---|---|---|---|
| Absorbance $\lambda_{max}$ (nm) | 379, 418 | 387, 432 | 396 | 389 |
| Emission $\lambda_{max}$ (nm) | 566 | - | - | - |

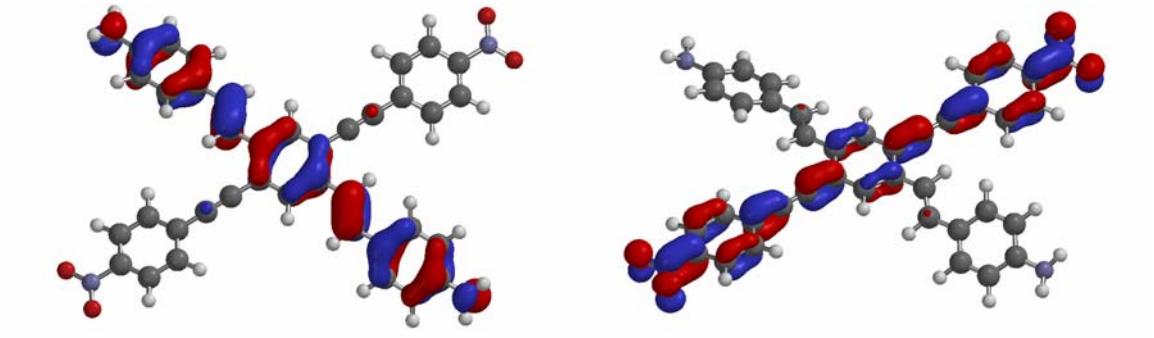

**Figure B.4**. Frontier orbitals for **B.5**. HOMO: -5.01 eV at left. LUMO: -2.81 eV at right. Values calculated by SPARTAN with B3LYP utilizing the 6-31G** basis set.

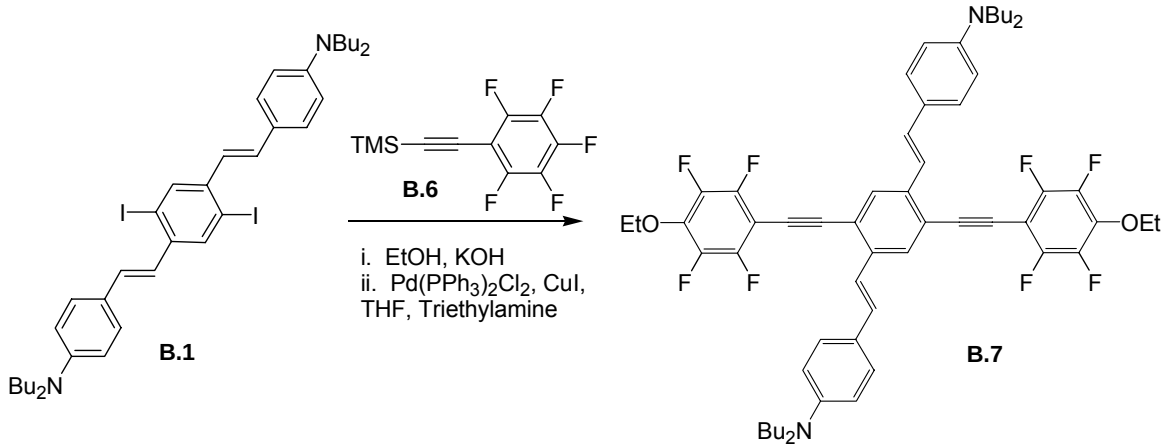


**Scheme B.3**. The formation of **B.7** from the previously described **B.1**.

Compound **B.7**: **B.6** (1.00 g, 3.78 mmol) was combined with 2.0 mL of EtOH and 1.0 g of KOH. After 10 min, **B.1** (789 mg, 1.00 mmol), $(PPh_3)_2PdCl_2$ (5.0 mg, 7.1 μmol), CuI (5.0 mg, 33 μmol) and 6.0 mL of triethylamine/THF 1:1 were added while under nitrogen purge. The reaction was allowed to progress over 24 h. The crude reaction mixture

was precipitated from dichloromethane into hexane and a second time from dichloromethane into cold methanol. $^{1}$H NMR determined the product still contained impurities (deemed later to be the addition of ethoxide to the fluorinated aromatic ring), so the product was purified by flash chromatography (dichloromethane/hexane, 1:1 as eluent). The resulting brilliant orange powder was recrystallized by evaporation of dichloromethane from methanol yielding crystals suitable for crystallographic analysis which ultimately determined the source of the additional peaks in the NMR spectrum. 13C was not feasible due to the highly fluorinated ring system producing a forest of peaks. Yield: 65% (after multiple purification steps). MP: 173-174$^{o}$. IR: 3034.8, 2965.4, 2860.2, 2210.3, 1603.7, 1578.6, 1521.7, 1497.6, 1442.7, 1400.2, 1390.6, 1365.5, 1274.9, 1217.0, 1196.8, 1186.1, 1127.3, 1026.1, 983.6, 956.66, 893.0, 805.2, 683.7. $^{1}$H NMR (300 MHz, $CDCl_3$): $\delta$ = 7.88 (s, 2H), 7.47 (m, 6H, $J_{3\ H,H}$ = 16.15 Hz), 6.67 (d, 2H, $J_{3\ H,H}$ = 8.57 HZ), 4.42 (q, 4H, $J_{3\ H,H}$ = 7.02 Hz), 3.34 (t, 8H, $J_{3\ H,H}$ = 7.27 Hz), 1.63-1.56 (m, 8H), 1.46-1.32 (m, 14H), 0.98, 0.93 (t, 12H, $J_{3\ H,H}$ = 7.34 Hz).

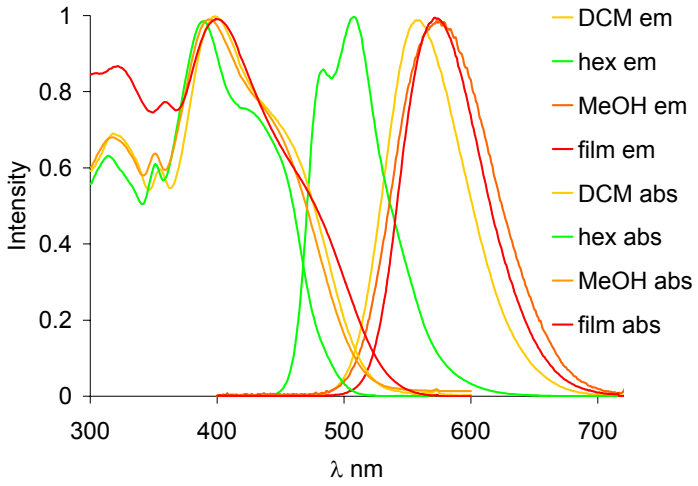


**Figure B.5**. Absorbance and emission spectra for **B.7**.

**Table B.3**. Summary of optical data for compound **B.7**.

| | Hexane | DCM | MeOH | Thin film |
|---|---|---|---|---|
| Absorbance $\lambda_{max}$ (nm) | 390 | 400 | 396 | 403 |
| Emission $\lambda_{max}$ (nm) | 485, 509 | 560 | 577 | 574 |

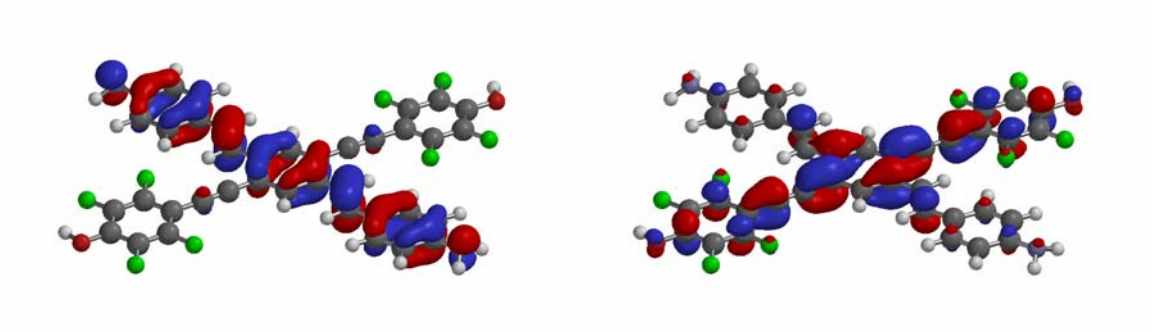

**Figure B.6**. Frontier orbitals for **B.7**. HOMO: -5.01 eV at left. LUMO: -2.81 eV at right. Values calculated by SPARTAN with B3LYP utilizing the 6-31G** basis set.

Summary of cyclic voltametry: Methods are as previously reported for characterization of related crucifroms. **B.3** showed two oxidation peaks, and the onset of a reduction peak. **B.5** showed one oxidation peak and a lowered reduction peak and the onset of a second reduction peak. **B.7** showed four oxidation peaks and the onset of a reduction peak.

**Table B.4**. Summary of cyclic voltametry data and calculated bandgaps.

| | **B.3** | **B.5** | **B.7** |
|---|---|---|---|
| | Oxidation [V]: | | |
| $E_{1/2}$ | 0.71 | 0.88 | 0.67 |
| Peak | 0.74 | 1.06 | 0.76 |
| HOMO | 5.21 | 5.38 | 5.17 |
| | Reduction [V]: | | |
| $E_{1/2}$ | -1.44* | -0.81 | -1.54* |
| Peak | - | -0.89 | - |
| LUMO | 3.06* | 3.69 | 2.96* |
| Band gap | 2.15* | 1.69 | 2.21* |
| | Quantum Chemical Calculations [eV]: | | |
| HOMO | -4.79 | -5.01 | -4.65 |
| LUMO | -2.48 | -2.81 | -1.96 |
| Band gap | 2.31 | 2.2 | 2.69 |

* represents a minimum value. Only onsets of reduction were observed

# Appendix C

# TEM and SEM Images

## C.1 Introduction

The ordering of molecules on the nano- and mesoscale is of fundamental interest in the increasing drive to miniaturize (or nanosize) the components of most objects in our everyday lives. From pants to electronics, nanotechnology will have a profound impact on our world today and most certainly in the future.

A frequent step in the characterization of any new compound in our labs was the imaging of various morphologies produced by aggregation, precipitation, explosion, drop-casting, spin-casting or annealing. In some cases the results were included in publications forming the basis for some of the previous chapters. However, there are number of images that could not be incorporated into publications for lack of space or for loss of explanation or reproducibility.

A brief explanation is offered for all of the images whether it be the supposed conditions under which the material was produced or the reaction conditions which produced the compound in question.

## C.2 Wires and fibers

Wires and fibres seem to result from the combination of polar and non-polar monomers. Similar structures have been shown Hamilton et al. Show Figure.

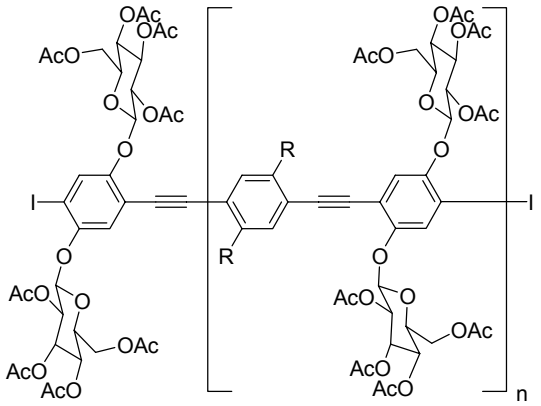


**C.1**

**Figure C.1**. Sugar polymer **C.1** utilized for the mesostructures shown in Figure C.2.

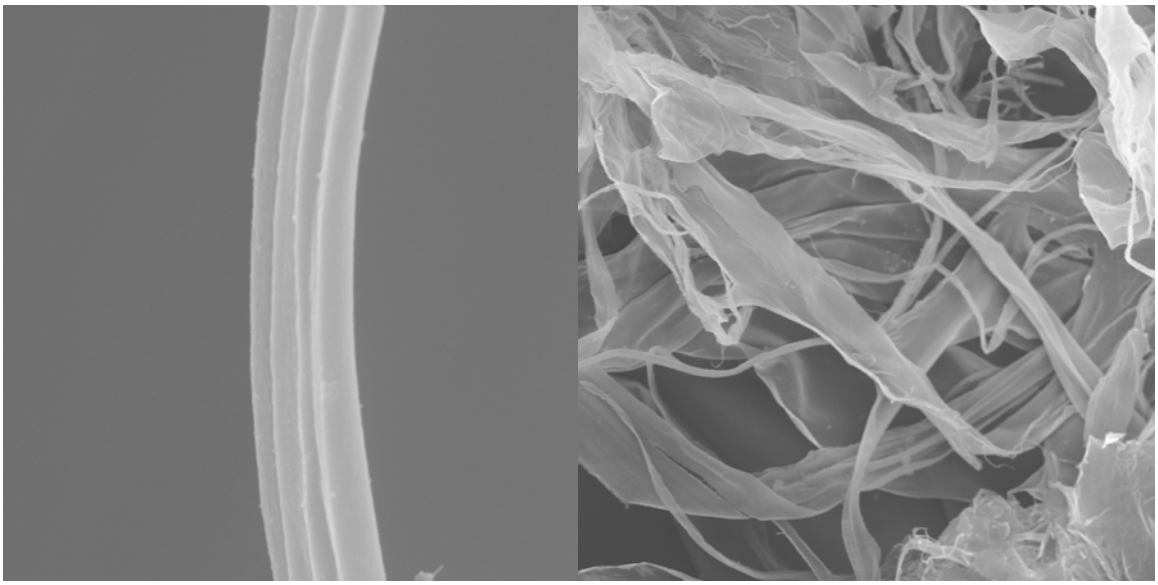

**Figure C.2**. At left an example of a multi-fibre ribbon formed from **C.1** in DMSO solution precipitated into water; picture width is 22.5 μm. At right, a collection of ribbons; picture width is 225 μm.

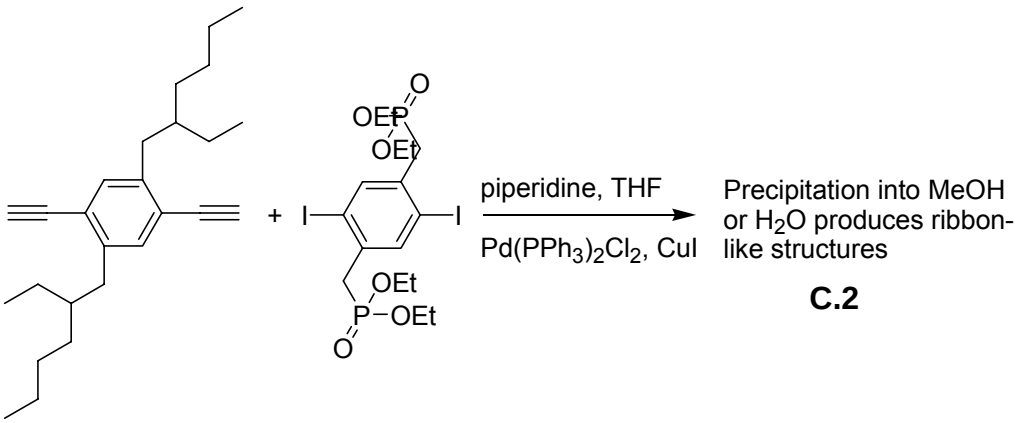


**Scheme C.1**. Formation of unknown polymeric material **C.2**. Composition and structure are difficult to discern from NMR and IR.

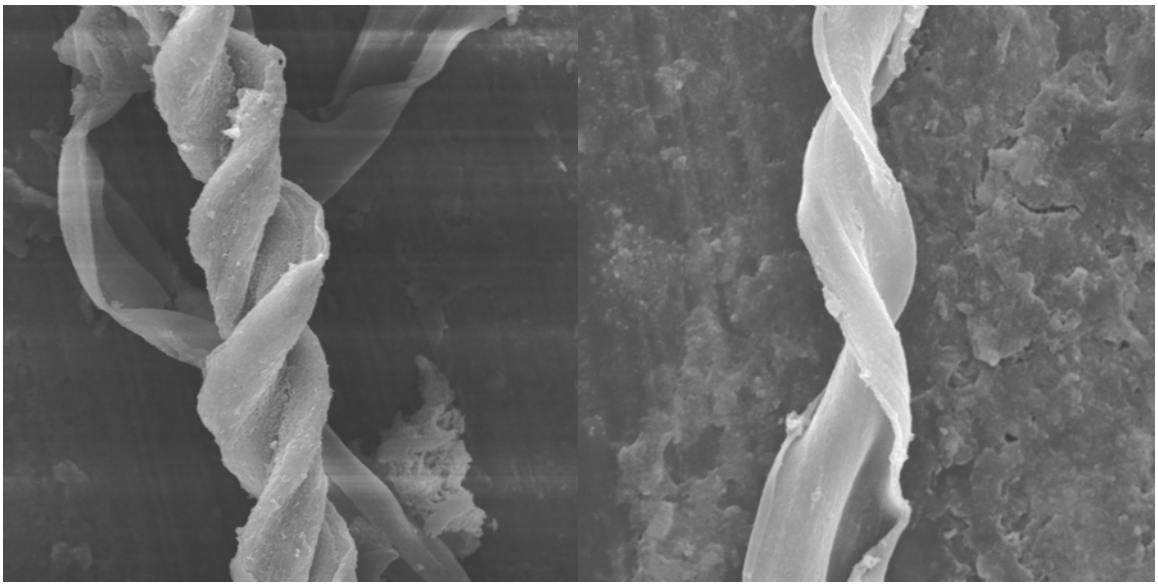

**Figure C.3**. At left, a helical ribbon; picture width is 129 μm. At right, another helical ribbon; picture width is 90 μm.

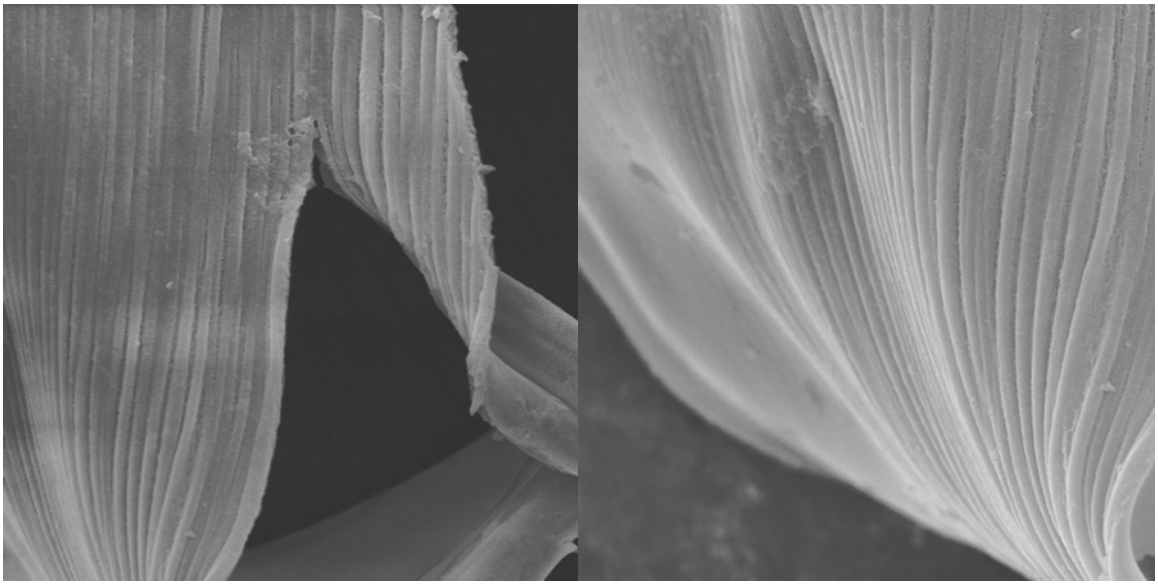

**Figure C.4**. At left, a sheet of fibres; picture width is 129 μm. At right, another sheet; picture width is 90 μm.

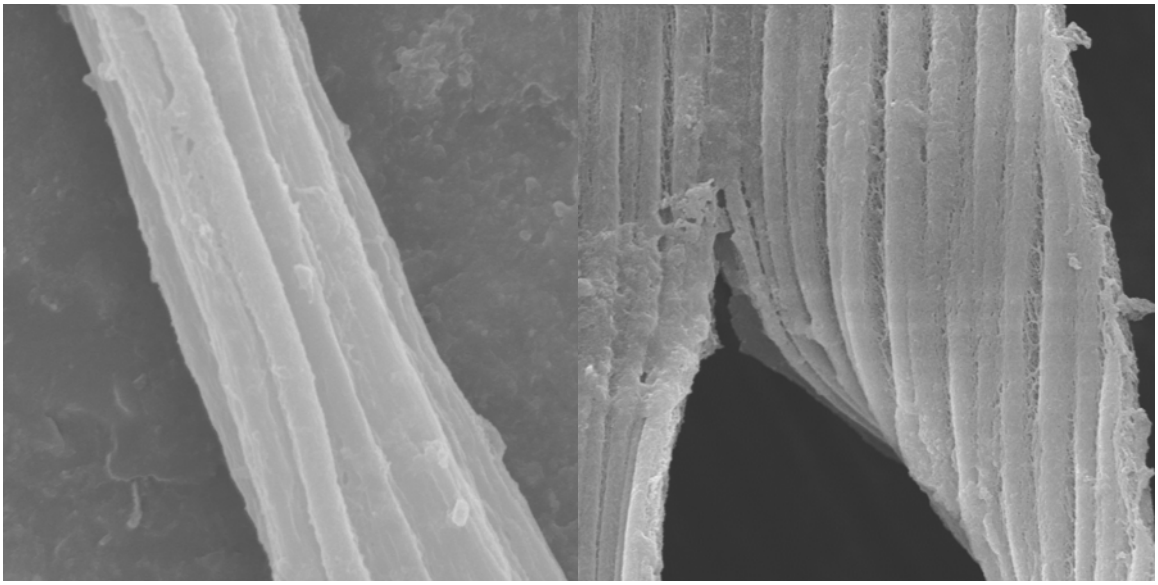

**Figure C.5**. At left, close up of a multi-fibred ribbon; picture width is 18 μm. At right, a split in a sheet; picture width is 18 μm.

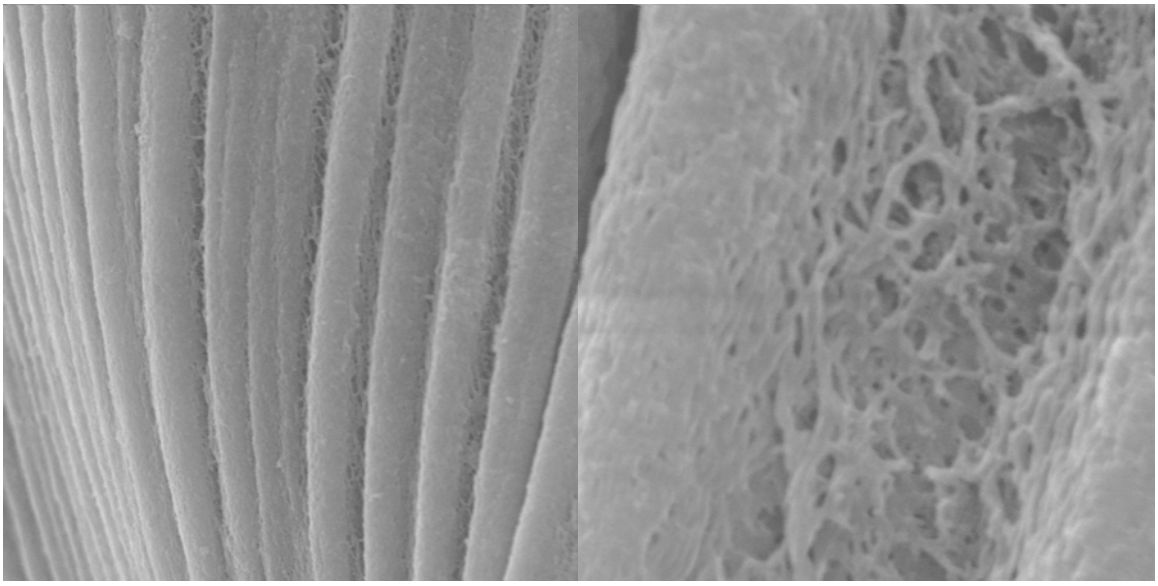

**Figure C.6**. At left, close up of a multi-fibred sheet; picture width is 15 μm. At right, between the individual fibres in a sheet appears a network of smaller fibres; picture width is 8.1 μm.

## C.3 Microspheres and Microflowers

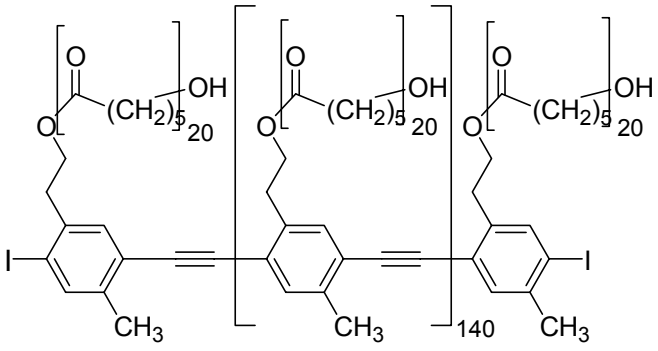


**C.3**

**Figure C.7**. Structure of polymer **C.3** utilized to form microspheres shown in Figure C.8.

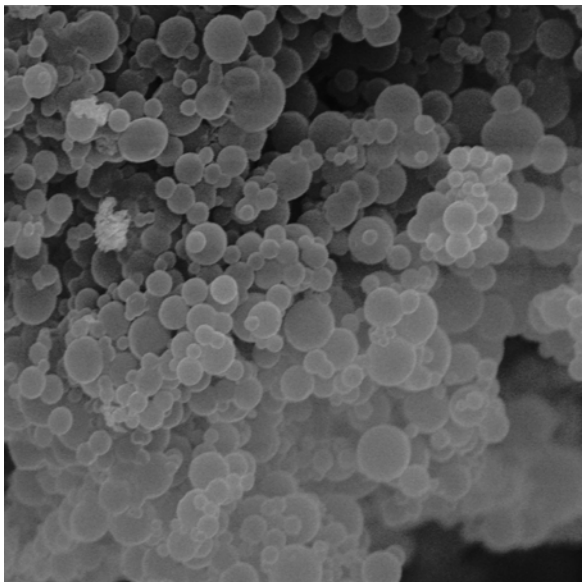

**Figure C.8**. Microspheres formed from polymer **C.3**[1]. Picture width is 45 μm.

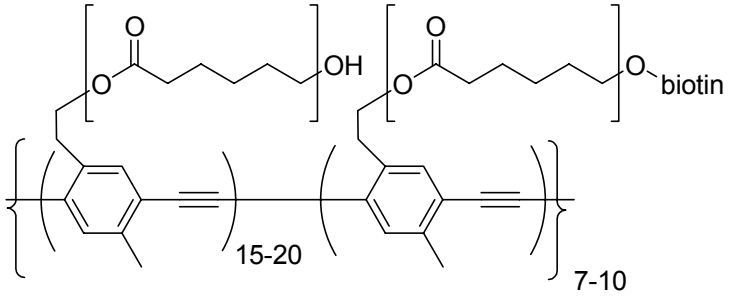


**C.4**

**Figure C.9**. Structure of polymer **C.4** utilized to form microflowers.

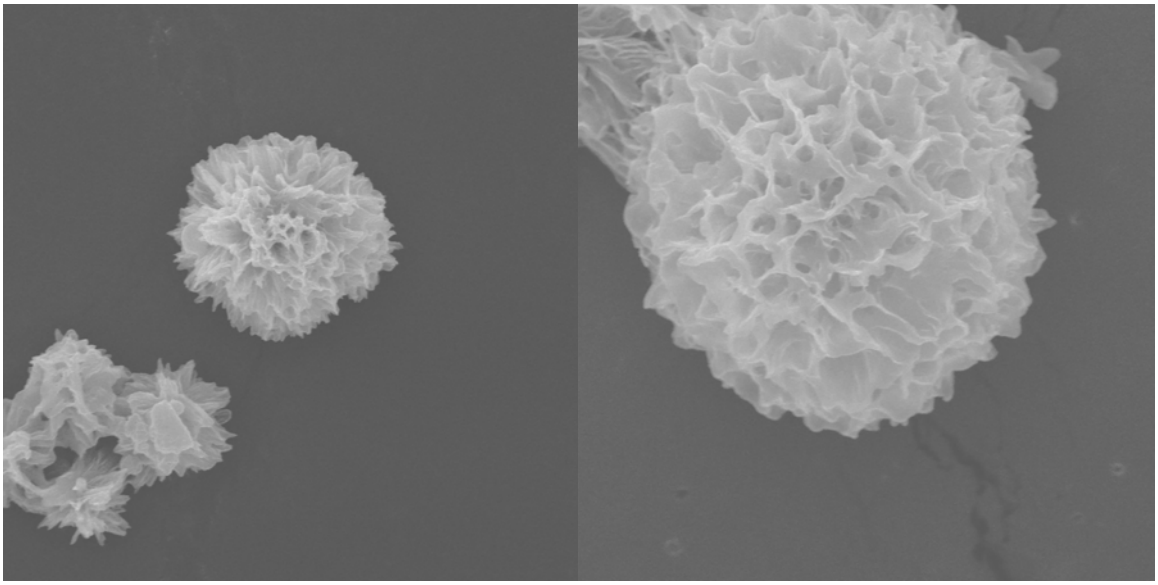

**Figure C.10**. Examples of microflowers formed by the method described in reference 1. Picture width at left, 53 μm; picture width at right, 18 μm.

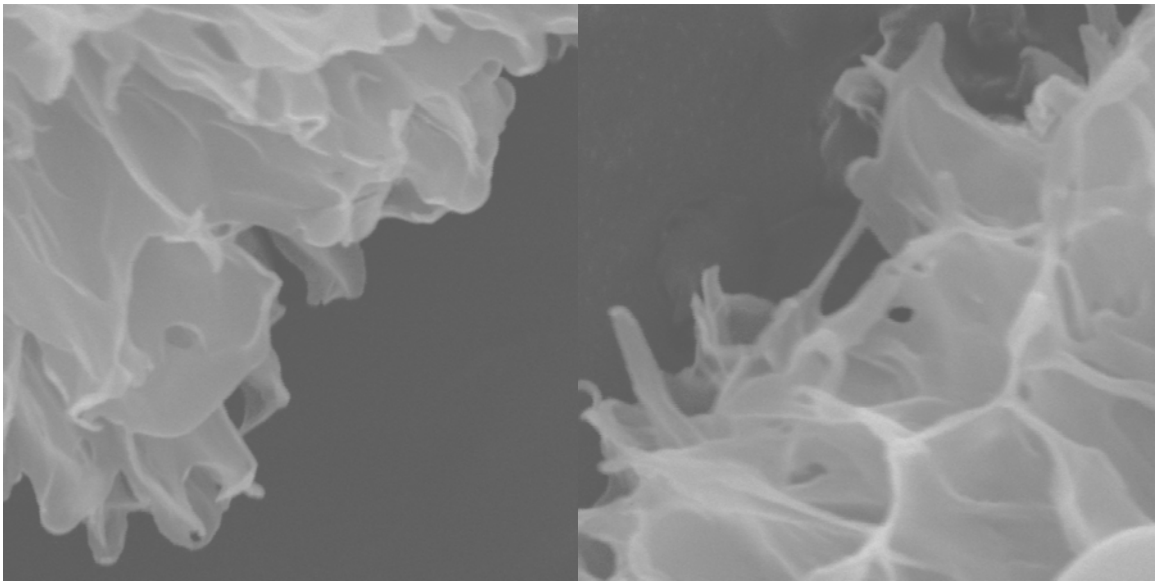

**Figure C.11**. Close ups of the microflowers showing the delicate structure at the edges. Picture width at left, 4.1 μm; picture width at right, 13.0 μm.

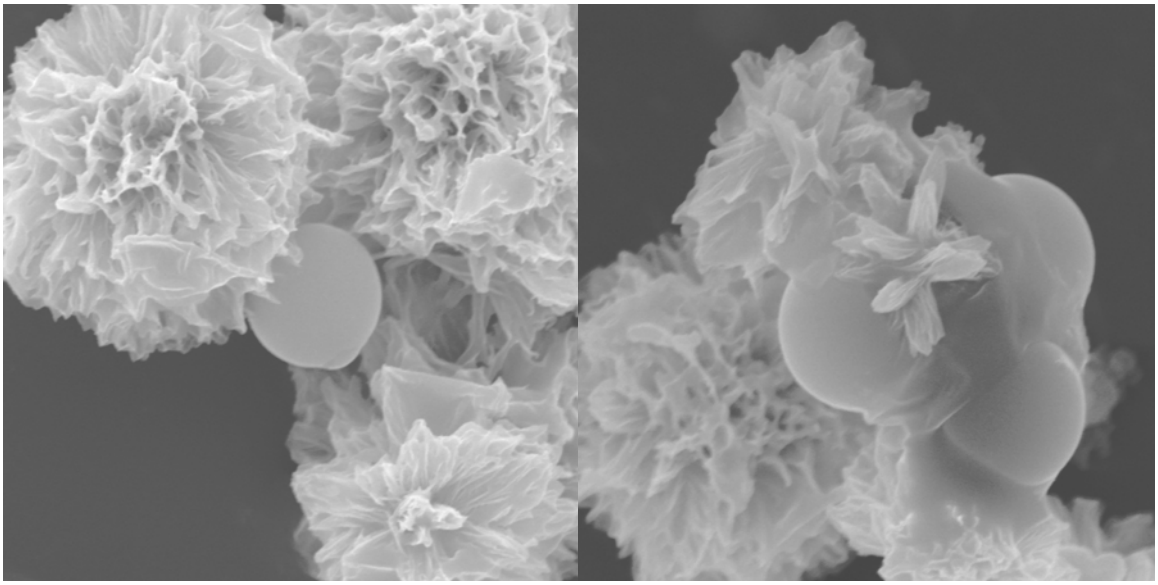

**Figure C.12**. When microflowers of the biotinylated polymer **C.4** were exposed to streptavidin coated microspheres[3], aggregates were formed. The pictures are reminiscent of phagocytosis. Picture width at left, 25.7 μm; picture width at right, 22.5 μm.

## C.4 References and Notes


1. Kietzke, T.; Neher, D.; Landfester, K.; Montenegro, R.; Guntner, R.; Scherf, U. *Nat. Mater.* **2003**, *2*, 408.

2. Caswell, K. K.; Wilson, J. N.; Bunz, U. H. F.; Murphy, C. J. *J. Am. Chem. Soc.*, **2003**, *125*, 13914.

3. Bangs Laboratories streptavidin coated microspheres: Product Code CP01N/5622.